Universitat Ramon Llull

TESIS DOCTORAL

Título	DEVELOPMENT OF BIOACTIVE IMPLANT PLATFORMS TO ASSIST CARDIAC TISSUE REPAIR AFTER MYOCARDIAL INFARCTION
Realizada por	Cristina Castells i Sala
en el Centro	IQS School of Engineering
y en el Departamento	de Bioingeniería
Dirigida por	Dr. Carlos E. Semino

C. Claravall, 1-3
08022 Barcelona
Tel. 936 022 200
Fax 936 022 249
E-mail: urlsc@sec.url.es
www.url.es

A tot aquell que ha estat al meu costat
durant aquesta etapa de la meva vida,
en algún moment o altre,
d'una manera o una altra.

"It is a miracle that curiosity survives formal education"

Albert Einstein (1879-1955)

"Prediction is very difficult, especially about the future"

Niels Bohr (1885-1962)

"If you want to change the world in some big way,
that's where you should start, biological molecules."

Bill Gates (1955)

ACKNOWLEGMENTS

Semblava que el dia no arribaria, però si, ha arribat, i aquí estem al final d'un viatge llarg i dur però alhora dolç i emocionant. Els últims quatre anys (aviat es diu) han tingut moments de tot tipus, alegres, tristos, eufòrics, depriments, motivants, desesperants i això només per a mi; no vull saber el que han representat per aquells que han estat més a prop meu en un moment o altre, ja que els meus canvis d'humor poden haver-los acostat a la bogeria. En aquest punt del viatge, i després de donar-hi tantes voltes i marejar tant al personal, no voldria acabar sense agrair a tots aquells que heu estat al meu costat, el recolzament que m'heu aportat. Poder no trobeu el vostre nom entre aquestes línies doncs estic contenta de dir que hi ha massa gent a la qual he d'agrair alguna cosa, però espero us sentiu identificats en algun dels següents paràgrafs.

Primer de tot, vull donar les gràcies al Dr. Semino. "*Carlos, mucha gracias por ofrecerme trabajar en tu laboratorio y darme la oportunidad de hacer un doctorado y trabajar contigo en un proyecto de estas características. A tu lado me he sumergido en el mundo de la biología molecular a niveles que desde mi punto de vista químico nunca pensé que llegaría. Gracias por transmitirme la pasión por la ciencia y el afán de superación en momentos en los que no creía que pudiera salir nada de esos volúmenes tan pequeños. Muchísimas gracias por todo.*"

També vull agrair al a tots els integrants del projecte Europeu RECATABI l'ajuda que m'han donat en tot moment i els diversos punts de vista dels que he pogut gaudir. Per mi ha sigut una experiència molt rica poder treballar amb especialistes de transfons tant variats, des de biòlegs i veterinaris, passant per químics especialistes en ciència dels materials fins a cirurgians cardíacs. Moltes gràcies per obrir-me la porta al món de la cardiologia, el qual he trobat realment apassionant . Concretament vull donar les gràcies a el Dr. Manuel Monelon Pradas, la Dra. Ana Vallés-Lluch, la Dra. Cristina Martínez-Ramos i la Maria Arnal-Pastor del Centre de Biomaterials i Enginyeria de Teixits de la Universitat Politècnica de València; a el Dr. Toni Bayes-Genis i la Dra. Carolina Soler-Botija del programa de recerca Heart Failure and Cardiac Regeneration (ICREC) de l'Institut Germans Trias i Pujol (IGTP); a el Dr. Juan Carlos Chachques del Departament de Cirurgia Cardiovascular de l'hospital Pompidou de Paris; i a el Dr. Alexander Deten del Fraunhofer IZI de Leipzig. Treballant amb tots vosaltres realment puc dir que he crescut com a científica i he aprés el que significa col·laborar amb grups interdisciplinars. Moltíssimes gràcies a tots, ha sigut una gran experiència. Vull fer un incís especial per la Cris. "*Ha sido un placer conocerte, con tu energía y tu constante y permanente felicidad. Curiosamente este proyecto te ha convertido en una gran amiga a la que me alegra haber encontrado. Eres un sol.*"

Per una altra banda, vull donar les gràcies a aquells que tot i no estar al llarg de tota la tesi, en algun moment o altre han tingut quelcom a veure en el seu desenvolupament, ja sigui directe o indirectament. "*Vielen Dank Frau Dr. Bianca M. Bussmann und Herrn Dr. Sven Reiche vom Translationszentrum für Regenerative Medizin in Leipzig. Ihr habt mir eine unterschiedliche Arbeitsweise gezeigt und mir gelernt, an das Warum der Dinge zu denken. Außerdem habt ihr mir die beste Art und Weise gezeigt, jeden Schritt zu realisieren. Vielen Dank auch an John für die Zusammenarbeit mit mir im Labor und dafür, dass ihr mir Techniken gelenrt habt, die ich bis dato nie durchgeführt hatte"*.Mil gràcies a la Dra. Maria Pilar Armengol responsable del servei de genòmica del IGTP de l'Hospital Germans Tries i Pujol de Badalona. No només m'has ajudat amb la part tècnica sinó que m'has ensenyat mil "intríngulis" de la PCR a temps real. Ha estat un plaer conèixer-te i espero trobar més gent com tu en el camí que la recerca em depari. "*Quiero agradecer también al Dr. Jesús Otero del Hospital Universitario de Asturias por facilitarnos los fibroblastos humanos los cuales nos han sido tan útiles para testar nuestros sistemas.*" També al Dr. Juli Bagó per marcar les cèl·lules que hem fet servir per als experiments *in vivo.* Al Dr. Salvador Borrós, director del laboratori de Materials de l'IQS, no puc deixar d'agrair-li les facilitats brindades per a l'ús dels equips d'humectabilitat, reometria i plasma, però també per els ànims i les interesants converses en els passadissos. Mil milions de gràcies a en Benja i la infinita paciència que ha tingut amb mi i amb els meus cops de cap contra els conceptes "elèctrics". I per últim però no menys important gràcies Francesc i Allan per ajudar-me a millorar la redacció d'aquesta tesis.

A títol més personal, vull començar per aquelles persones amb les que he compartit el dia a dia. Primer de tot, i amb menció especial a les quatre persones amb qui vaig començar aquest viatge: Núria, Tere, Mire i Vero. Nenes ha estat un plaer compartir aquesta etapa de la meva vida amb vosaltres. Núria els nostres vinets després d'hores i hores intentant posar el RAD en les membranes són inoblidables i no diré irrepetibles perquè espero repetir-ho sempre que sigui possible tot i que estiguem cada una a una ciutat diferent. Mire, Tere, Vero amb vosaltres el camí s'ha fet infinitament més interessant i fàcil. Us trobaré molt a faltar (bé ja us hi trobo doncs soc la última que encara ronda per aquí). Per una altra banda també vull agrair a la Lourdes i en Javi les hores de feina i anades d'olla compartides. Amb vosaltres la ciència s'ha fet més intensa i també més fàcil d'atacar. Heu convertit l'electro-estimulació i l'epigenètica en reptes abordables. No puc oblidar-me però de la resta de gent del laboratori amb la que no he treballat directament però que m'heu fet gaudir de l'experiència: Cate, Àlex, Desi, Melva, Raphaella, Anna, Juli, Oscar, Sílvia, Ana i Astrid. Anna, et dec un incís especial. Has aparegut molt al final de la meva tesis però aquest últim any t'has convertit en una gran amiga. Merci per els bon àpats, les bones xerrades, l'iniciació al món del cine i la música moderneta i per tot el que m'has aportat i sé que continuaràs aportant. Vull donar també les gracies als que m'heu

aguantat més aquest últims mesos durant els dinars: "*Cate, Miquel i Astrid lunch time with all of you have been really tasty and full of chocolate.*"

El laboratori d'Enginyeria de Teixits va íntimament lligat al de Biomaterials. Tot i tenir estires i arronses que ens han fet la vida més interessant he trobat grans persones i amics en aquest laboratori que compartim: Pri, Sejin, Pau, Ingrid, Pere, Mariana, Oscar, Leti i als que segur que em deixo. Hem passat grans moments junts després d'hores de feina. Els petits moment de cafetons, cervesetes, festetes i activitats variades han sigut tots i cada un d'ells especials a la seva manera i sé que els trobaré molt a faltar. No em vull oblidar de els bioquímics amb qui més he tractat i he pogut recórrer en tot moment, i especialment a la Victoria i la Cristina. Vic merci per ser-hi en tot (i quan dic tot vull dir tot) moment en tots els àmbits i instants de la meva vida.

Fora del laboratori també hi ha moltes persones que m'han aguantat amb paciència i que han sigut amb mi des de que ens hem creuat en el camí de la vida. Als Lloretencs i especialment la Mimar, en Cesc, la Moni, la Yaiza i la Clàudia els vull agrair el ser-hi sempre i, tot i divergir camins, aparèixer quan se'ls fa falta. Als companys de carrera, que tot i trobar-nos poc aconseguim mantenir-nos al dia i es preocupen pel que faig i com em va. M'encanta que a aquestes altures, després de tant anys i dels tombs que dóna la vida pugui dir que encara us tinc al meu costat. Gracies a tots els que m'heu recolzat i animat en algun moment. A en Javi li vull agrair el temps que hem compartit en tots els aspectes i especialment parlant de ciència i animant-nos l'un a l'altre a continuar endavant quan tot plegat semblava que no tenia sortida.

Vull acabar fent un incís especial a la meva família, a tots i cada un d'ells, els que hi son i els que ja han marxat però que sempre s'han preocupat tant per mi, per com em van les coses i que m'han recolzat en totes les meves decisions. Els que sempre han estat i sé que sempre estaran al meu costat passi el que passi. Especialment als meus pares que han fet grans esforços perquè jo sigui on soc ara i que han tingut la paciència d'educar-me per arribar-hi. I al meu germà li he d'agrair com li treu ferro als meus suposats problemes, com m'ajuda a deixar d'ofuscar-me per les coses que no tenen solució i com em fa riure en tot moment. Gràcies per fer-me veure les coses des d'un altre punt de vista quan ho necessito.

Iaia, ho he aconseguit, he acabat el llibre.

Moltes gràcies a tots,

CRIS

Aquesta tesis ha sigut possible gràcies al projecte europeu del 7º programa marco RECATABI y el pressupost del IQS per al laboratori d'Enginyeria de Teixits.

SUMMARY

The irreversible necrosis of heart muscle (myocardial infarction, MI) occurs when ischemia exceeds a critical threshold and overwhelms myocardial cellular repair mechanisms. After MI, myocardial tissue lacks the ability to significantly regenerate itself and as a consequence, ischemia might cause moderate or severe tissue death. Tissue Engineering is an emerging interdisciplinary field focused on the obtaining of three-dimensional (3D) constructs with two different purposes: provide a set of biomedical tools with potential applicability in tissue replacement, repair and regeneration; or enable the *in vitro* study of cardiac human physiology and physiopathology more accurately. In this work, we have developed and analyzed a 3D *in vitro* model based on RAD16-I self-assembling peptide and a bioactive implant for cardiac tissue repair in the framework of RECATABI European Project.

3D models can help us to study the biophysical, biomechanical and biochemical parameters that regulate cell differentiation. In this thesis, we have developed a 3D *in vitro* model to analyze the behavior of subcutaneous adipose derived progenitor cells (subATDPCs) in terms of viability, growth, and gene expression, under different stimuli. Moreover, a novel and simple method to study the effect of electrical stimulus on cells growing in the 3D model has been achieved. The goal of these *in vitro* models is to better understand the behavior that these cells could have after their *in vivo* implantation with the hope to improve their performance in terms of regeneration or repair of the infarcted tissue.

Stem cells have been previously proposed to be grafted into the infarcted area to contribute to the generation of new myocardial tissue. We hypothesize that this mechanism could be enhanced by the application of a bioactive implant that could maintain the cells in the implanted site, afford the mechanical heart behavior and, at the same time, provide to the implanted cells a proper microenvironment. Therefore, we have prepared a composite obtained from the combination of RAD16-I included within microporous of elastomeric membranes. The goal of the present study is to evaluate cell survival and growth, seeding capacity and gene expression of subATDPCs in the new synthetic composite scaffold platform. We have described the development and characterization of bioimplants based on two different elastomeric membranes: poly(ethyl acrylate) (PEA), and poly(caprolactone 2-(methacryloyloxy)ethyl ester, (PCLMA). Both biomaterials are a good support for cell delivery and elastic enough to withstand the stresses arising from the heartbeat. Additionally, the developed composites equally facilitated the propagation of electrical pulses and maintained subATDPCs gene expression. We have proposed that the bioactive implants (elastomeric membranes with self-assembling peptide, and subcutaneous adipose tissue derived progenitor cells) could increase the efficacy of future cardiac cell therapy by improving cell immobilization and survival at the affected site.

RESUMEN

La necrosis irreversible del músculo cardíaco se conoce como infarto de miocardio (MI) y se da cuando la isquemia supera el umbral crítico y rebasa los mecanismos celulares de reparación. Después de un MI, el tejido cardíaco no tiene la capacidad suficiente de autoregeneración y como consecuencia, la isquemia puede causar la muerte, moderada o severa, del tejido. La ingeniería de tejidos es un campo emergente interdisciplinar enfocado a obtener cultivos tridimensionales (3D) con dos propósitos distintos: aportar herramientas biomédicas con potencial aplicación en la substitución, reparación y regeneración del tejido; o permitir el estudio *in vitro* de la fisiología y la patofisiología de manera más precisa. En la presente tesis se ha desarrollado y analizado un modelo *in vitro* 3D basado en el péptido autoensamblable RAD16-I y un implante bioactivo para la reparación del tejido cardíaco dentro del marco del proyecto europeo RECATABI.

Los modelos 3D pueden ayudarnos a estudiar los parámetros biofísicos, biomecánicos y bioquímicos que regulan la diferenciación celular. En esta tesis, hemos desarrollado un modelo 3D para analizar el comportamiento de células progenitoras derivadas de tejidos adiposo subcutáneo (subATDPCs) en términos de viabilidad, crecimiento y expresión génica, bajo la influencia de diferentes estímulos. Por otro lado, se ha desarrollado un método simple y novedoso para el estudio del efecto de un estímulo eléctrico en células encapsuladas en el modelo 3D. El objetivo final de este modelo *in vitro* es entender mejor el comportamiento que estas pueden tener células *in vivo* después de su implantación. De esta manera se espera poder mejorar su actuación en términos de regeneración o reparación del tejido infartado.

Se ha propuesto con anterioridad que el injerto de células progenitoras en el área infartada puede contribuir en la generación de un nuevo tejido de miocardio. Nuestra hipótesis se basa en que este mecanismo puede ser mejorado con la aplicación de un implante bioactivo que pueda mantener las células en la localización de implantación, soportar el comportamiento mecánico del corazón y a la vez proporcionar un microambiente adecuado a las células implantadas. Con estos objetivos se preparó un material combinado consistente en la inclusión del RAD16-I dentro de los microporos de membranas elastoméricas. El objetivo de este estudio es evaluar la capacidad de siembra de esta plataforma y la supervivencia, crecimiento y expresión génica de las subATDPCs. Se describe el desarrollo y caracterización de bioimplantes basados en dos membranas elastoméricas: poli etil acrilato (PEA) y policaprolactona 2-metacriloxiloxi etil ester (PCLMA). Ambas son buenos materiales de soporte para la implantación de células y también son suficientemente elásticas para soportar los esfuerzos resultantes del latido del corazón. Se ha observado que los dos materiales compuestos facilitan la propagación de los impulsos eléctricos y permiten el mantenimiento de la expresión génica de las subATDPCs. Se propone que los implantes bioactivos (membranas elastomérica con péptido autoensamblable y subATDPCs) pueden mejorar la eficacia de futuras terapias celulares, aumentando la inmovilización y supervivencia de las células en el área afectada.

RESUM

La necrosi irreversible del múscul cardíac es coneix com infart de miocardi (MI) i es dóna quan la isquèmia supera el llindar crític y depassa els mecanismes cel·lulars de reparació. Després d'un MI, el teixit cardíac no té la capacitat suficient d'autoregeneració i com a conseqüència, la isquèmia pot causar la mort, moderada o severa, del teixit. L'enginyeria de teixits és un camp emergent interdisciplinari enfocat a l'obtenció de cultius tridimensionals (3D) emprats per a dos propòsits diferents: aportar eines biomèdiques amb potencial aplicació en la substitució, reparació i regeneració del teixit; o permetre l'estudi *in vitro* de la fisiologia i la fisiopatologia de manera més precisa. En aquesta tesi s'ha desenvolupat i analitzat un model 3D *in vitro* basat en el pèptid autoensamblant RAD16-I, i un implant bioactiu per a la reparació del teixit cardíac dins del marc del projecte europeu RECATABI.

Els models 3D poden ajudar-nos a estudiar els paràmetres biofísics, biomecànics i bioquímics que regulen la diferenciació cel·lular. En la present tesis, s'ha desenvolupat un model 3D per analitzar el comportament de cèl·lules progenitores derivades de teixit adipós subcutani (subATDPCs) en termes de viabilitat, creixement i expressió gènica, sota la influència de diferents estímuls. Per una altra banda, s'ha desenvolupat un mètode simple i innovador per a l'estudi de l'efecte de l'estímul elèctric en cèl·lules cultivades en el model 3D proposat. L'objectiu final d'aquest model *in vitro* és entendre millor el comportament que poden tenir aquestes cèl·lules *in vivo* després de ser implantades. D'aquesta manera s'espera poder millorar la seva actuació en la regeneració o reparació del teixit infartat.

S'ha proposat amb anterioritat que l'empelt de cèl·lules progenitores en l'àrea afectada pot contribuir en la generació d'un nou teixit de miocardi. La nostra hipòtesi es basa en que aquest mecanisme es pot millorar amb l'aplicació d'un implant bioactiu que pugui mantenir les cèl·lules en la localització d'implantació, suportar el comportament mecànic del cor i a la vegada proporcionar un micoambient adequat per a les cèl·lules implantades. Amb aquest objectius, es va preparar un material combinant consistent en la inclusió del RAD16-I dins dels microporus de membranes elastomèriques. L'objectiu d'aquest estudi és avaluar la capacitat de sembra d'aquesta plataforma i la supervivència, creixement i expressió gènica de les subATDPCs en el material combinat. Es descriu el desenvolupament i caracterització de bioimplants basats en dues membranes elastomèriques: polietilacrilat (PEA) i policaprolactona 2-metacriloxiloxi etil ester (PCLMA). Ambdues són bons materials de suport i també són suficientment elàstiques per a suportar els esforços resultants del batec del cor. A més, ambdós materials compostos faciliten la propagació dels impulsos elèctrics i permeten el manteniment d'expressió gènica de les subATDPCs. Es proposa doncs que els implants bioactius (membranes elastomèriques amb pèptid autoensamblant i subATDPCs) poden millorar l'eficàcia de futures teràpies cel·lulars augmentant la immobilització i supervivència de les cèl·lules en l'àrea afectada.

TABLE OF CONTENTS

LIST OF FIGURES

CHAPTER 3

CHAPTER 4

LIST OF TABLES

LIST OF ABREVIATIONS[i]

A – Alanine

Aa 2P– Ascorbic acid 2-phosphate

ACTN1 – alpha actinin 1protein

ACTN1 – alpha actinin 1 gene

ADSC – Adipose derived stem cell

ATDPCs – Adipose Tissue Derived Progenitor Cells

Ao - Aorta

ASCs – Adult Stem Cells

ATMPs – Advanced-therapy medicinal products

AV – Atrioventricular

BM-MSCs – Bone marrow mesenchymal stem cells

BMP-2 – Bone Morphogenic Protein 2

BMP-4 – Bone Morphogenic Protein 4

BM-MNCs – Bone marrow mononucleated cells

BSA – Bovine serum albumine

CABG – Coronary Artery Bypass Grafting

CD – Circular Dichroism

cDNA – complementary deoxyribonucleic acid

CHD – Coronary Heart Disease

CLMA – Caprolactone methacryloxyl ethyl ester

CMs – Cardiomyocytes

CMV - Cytomegalovirus

CSCs – Cardiac Stem Cells

CTE – Cardiac Tissue Engineering

cTnI – cardiac Troponin I

cTnT – cardiac Troponin T

CVD – CardioVascular Disease

Cx43 – Connexin 43

D – Aspartic Acid

DAPI - 2-(4-Amidinophenyl)-6-indolecarbamidine dihydrochloride

DMA – Dynamic Mechanical Analysis

DMSO – Dimethyl sulfoxide

DNA – Deoxyribonucleic acid

dNTPs – deoxynucleotide thriphosphates

D&P staining – DAPI and Phalloidin staining

DV – Diastolic Volume

E – Glutamic Acid

E – Young modulus

EA – Ethyl acrylate

ECM – Extracellular Matrix

EF – Ejection fraction

EHT – Engineered Heart Tissues

eGFP – Enhanced green fluorescent protein

ES – Electrical Stimulation

ESCs – Embryonic Stem Cells

EtBr – Ethidium homodimer-1 bromide

EWC – Equilibrium water content

FAT – Fatty Acid Traslocase

FBS – Fetal Bovine Serum

FGF – Fibroblast Growth Factor

FITC-dextran - fluorescein isothiocyanate-dextran

G – Glycine

G' – Storage Modulus

GATA4 – GATA binding protein 4

GATA4 - GATA4 gene

GF – Growth Factor

GJA1 – Gap junction protein, alpha 1

GJA1 – GJA1 gene

GCP – Good clinical practice

GLP – Good laboratory practice

GMP – Good manufacturing practice

hcTnIp – human cardiac Troponin I promoter

hNDF – human normal dermal fibroblasts

HS – Horse Serum

hUVECs – human Umbilical Vein Endothelial Cells

ICREC – Insuficiéncia Cardíaca REgeneració Cardíaca group

IGF-I – Insulin Growth Factor I

IGTP - Institute Germans Trias i Pujol

IMDM – Iscove's Modified Dulbecco's Medium

iPSCs – Induced Pluripotent Stem Cells

ISL1 – Insulin Gene Enhancer protein

ISL1 – Insulin Gene Enhancer gene

ISSCR – International Society for Stem Cell Research

ITS – Insulin-Transferrin-Selenium

K - Lysine

LA – Left Atrium

LAD – Left anterior descending

LV – Left Ventricle, Left Ventricular

LVEF - Left ventricular ejection fraction

L&D assay – Live and Dead assay

MAGNUM – Myocardia Assistance by Grafting a New bioartificial Upgraded Myocaridum

MC3T3 – cells of mouse calvaria

MEFs – Mouse Embryonic Fibroblasts

MEF2C – Myocyte Enhancer Factor-2 Polypeptide-C

MEF2C – MEF2C gene

MEF2 – MADS box transcription enhancer factor 2

mESC – Mouse Embryonic Stem Cell

MHC – Myosin Heavy Chain

MI – Myocardial Infarction

MMP - Metalloproteases

MSC – Mesenchymal Stem Cell

MTT – [(3-(4,5-dimethylthiazol-2-yl)2,5-diphenyltatrazolium bromide]

NAD(P)H – Nicotinamide Adenine Dinucleotide Phosphate

NCBI – National Center for Biotechnology Information

NKX2.5 – NK2 Transcription Factor Related Locus-5

NKX2.5 – NKX2.5 gene

no ES – without electro-stimulation

NSF – National Science Foundation

NWs – Nanowires

OCT – Optimal cutting temperature

PA – Pulmonary Artery

PB – Phosphate buffer

PBSA – Phosphate buffer saline with BSA

PBST – Phosphate buffer saline

PBST – Phosphate buffer saline 0.1 % Tween

PCI – Percutaneous Coronary Intervention

PDGF – Platelet-Derived Growth Factor

PEA - poly(ethyl acrylate)

PEA/PHEA (90:10) – copolymer of poly(ethyl acrylate) and poly (hydroxyl ethyl acrylate) (PEA/PHEA) in a blending ratio of 90:10

PED – Poly(aliphatic/aromatic-ester)

PEG – Polyethylene glycol

PEUU – Poly(ester urethane urea)

PFA – Paraformaldehyde

PGs - Proteogycans

PGA – Polyglycolic acid

PGS – Poly(glycerol sebacate)

PLA – Polylactic acid

PLCA – Poly(L-lactic acid)-copoly-(3-caprolactone)

PLCL – Poly(L-lactic acid)-co-poly-(3-caprolactone)

PLGA – Poly(D,L-lactic-co-glycolic acid)

PLuc – Promoter-less luciferase

PMMA – poly(methyl methacrylate)

POC – Poly(1,8-octanediol-co-citrate)

P/S – Penicillin/Streptomicin

PVDF – Polyvinylidene fluoride

qRT-CPR – quantitative reverse transcriptase polymerase chain reaction

R - Arginine

RA – Right Atrium

Ra – Retinoic acid

RAD16-I – RAD16-I self-assembling peptide

RAD16-I/RADRGD – RAD16-I self-assembling peptide combined with RAD16-I self-assembling peptide containing RGD motifs

RAD16-I+Hep – RAD16-I peptide-heparin composite

RADRGD – RAD16-I self-assembling peptide containing RGD motifs

RECATABI – REgeneration of CArdiac Tissue Assisted by Bioactive Implant

RGD – Arginine-Glycine-Aspartic acid adhesion motif

RLuc – Renilla luciferase

RFP – Red fluorescent protein

RNA – Ribonucleic acid

RT-PCR – Reverse Transcriptase polymerase chain reaction

RV – Right Ventricle

RM – Regenerative Medicine

SA – Sinoatrial

SAP – Self-assembling Peptide

SC – Stem cell

SCID – Severe combined immunodeficiency

SEM – Scanning electron microscopy

SERCA2 – Sarcoplasmic/Endoplasmic Reticulum Calcium ATPase 2

SERCA2 – SERCA2 gene

subATDPCs – subcutaneous adipose tissue-derived stem cells

T - Temperature

TBX5 – T-box transcription factor 5

TBX5 – TBX5 gene

TE – Tissue Engineering

TGF-β1 – Transformig Growth Factor Family β,1

TRITC - Tetramethylrhodamine

UPC – Universitat Politècnica de Catalunya

UPV - Universitat Politècnica de València

USD – United States Dollars

VC – Vena Cava

$VEGF_{165}$ – Vascular Endothelial Growth Factor 165

2D – Two-dimensional

3D – Three-dimensional

5-aza – 5-azacytidine

α-MEM – alpha Minimum Essential Media

π – Porosity

ρ – Electrical resistivity

[i] The nomenclature used in this thesis for gene and protein is based one HUGO Gene Nomenclature Committee guidelines. Gray KA, Daugherty LC, Gordon SM, Seal RL, Wright MW, Bruford EA. **genenames.org: the HGNC resources in 2013.** Nucleic Acids Res. 2013 Jan;41(Database issue):D545-52. doi: 10.1093/nar/gks1066. Epub 2012 Nov 17 PMID:23161694

PREFACE: Our inquisitiveness

Castells-Sala C, *et. al.* 2013 Current Applications of Tissue Engineering in Biomedicine *Biochips and Tissue Chips* 0–14 (REVIEW)

Overview

The aim of this section is to introduce the field in which all the work presented in the next chapters will be enclosed, the Tissue Engineering (TE) field. The investigation within this radically new concept for the treatment of disease and injury has increased during the last decades. It involves the use of molecular and cell biology technologies combined altogether with material science with the hope to promote mechanisms of tissue regeneration in situations where evolution has determined that adult humans no longer have this privilege[1]. In this brief introduction, I will present an abridged journey through the history describing the main players and their seminal discoveries that lead to the founding of the field.

A little of history

"The tails of lizards and of serpents, if they be cut off, will grow again"
Aristotle, History of Animals, Book II, Chap 17, 508b 4-7

Throughout history, the generation of artificial tissues, organs or even more complex organisms from simpler pieces has been deeply embedded in people's imagination and considered a myth or dream. There are many examples that reflect the human desire to be able to create, by themselves, living individuals or at least parts of them. Just 278 years AD, Fra Angelico painted "The Healing of Justinian" (Figure 1A, a), which illustrates the legend of St. Cosmas and St. Damien replacing an injured leg for a homograft onto a soldier. From the time of the ancient Romans, and until the 19th century, it was generally accepted that some life forms arose spontaneously from non-living matter (spontaneous generation). During the transition from the Middle Ages to the Renaissance in Europe, the hope and belief that living organisms could be generated by alchemy took Theophrastus von Hohenheim (Figure 1, d) to attempt the creation of human life by mixing chemical substances in a defined environment. Later on, as science and medicine progressed, the idea that life could be created by scientific means was represented in a multitude of stories, paintings and films. A remarkable example in literature and cinema is the history of Frankenstein (Figure 1A, b), which describes the vitalization of a creature reassembled from different body parts[2]. The creation of live from inert material was decisively dispelled during the 19th century by Louis Pasteur, who enlarges the work performed by investigators such as Francesco Redi and Lazzaro Spallanzani. Finally, advances in germ theory[I] and cell theory[II] definitely displaced the ideas of spontaneous generation[3].

[I]GERM THEORY (Girolmo Fracastoro): States that certain diseases are caused by microorganisms. Proposed in the mid-16th century and gained widespread credence when sustained by scientific discoveries of the 17th and late 19th century.

[II] CELL THEORY (Matthias Schleiden and Theodor Schwamm). States that: (1) all living organsims are composed of one or more cells, (2) the cell is the more basic unit of life, and (3) all cells arise from pre-existing living cells

The creative and curious nature of humans, along with our endless imagination are the engines that push us to envision beyond the limits of science; rationality and progress then, take those dreams into reality.

A determined observation of nature shows a high diversity of organisms capable of growing new parts of their bodies with the aim to replace those that are damaged (Figure 1B).

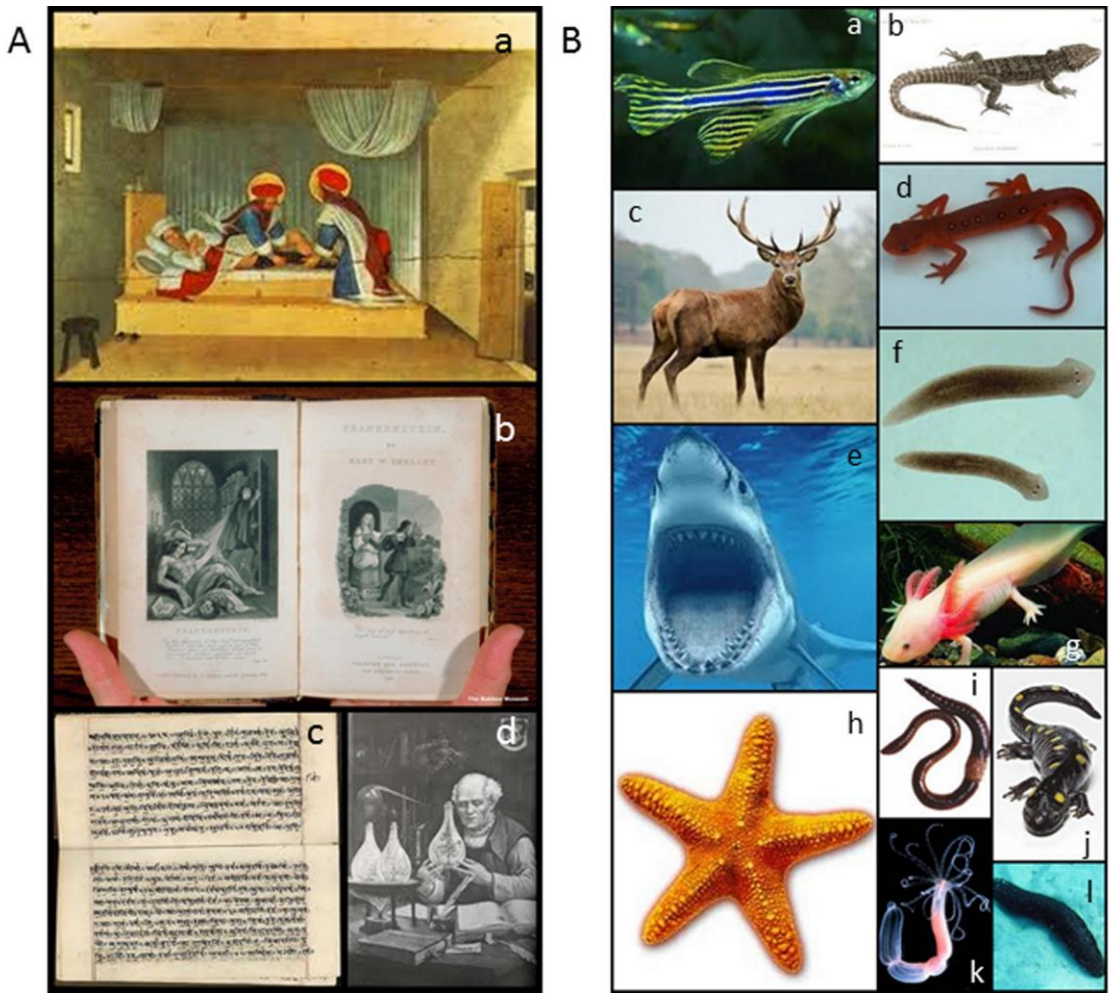

Figure 1: The origin and inspiration of Tissue Engineering. *(A) Remarkable artistic references of the desire to create:* (a) "Healing of Justinian" Fra Angelico (1455, Roma), (b) Frankenstein by Mary Shelley (1818, London), (c) Sanskrit text (3000-2500 BC, India) and (d) Theophrastus von Hohenheim (1493-1541, German-Swiss alchemist and physician) *(B) Nature inspiration. Important examples of organisms capable to regenerate*: (a) Zebrafish (b) Lizard (c) Deer Antler (d) Newt (e) Shark teeth (f) Planarian (g) Axolotl (h) Starfish (i) Annelid (j) Spotted salamander (k) Hydra (l) Sea cucumber.

Regeneration can be defined as the process of renewal, restoration, and growth that makes genomes, cells, organisms, and ecosystems resilient to natural fluctuations or events that cause disturbance or damage[4]. It is a fundamental attribute of all living organism and can be complete, when the new tissue results the same as the lost one, or incomplete when it takes place healing by fibrosis (e.g. scar formation). Complete tissue regeneration occurs through the activation of developmental processes to restore the missing or damaged structures. It has long been observed that, even though there is a great diversity in the regeneration ability among different animals,

many of the developmental molecules are shared by organisms as different as hydras and humans. This suggests that the underlying molecular machinery is probably the same. These facts have drawn the attention to the study of animal regeneration. Apart from being a fascinating biological issue, the acquired knowledge on how regeneration takes place naturally can provide very important insights into the creation of new functional tissues for eventual medical use[4]. The idea is to recreate *in vitro* the biological, biophysical and biomechanical conditions that occur in regeneration environments to draw out the intrinsic ability of differentiated cells to develop a tissue-like structure[5].

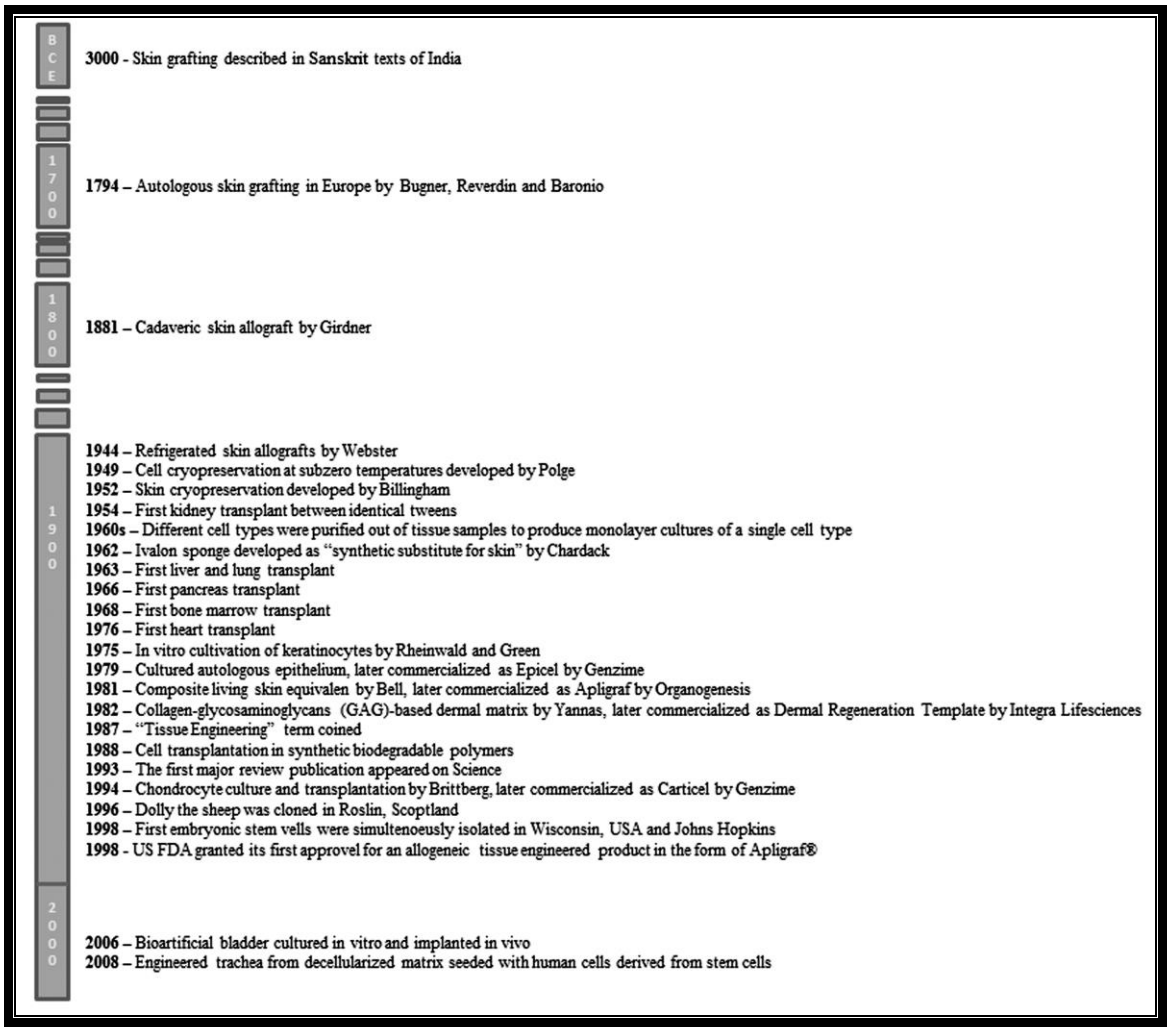

Figure 2: Important outcomes in the field of Tissue Engineering.

In terms of scientific progress, the first tissue-based therapies were skin grafting techniques performed by Hindus in 3000-2500 BC, which were documented in Sanskrit texts (Figure 1A, c). More recently, in 1794 the first autologous skin grafting was reported, and almost 100 years later the first cadaveric skin allograft was prepared. During the 20th century TE and regenerative medicine have advanced, grown and developed by leaps and bounds. Between 1954 and 1976 transplantations of kidney, liver, lung, pancreas, bone marrow, and heart were achieved. At

cellular level, cryopreservation at subzero temperatures was developed in 1949 and 10 years later, the purification of different cell types to produce monolayer cultures of single cell types was accomplished. Also during this century the production of synthetic substitutes was gradually developed. Additionally, several tissue-engineered skin and subsequently cartilage products were successfully commercialized[6] (see Figure 2).

Tissue Engineering

" *Tissue Engineering is the application of the principles and methods of engineering and life sciences toward the fundamental understanding of structure-function relationships in normal and pathologic mammalian tissue and the development of biological substitutes to restore, maintain, or improve function*".
National Science Foundation (NSF) – 1987

After its official definition in 1987 by NSF, the field of TE becomes a rapidly growing scientific area mainly focused on the development of tissue and organs substitutes, but also a useful tool for the obtaining of *in vitro* models (see Figure 3).

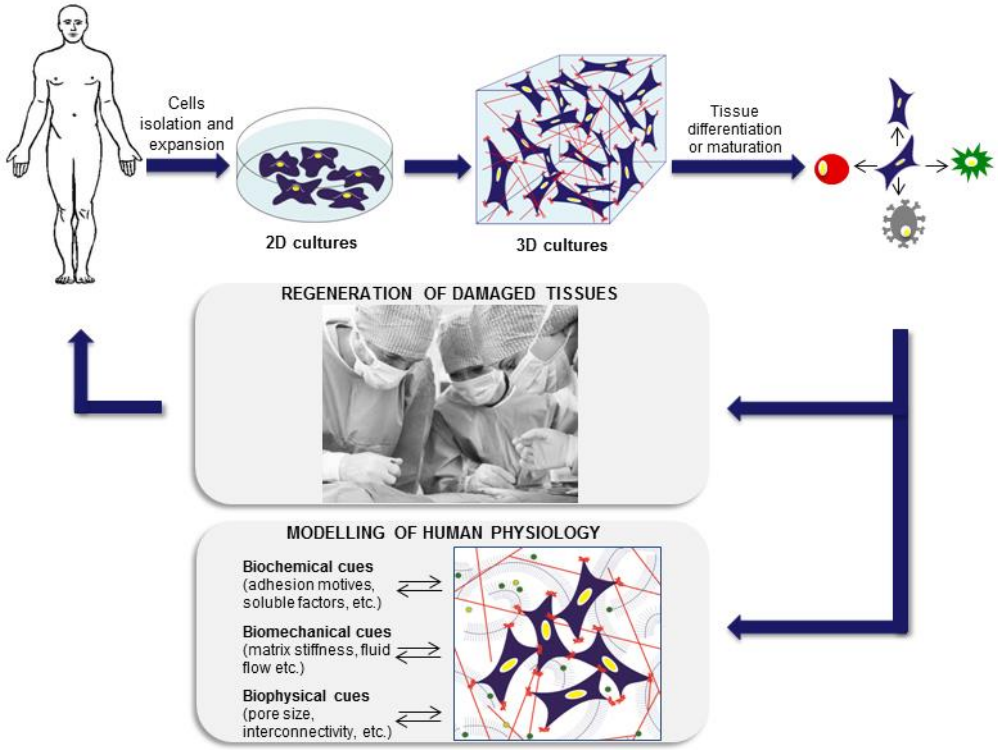

Figure 3: Tissue Engineering principles. Cells are isolated from human or animal sources and expanded on two-dimensional cultures. Next, cells are embedded in an extracellular matrix analogue (scaffold), which facilitates proper cellular organization. This engineered tissue is implanted in the patient to promote regeneration of damaged tissue. Alternatively, it can be used *in vitro* to study human physiology and pathophysiology more accurately than with two-dimensional cultures. Castells-Sala *et. al.* 2013.

It is well known that biological tissues consist of cells, extracellular matrix (ECM) and signaling systems. The combination of these three components plays a crucial role in the differential activation of genes or cascades of genes responsible for signaling tissue building and differentiation[7]. By learning from nature, TE uses combinations of cells, scaffolds and/or

biologically active molecules to develop the desired substitute. In most cases a three-dimensional (3D) construct is produced allowing the control of biological, biophysical and/or biomechanical parameters in the laboratory[8]. Not surprisingly, TE is an interdisciplinary field that brings together specialists from as different areas as cell and developmental biology, basic medical and veterinary sciences, biophysics and biomechanics, transplantation science, biomaterials and biomechanical engineering.

The obtained 3D constructs are used for two purposes, each one independently useful, yet related between one another:

Provide a set of biomedical tools with potential applicability in tissue replacement, repair, and regeneration

Yearly, millions of people suffer tissue loss or end-stage organ failure, and it is one of the most frequent, devastating, and costly problems for healthcare nowadays. Current treatments are associated with transplants, mechanical devices, surgical reconstructions or supplementation of metabolic products. Although these therapies have saved and improved countless patient lives, they still present associated problems[9]:

- Organ transplants show important limitations such as transplant rejection and lack of donors to cover the worldwide demand.
- Mechanical devices are not capable of accomplishing all tissue functions and cannot prevent progressive deterioration or be compatible with tissue/organ growth.
- Surgical reconstruction can result in long-term difficulties since the organs used for the replacement consist of different tissue and cannot properly function in the new environment.
- The supplementation of metabolic products does not solve the lack of physiological feedback mechanisms, which may lead to acute or long-term complications.

Therefore, TE arises from the need to provide more definitive solutions to tissue repair in clinic. This is achieved by the development of *in vitro* devices that could repair the damaged tissue *in vivo*[10].

Enable the in vitro study of human physiology and physiopathology more accurately

Knowledge of human physiology and physiopathology is of great interest for medicine professionals in order to find the best procedure when a particular health problem is faced. Unfortunately, the complexity of the human body makes it difficult to analyze each factor separately. To solve these issues, TE uses 3D constructs, which allow the study of human physiology and physiopathology *in vitro*[8,11].

In vitro human models help to identify and comprehend the factors that drive cellular processes. In particular, the idea is to deconstruct the complex cellular microenvironment into simpler systems in order to analyze the role of different chemical, mechanical and/or physical factors. In fact, these models fulfill the need for reductionist approaches to understand the *in vivo* molecular mechanisms, which rule human physiological as well as pathological processes and in turn, better predict the effect of drugs and medical therapies. A lot of research is focused on the study of different disorders such as arrhythmia[12], skin fibrosis[13] and wound healing[14,15], and the comprehension of the biological function and development of healthy organs such as skin[16–19], blood-brain barrier[20], and mammary gland[10,21].

Tissue Engineering components

TE involves three basic elements: cells, scaffolds and biomolecules. It is necessary to carefully choose which combination better fits the desired application. The mix of the three elements produces a very complex structure, while simpler than *in vivo*, it is still very challenging to design properly. To fully understand the parts that make up these structures the individual blocks are described here shortly:

Cells

It has been demonstrated that the use of living cells results in a higher degree of tissue function than the use of chemotactic agents, growth factors (GFs) or hormones to stimulate development. Cells are able to create or recreate functional structures using pre-programmed information and signaling. Today, there are still much needs to be learned in regard to their behavior for the creation of body structures before its medical use can become a reality[7].

Some TE approaches are focused on a guided regeneration of tissue using materials that serve as templates for ingrowth of host cells and tissues, while others implant cells as a part of the engineered device. One of the most important issues is the selection of the cell source depending on the final application. This step becomes critical, especially when the strategies mentioned above are designed to be clinically applied. In general, cells should fulfill a basic requirement: to be integrated in the specific tissue and segregate GFs and cytokines that activate the endogenous tissue regeneration program. The first approach in cell-based techniques is the use of native resident cells (progenitor and/or functional); unfortunately, some specific cell types are difficult to obtain and grow in large amounts *in vitro*. As a consequence stem cells have emerged as a promising alternative[22].

Stem cells are unspecialized cells that maintain the ability to preserve developmental potential and are capable of renewing themselves through mitotic cell division. They are able to undergo a diverse range of cell specialization through a process called differentiation, which is induced

by certain physiologic or experimental conditions. Intrinsic factors of the cells (signals inside the cells, gene expression) as well as extrinsic ones (signals from outside, chemicals, physical contact and certain molecules) that trigger each stem cell undergo differentiation are just beginning to be understood. Nevertheless, it is known that the action of these signals causes the DNA to acquire concrete epigenetic marks that can be passed on through cell division, and direct the specific genes to be expressed and transcribed at protein level for each cell type[23].

Stem cells can be divided into two big groups: Embryonic Stem Cells (ESCs) and Adult Stem Cells (ASCs). ESCs are pluripotent cells that are able to differentiate into any lineage while ASCs are multipotent. Although ESCs have higher capacity to differentiate than ASCs, their use is highly restricted due to ethical controversies and their potential to produce teratomas. As a consequence, ASCs seem to be more appropriate for TE[24,25]. For instance, ASCs and tissues derived from them are currently believed to be less likely to initiate rejection after transplantation[26]. Research on ASCs is progressing rapidly and up today, they have been isolated from different tissues including bone marrow[27], muscle and adipose tissue[28], and umbilical cord[29,30].

There is still much work to be done in order to understand stem cells capabilities, but their unique regenerative abilities can offer new insights into the TE field. Therefore, one of the challenges the scientific community has to cope with is to understand the principles of cell biology to apply the knowledge with the aim to obtain better tissue or organ substitutes.

Concurrently, it is also important to develop techniques to maintain alive the large masses of cells needed both *in vitro* and *in vivo.* In this aspect enormous challenge in which significant advances have already been made is still under development. For example *in vitro* flow bioreactors for maintenance of cell mass have improved during the recent years.

Although this work will be mainly focused on the use of ASCs, it is important to briefly mention induced pluripotent stem cells (iPSCs). This type of cells were presented in the scientific community by Yamanaka and collaborators in 2006[31,32]. Basically, iPSCs are somatic cells that have been reprogrammed to a pluripotent state through the introduction of a defined set of transcription factors. The main advantages of these cells are their autologous character, their differentiation capacity and the robustness and simplicity of the reprogramming procedure. However, there are several barriers to overcome before extensively using iPSCs in TE. Specifically, the molecular mechanisms underlying reprogramming should be precisely characterized before its use in clinical applications[33,34].

Scaffolds

The second major goal of TE field is the design of scaffolds able to recreate the *in vivo* milieu of cells, which is mainly provided by the ECM. Due to the huge diversity of TE potential applications, the task to develop a biomaterial to be used as cell scaffold results to be quite arduous. The designed material can be permanent or biodegradable, natural, synthetic or hybrid and need to be compatible with the living system *in vitro* and *in vivo*. Moreover, these structures should incorporate the appropriate biophysical, biomechanical and biochemical cues that guide cell proliferation, differentiation, maintenance, and function[35]. The difficulty lies in the fact that each design should focus in the specific considered therapy and therefore different scaffolds with different properties need to be delineated.

Regarding biophysical signaling, an essential function of the ECM is to give anchorage and mechanical signaling to cells. For this reason, the understanding of the interface between the cells and the implant site is an important assessment for the optimization of the scaffold. Interestingly, the ECM highly porous nanostructure provides the cells a proper 3D microenvironment and imparts biochemical signaling through two mechanisms: (*i*) the binding of a wide variety of soluble GFs, enzymes and other effector molecules controlling their diffusion and local concentrations and (*ii*) the exposure of specific motifs that are recognized by cellular adhesion receptors. As a result, ECM is dynamically integrated with the intracellular signaling pathways regulating gene expression and participating in cell phenotype determination[36–39]. Additionally, the cells are able to sense the matrix stiffness, which also results in mechanical signaling. Cells routinely contract to pull on the milieu where they are attached, generating internal tension. This mechanical stimulus is translated into a chemical response through a process known as mechanotransduction, which has been reported to directly influence cell function (e.g. proliferation, differentiation, maintenance, survival)[40–42]. Due to the complexity and interaction among all these cues, TE focuses on mimicking the most relevant ECM properties to develop custom-tailored scaffolds depending on the tissue to be recreated[36,43,44]. Specifically, parameters as scaffold pore size, chemical signaling motifs and stiffness should be carefully examined.

Besides particular parameters, an ideal biomaterial designed for clinical applications should fulfill a serial of requirements. First of all, biocompatibility and biodegradability are required to allow scaffold replacement by proteins synthesized and secreted by native or implanted cells[44–46]. Additionally, the material must be clinically compliant (that means, covering Good Manufacturing Practice standards, GMP) to minimize inflammatory and immunological response avoiding further tissue damage[44]. Moreover, since cell degradation products are toxic to other cells, it would be important for the material to allow host macrophages to infiltrate and

remove cellular debris[47]. Finally, material production, purification and processing should be easy and scalable[35,48].

Scaffolds for TE can be divided in natural and synthetic, depending on their origin. Natural scaffolds are readily accessible and provide a broad range of cues that during an *in vivo* assay participate in the process of morphogenesis and function acquisition of different cell types. However, its composition strongly depends on the specific animal origin as well as on the isolation and purification procedures, compromising assay reproducibility[8,44]. On the other hand, synthetic scaffolds can be custom-tailored to mimic specific ECM properties, providing controllable cellular environments. Paradoxically, this advantage makes this class of biomaterials far more challenging because a wide range of factors needed to be identified and precisely incorporated. Indeed, unless the application of surface-modifications (adhesion of peptides or biological molecules), synthetic scaffolds only serve to hold and guide cells in a 3D space until they produce their own physiological matrix environment[8,47,49].

Biomolecules

Besides an appropriate scaffold and cell source, signaling molecules represent an interesting tool in TE to modulate several aspects of cell biology, from proliferation capacity to specific phenotypic features of fully differentiated cells[43,50,51]. In the cellular milieu, the presence and gradient of soluble factors such as GFs, chemokines and cytokines play an important role in biological phenomena such as chemotaxis, morphogenesis and wound healing. In particular, these signals are tightly controlled and unique to each organ and for this reason what happens to a cell depends on their location[7].

Signaling molecules used in TE can be added to the culture media as soluble factors or attached to the scaffold by means of covalent and non-covalent interactions. First of all, the direct delivery of these molecules into the media is frequently used to *in vitro* evaluate the effect of these cues. However, these biomolecules are rapidly degraded and deactivated by some cell-secreted enzymes, responsible for their short biological half-live. For this reason, for clinical application, the bounding of these factors to the matrix is highly extended with the aim to protect them from degradation[52]. Additionally, the controlled release of different factors from scaffolds allows their constant renewal, having a great potential to direct tissue regeneration and formation. Several matrix systems, microparticles and encapsulated cells have been reported to locally deliver bioactive factors and to maintain effective concentrations for their use in the application areas, such as musculoskeletal, neural and hepatic tissue[53–55].

.

BIBLIOGRAPHY

1. Williams, D. Benefit and risk in tissue engineering. *Mater. Today* **7,** 24–29 (2004).

2. Meyer, U. in *Fundam. Tissue Eng. Regen. Med.* 5–12 (2009).

3. Levine, R. & Evers, C. The Slow Death of Spontaneous Generation (1668-1859). *Natl. Heal. Museum* (1999).

4. Carlson, B. M. *Principles of Regenerative Biology*. (2011). at <http://books.google.es/books/about/Principles_of_Regenerative_Biology.html?id=f_Epd5lHTNkC&redir_esc=y>

5. Quintana, L. *et al.* Early Tissue Patterning Recreated by Mouse Embryonic Fibroblasts in a Three-Dimensional Environment. *Tissue Eng.* **15,** 45–54 (2009).

6. Berthiaume, F., Maguire, T. J. & Yarmush, M. L. Tissue engineering and regenerative medicine: history, progress, and challenges. *Annu. Rev. Chem. Biomol. Eng.* **2,** 403–30 (2011).

7. Lanza, R., Langer, R. & Vacanty, J. *Principles of Tissue Engineering*. (2000).

8. Griffith, L. G. & Swartz, M. A. Capturing complex 3D tissue physiology in vitro. *Nat. Rev. Mol. Cell Biol.* **7,** 211–24 (2006).

9. Lalan, B.a., S., Pomerantseva, M.D., I. & Vacanti, M.D., J. P. Tissue Engineering and Its Potential Impact on Surgery. *World J. Surg.* **25,** 1458–1466 (2001).

10. Castells-Sala, C. *et al.* Current Applications of Tissue Engineering in Biomedicine. *Biochips and Tissue Chips* 0–14 (2013). doi:10.4172/2153-0777.S2-004

11. Pampaloni, F., Reynaud, E. G. & Stelzer, E. H. K. The third dimension bridges the gap between cell culture and live tissue. *Nat. Rev. Mol. Cell Biol.* **8,** 839–45 (2007).

12. Thompson, S. a *et al.* Engraftment of human embryonic stem cell derived cardiomyocytes improves conduction in an arrhythmogenic in vitro model. *J. Mol. Cell. Cardiol.* **53,** 15–23 (2012).

13. Moulin, V. J. Chapter 19 Reconstitution of Skin Fibrosis Development Using a Tissue Engineering Approach. **961,** 287–303

14. Li, Y.-C., Chen, C.-R. & Young, T.-H. Pearl extract enhances the migratory ability of fibroblasts in a wound healing model. *Pharm. Biol.* **51,** 289–97 (2013).

15. Van den Broek, L. J., Niessen, F. B., Scheper, R. J. & Gibbs, S. Development, validation and testing of a human tissue engineered hypertrophic scar model. *ALTEX* **29,** 389–402 (2012).

16. Paquet, C. *et al.* Tissue engineering of skin and cornea: Development of new models for in vitro studies. *Ann. N. Y. Acad. Sci.* **1197,** 166–77 (2010).

17. Bellas, E., Seiberg, M., Garlick, J. & Kaplan, D. L. In vitro 3D full-thickness skin-equivalent tissue model using silk and collagen biomaterials. *Macromol. Biosci.* **12,** 1627–36 (2012).

18. Fernandez, T. L., Dawson, R. a, Van Lonkhuyzen, D. R., Kimlin, M. G. & Upton, Z. A tan in a test tube - in vitro models for investigating ultraviolet radiation-induced damage in skin. *Exp. Dermatol.* **21,** 404–10 (2012).

19. Krishnan, R. *et al.* Polysaccharide nanofibrous scaffolds as a model for in vitro skin tissue regeneration. *J. Mater. Sci. Mater. Med.* **23,** 1511–9 (2012).

20. Lippmann, E. S., Al-Ahmad, A., Palecek, S. P. & Shusta, E. V. Modeling the blood-brain barrier using stem cell sources. *Fluids Barriers CNS* **10,** 2 (2013).

21. Wang, X., Reagan, M. R. & Kaplan, D. L. Synthetic adipose tissue models for studying mammary gland development and breast tissue engineering. *J. Mammary Gland Biol. Neoplasia* **15,** 365–76 (2010).

22. Bernstein, H. S. & Srivastava, D. Stem cell therapy for cardiac disease. *Pediatr. Res.* **71,** 491–499 (2012).

23. Gereige, L.-M. & Mikkola, H. K. A. DNA methylation is guardian of stem cell self-renewal and multipotency. *Nature* **41,** 1164–1166 (2009).

24. Naderi, H., Matin, M. M. & Bahrami, A. R. Review paper: critical issues in tissue engineering: biomaterials, cell sources, angiogenesis, and drug delivery systems. *J. Biomater. Appl.* **26,** 383–417 (2011).

25. Semino, C. E. Can we build artificial stem cell compartments? *J. Biomed. Biotechnol.* **3,** 164–169 (2003).

26. [World Wide Web site]. Bethesda; MD: National Institutes of Health; U.S. Department of Health and Human Service. What are the similarities and differences between embryonic and adult stem cells?. In Stem Cell Information. at < <http://stemcells.nih.gov/info/basics/pages/basics5.aspx>>

27. Clifford, D. M. *et al.* Long-term effects of autologous bone marrow stem cell treatment in acute myocardial infarction: factors that may influence outcomes. *PLoS One* **7,** (2012).

28. Qayyum, A. A. *et al.* Adipose-derived mesenchymal stromal cells for chronic myocardial ischemia (MyStromalCell Trial): study design. *Regen. Med.* **7,** 421–8 (2012).

29. Weber, B., Zeisberger, S. M. & Hoerstrup, S. P. Prenatally harvested cells for cardiovascular tissue engineering: fabrication of autologous implants prior to birth. *Placenta* **32 Suppl 4,** S316–9 (2011).

30. Cortes-Morichetti, M. *et al.* Association between a cell-seeded collagen matrix and cellular cardiomyoplasty for myocardial support and regeneration. *Tissue Eng.* **13,** 2681–7 (2007).

31. Yu, J. *et al.* Induced pluripotent stem cell lines derived from human somatic cells. *Science (80-.).* **318,** 1917–20 (2007).

32. Takahashi, K. & Yamanaka, S. Induction of pluripotent stem cells from mouse embryonic and adult fibroblast cultures by defined factors. *Cell* **126,** 663–76 (2006).

33. Zhu, Z. & Huangfu, D. Human pluripotent stem cells: an emerging model in developmental biology. *Development* **140,** 705–17 (2013).

34. Nishikawa, S., Goldstein, R. A. & Nierras, C. R. The promise of human induced pluripotent stem cells for research and therapy. *Nat. Rev. Mol. Cell Biol.* **9,** 725–729 (2008).

35. Dutta, R. C. & Dutta, A. K. Cell-interactive 3D-scaffold; advances and applications. *Biotechnol. Adv.* **27,** 334–339 (2009).

36. Frantz, C., Stewart, K. M. & Weaver, V. M. The extracellular matrix at a glance. *J. Cell Sci.* **123,** 4195–200 (2010).

37. Lu, P., Weaver, V. M. & Werb, Z. The extracellular matrix: a dynamic niche in cancer progression. *J. Cell Biol.* **196,** 395–406 (2012).

38. Juliano, R. L., Haskill, S. & Carolina, N. Signal Transduction from the Extracellular Matrix. *J. Cell Biol.* **120,** 577–585 (1993).

39. Kim, S.-H., Turnbull, J. & Guimond, S. Extracellular matrix and cell signalling: the dynamic cooperation of integrin, proteoglycan and growth factor receptor. *J. Endocrinol.* **209,** 139–51 (2011).

40. Wozniak, M. a & Chen, C. S. Mechanotransduction in development: a growing role for contractility. *Nat. Rev. Mol. Cell Biol.* **10,** 34–43 (2009).

41. Samuel, M. S. *et al.* Actomyosin-mediated cellular tension drives increased tissue stiffness and β-catenin activation to induce epidermal hyperplasia and tumor growth. *Cancer Cell* **19,** 776–91 (2011).

42. Janmey, P. a & Miller, R. T. Mechanisms of mechanical signaling in development and disease. *J. Cell Sci.* **124,** 9–18 (2011).

43. Sant, S., Hancock, M., Donnelly, J., Iyer, D. & Khademhosseini, A. Biomimetic gradient hydrogels for tissue engineering. *Can J Chem Eng* **88,** 899–911 (2010).

44. Karam, J.-P., Muscari, C. & Montero-Menei, C. N. Combining adult stem cells and polymeric devices for tissue engineering in infarcted myocardium. *Biomaterials* **33,** 5683–5695 (2012).

45. Polak, D. J. Regenerative medicine. Opportunities and challenges: a brief overview. *J. R. Soc. Interface* **7 Suppl 6,** S777–81 (2010).

46. Atala, A. Regenerative medicine strategies. *J. Pediatr. Surg.* **47,** 17–28 (2012).

47. Fernandes, S., Kuklok, S., McGonigle, J., Reinecke, H. & Murry, C. E. Synthetic matrices to serve as niches for muscle cell transplantation. *Cells. Tissues. Organs* **195,** 48–59 (2012).

48. Holmes, T. C. *et al.* Extensive neurite outgrowth and active synapse formation on self-assembling peptide scaffolds. *Proc. Natl. Acad. Sci. U. S. A.* **97,** 6728–33 (2000).

49. Genové, E., Shen, C., Zhang, S. & Semino, C. E. The effect of functionalized self-assembling peptide scaffolds on human aortic endothelial cell function. *Biomaterials* **26,** 3341–3351 (2005).

50. Lee, S. Cytokine delivery and tissue engineering. *Yonsei Med. J.* **41,** 704–19 (2000).

51. Even-Ram, S. & Yamada, K. M. Cell migration in 3D matrix. *Curr. Opin. Cell Biol.* **17,** 524–32 (2005).

52. Tayalia, P. & Mooney, D. J. Controlled growth factor delivery for tissue engineering. *Adv. Mater.* **21,** 3269–85 (2009).

53. Babensee, J. E., McIntire, L. V & Mikos, A. G. Growth factor delivery for tissue engineering. *Pharm. Res.* **17,** 497–504 (2000).

54. Wozney, J. M. & Seeherman, H. J. Protein-based tissue engineering in bone and cartilage repair. *Curr. Opin. Biotechnol.* **15,** 392–8 (2004).

55. Sohier, J., Moroni, L., Van Blitterswijk, C., De Groot, K. & Bezemer, J. M. Critical factors in the design of growth factor releasing scaffolds for cartilage tissue engineering. *Expert Opin. Drug Deliv.* **5,** 543–566 (2008).

CHAPTER 1 – INTRODUCTION: Focusing interests

Castells-Sala C and Semino C E (2012) Biomaterials for stem cell culture and seeding for the generation and delivery of cardiac myocytes. *Curr. Opin. Organ Transplant.* 17 681–7. (REVIEW)

1.1 BACKGROUND

1.1.1 Overview

According to the World Health Organization, cardiovascular diseases (CVDs) are the number one cause of death worldwide. CVD is an overarching term that refers to a group of diseases involving the heart and blood vessels. An estimated 17.3 million people died from CVDs in 2008, representing 30 % of all global deaths, and this number is predicted to increase and reach 24 million people by 2030[1,2]. Over 80 % of these deaths take place in low- and middle-income countries and occur almost equally in men and women[2]. CVDs include coronary heart disease (CHD) (heart attacks)[i], cerebrovascular disease (stroke)[ii], hypertensive heart disease[iii], peripheral arterial disease[iv], aortic disease[v], rheumatic heart disease[vi], and congenital heart disease[vii]. Significantly, heart attacks and strokes account for nearly the 80 % of deaths as can be observed in Figure 1.1-1.

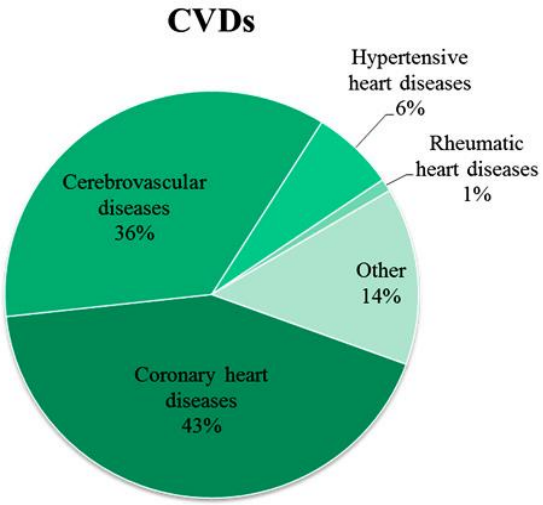

Figure 1.1-1: Cardiovascular diseases prevalence[3]**.** CVDs claim more lives than anything else, accounting for nearly one-third of deaths worldwide. Coronary heart disease results in the most fatal cardiovascular disorder. Data recorded from World Health Organization.

In 2010, the global cost of CVDs was estimated at USD 863 billion (an average per capita cost of USD 125), and it was estimated to rise to USD 1,044 billion in 2030[4]. About 80 % of coronary heart and cardiovascular cases are directly caused by behavior risk factors, including unhealthy diet, obesity, physical inactivity, tobacco, and harmful use of alcohol[2]. Therefore, the corrections of life habits can reduce premature death, clinical events, and public costs. Reducing

[i] Coronary heart disease: Blocking of heart's blood supply.
[ii] Cerebrovascular disease: Disturbing of blood supply to the brain.
[iii] Hypertensive heart disease: Complications of systemic arterial hypertension or high blood pressure.
[iv] Peripheral arterial disease: Blockage in the arteries of the limbs (usually legs).
[v] Aortic disease: Weakening of aorta wall and formation of bulges outwards.
[vi] Rheumatic heart disease: damage to the heart muscle and heart valves due to rheumatic fever, caused by streptococcal bacteria.
[vii] Congenital heart disease: malformations of heart structure existing at birth.

the incidence through lifestyle changes can save thousands of dollars, but in any case it is crucial to develop new strategies to treat this family of diseases.

CVDs encompass different illnesses with a variety of casuistry, so it is essential to focus on specific ailments. In this work, we will direct our attempts to the latest complication of CHD: the narrowing of the blood vessels that supply blood and oxygen to the heart. The blocking of blood supply to the heart leads to different diseases such as angina, heart attacks, arrhythmias, and at the end stage heart failure. The subject of our study will be the heart tissue damage produced due to heart attack (medically known as myocardial infarction, MI).

Current therapies for the treatment of MI include percutaneous coronary intervention (PCI), coronary artery bypass grafting (CABG), *dynamic latissiumus dorsi* cardiomyoplasty, cardiac bio-assist mechanical support, and pharmacological intervention. These therapies are capable of increasing patients' life expectancy a few years after MI, reducing early mortality. Despite the improved medical care and acute management of MI, survivors are susceptible to an increased prevalence of chronic heart failure due to muscular tissue death, which develop scarring, followed by ventricular remodeling and dilatation[5]. The removal of damaged heart tissues by ventriculoplasty results in the loss of a substantial portion of nondiseased myocardium, so this treatment is suitable only for severe dilated cardiomyoplasty[6]. To avoid heart failure, the last and only available treatment option with good long-term results is heart transplantation. Unfortunately, this treatment is limited due to the lack of donors and complications associated with immunological response. In this context, the design of new strategies that maintain the structural support necessary for effective cardiomyocyte (CM) contraction is of high interest.

The need for new therapies has grown in parallel to the evidence that heart muscle is capable of regeneration through the activation of cardiac stem cells or recruitment of stem cells (SCs) from other tissues[7]. Although this regenerative capacity is not enough to compensate the large-scale tissue lost after MI, the concept has opened a new field in heart therapies: cell transplantation. The major aim of cellular therapy is the recovery of cardiac function in the infarcted heart by regenerating lost myocardial tissue as well as its associated vasculature[8]. Current treatments under study consist in cellular cardiomyoplasty, where cells are directly injected or encapsulated in scaffolds and grafted into ischemic ventricles wall. These strategies show beneficial effects but are not fully developed yet. The exact beneficial mechanism of cell therapy in ischemic heart disease is not yet fully understood but possible mechanisms involve paracrine secretion of growth factors (GFs) and cytokines, improving neovascularization and angiogenesis[9]

In this context, a small consortium (RECATABI) was created with the objective to obtain a novel clinical platform to regenerate necrotic ischemic tissues after MI with a simple patch technology application. The consortium aimed to achieve this goal by manofacturing nanoscale

engineered biomaterials and scaffolds that mimic as much as possible the biomechanical and biophysical requirements of the implanted tissue. To accomplish this objective, it was needed the close collaboration of an interdisciplinary group of experts. In particular, the consortium was formed by experts in areas such as material sciences, tissue engineering (TE), stem cell technologies, clinical cardiovascular research, and industry:

- Dr. Manuel Monleón-Pradas (Center for Biomaterials and Tissue Engineering, Universitat Politècnica de València (UPV), València, Spain)
- Dr. Antoni Bayés-Genís (Heart Failure and Cardiac Regeneration (ICREC) Research Program, Health Research Institute Germans Trias i Pujol (IGTP), Cardiology Service, Hospital Universitari Germans Trias i Pujol, Badalona, Spain)
- Dr. Alexander Deten (Fraunhofer institute for Cell Therapy & Immunology, Leipzig, Germany)
- Dr. Juan Carlos Chachques (Department of Cardiovascular Surgery, Pompidou Hospital, Paris, France)
- Franck Tricot (Creaspine SAS)
- Dr. Carlos E. Semino (Department of Bioengineering, IQS-School of Engineering, Ramon Llull University, Barcelona, Spain)

The present thesis is enclosed within RECATABI European project and specifically focused on the *in vitro* work developed in Dr. Semino's group. Chapter 2 and Chapter 3 describe the development of *in vitro* models for the characterization of cardiomyogenic potential of subATDPCs. On the other hand, Chapter 4 is focused on the assembling and analysis of a bioactive device for the treatment of ischemic tissue after MI. An overview of the most relevant results obtained during RECATABI project is also provided at the end of Chapter 4.

1.1.2 Heart physiology

The heart is a muscular organ, about the size of a fist, which lies in the center of the thoracic cavity encased in a double-walled membrane sac called the Pericardium[10,11]. Pericardium contains a layer of pericardial fluid that lubricates the external surface of the heart as it beats. The heart is responsible for pumping blood throughout arteries and veins supplying nutrients (picked up from the intestine) and oxygen (collected from the lungs) all over the body. Functionally, it is divided into left and right halves by a central wall (septum). Each half functions as an independent pump that consists of an atrium and a ventricle. These two pumps promote pulmonary circulation (flow within the lungs through the pulmonary vein) and systemic circulation (flow within the rest of the body through the aorta artery). A scheme is presented in Figure 1.1-2.

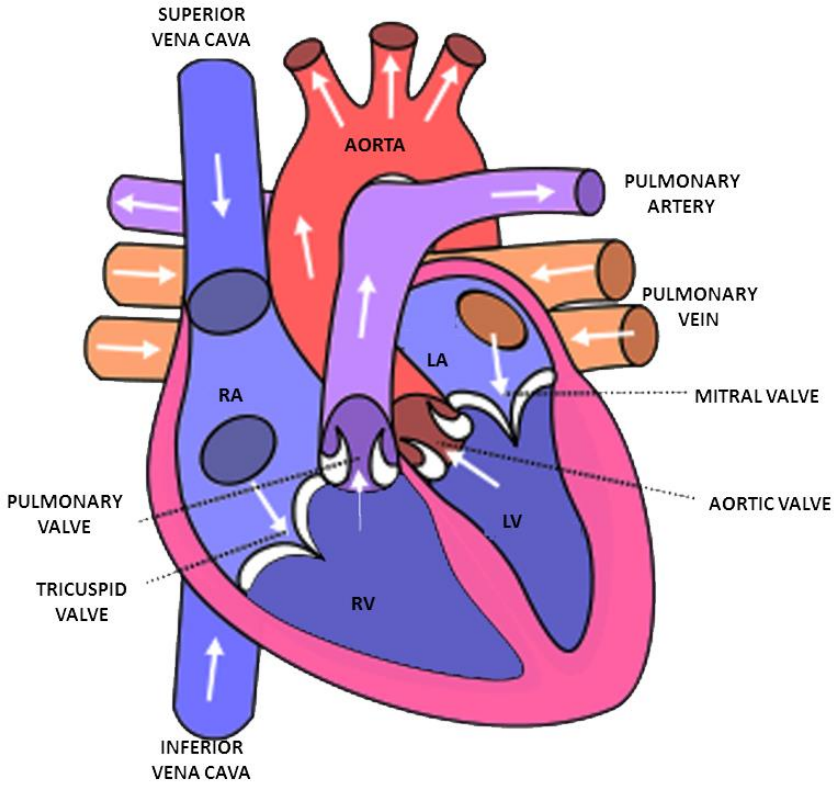

Figure 1.1-2: Cardiovascular system function[12]**.** Anterior (frontal) view of the opened heart. White arrows indicate normal blood flow. Blood containing low oxygen concentration circulates through the vena cava (VC both superior and inferior) that flows into the right atrium (RA). From there, the blood passes to the right ventricle (RV) which pumps the blood through the pulmonary artery (PA) to the lungs where it is re-oxygenated. Blood with high oxygen concentration returns to the heart through the pulmonary vein to the left atrium (LA) and the left ventricle (LV) pumps it all along the body through the aorta (Ao). Running across the surface of the ventricles, there are shallow grooves containing the coronary arteries and coronary veins, which supply blood to the heart muscle. Original image created by Eric Pierce and licensed under the creative Commons Attribution Share-Alik 3.0 license.

Cardiac cycle

A single cycle of cardiac activity can be divided into two movements: systole (muscular contraction) and diastole (muscular dilatation) as it is graphically observed in Figure 1.1-3. A lower pressure in the ventricles than in the atria produces the opening of atrioventricular valves (tricuspid and mitral valves), and consequently the blood flows into the relaxed ventricles. At this point, the contraction of the atria (atrial systole) completes the ventricular filling. Subsequently, the ventricular contraction causes the atrioventricular valves to close, signaling the beginning of ventricular systole. The semilunar valves (pulmonary and aortic) remain closed during this period, but the increase of ventricular pressure due to contraction causes their opening. When ventricles relax, and the pressure decreases, the semilunar valves close and the ventricular diastole begins. The atrioventricular valves remain closed until the pressure in the ventricles is lower than in the atria and the cycle re-starts. Since ventricles are responsible for pumping the blood out of the heart, their walls need to be strong; therefore, they include most part of cardiac muscle cells[10,11].

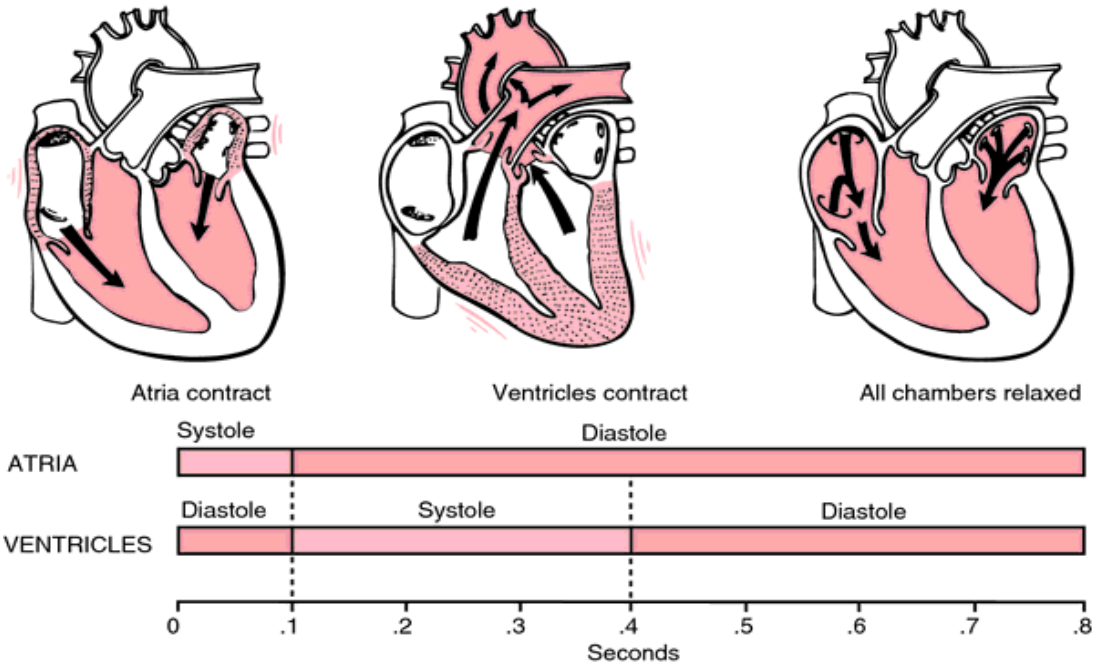

Figure 1.1-3: Cardiac cycle. A single cycle of cardiac activity can be divided into two movements: systole (muscular contraction) and diastole (muscular dilatation). The stiffness of heart muscle is 10KPa at the beginning of diastole and up to 200-500 KPa at the end of diastole. Image from Mosby's Medical Dictionary, 8th edition. © 2009, Elsevier.

Heart at cellular level

The cardiac wall is divided in three layers (see Figure 1.1-4): Epicardium, Myocardium and Endocardium.

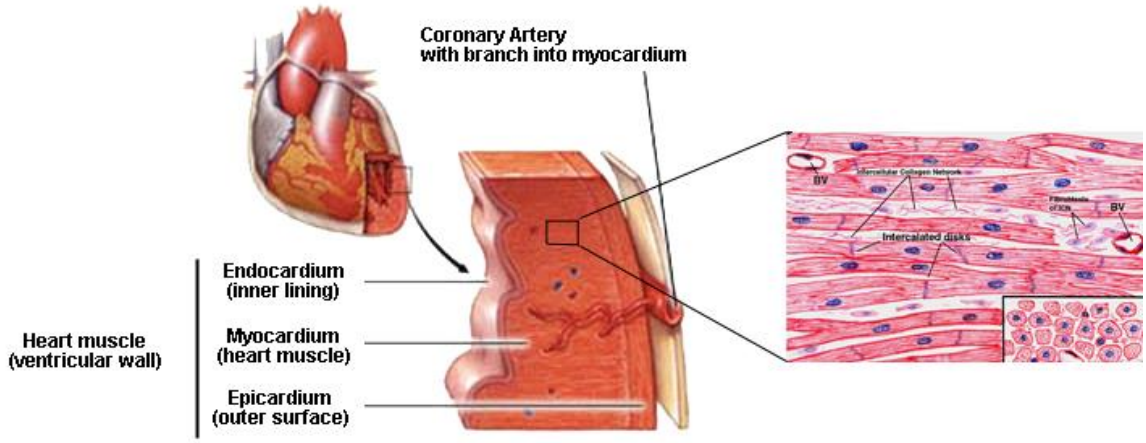

Figure 1.1-4: Cardiac muscular tissue layers. Cardiac muscular tissue is divided into three layers: epicardium, myocardium and endocardium. Myocardium is formed by cardiomyocytes that are faintly striated, branching, mononucleated cells connected by means of intercalated disks to form a functional network. Intercalated disks are anchoring structures containing gap junctions. This tissue is irrigated by coronary arteries with branches to the myocardium. The heart itself is contained in a sac called pericardium which plays roles such as fix the heart, limit its motion, prevent overfilling, lubricate and protect from infection. Image adapted from ©Mayo Foundation for Medical Education and research.

- *Epicardium*: Outer layer of the heart composed of connective tissue and covered by epithelium. It provides an outer protective layer for the heart.
- *Myocardium*: It is the muscular tissue of the heart wall and rests between epicardium and endocardium.
- *Endocardium*: Thin serous membrane that lines the interior of the heart. It is composed of loose connective tissue and simple squamous epithelial tissue.

In this work we will fix our attention on myocardium. It is composed of cells surrounded by an extracellular matrix (ECM) spatially organized into a complex 3D architecture to allow coordinated contraction and electrical pulse propagation. The cells that form the heart tissue can be divided into two major categories: excitable and non-excitable. The excitable ones are able to produce action potentials and include cardiac myocytes, pacemaker cells, Purkinje cells, and smooth muscle cells. On the other hand, non-excitable cells do not generate action potentials and include fibroblasts, endothelial cells, and adipocytes. Cardiac myocytes are organized within muscular fibers with changing orientation across the ventricular wall up to 180º (cardiac bundles). At the same time, these muscular fibers are organized into myocardial laminas 4-6 myocytes thick separated from neighboring laminas by extracellular collagen. The particular arrangement of the ventricular myocytes influences the mechanical and electrical function of the heart and small changes can lead to severe damages in these functions[13].

Heart beating

Heart beating is conducted by the contraction and relaxation of cardiac muscles. This involuntary beating is guided by a network of nerve fibers obtaining an efficient wave-like pumping action (Figure 1.1-5). Pacemaker cells are responsible for initiating this contraction: these cells have specialized membrane that allows sodium, calcium, and potassium to cross, causing cell depolarization. This depolarization is the moving force that initiates the sending of electrical impulses through heart wall, which triggers each heartbeat. Pacemaker cells are localized in the right atrium, in an area known as sinoatrial node (SA node). The impulse generated spreads through the atria to the atrioventricular node (AV node), situated in the lower portion of the right atrium. The AV node in turn sends an impulse through the nerve network to the ventricles initiating the contraction of the ventricles and creating a delay of 0.1 seconds to ensure that all the blood from the atria has been ejected to the ventricles before their contraction. The nerve network is formed by Purkinje fibers, specialized CMs that conduct cardiac action potentials more quickly and efficiently than any other cells in the heart. This cycle occurs approximately 70 times per minute. Electromechanical coupling of CMs is crucial for their synchronous response to electrical pacing signals[14].

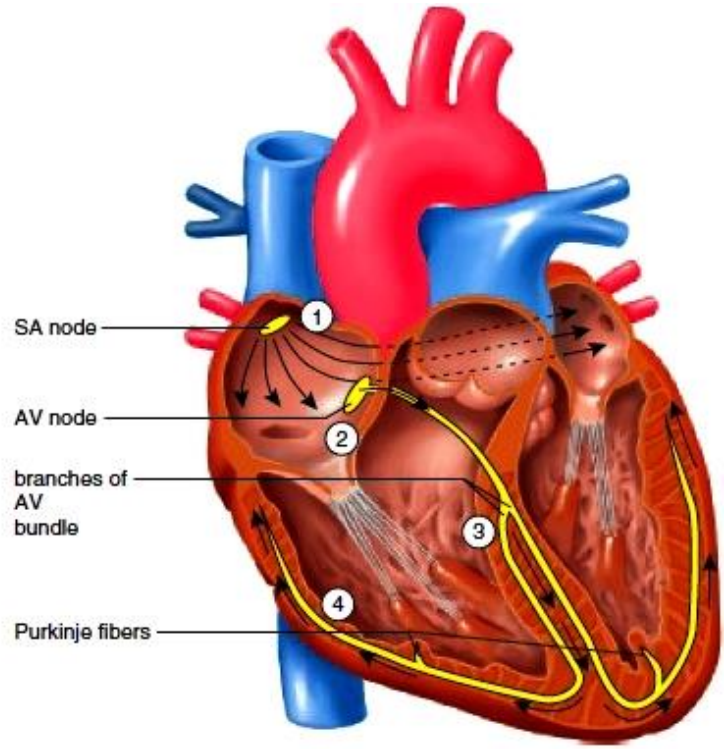

Figure 1.1-5: Electrical conduction system. (1) Stimulus originates in the Sinoatrial (SA) node and travels across the walls of the atria, causing them to contract. (2) Stimulus arrives at the Atrioventricular (AV) node and travels along the AV bundle. (3) Stimulus descends to the apex of the heart through the bundle branches. (4) After stimulus reaches the Purkinje fibers, the ventricles contract. Image adapted from www.melbourneheartcare.com.

1.1.3 Myocardial Infarction

MI[15,16] is the irreversible necrosis of the heart muscle. It occurs when ischemia exceeds a critical threshold and overwhelms myocardial cellular repair mechanisms designed to maintain normal operating function and homeostasis. Coronary arteries transport the essential nutrients to the heart and its steady supply allows the heart to pump blood continuously to the rest of the body. Concerning to the pathological process, most MI are caused by a disruption in the vascular endothelium associated with an unstable build-up of plaque. This stimulates the formation of an intracoronary thrombus, which results in coronary artery blood flow occlusion. If such an occlusion persists for more than 20 minutes, irreversible myocardial cell damage and cell death will occur. Nearly 70 % of MIs involve left ventricle (LV), in part because it has the most part of muscular mass and is more sensitive to oxygen supply.

The accumulation of this plaque over time is known as atherosclerosis, and it occurs over a period of years to decades. Research suggests that CHD begins with damage to the lining and inner layers of coronary arteries, and continues with the deposition of calcium, fatty substances, cholesterol, cellular waste products, and other cellular substances in the inner lining of an artery. It is important to notice that these products are present in healthy individuals, but its quantity is critical. Several factors have been reported to contribute to the coronary arteries damage including smoking (even secondhand smoke), high amount of certain fats and cholesterol in the

blood, high blood pressure, high amounts of sugar in the blood, and blood vessel inflammation, between others.

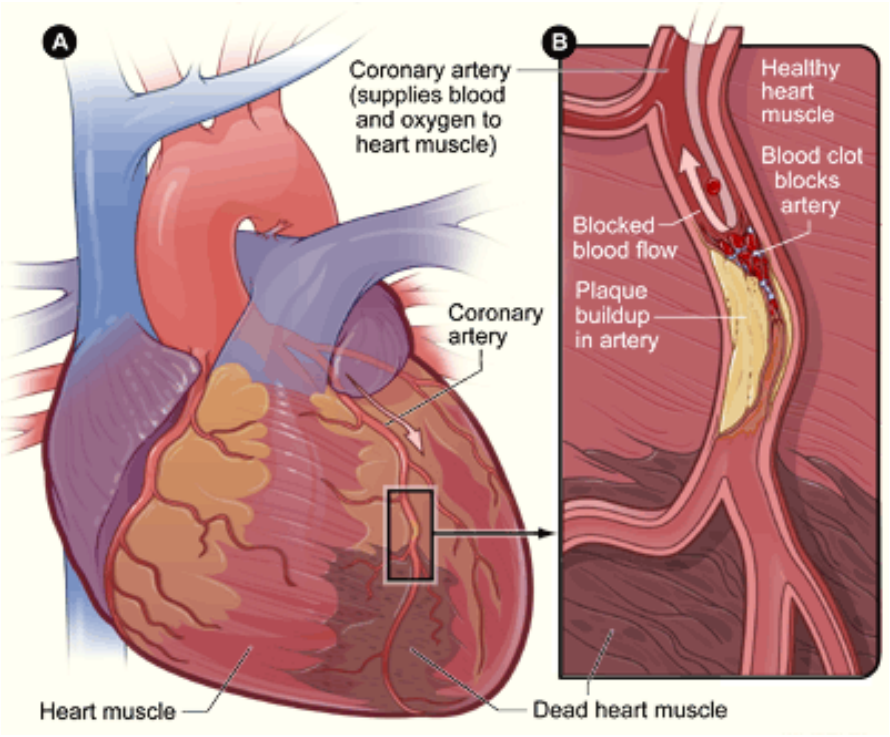

Figure 1.1-6: Myocardial infarction. (A) Heart presenting necrotic heart muscle caused by heart attack. (B) Cross-section of a coronary artery with plaque build-up and blood clot. Image adapted from https://www.nhlbi.nih.gov/health/health-topics/topics/heartattack/

Reduced blood supply leads to cell death. It first occurs in the area of muscular wall most distal to the arterial blood supply: the endocardium. As the duration of the occlusion increases, the area of myocardial cell death enlarges, extending from the endocardium to the myocardium and ultimately to the epicardium. The area of myocardial cell death then spreads laterally. Generally, after a 6- to 8-hour period of coronary occlusion, most of the distal myocardium has died. The severity of a MI depends on three factors: the level of the occlusion in the coronary artery, the length in time of the occlusion, and the presence or absence of collateral circulation. In general it can be pustule that:

- The more proximal the coronary occlusion, the more extensive the amount of myocardium that will be at risk of necrosis.
- The larger the necrotic area, the greater the chances of death because of mechanical complication or pump failure.
- The longer a vessel occlusion persists, the higher the chances of irreversible myocardial damage distal to the occlusion.

The goals of therapies to be used immediately after MI include the expedient restoration of normal coronary blood flow and salvaging as much functional myocardium as possible. These

goals can be achieved by a number of medical interventions and adjunctive therapies. In any case, after the restoration of blood flow, as an adult heart is not able to repair the damaged tissue, a scar is formed on the damaged cardiac tissue. Scar formation is crucial for rapid handling and seclusion of the lesion from healthy tissue, preventing a cascade of uncontrolled deleterious events[17]. However, the newly formed tissue does not have contractile, mechanical, and electrical properties of normal myocardium, which reduce the pumping efficiency of ventricles. Different compensatory mechanisms are activated in response to reduced cardiac output, maintaining initially acceptable levels. Ultimately, these compensatory systems place an extra burden on the weakened heart muscle, initializing a downward spiral of cardiac function which leads to heart failure[18]. Heart failure after a MI is often progressive. After CMs' death, macrophages, monocytes, and neutrophils migrate into the infarct area, initiating the inflammatory response. Subsequently, matrix metalloproteases (MMPs) are activated and the infarct starts to expand due to the weakening of the collagen scaffold. The damaged wall undergoes progressive remodeling, wall thinning, and chamber dilatation, with CMs slippage and fibroblast proliferation[19]. This increase of fibrillar, cross-linked collagen deposition helps to resist the deformation and rupture[20], but interferes in the migration and engraftment of the cells. Additionally, the ischemic heart results to be a hostile environment for the cells due to local hypoxia, acidosis, lack of substrates, and accumulations of metabolites[21]. New therapies are required to prevent the progression of pathological remodeling and cell death, as well as to induce tissue recovery in the affected areas[22].

Regenerative medicine aims to achieve the restoration of tissue structure and organ function, thus delaying or preventing disease progression. The desired outcome would be the maintenance of normal ventricular function and anatomy, replacement of lost CMs post-MI, prevention of LV wall thinning, and improvement in overall cardiac output towards physiological levels (average of 5.6 L/min for human males and 4.9 L/min for human females). With the aim to achieve these goals, Cardiac Tissue Engineering (CTE) is nowadays under study as an approach to support cell-based therapies and enhance their efficacy[22].

1.1.4 Cardiac Tissue Engineering

Regenerative medicine is undergoing experimental and clinical trials in cardiology, in order to limit the consequences of MI[23]. Its ultimate aim is to protect the infarcted heart from the progressive increase in cavity dilatation, decrease in wall thickness, and deterioration of ventricular function along time[17]. This can be fulfilled from different approaches:

1. Direct injection of isolated cell suspensions[24–27].
2. Biomaterials application to restrain ventricular cavity dilatation.

3. Injection of biomaterials with or without cells and/or growth factors (GFs) [28–34] into the myocardium to create *in situ* engineered cardiac tissue.
4. *In vivo* implantation of *in vitro* engineered cardiac tissue with or without cells and/or GFs[19,35–38].

The direct delivery of cell suspensions is known as cellular cardiomyoplasty. It is well established that this technique has the potential to influence in the reconstruction of myocardium *in situ*[19]. Resident stem cells or exogenous progenitor cells administrated in the proximity of the lesion can modify the microenvironment by secreting cytokines that favor cell homing, growth, and differentiation[17]. Many benefits have been reported: (1) reduction of size and fibrosis of infarct scars; (2) limitation of adverse post-ischemic remodeling; and (3) improvement of diastolic function[23]. Unfortunately, direct cell loading in the affected tissue presents many problems related to low cell engraftment (blood pumping washes out most of the injected cells from the target site), and poor cell survival (approximately 90 % of delivered cells die). Therefore, after many years of cardiomyoplasty trials the efficacy of the benefits observed resulted to be very limited due cell engraftment and survival efficiency.

To improve the efficiency of cellular therapy, an efficient cell delivery system is essential. CTE, which includes de use of biomaterials, emerged as an interesting approach. There are three primary strategies: (1) *in situ* TE where cells and biomaterials are directly injected in the myocardium; (2) *in vitro* TE that embeds the cells in 3D scaffolds to develop tissue constructs for *in vivo* implantation; and (3) scaffold free TE (cell sheets, cell bodies, core shell, and aggregates)[39,40]. The association of cells with biomaterials could provide an appropriate milieu where cells can grow in a 3D fashion and at the same time offer a support for the implantation step. The proper design, fabrication, and characterization of the material required to guide tissue development, and in some cases, support the organ, is required[18]. The right microenvironment as well as mechanical and topological cues may even reverse remodeling and boost cardiac regeneration[41]. Specifically, the milieu provides physical (e.g. dimensionality, topology), chemical (e.g. GF, cytokines, cell-adhesion complexes), and mechanical (e.g. stiffness) cues, facilitating cells integration and further cardiac regeneration[42].

Thus, CTE approach constitutes an attractive alternative since it provides the opportunity to deliver a large number of cells that are already organized in a natural or artificial ECM. The expectation of CTE lies in the repair of damaged tissues and organs, and also the production of relevant *in vitro* tissues for successful implantation[43]. Major issues still need to be solved, and bed-to-bench follow-up is paramount to foster clinical implementations[44]. The development of these therapies requires a multidisciplinary approach in order to optimize cell source, scaffolding design, and interaction of soluble biomolecules with and extracellular milieu[45].

Cells for Cardiac Tissue Engineering

It has been reported that MI involves the loss of 1-1.5 billion (10^9) CMs, compromising considerable amounts of myocardial cell mass[46]. For this reason, many CTE approaches are based on using new cells to replenish the damaged myocardium. Cell implantation strategies for heart failure have been designed to replace damaged cells or to produce new fibers creating contractile tissue[23]. But which kind of cell is the best candidate? Several stem and progenitor cells types from autologous and allogeneic donors are being tested to find the most appropriate candidate (Figure 1.1-7). Interestingly detailed reviews have been published regarding advantages, drawbacks, and different advances developed in this issue[7,19,47–52]. Here, a short overview of the cell types under study is provided.

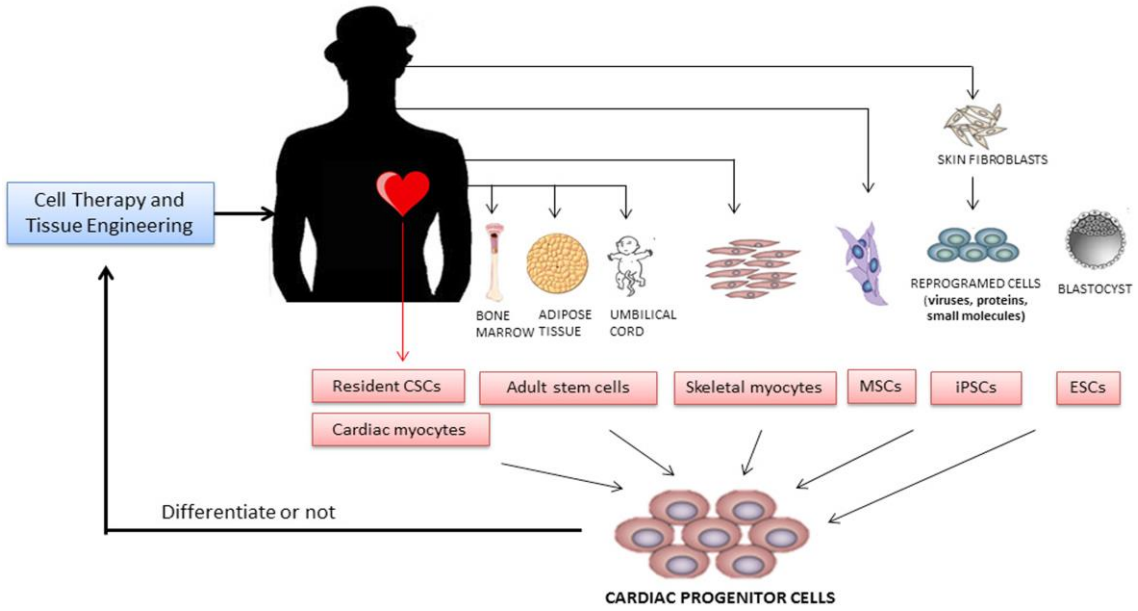

Figure 1.1-7: Cells under study for their application in Cardiac Tissue Engineering. Different cell types have been analyzed clinically with good results in terms of security, but heterogeneous results in terms of efficacy. Different regenerative mechanisms of implanted cells have been described: (1) transplanted cells could directly transdifferentiate into CMs; (2) paracrine effects could induce the growth of resident CMs; (3) resident endogenous myocardial stem cells may be stimulated; and (4) cell fusion between transplanted cells and resident CMs could be induced[5].

CARDIAC MYOCYTES[53]: They are the major cell type of cardiac muscle tissue. The primary goal of cardiac cell therapy consists in increasing the number of contractile cells in the necrotic zone to improve systolic heart function. Consequently, CMs were the first obvious source of cells due to their natural electro-physiological, structural, and contractile properties. These cells are able to engraft successfully in the resident myocardium improving its contractility. However, differentiated CMs dissociated from heart tissue are difficult to obtain and expand since they depend on heart biopsies or donations.

SKELETAL MYOBLATS[53,54]: Skeletal muscular fibers harbor an endogenous reservoir of tissue-committed precursor cells. Their use in cardiac repair is motivated by their clinically attractive

characteristics: (1) autologous origin with easy accessibility and without immune rejection or ethical concern, (2) high degree of scalability, (3) myogenic lineage that reduces the risk of tumor formation, and (4) high resistance to ischemia. However, they do not functionally integrate with the host cardiac tissue due to their incapability to form the appropriate gap junctions as a result, they can produce arrhythmias.

CARDIAC STEM CELLS (CSCs)[55]: The identification of a reservoir of resident stem cells in the heart appeared as a huge promise for cardiac regeneration since they are tissue specific and pre-committed to a cardiac fate. These cells are capable of differentiating into CMs, vascular smooth muscle cells, and endothelial cells. However, isolating and expanding them from cardiac biopsies represents a challenge.

EMBRIONIC STEM CELLS (ESCs): They are pluripotent, undifferentiated cells and, therefore, have the ability to differentiate into different specialized cells. They are able to grow and divide indefinitely, but their cellular mechanisms and signaling pathways are not fully understood. Although their cardiomyogenic potential, implanting ESC (or its cardiogenic derivate) *in vivo* might have the risk of producing teratomas[19,43,56,57] or/and induce arrhythmias[52,58]. Additionally to the biologic drawbacks, the clinical use of ESCs is severely limited due to ethical concerns and political discussion.

INDUCED PLURIPOTENT STEM CELLS (iPSCs)[59]: The main benefits of these cells are (1) their autologous character, (2) their differentiation capacity, and (3) the robustness and simplicity of reprogramming procedure[7,60]. Additionally, they are free of political and ethical debate. In mice hearts, these cells reduced cardiac cell loss, decreased fibrotic scar formation, and significantly improved cardiac function[5,25]. However, there are many barriers to overcome before its clinical use can be envisioned. Recent studies have revealed that iPSCs contain epigenetic features that indicate either incomplete or aberrant reprogramming. Additionally, some established iPSCs are genetically unstable, exhibiting large-scale genomic rearrangement, copy-number variation and abnormal karyotype[61].

ADULT STEM CELLS (ASCs): An adult stem cell is an undifferentiated cell found among differentiated cells in a tissue or organ that can self-renew and produce a progenitor cell. These cells can differentiate to yield some or all of the major specialized cell types of the tissue or organ in question. The primary role of ASCs in a living organism is to maintain and repair the tissue in which they are found. They have been isolated from a range of sources including bone marrow[62], muscle tissue, adipose tissue[63], and umbilical cord[64,65]. Principal advantages of ASCs are based on their autologous character, avoiding immunogenic reactions and tumor formation. Indeed, most of the research in cardiovascular regenerative therapies has been conducted using

bone marrow-derived stem cells, a specific type of ASC. It has been demonstrated that their administration can improve cardiac function in animal models of MI and develop vasculogenesis in ischemia models. Mesenchymal stem cells (MSCs)[66] is a subpopulation of bone-marrow stem cells[5], which have been reported to be capable of forming cardiac lineage cells *in vitro* and *in vivo*. Interestingly, MSCs can be obtained from other sources, such as adipose tissue, placenta, and umbilical cord[51]. They are easy to isolate and cultivate. Importantly, it has been reported that their therapeutic potential resides in the ability to directly differentiate into cardiac tissue, and exert paracrine signaling through the release of soluble biomolecules such as GFs[19].

It is not trivial to choose the most adequate cellular type for CTE. At microscopic level, the engrafted cells have to survive, and migrate from the seeding site to the border of damaged area, invade the infarcted zone, grow and differentiate. For this purpose, cells need the formation of adherent and gap junctions with the resident cells to anchor properly to the host myocardium. Interaction between integrin receptors on progenitor cells and ECM proteins is fundamental for cell loading, division, and maturation[17]. On the other hand, technically speaking, finding the best cell source for cardiac repair remains a major obstacle because of the difficulty on isolating and expanding autologous sources, ethical issues surrounding certain cell types and the inability of one cell source to fully replenish all necessary cell types[20]. Ideally, for clinical application, the cells used for CTE must accomplish the subsequent requirements [67,68]:

1. Amenability to large-scale expansion. Recent advances in large-scale bioreactor technologies adequately address this issue, being operable in accordance to good manufacturing practice (GMP) regulations.
2. Feasibly engrafting within damaged areas.
3. Migration potential.
4. Capability to differentiate into new CMs coupled electromechanically with neighboring cells and other mature cell types such as endothelial cells or fibroblasts.
5. Avoid tumor formation and arrhythmias induction. Tumorigenicity may be controllable by stringent selection of terminally differentiated somatic derivatives. Conversely, arrhythmogenicity appears more difficult to control[40].

In this project, adipose-derived progenitor cells (ATDPCs) were selected. These cells can be easily isolated and cultured *in vitro*. Interestingly, they express markers associated with MSCs and maintain their multipotenciality to differentiate into chondrocytes, osteoblasts, endothelial cells, and CMs. The differentiation capacity and paracrine activity of these cells make them an optimal candidate for the treatment of a diverse range of diseases. Four different possible fates

of ADPCs are described by Choi *et al.*[69]: (1) differentiating into cardiac muscles by direct contact with adjacent resident CMs; (2) differentiating into smooth muscle cells that have migrated to and surrounded immature vessels; (3) adipogenic differentiation and (4) secreting pro-angiogenic factors to recruit endogenous endothelial cells[19]. MSCs were discarded because although they can partially transdifferentiate into cardiomyogenic lineage, they rapidly undergo senescence during *in vitro* expansion.

Biomaterials for Cardiac Tissue Engineering

In ischemic disease, ECM is both chemically and morphologically modified. Therefore, the development of a milieu that closely mimics the native tissue architecture is of high interest[23,52]. There are various critical aspects to address for the design of the material: (1) cell anchorage in the scaffold, (2) nutrients and other small molecules diffusion, (3) vascular integration, (4) cellular organization, and (5) vascularization to enhance cell survival of the engrafted cells[18,70]. The selected biomaterial for CTE must accomplish the subsequent basic requirements:

1. *Biomimetism:* mimic the ECM and fit the structural and mechanical properties of the native myocardium. In particular, it should be stress and strain-resistant, but elastic enough to transmit contractile forces[71], due to the constant expansion and contraction of the heart tissue. Additionally, the material must integrate with the endogenous electrical pattern of the heart, propagating the internal wave front.
2. *Biocompatibility:* avoid rejection or immune response, presenting a good interaction with the host.
3. *Biodegradability:* in case to be biodegradable, the degradation products must be non-toxic and readily removed from the body.
4. *Cell friendly*: enhance cell survival, adhesion and rapid vascularization[7,72]. Additionally it must allow host macrophage infiltration in order to remove cellular debris[8].
5. *Cost effective*: easily accessible and reasonably affordable.

Biomaterials give cells multiple physical, mechanical and chemical cues to guide their growth, function, self-renewal and differentiation. In order to design a suitable biomaterial, there are large number of parameters to be considered[19,45]. Regarding physical signaling, scaffold internal structure (e.g. size and interconnectivity of pores) determines the transport of nutrients, metabolites and regulatory molecules[19,43], and at the same time the accommodation of the cells, and their organization into functional tissues. For instance, it has been largely demonstrated that extremely large pores could avoid vascularization (endothelial cells are not capable of bridging pores larger than their diameter), but pores smaller than 100 μm can influence diffusion. From the chemical perspective, the scaffold has an important role in cellular attachment and differentiation. Specifically, it has been reported that properties such as wettability, charge,

chemistry, roughness and stiffness play an essential role in determine whether cells are able to adhere. Finally, its elasticity must be precisely controlled because it should not negatively affect heart performance. Besides, a compromise between the complete degradation and the mechanical support is needed. Biomaterials have been successfully used to constrain the post-MI failing heart, preventing it from further remodeling and dilatation[18,41].

CTE uses both natural and synthetic materials. Up to date, most research is focused on natural biomaterials due to their early commercial availability and the potential advantage of biologic recognition[7]. Nevertheless, the use of synthetic scaffolds is also of high interest. This type of materials has a wide diversity of properties, which can be tailored with respect to mechanical, chemical and physical signaling. The most important quality of this group of materials is that the synthesis conditions can be fixed to get defined properties without batch-to-batch variations and with known composition (desired porosity, mechanical stability and degradation properties). However, their origin leads to limited cellular interactions. Some examples of materials used nowadays in CTE are presented in Table 1.1-1.

Table 1.1-1: Materials currently used in Cardiac Tissue Engineering[73]. Image from Castells-Sala *et. al.*

Biomaterials			
Origin		Types	
Natural	Synthetic	Injectable	Noninjectable
Collagen	PLA	Glues,	Porous scaffolds
Silk	PGA	Self-assembling Peptides	Natural ECM
Chitosan	PLCA		Gels
Alginate			Nanobiomaterials
Fibroin			Sponges

ECM, extracellular matrix; PGA, Poly (glycolic acid); PLA, Poly (lactic acid); PLCA, Poly (L-lactic acid)-copoly-(3-caprolactone).

Besides material composition, the methodology used for its implantation is also important. In this field, injectable scaffolds have been widely studied as vehicles for cell delivery with the aim to maximize cell retention, and survival in the ischemic area. Injectable therapies are beneficial to avoid invasive chirurgical treatments, but their major challenge resides in the demanded properties. For practical reasons, the material needs to remain liquid until its injection and then solidify quickly after delivery, presenting the features described above. The difficulty of this technique falls on the continuous contraction-relaxation cycles present in the heart, and, therefore, the integration of muscular, vascular and connective tissue compartments between graft and host is really challenging. Although injectable biomaterials seem like a more desirable approach from the chirurgic point of view, the need to maintain the material in a liquid phase until injection made of non-injectable materials an interesting alternative[74]. Several studies have been focused on the scaffold itself. Many materials are able to induce a cellular response from the host tissue[52], but they also serve as a 3D environment and a vehicle for cells[18]. A scheme of

different biomaterials platforms is presented in Figure 1.1-8, and examples of both kinds of materials are presented on Table 1.1-1.

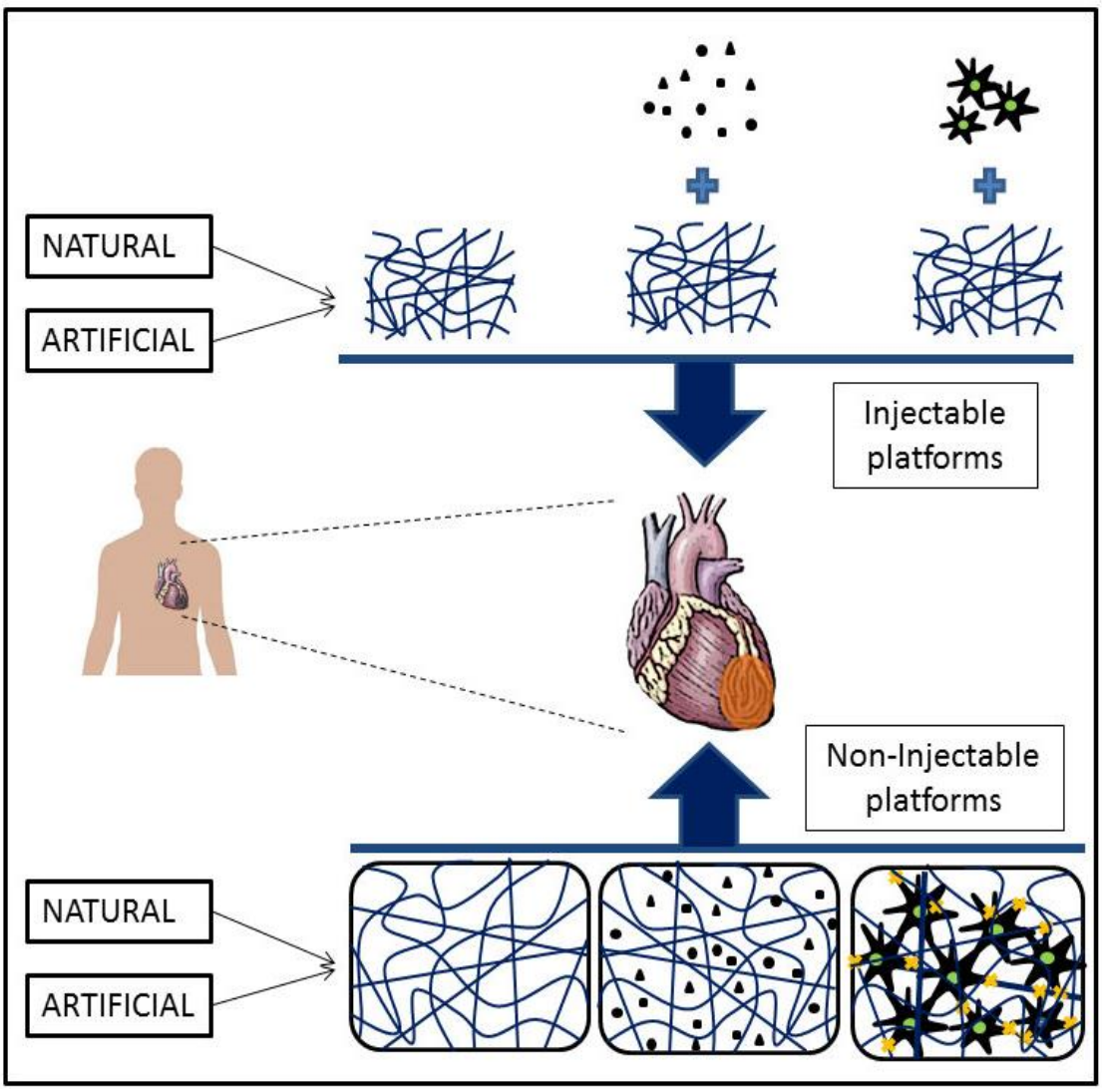

Figure 1.1-8: **Biomaterials platforms mainly used in Cardiac Tissue Engineering**[73]**.** Natural and artificial biomaterials are used in the development of injectable and non-injectable biomaterial platforms to assist cardiac tissue repair and regeneration after acute or chronic MI. Injectable systems usually are composed of a liquid material (hydrogel) scaffold, whereas non-injectable biomaterials are composed of solid materials with tuned stiffness values as well as variable mesh and porous sizes. Both platforms could include the use of GFs and cytokines (triangle, square, and circle dots), cells (star-like shape), or both. From Castells-Sala *et. al.* 2012.

RECATABI project bets on a combination of two synthetic biomaterials: an elastomeric microporous membrane to provide mechanical support to cells and a self-assembling peptide (SAP) nanofiber gel to provide an adequate microenvironment within the membrane's pores. The results obtained combining these materials for cell culture and further *in vivo* application are presented in Chapter 4.

1.1.5 Cardiac markers analyzed

Heart is the first organ to form and function in the embryo. Its development requires cell specification, cell differentiation, cell migration, morphogenesis, and interaction among cells. This process can be divided in three steps: (1) determination of the cardiac field in the mesoderm; (2) differentiation of cardiac precursor cells; and (3) heart maturation. The identity of the progenitor cells during early cardiogenesis is regulated by tightly coordinated, spatially and temporally active signaling pathways and molecular mechanisms. This leads cells to a progressive restriction of undifferentiated progenitors to the different cardiovascular lineages (Figure 1.1-9). The molecular identity of these inductive signals is not well understood, but various transcription factors that may regulate cardiac commitment and differentiation have been isolated. The understanding of this molecular basis could facilitate the investigation of stem cell-based regenerative therapies, since it would allow the development of more extensive strategies in CMs differentiation or even the identification of new cell types with CM potential[75].

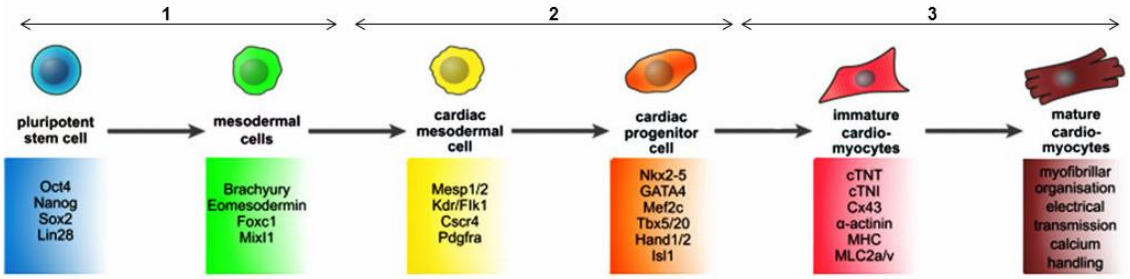

Figure 1.1-9: Sequential steps in cardiac differentiation *in vitro* from pluripotent stem cells to functional cardiomyocytes[75]. Cardiac development starts with the commitment of undifferentiated pluripotent stem cells of the inner cell mass of blastocysts to mesodermal restricted derivatives during embryonic development. Typical markers and characteristics for the different cell types are indicated. Structural and functional maturation is not well understood. Maturation might be provoked by hormones, organization in 3D engineered heart tissues (EHTs), and electrical and mechanical stimulation. Image adapted from Cyganek 2013.

In this thesis the cardiomyogenic potential of the cells cultured in different conditions (2D and 3D environment) and stimulation protocols (chemical and electrical) is assessed by analyzing the expression of early and definitive cardiac markers. A brief description of the analyzed markers is presented below:

Early cardiac markers

- ***GATA binding protein 4 (GATA4).*** GATA factors comprise a small family of highly conserved zinc finger transcription factors that play critical roles in gene activation in multiple cell lineages. They are involved in the development of the cardiovascular, hematopoietic, digestive, and reproductive systems. GATA4 is an essential transcription factor for normal heart morphogenesis that regulates the survival, growth, and proliferation of CMs[76]. It is one of the earliest transcription factors expressed in

developing cardiac cells, and continues to be expressed in CMs. Its function consists on binding to DNA and determining which genes get active or shut off.

- ***Myocyte Enhancer Factor-2 Polypeptide-C (MEF2C).*** Member of the MADS box transcription enhancer factor 2 (MEF2) family proteins, which play a key role in myogenesis[77]. MEF2 family of transcription factors has long been associated with regulation of myocardial-expressed genes, including cardiac alpha-actin (ACTN1) and myosin heavy chain (MHC)[78]. The encoded protein, MEF2C, has both trans-activating and DNA binding activities. It is possible that this protein plays a role in maintaining the differentiated state of muscle cells. It is also involved in vascular development.
- ***NK2 Transcription Factor Related Locus-5 (NKX2.5).*** Also called Csx, this gene encodes a homeobox-containing transcription factor that functions in heart formation and development. NKX2.5 is the earliest known marker of vertebrate heart development. The overexpression or loss-of-function mutations studies in frogs, zebrafish, mice and humans have demonstrated that NKX2.5 can induce myocardial gene expression, and that it is necessary for the specification of the right ventricle, heart looping and atrial septation[79]. It is also involved in the AV node function and intimately cooperates with GATA4 for the differentiation into beating CMs. NKX2.5 has been shown to interact with TBX5[80].
- ***T-box Transcription Factor 5 (TBX5).*** TBX5 belongs to the T-box gene family. Its members share a highly conserved 180-amino- acid domain required for DNA binding [81]. TBX5 gene is critical for the development of the heart. The encoded protein regulates the activity of other genes by attaching to specific regions of DNA. In situ hybridization studies in mouse, chick and humans show that it is expressed in the cardiac crescent early in the developing heart and subsequently in an asymmetric fashion in the left ventricle and on the left side of the ventricular septum[82].The T-box 5 protein is also critical for the formation of the electrical system that coordinates contractions of the heart chambers. It has been shown to interact with NKX2.5, GATA4 and MEF2C to synergistically activate target genes expression in CMs [83].

Definitive cardiac markers

- ***Alpha-actin 1(ACTN1).*** Alpha actin belongs to the spectrins gene superfamily, which represents a diverse group of cytoskeletal proteins. It is a marker of mature CMs, but it is also expressed in cardiac progenitor cells. Therefore, it could be also considered an early cardiac marker. This type of actin is specifically expressed in myoblast cytoskeleton and is the major constituent of the contractile apparatus[84].
- ***Connexin43 (Cx43) or gap junction protein, alpha 1 (GJA1).*** GJA1 is a member of the connexin gene family. It encodes for a protein component of gap junctions, which are

composed of arrays of intercellular channels that provide a route for the diffusion of low molecular weight materials from cell to cell. Gap junctions mediate electrical coupling between cardiac myocytes, forming the cell-to-cell pathways for propagation of the precisely orchestrated patterns of current flow that govern the regular rhythm of the healthy heart. The encoded protein is the major protein of gap junctions in the heart. It has been established unequivocally that mammalian CMs express Cx40, Cx43, and Cx45, but different tissues of the heart express different amounts and combinations of these connexins. The major cardiac gap junction protein, Cx43, is expressed in atrial and ventricular muscle[85].

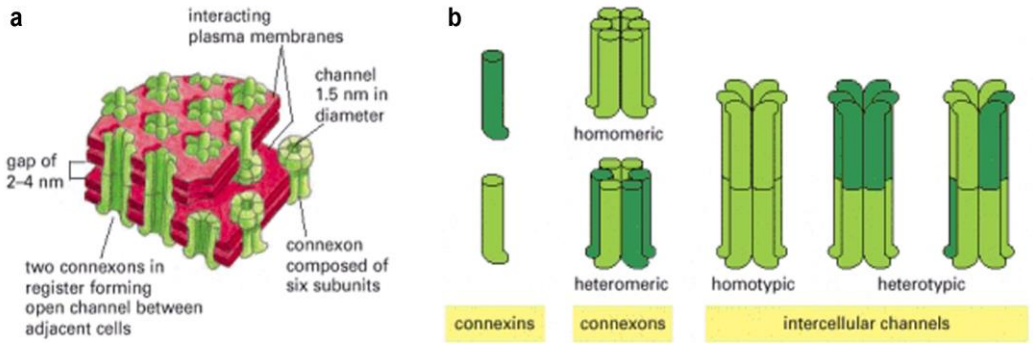

Figure 1.1-10: Cardiac gap junctions. Specialized intercellular connection between two cells, that allows the pass of molecules and ions, freely. (a) A 3D drawing showing the interacting plasma membranes of two adjacent cells connected by gap junctions. The lipid bilayers (red) are penetrated by protein assemblies called connexons (green). (b) The connexons are composed of 6 connexins. The connexons can be homomeric or heteromeric, and the intercellular channels can be homotypic or heterotypic. Several gap juncions channels (hundreds) assemble within a macromelecular complex called gap junction plaque. Image adapted from Molecular Biology of the Cell. 4th edition[86].

- ***Myosin Heavy Chain (MHC).*** Myosins are a family of ATP-dependent protein well known for their role in muscle contraction and their involvement in a wide range of eukaryotic motility processes. Muscle myosin contains 2 heavy chain subunits, 2 alkali light chain subunits, and 2 regulatory light chain subunits. This gene encodes the heavy chain subunit of cardiac myosin predominantly expressed in normal human ventricle. The abundance of this protein correlates with the contractile velocity of cardiac muscle[84].
- **Troponin.** It is a 3-unit complex of troponin T (tropomyosin binding), I (inhibitory) and C (calcium binding). This thin filament is associated with the regulatory complex of the contractile system of skeletal and cardiac muscle. The principal role of this complex is to control the calcium mediated interaction between actin and myosin. Troponin C binds calcium released out of the sarcoplasmic reticulum after stimulation; Troponin T (cTnT) connects the troponin complex to tropomyosin regulating muscle contraction in response to alteration in intercellular calcium concentration; and Troponin I (cTnI) prevents the connection between actin and myosin without stimulus. In contrast with

other multigene families, the skeletal and cardiac proteins are not derived from alternative splicing of exons from a single gene [87], therefore, they have, theoretically, the potential of being unique to the myocardium. Indeed, cTnI has only been identified in the myocardium[88].

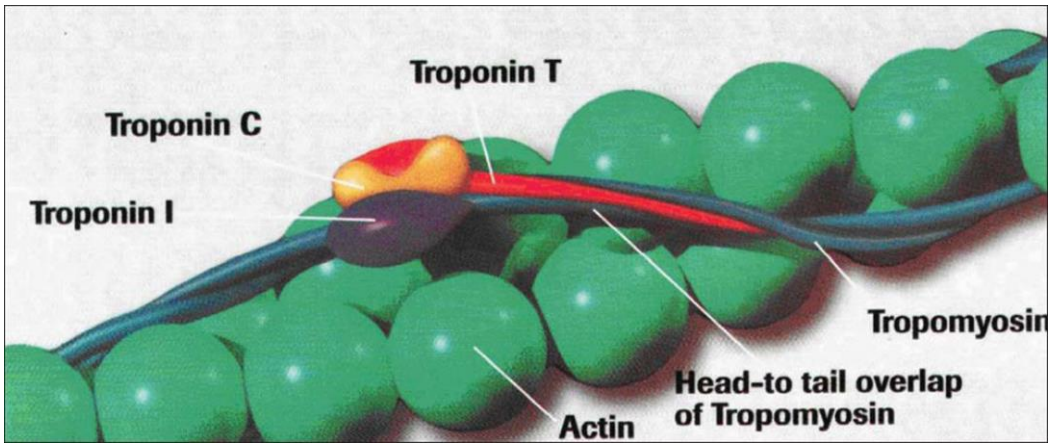

Figure 1.1-11: Arrangement of Troponins I, C and T with tropomyosin and actin in the heart muscle fibers. These are located at regular intervals along the length of actin filaments and play a key role in muscle contraction. Image adapted from Chaikhouni A *et. al.*[89].

1.2 MOTIVATIONS AND GENERAL AIMS

From their beginnings, the Tissue Engineering Laboratory directed by Dr. Semino has been fully immersed in the study of three-dimensional (3D) environment effect on cell behavior. The principal hypothesis of the group is that the recreation of key biological, biophysical and biomechanical parameters of a healthy tissue would allow a damaged tissue function recovery. The system used in our laboratory is based on the synthetic matrix of self-assembling peptide RAD16-I[90] (see Chapter 2), that allows studying different aspects of cellular behavior such as proliferation, maintenance, and acquisition of complex cellular structures with characteristics of tissues and organs.[91]. Additionally, these 3D systems achieve to mimic the *in vivo* milieu, recreating structural patterns that allow proper organization of the ECM and increasing cell capacity of differentiation and proliferation. In this context, during the last years, the group has obtained a series of study models working with adult cells: MC3T3[92] (cells of mouse calvaria), MEF[93,94] (Mouse Embryonic fibroblasts), hNDF[95] (normal human dermal fibroblasts); and embryonic stem cells: mESC[96] (Mouse Embryonic stem cells).

Meanwhile, the RECATABI European project coordinated from our laboratory proposed to develop a bioengineering platform to implant subcutaneous Adipose Tissue-Derived Progenitor Cells (subATDPCs) in the damaged tissue of the heart after MI, with the aim to promote function recovery. The 3D mentioned systems provide the cells great freedom of migration, leading to the formation of intracellular contacts and resulting in the appearance of emergent properties of self-organization acquisition. However, their mechanical performance is not suitable for their direct introduction in a highly stressed tissue such as the heart. Therefore, the combination of RAD16-I with elastomeric membranes (to provide mechanical support) was proposed for the culture of subATDPCs and subsequent implantation of the platform in animal models (mice and sheep).

Thus, the general objectives of the present thesis, which will be addressed separately in the next three chapters, are the following:

- To obtain an *in vitro* model to study the behavior of subATDPCs in a truly 3D environment for the understanding of key biological, biophysical and biomechanical parameters regulating the cardiac differentiation process (Chapter 2).

- To obtain a system to analyze the effect of electrical stimulation in the developed *in vitro* 3D model (Chapter 3).

- To evaluate innovative combinations of scaffolds and cells for novel cell-delivery system to ensure high cell survival and enhanced tissue integration after implantation (Chapter 4).

1.3 BIBLIOGRAPHY

1. Mathers, C. & Loncar, D. Projections of global mortality and burden of disease from 2002 to 2030. *PloS med* **3,** e442 (2006).

2. Organization, W. H. Global status report on noncommunicable disaeses 2010. (2011).

3. Cannon, B. Cardiovascular disease: Biochemistry to behaviour. *Nature* **493,** S2–3 (2013).

4. World Economic Forum & Harvard School fo Public Health. *The Global Economic Burden of Non-communicable Diseases*. (2011). at <http://www3.weforum.org/docs/WEF_Harvard_HE_GlobalEconomicBurdenNonCommunicableDiseases_2011.pdf>

5. Doppler, S. a, Deutsch, M.-A., Lange, R. & Krane, M. Cardiac regeneration: current therapies-future concepts. *J. Thorac. Dis.* **5,** 683–97 (2013).

6. Heng, B. C., Haider, H. K., Sim, E. K.-W., Cao, T. & Ng, S. C. Strategies for directing the differentiation of stem cells into the cardiomyogenic lineage in vitro. *Cardiovasc Res* **62,** 34–42 (2004).

7. Karam, J.-P., Muscari, C. & Montero-Menei, C. N. Combining adult stem cells and polymeric devices for tissue engineering in infarcted myocardium. *Biomaterials* **33,** 5683–5695 (2012).

8. Fernandes, S., Kuklok, S., McGonigle, J., Reinecke, H. & Murry, C. E. Synthetic matrices to serve as niches for muscle cell transplantation. *Cells. Tissues. Organs* **195,** 48–59 (2012).

9. Haneef, K. *et al.* Development of bioartificial myocardium by electrostimulation of 3D collagen scaffolds seeded with stem cells. *Heart Int.* **7,** e14 (2012).

10. Klabunde, R. *Cardiovascular Physiology Concepts*. (2012).

11. Pearson. in *Hum. Physiol. an Integr. approach* 462–508 (2012). at <http://www.pearsonhighered.com/silverthorn6einfo/assets/pdf/silverthorn-ch14.pdf>

12. Peeters, T. H. J. M. GPU-based Visualization Techniques for the Interactive Exploration of Diffusion MRI Data. (2009).

13. Arnal-Pastor, M., Chachques, J. C., Monleón Pradas, M. & Vallés-Lluch, A. in *Regen. Med. Tissue Eng.* (Andrades, A.) 275–303 (2013). doi:10.5772/56076

14. Ravichandran, R., Venugopal, J. R., Sundarrajan, S., Mukherjee, S. & Ramakrishna, S. Cardiogenic differentiation of mesenchymal stem cells on elastomeric poly (glycerol sebacate)/collagen core/shell fibers. *World J. Cardiol.* **5,** 28–41 (2013).

15. Crowley, L. *An Introduction to Human Disease: Pathology and Pathophysiology Correlations*. 786 (Jones & Bartlett Publishers, 2009). at <http://books.google.com/books?id=Cflyw-sfn0AC&pgis=1>

16. Braun, C. A. & Anderson, C. M. *Pathophysiology: Functional Alterations in Human Health*. 518 (Lippincott Williams & Wilkins, 2007). at <http://books.google.com/books?id=hRoRff4PH6wC&pgis=1>

17. Anversa, P., Kajstura, J. & Leri, A. in *Hear. Fail. A Companion to Braunwald's Hear. Dis.* 48–72 (Elsevier Inc., 2004). doi:10.1016/B978-1-4160-5895-3.10004-X

18. Jawad, H., Lyon, A. R., Harding, S. E., Ali, N. N. & Boccaccini, A. R. Myocardial tissue engineering. *Br. Med. Bull.* **87,** 31–47 (2008).

19. Venugopal, J. R. *et al.* Biomaterial strategies for alleviation of myocardial infarction. *J. R. Soc. Interface* **9,** 1–19 (2012).

20. Christman, K. L. & Lee, R. J. Biomaterials for the treatment of myocardial infarction. *J. Am. Coll. Cardiol.* **48,** 907–13 (2006).

21. Stamm, C., Nasseri, B., Choi, Y.-H. & Hetzer, R. Cell therapy for heart disease: great expectations, as yet unmet. *Heart. Lung Circ.* **18,** 245–56 (2009).

22. Nunes, S. S., Song, H., Chiang, C. K. & Radisic, M. Stem cell-based cardiac tissue engineering. *J. Cardiovasc. Transl. Res.* **4,** 592–602 (2011).

23. Chachques, J. C. Development of bioartificial myocardium using stem cells and nanobiotechnology templates. *Cardiol. Res. Pract.* **2011,** 806795 (2010).

24. Murry, C. E., Field, L. J. & Menasché, P. Cell-based cardiac repair: reflections at the 10-year point. *Circulation* **112,** 3174–83 (2005).

25. Wang, F. & Guan, J. Cellular cardiomyoplasty and cardiac tissue engineering for myocardial therapy. *Adv. Drug Deliv. Rev.* **62,** 784–97 (2010).

26. Patel, A. N. & Genovese, J. A. Stem cell therapy for the treatment of heart failure. *Curr. Opin. Cardiol.* **22,** 464–70 (2007).

27. Pendyala, L. *et al.* Cellular cardiomyoplasty and cardiac regeneration. *Curr. Cardiol. Rev.* **4,** 72–80 (2008).

28. Li, Z., Guo, X. & Guan, J. A Thermosensitive Hydrogel Capable of Releasing bFGF for Enhanced Differentiation of Mesenchymal Stem Cell into Cardiomyocyte-like Cells under Ischemic Conditions. *Biomacromolecules* **13,** 1956–64 (2012).

29. Huang, C., Wei, H., Yeh, Y., Wang, J. & Lin, W. Injectable PLGA porous beads cellularized by hAFSCs for cellular cardiomyoplasty. *Biomaterials* **33,** 4069–77 (2012).

30. Liu, Z. *et al.* The influence of chitosan hydrogel on stem cell engraftment, survival and homing in the ischemic myocardial microenvironment. *Biomaterials* **33,** 3093–106 (2012).

31. Kadner, K. *et al.* The beneficial effects of deferred delivery on the efficiency of hydrogel therapy post myocardial infarction. *Biomaterials* **33,** 2060–6 (2012).

32. Reis, L. a *et al.* A peptide-modified chitosan-collagen hydrogel for cardiac cell culture and delivery. *Acta Biomater.* **8,** 1022–36 (2012).

33. Cheng, K. *et al.* Intramyocardial injection of platelet gel promotes endogenous repair and augments cardiac function in rats with myocardial infarction. *J. Am. Coll. Cardiol.* **59,** 256–64 (2012).

34. Johnson, T. & Christman, K. Injectable hydrogel therapies and their delivery strategies for treating myocardial infarction. *Expert Opin. Drug Deliv.* **10,** 59–72 (2013).

35. Naderi, H., Matin, M. M. & Bahrami, A. R. Review paper: critical issues in tissue engineering: biomaterials, cell sources, angiogenesis, and drug delivery systems. *J. Biomater. Appl.* **26,** 383–417 (2011).

36. Vunjak-Novakovic, G., Lui, K. O., Tandon, N. & Chien, K. R. Bioengineering heart muscle: a paradigm for regenerative medicine. *Annu. Rev. Biomed. Eng.* **15,** 245–67 (2011).

37. Ptaszek, L. M., Mansour, M., Ruskin, J. N. & Chien, K. R. Towards regenerative therapy for cardiac disease. *Lancet* **379,** 933–942 (2012).

38. Rane, A. a & Christman, K. L. Biomaterials for the treatment of myocardial infarction a 5-year update. *J. Am. Coll. Cardiol.* **58,** 2615–29 (2011).

39. Song, H. *et al.* Interrogating functional integration between injected pluripotent stem cell-derived cells and surrogate cardiac tissue. *Proc. Natl. Acad. Sci. U. S. A.* **107,** 3329–3334 (2010).

40. Karikkineth, B. C. & Zimmermann, W.-H. Myocardial tissue engineering and heart muscle repair. *Curr. Pharm. Biotechnol.* **14,** 4–11 (2013).

41. Marion, M. H. van, Bax, N. A. M., Spreeuwel, A. C. C. van, van der Schaft, D. W. J. & Bouten, C. V. C. Material-based engineering strategies for cardiac regeneration. *Curr. Pharm. Des.* **20,** 2057–68 (2014).

42. Kuraitis, D., Giordano, C., Ruel, M., Musarò, A. & Suuronen, E. J. Exploiting extracellular matrix-stem cell interactions: a review of natural materials for therapeutic muscle regeneration. *Biomaterials* **33,** 428–43 (2012).

43. Naderi, H., Matin, M. M. & Bahrami, A. R. Review paper: critical issues in tissue engineering: biomaterials, cell sources, angiogenesis, and drug delivery systems. *J. Biomater. Appl.* **26,** 383–417 (2011).

44. Giraud, M.-N., Guex, A. G. & Tevaearai, H. T. Cell therapies for heart function recovery: focus on myocardial tissue engineering and nanotechnologies. *Cardiol. Res. Pract.* **2012,** 971614 (2012).

45. Lundberg, M. S. Cardiovascular tissue engineering research support at the National Heart, Lung, and Blood Institute. *Circ. Res.* **112,** 1097–103 (2013).

46. Debayon, P., Mathews, S. S. & Nilanjana, M. Mesenchymal stem cell: present challenges and prospective cellular cardiomyoplasty approaches for myocardial regeneration. *Antioxid. Redox Signal.* **11,** 1841–55 (2009).

47. Lui, K. O., Bu, L., Li, R. A. & Chan, C. W. Pluripotent stem cell-based heart regeneration: from the developmental and immunological perspectives. *Birth Defects Res. C. Embryo Today* **96,** 98–108 (2012).

48. Abdelli, L. S., Merino, H., Rocher, C. M. & Singla, D. K. Cell therapy in the heart. *Can. J. Physiol. Pharmacol.* **315,** 307–315 (2012).

49. Hoover-Plow, J. & Gong, Y. Challenges for heart disease stem cell therapy. *Vasc. Health Risk Manag.* **8,** 99–113 (2012).

50. Oldroyd, K. G., Berry, C. & Bartunek, J. Myocardial repair and regeneration: bone marrow or cardiac stem cells? *Mol. Ther.* **20,** 1102–5 (2012).

51. Gnecchi, M., Danieli, P. & Cervio, E. Mesenchymal stem cell therapy for heart disease. *Vascul. Pharmacol.* **57,** 48–55 (2012).

52. Liu, J. *et al.* Generation, Characterization and Potential Therapeutic Applications of Cardiomyocytes from Various Stem Cells. *Stem Cells Dev.* **21,** 2095–110 (2012).

53. Dowell, J. D., Rubart, M., Pasumarthi, K. B. S., Soonpaa, M. H. & Field, L. J. Myocyte and myogenic stem cell transplantation in the heart. *Cardiovasc. Res.* **58,** 336–50 (2003).

54. Menasché, P. Skeletal myoblasts and cardiac repair. *J. Mol. Cell. Cardiol.* **45,** 545–53 (2008).

55. Bollini, S., Smart, N. & Riley, P. R. Resident cardiac progenitor cells: at the heart of regeneration. *J. Mol. Cell. Cardiol.* **50,** 296–303 (2011).

56. Kleger, A. & Liebau, S. Calcium-activated potassium channels, cardiogenesis of pluripotent stem cells, and enrichment of pacemaker-like cells. *Trends Cardiovasc. Med.* **21,** 74–83 (2011).

57. Chong, J. J. H. Cell Therapy for Left Ventricular Dysfunction: An Overview for Cardiac Clinicians. *Heart. Lung Circ.* **21,** 532–42 (2012).

58. Mullenix, P. S., Huddleston, S. J., Stojadinovic, A., Trachiotis, G. D. & Alexander, E. P. A new heart: somatic stem cells and myocardial regeneration. *J. Surg. Oncol.* **105,** 475–80 (2012).

59. Pawani, H. & Bhartiya, D. Pluripotent stem cells for cardiac regeneration: Overview of recent advances & emerging trends. *Indian J. Med. Res.* **137,** 270–82 (2013).

60. Ptaszek, L. M., Mansour, M., Ruskin, J. N. & Chien, K. R. Towards regenerative therapy for cardiac disease. *Lancet* **379,** 933–942 (2012).

61. Bernstein, H. S. & Srivastava, D. Stem cell therapy for cardiac disease. *Pediatr. Res.* **71,** 491–499 (2012).

62. Clifford, D. M. *et al.* Long-term effects of autologous bone marrow stem cell treatment in acute myocardial infarction: factors that may influence outcomes. *PLoS One* **7,** e37373 (2012).

63. Qayyum, A. A. *et al.* Adipose-derived mesenchymal stromal cells for chronic myocardial ischemia (MyStromalCell Trial): study design. *Regen. Med.* **7,** 421–8 (2012).

64. Weber, B., Zeisberger, S. M. & Hoerstrup, S. P. Prenatally harvested cells for cardiovascular tissue engineering: fabrication of autologous implants prior to birth. *Placenta* **32 Suppl 4,** S316–9 (2011).

65. Cortes-Morichetti, M. *et al.* Association between a cell-seeded collagen matrix and cellular cardiomyoplasty for myocardial support and regeneration. *Tissue Eng.* **13,** 2681–7 (2007).

66. Cashman, T. J., Gouon-Evans, V. & Costa, K. D. Mesenchymal stem cells for cardiac therapy: practical challenges and potential mechanisms. *Stem Cell Rev.* **9,** 254–65 (2013).

67. Soler-Botija, C., Bagó, J. R. & Bayes-Genis, A. A bird's-eye view of cell therapy and tissue engineering for cardiac regeneration. *Ann. N. Y. Acad. Sci.* **1254,** 57–65 (2012).

68. Bayes-Genis, A. *et al.* Chimerism and microchimerism of the human heart: evidence for cardiac regeneration. *Nat. Clin. Pract. Cardiovasc. Med.* **4 Suppl 1,** S40–5 (2007).

69. Choi, Y. S., Matsuda, K., Dusting, G. J., Morrison, W. A. & Dilley, R. J. Engineering cardiac tissue in vivo from human adipose-derived stem cells. *Biomaterials* **31,** 2236–2242 (2010).

70. Curtis, M. W. & Russell, B. Cardiac tissue engineering. *J. Cardiovasc. Nurs.* **24,** 87–92 (2009).

71. Demirbag, B., Huri, P. Y., Kose, G. T., Buyuksungur, A. & Hasirci, V. Advanced cell therapies with and without scaffolds. *Biotechnol. J.* **6,** 1437–53 (2011).

72. Sant, S., Hancock, M. & Donnelly, J. Biomimetic gradient hydrogels for tissue engineering. *engineering* **88,** 899–911 (2010).

73. Castells-Sala, C. & Semino, C. E. Biomaterials for stem cell culture and seeding for the generation and delivery of cardiac myocytes. *Curr. Opin. Organ Transplant.* **17,** 681–7 (2012).

74. Cheng, K. *et al.* Functional performance of human cardiosphere-derived cells delivered in an in situ polymerizable hyaluronan-gelatin hydrogel. *Biomaterials* **33,** 5317–5324 (2012).

75. Cyganek, L. Cardiac Progenitor Cells and their Therapeutic Application for Cardiac Repair. *J. Clin. Exp. Cardiolog.* **01,** (2013).

76. Holtzinger, A., Rosenfeld, G. E. & Evans, T. Gata4 directs development of cardiac-inducing endoderm from ES cells. *Dev. Biol.* **337,** 63–73 (2010).

77. Wilson-Rawls, J., Molkentin, J. D., Black, B. L. & Olson, E. N. Activated Notch Inhibits Myogenic Activity of the MADS-Box Transcription Factor Myocyte Enhancer Factor 2C. *Mol. Cell. Biol* **19,** 2853 (1999).

78. Lockhart, M. M. *et al.* Mef2c regulates transcription of the extracellular matrix protein cartilage link protein 1 in the developing murine heart. *PLoS One* **8,** e57073 (2013).

79. Horb, M. E. & Thomsen, G. H. Tbx5 is essential for heart development. *Development* **126,** 1739–51 (1999).

80. Nemer, G. & Nemer, M. Regulation of heart development and function through combinatorial interactions of transcription factors. *Ann. Med.* **33,** 604–10 (2001).

81. Moskowitz, I. P. G. *et al.* The T-Box transcription factor Tbx5 is required for the patterning and maturation of the murine cardiac conduction system. *Development* **131,** 4107–16 (2004).

82. Ghosh, T. K. *et al.* Characterization of the TBX5 binding site and analysis of mutations that cause Holt-Oram syndrome. *Hum. Mol. Genet.* **10,** 1983–94 (2001).

83. Wang, C., Cao, D., Wang, Q. & Wang, D.-Z. Synergistic activation of cardiac genes by myocardin and Tbx5. *PLoS One* **6,** e24242 (2011).

84. Center, C. H. G., Genetics of Molecular, D. & the Weizmann Science, I. of. Gene Cards. *1996*

85. Kanno, S. & Saffitz, J. E. The role of myocardial gap junctions in electrical conduction and arrhythmogenesis. *Cardiovasc. Pathol.* **10,** 169–77 (2001).

86. Alberts, B. *et al. Molecular Biology of the Cell.* (2002).

87. Messner, B., Baum, H., Fischer, P., Quasthoff, S. & Neumeier, D. Expression of messenger RNA of the cardiac isoforms of troponin T and I in myopathic skeletal muscle. *Am. J. Clin. Pathol.* **114,** 544–9 (2000).

88. Sharma, S., Jackson, P. G. & Makan, J. Cardiac troponins. *J. Clin. Pathol.* **57,** 1025–6 (2004).

89. Chaikhouni, A. & Al-Zaim, H. Troponin I Levels after coronary bypass operations in Aleppo, Syria. *Off. J. Gulf Hear. Assoc.* **8,** 6–9 (2007).

90. Zhang, S., Ellis-behnke, R. & Zhao, X. *Scaffolding in Tissue Engineering. CHAPTER 15: PuraMatrix : Self-assembling Peptide Nanofiber Scaffolds*. 217–248 (2006).

91. Semino, C. E. Can we build artificial stem cell compartments? *J. Biomed. Biotechnol.* **3,** 164–169 (2003).

92. Marí-Buyé, N., Luque, T., Navajas, D. & Semino, C. C. E. Development of a three-dimensional bone-like construct in a soft self-assembling peptide matrix. *Tissue Eng. Part A* **19,** 870–881 (2013).

93. Quintana, L. *et al.* Early Tissue Patterning Recreated by Mouse Embryonic Fibroblasts in a Three-Dimensional Environment. *Tissue Eng.* **15,** 45–54 (2009).

94. Fernández-Muiños, M. T. Effect of the microenvironment in the in vitro chondrogenic and osteogenic differentiation of mouse embryonic fibroblasts. (2013).

95. Bussmann, B. M. *et al.* Chondrogenic potential of human dermal fibroblasts in a contractile, soft, self-assembling, peptide hydrogel. *J. Tissue Eng. Regen. Med.* (2013). doi:10.1002/term.1766

96. Garreta, E., Genové, E., Borrós, S. & Semino, C. E. Osteogenic differentiation of mouse embryonic stem cells and mouse embryonic fibroblasts in a three-dimensional self-assembling peptide scaffold. *Tissue Eng.* **12,** 2215–27 (2006).

CHAPTER 2: Three-dimensional cultures of subcutaneous adipose tissue derived progenitor cells based in RAD16-I modified with RGD motifs and heparin polysaccharide

Castells-Sala C, *et.al.*. (under preparation) Three-dimensional cultures of subcutaneous adipose tissue derived progenitor cells based in RAD16-I.

2.1 BACKGROUND

2.1.1 Overview

After myocardial infarction (MI), the principal purpose of medical practice is to reconstitute the blood flow towards the affected area as soon as possible, to avoid at the maximum extent the formation of necrotic tissue. Unfortunately, it is not always possible, and the prolonged ischemia produces a high degree of cardiomyocyte (CM) death, which leads to a reduction of heart normal function. With the aim to restore this function, big efforts are being focused in the delivery of cells to the damaged site. Although the present clinical trials of cell therapy to provide a "proof of concept" of its viability, the encouraging results observed have a limited success in damaged myocardium regeneration[1]. Valuable lessons can be learnt from human myocardium and stem cell (SC) biology that would help scientists to develop new effective, safe and affordable regenerative therapies. Therefore, *in vitro* and *in vivo* models are nowadays being widely studied.

Humans heart is one of the organs with lowest regenerative capacity, but hearts innate ability to regenerate has been extensively reported in amphibians[2], fish, and recently in developing mammals[3]. Zebrafish[4] *in vitro* model is one example of particular importance in Cardiac Tissue Engineering (CTE) due to its ability to regenerate approximately 20 % of its resected ventricular mass two months following heart injury[3,5]. Interestingly, this heart muscle regeneration does not make use of SC, instead, mature heart muscle cells regress to SC-like state and re-differentiate. Whereas, in adult mammals the situation seems to be different. Typically, mammalian hearts respond to injury by scarring, whereby the damaged cardiac muscle is replaced by fibrotic scar tissue[6].

In vivo models are of high interest, but their high-complexity limit the possibility to analyze specific factors. Although the long-term goal of tissue engineering (TE) is to enhance *in vivo* regeneration, it also allows developing strategies to study such factors in a more controlled manner. Therefore, in a short-term approach TE can help to improve our understanding of how cells respond biochemically and in terms of spatial organization to the features found in their native environment, and to specific induction factors. These *in vitro* models also provide accurate approaches that may guide the creation of three-dimensional (3D) engineered cell aggregates. In this sense, innovations in the fields of biomaterials scaffolds, tissue matrix environment, and chemical or biological scaffolds are under development to understand the cellular response[7].

Cells introduced in the infarcted myocardium are hoped to induce angiogenesis, inhibit apoptosis, help to recover hibernating myocardium, activate endogenous repair mechanisms,

and create a new contractile tissue[8]. There is a strong possibility that implanting undifferentiated SC *in vivo* lead to a low engraftment and as a consequence to limited myocardial regeneration effect. Therefore, it is possible that some degree of cardiomyogenic differentiation of SC *in vitro* prior to transplantation would help to solve these issues. Additionally, this pre-differentiation may also alleviate the probability of spontaneous differentiation of SC into undesired lineages and reduces the risk of teratoma formation[9]. Moreover, it is likely that, without previous differentiation, only a small fraction of the transplanted cells would differentiate into the cardiomyogenic lineage, thus reducing the efficacy of the therapy. The development of efficient protocols for directly cardiomyogenic differentiation *in vitro* is thought to provide a much more amenable model to molecular characterization and genetic manipulation[1].

In this chapter, we describe an *in vitro* model of subcutaneous adipose tissue derived progenitor cells (subATDPCs) in a 3D system with the aim to analyze its cardiogenic potential before implantation in animal models.

2.1.2 *In vitro* models

The major process to reverse the left ventricular remodeling would be the enhancement of CMs regeneration as well as stimulation of neovascularization within the affected area of the myocardium. While animal models clearly have shown benefits of SC therapy to improve cardiac function after MI and ischemic heart failure, clinical trials in humans have shown to provide restricted benefits[10]. Animal models display the integrated responses that result from complex interactions between tissues and organs. Nonetheless, they fail to capture important facets of human responses, and they are very costly, time-consuming, and ethically controversial[11–13]. However, it has been widely proposed that understanding the underlying biology is the first step to a successful breakthrough in the development of new and efficient therapies. To achieve this goal the complex cellular microenvironment needs to be deconstructed into simpler and predictable systems. Decompose 3D microenvironments and the associated processes into adhesive, mechanical, and chemical components will aid in the understanding of the fundamental mechanisms that guide these processes[14]. Additionally, it would help researchers to identify and analyze the role of specific critical factors in human physiology and pathophysiology, or regulate SC fate. These approaches have already provided useful tools for controlling cell differentiation with potential clinical application and could also be precious to accelerate translational research[11].

Life is not entirely flat: the milieu is a crucial fate determinant

Functional systems consist of cells growing in two dimensions (2D) and cells growing in 3D structures. Both environments are in close contact and interact one to each other. A high

percentage of *in vivo* cells are organized in a 3D microenvironment (provided by the extracellular matrix, ECM), but their study *in vitro* has mostly been performed in 2D Petri dishes. Studies in standard cell cultures have produced many important conceptual advances. However, the change from a 3D *in vivo* milieu to a 2D tissue culture substrate, could lead to a differential cell behavior. Specifically, they can differ considerably on their morphology, cell-cell and cell-ECM interactions, and gene expression patterns from those growing in more physiological 3D environment (see Figure 2.1-1)[11,12,14]. This fact can be explained due to the unnaturally polarization found in 2D platforms for cells that are used to grow in a 3D milieu. In these systems cells have one side attached to a rigid and flat substrate and the other one exposed to culture media, what reduce cell-cell and cell-ECM interactions[15]. Additionally, the accessibility to the soluble factors (cell secreted factors and exogenous added factors) in 2D systems is quite easy since they are free to mix convectively through the medium, leading to a rapid equilibration. Therefore, conventional 2D cell cultures, in which cells grown in physiological constrained conditions, do not mimic adequately *in vivo* systems, which limits their potential to predict the cellular responses of real organisms[12,16].

The 3D *in vitro* models were developed to recreate the *in vivo* cellular environment offered by the ECM and neighboring cells. This new milieu provides unique perspectives on the behavior of the cells, developing tissues and organs[11]. During the last two decades, significant discoveries have shown that ECM plays an important role in the behavior of biological tissues. The interactions between cells and the ECM can determine whether a given cell undergoes proliferation, differentiation, apoptosis or invasion[15,16]. Additionally, it has been widely reported the great importance of the direct connection between cells and the ECM through integrin receptors.

In this context, 3D models, which are constituted by cells, 3D matrices (natural or synthetic) and effector molecules, fulfill the need for reductionist approaches to understanding *in vivo* molecular mechanisms (see Figure 2.1-1)[11]. These models have the potential to improve the physiological relevance of cell-based assays and advance the quantitative modeling of biological systems from cells to organisms[12]. They allow the cells to integrate many external cues (including those that arise from various ECM components, mechanical stimulation, and soluble signals from adjacent and event distant cells) to generate a basal phenotype and respond to perturbations in their environment. Additionally, these models mimic the limited access to the soluble factors due to structural features such as pore size, interconnectivity, gel dimensions, cell density, and solute size and charge[14]. The 3D structure also allows having adhesions distributed in all three dimensions without prescribed polarity.

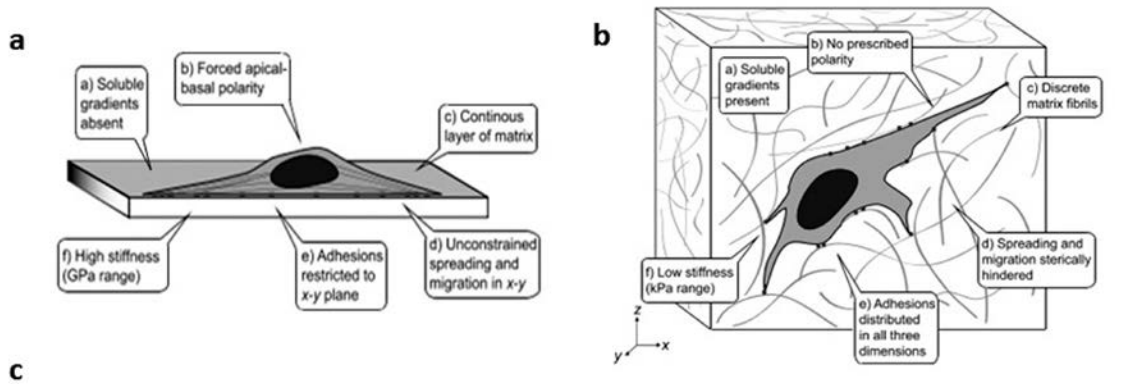

c

Biological Function	2D versus 3D	Regulatory Mechanisms
Cell Shape	Loss of epithelial cell polarity and altered epithelial and fibroblast shape in 2D	Growth factor receptors and pathways; cell-adhesion signals associated with cell survival and matrix plasticity
Gene Expression	Cells in 2D versus 3D often have different patterns of gene expression	ECM, hormones, and adhesion molecules
Growth	3D matrix-dependent regulation of cell growth	Adhesion and growth factor-related pathways plus survival or apoptotic genes
Morphogenesis	3D matrix-induced vessel sprouting and gland branching	ECM, adhesion, growth factor-related pathways and apoptotic genes
Motility	Altered single and collective cell motility patterns in 3D matrices	ECM and its regulators; adhesions and growth factor-related pathways; phospholipids
Differentiation	3D matrix-induced cell differentiation	ECM and growth factors; motor molecules

Figure 2.1-1: Cell and tissue organization in 2D vs. 3D cultures. The cues encountered by a cell are strikingly different between an ECM- coated glass or plastic surface (2D) and a typical 3D ECM**.** a) A cell growing on 2D flat surface. b) Cell cultured in 3D *in vitro* model mimicking the natural ECM. c) Biological function comparison of cells growing on 2D surface vs. 3D system. Image adapted from Baker *et. al.* 2012 [11,14]

In vitro 3D approaches enable a more accurate study of the molecular mechanisms underlying human diseases and better prediction of drugs and therapies effect, compared to 2D systems[15,17–20]. In any 3D model system, the particular cellular and matrix microenvironment provided to cells can substantially influence the experimental outcome.

Extracellular matrix

Within the most part of pluricellular organisms, the cells are organized in cooperative groups called tissues. The cells secrete various macromolecules that interact one to each other forming a complex network known as ECM. This structure is involved in the maintenance of the tissue structure and possesses a reticular organization where the cells can migrate and interact one to each other (Figure 2.1-2)[21]. There is a serial of essential components found in ECM, which composition varies between tissues. From merely structural point of view, collagens provide strength to the tissues, elastin ensures tissue flexibility, and glycoproteins maintain tissue cohesiveness. Another important element is the ground substance that fills the gaps between protein fibers of the ECM. This gel-like substance is composed of different types of polysaccharides, mainly glycosaminoglycans (GAG), and to a less extent some adhesion glycoproteins. This complex structure controls the bulk and local mechanical environment. Additionally, it contributes to the microenvironment through their own signaling moieties and

their ability to bind growth factors (GFs), cytokines, enzymes, and other diffusible molecules. This property to bind soluble effector molecules significantly slows their diffusion and therefore, serves to fine tune their local concentrations and gradients[11,13]. Therefore, both the molecular composition and physical properties of the ECM are necessary for the control of fundamental cell processes. Additionally, ECM integral role in regulating the spatial distribution of nutrients, gases, and soluble effector molecules also play an essential role[14]. It is also important to mention that cells secrete their own ECM, which becomes incorporated into the local environment[13].

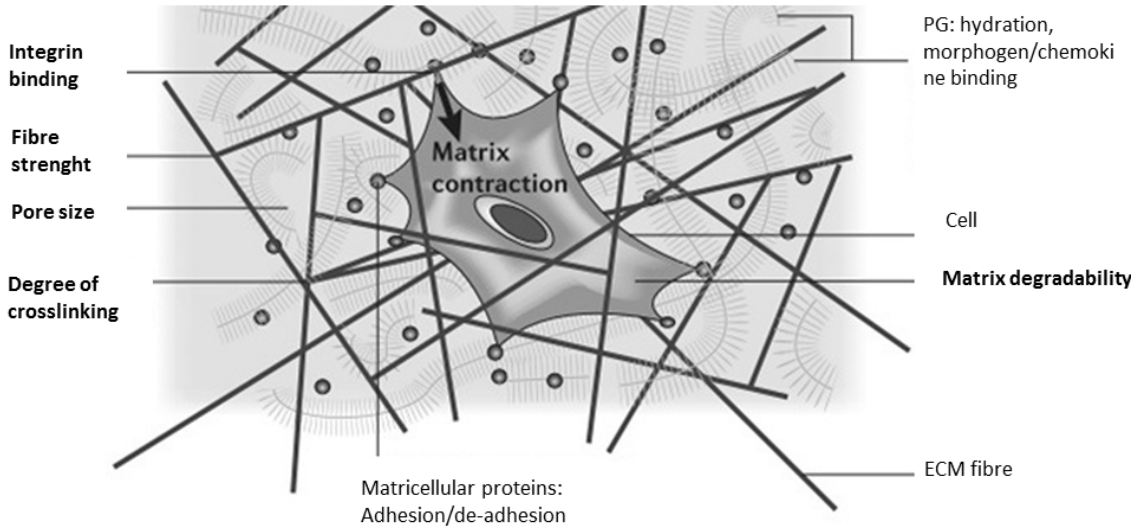

Figure 2.1-2: Extracellular matrix. The composition, architecture, and degree of crosslinking dictate the mechanical properties of ECM and control the transmission of mechanical forces to cells. Collagen fibers resist tensional and compaction forces, while proteoglycans (PGs) control hydration. PGs also hinder protein transport by their high, fixed charge density. Matrix composition also controls cell adhesion and migration. Furthermore, its sensibility to proteolytic enzymes will determine the ability of the cell to remodel the matrix and migrate through it. Image adapted from Griffith *et. al.* 2006[13].

Cell-ECM interactions: integrin and non-integrin receptors

Cell adhesion is fundamental for tissue formation and integrity. Moreover, for TE strategies it is essential to know how cells can interact with the ECM and transduce the information received by extracellular molecules into an intracellular event[22]. Adhesion molecules are functional receptors expressed in the cellular membrane that actively participate in physiologic and pathologic phenomena. Their underlying characteristic is their capacity of transducing signals and modulate signaling cascades. Cell surface possesses two kinds of receptors: integrin and non-integrin receptors.

Integrins are heterodimeric transmembrane receptors and the major group of adhesion receptors that connect cells to components of the ECM (Figure 2.1-3)[23]. In the case of human cells, it has been identified 18 α-subunits and 8 β-subunits which gives rise up to 24 distinct integrin heterodimers[24]. Both the integrin α and β subunits are type I transmembrane glycoproteins with

large extracellular domains followed by single-spanning transmembrane domains, with the exception of β4, which has a short cytoplasmic domain[25].

The cytoplasmic domains of both subunits are connected to the actin cytoskeleton of the cell via associated proteins also known as adaptor proteins[23]. This particular structure connects cells mechanically with their surrounding environment acting as "cellular sensors". Integrins work in a bidirectional signaling manner[24]. On one direction, the adhesiveness of integrins can be dynamically regulated in response to cytokines, chemokines or other stimuli in a process known as inside-out signaling. On the other direction, specific ligand binding as well as mechanical forces generate outside-in signals that trigger intracellular signal transduction cascades[23,25]. These signal transduction cascades play a crucial role in a wide number of cellular processes both physiological[23,26] and pathological[26–28]. In conclusion, cell surface integrin receptors and the contractile cytoskeleton pull against the ECM to sense the stiffness of the microenvironment, which initiate specific cellular responses by, for example, modulating changes in gene expression.

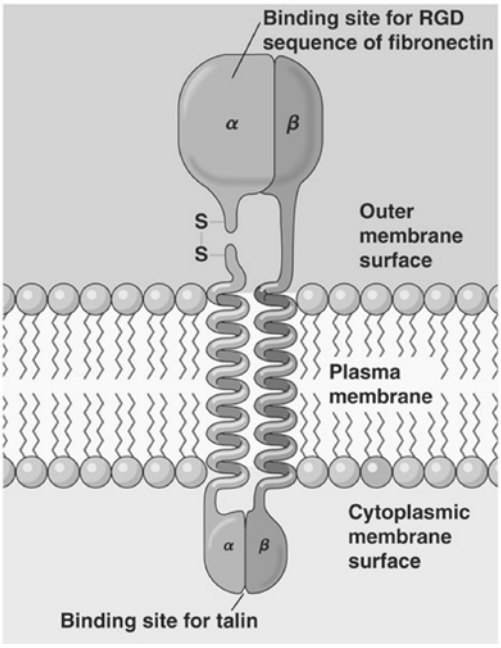

Figure 2.1-3: Integrin scheme. Transmembrane integrin receptors mediate cell adhesion. The extracellular head region generally binds ECM basement membranes or connective tissue, but it also can bind neighboring cells, bacterial polysaccharides, or viral coat proteins. Through all these interactions, integrins mediate different processes: (1) stable adhesion to basement membranes, (2) formation of ECM and migration on such matrices, (3) formation of platelet aggregates, (4) establishment of intercellular junctions in the immune system, and (5) bacterial and viral entry during infectious diseases. Furthermore, integrin-mediated adhesion modulates signaling cascades in control of cell motility, survival, proliferation, and differentiation. Image adapted from Pearson Education Inc.[29].

Non-integrin receptors are a wide range group of cell surface receptors not as widely studied as integrins. Proteoglycans, CD36, and laminin-binding proteins belong to this group and are the most analyzed. Among proteoglycans, syndecan and CD44 are the most widely studied. The first one is a transmembrane proteoglycan which GAG side chains are represented by

chondroitin sulfate and heparin sulfate[22]. Syndecan surface receptors bind to collagens, fibronectin, thrombospondin, and other ECM receptors[22]. CD44 is a cell surface glycoprotein which carries N- and O-linked sugars and GAG side chains[22]. It binds to type I and IV collagens and hyaluronan playing a vital role in cell adhesion and movement[22]. On the other end, CD36, also known as FAT (fatty acid translocase) is an integral membrane protein found on the surface of many cell types. It binds many ECM ligands including collagen, thrombospondin, anionic phospholipids, and oxidized LDL. Additionally, it directly binds to long chain fatty acid acids and may function in the transport and/or as a regulator of fatty acid transport[30]. In the case of laminin-binding proteins it is known that cells express many proteins (integrin receptors between them) that bind to laminin. The non-integrin receptor most amply studied is the 67 kDa laminin receptor (67LR) since it is an important molecule both in cell adhesion to the ECM and in signaling transduction following this binding event. This protein also plays critical roles in the metastasis of tumor cells[31].

Cell-cell interactions

Mammalian cells are in close contact and communicate one to each other. They are able to coordinate their behavior sending and receiving a variety of chemical signals. This ability is the hallmark of multicellular organisms. Therefore, cell-cell communication refers to the direct interaction between cell surfaces[32], which allow them to communicate in response to changes in their environment. Cell-cell communication via cell adhesion is critical for assembling cells into tissues, controlling cell shape and cell function. The major cell-cell adhesion sites are: tight junctions, anchoring junctions, and communication junctions. This division is based upon the function they serve[21,32].

Also called occluding junctions, tight junctions form the closest contact between adjacent cells, preventing small molecules from leaking between the cells and through the sheet (Figure 2.1-4a). This allows the sheet of cells to act as a cellular filament space wall within the organ, keeping molecules on one side or the other. Anchoring junctions mechanically attach the cytoskeleton of one cell to the cytoskeletons of other cells or to the extracellular matrix. They are commonest in tissues subject to mechanical stress, such as muscle and skin epithelium[32,33].

Anchoring junctions are multiprotein complexes found in all cell types where they stabilize the cells position, provide stability and rigidity, and support tissue integrity by holding cell sheets together (Figure 2.1-4b). Additionally, anchoring junctions regulate the motility of both single cells and cellular masses through their substrates. These anchor points are highly dynamic, primarily associated with actin filaments, and come in many different forms[34]. Anchoring junctions called desmosomes connect the cytoskeletons of adjacent cells while hemidesmosomes anchor epithelial cells to the basement membrane. Proteins called cadherins,

most of which are single-pass transmembrane glycoproteins, are responsible for creating the critical link[32].

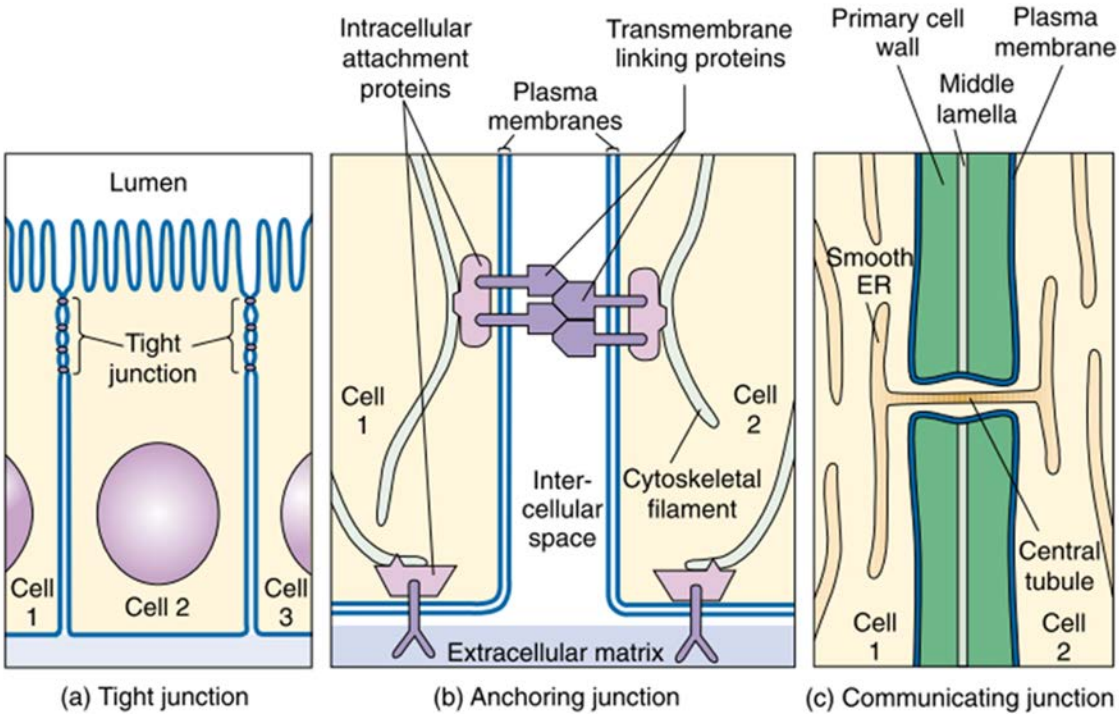

Figure 2.1-4: Types of cell junctions. These three models represent current thinking on how the structures of the major types of cell junctions facilitate their function. (a) Tight junction, (b) Anchoring junction, and (c) Communication junction. *From Biology. Chapter 7: Cell-cell interactions*[32].

The third group of cell-cell adhesion sites is communicating junctions, which allows the direct transfer of a chemical signal from one cell to an adjacent one (Figure 2.1-4c). In animals, these direct communication channels between cells are called gap junctions. Gap junctions are aggregates of intercellular channels composed of connexons, which are constituted by six identical transmembrane proteins (see Figure 1.1-10). The proteins within a connexon (called connexins) are arranged circularly to create a channel. A gap junction is formed when the connexons of two cells align perfectly, creating an open channel spanning the plasma membranes of both cells. These channels establish direct physical connections that link the cytoplasm of two cells together. The direct connection allows the transfer of small substances such as salts, sugars and amino acids, but prevent the passage of larger molecules such as proteins. The ability of adjacent cells to share ions through low-resistance pathways is fundamental to the function of electrically excitable cells, such as neurons, heart, and smooth muscle[32,35].

2.1.3 Self-assembling peptides as three-dimensional scaffolds

An overwhelming number of biomaterials have been developed to study, as well as to direct, cellular interactions in 3D[14]. Not only the theoretical base but also the technical procedure needs to be widely analyzed. These systems typically begin with a liquid precursor containing suspended cells, which gels or solidifies in a cytocompatible and hydrated manner[14]. The resulting gels might be porous to enable nutrient and waste exchange, and need to possess sufficiently mechanical properties to be self-supporting. Nanomaterials are emerging as the principal candidates to ensure the achievement of a proper instructive cell niche with good drug release/administration properties[36].

The discovery and development of self-assembling peptides (SAPs) revolutionized the TE community. By definition, self-assembly is the spontaneous organization of molecules into structurally well-defined arrangements, under thermodynamic equilibrium conditions, due to no covalent interactions[37,38]. Self-assembly is ubiquitous in nature. It has been observed that under variety of conditions, amphiphilic molecules spontaneously assemble into aggregates with tunable size and structure in response to change in their physical properties[39]. The nanofibers are 1000-fold smaller than synthetic polymer microfibers and similar in scale to ECM. This property allows mimicking better the 3D environment found *in vivo*. A widely studied SAP was EAK16-II, a 16 amino acid peptide found as a segment in the yeast protein, Zuotin. Its peculiarity is the alternating alanine (A, neutral charge), charges of glutamic acid (E, negative charge), and lysine (K, positive charge) with regularity: Ac-AEAEAKAKAEAEAKAK-NH2. This particularity creates a secondary bipolar structure that induce the self-assembly in high ionic strength medium. The interactions obtained after the self-assembly are weak and non-covalent (hydrogen bonds, ionic bonds, hydrophobic interactions, van der Waals interactions, and water-mediated hydrogen bonds)[40]. This type of nanofiber structure is stable under changes in temperature (T), pH, concentration of denaturing agents (urea, guanidinium hydrochloride), and degradation by proteolytic enzymes *in vitro*[39,41].

SAPs can be classified in three main blocks: (1) Type I, which forms β-sheet structures, (2) Type II, which forms both β-sheet and α-helix structures, and (3) Type III, which forms monolayers on surfaces. SAPs included in the first group are subclassified according to the scheme of repeating residues in each face of the peptide. Depending on the alternating positively and negatively charged arrangement of amino acids, peptides are divided in several moduli: (I) -+-+-+-+, (II) --++--++, and so on. The number following the peptide name is the modulus that belongs to. The most hopeful property of EAK16-II is its apparent lack of toxicity. Other SAPs models have been discovered with the same properties as EAK16-II. In this work, we focus our attention in RAD16-I[41].

PuraMatrix™ / RAD16-I Self-assembling peptide

RAD16-I (AcN-RADARADARADARADA-CNH2, R= Arginine (positive charge); A= Alanine (neutral charge); and D= Aspartic Acid (negative charge)) is a 16-residue peptide, member of the ionic self-complementary oligopeptide family. This type of oligopeptides consists of internally periodic repeats of alternating ionic hydrophilic and hydrophobic residues forming a β-sheet. The structure of the β-sheet present two differentiated surfaces: 1) one polar surface with regular repeating charged ionic side chains and, 2) a non-polar surface with alanine residues. Due to this structure, all charged amino acids lie on the same side providing them the capacity of self-assemble in the presence of monovalent cations. The self-assembly ends in the development of a nanofiber network with pores of 5-200 nm in diameter and over 99 % water content (Figure 2.1-5)[37,38]. The ionic side chains, complementary one to each other, form intermolecular ionic bonds, while methyl groups of alanine residues form hydrophobic β-sheet interactions (Figure 2.1-5c). Other features, like the intermolecular hydrogen bonds in conventional β-sheet, contribute to the formation and stability of the structure[42].

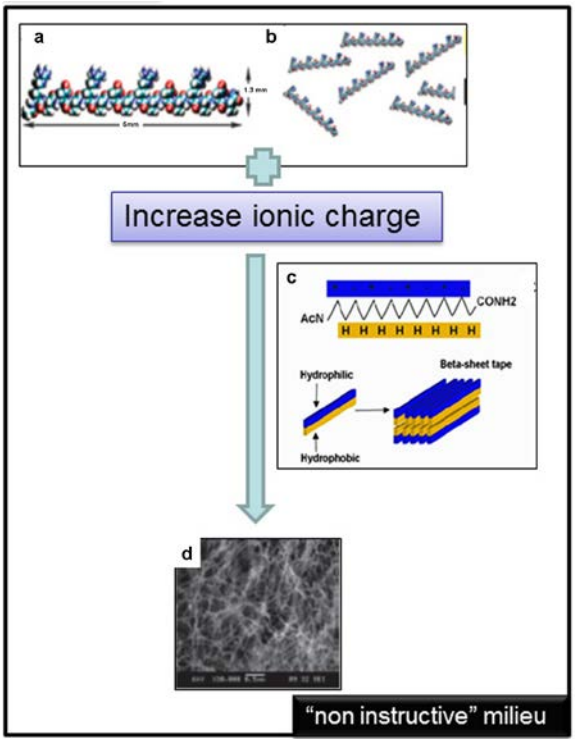

Figure 2.1-5: **Self-assembling process of RAD16-I peptide.** (*a*) Molecular model of the RAD16-I molecular building block. (*b*) Molecular model of RAD16-I molecules undergoing self-assembly. (*c*) RAD16-I peptide is formed by alternating hydrophilic and hydrophobic amino acids forming an antiparallel β-sheet configuration that self-assembles into nanofiber network. Increasing the ionic strength and adjusting pH to neutrality the peptide easily turns into a gel[43]. (d) The self-assembling peptide is examined by using scanning electron microscopy. (Scale bar, 500 nm.)[44].

It has been reported that the ionic strength (within a range) increase the stability of β-sheet structure inducing some order, and leads the self-assembly into a peptide matrix[45]. Monovalent ions do not have a particular position in the matrix structure, but their role is important because

they are the driving force that stimulate the self-assembly. These matrices are chemically and physically stable under physiological conditions and do not dissolve with heat neither in acidic or alkaline solutions nor dissolve upon addition of guanidine hydrochloride, SDS/urea or a variety of proteolytic enzymes[46,47]. Additionally, it has been demonstrated that RAD16-I produces no noticeable immune response, nor inflammatory reaction in animals, nor cytotoxicity[41].

Although RAD16-I has been shown to support attachment and/or differentiation of a variety of cell types, it does not contain any specific peptide signaling motif. Therefore, this environment can be defined as "non-instructive" milieu from the point of view of cell receptor recognition/activation[48].

During the last years, *Semino and collaborators* have been studying the effect of three-dimensional milieu based on RAD16-I in the behavior of different cell types. Indeed, *Garreta et.al*. cultured mouse Embryonic Stem Cells (mESC) and Mouse Embryonic Fibroblasts (MEFs) encapsulated in RAD16-I with the aim to analyze the differentiation into osteoblast-like cells. It was shown that mESCs acquired an osteoblast-like phenotype when cultured both in 2D and 3D conditions, but MEFs only underwent osteoblast differentiation when cultured in 3D RAD16-I system and induced with osteogenic inductors[49,50]. Another approach using this peptide scaffold is the one proposed by *Quintana et.al.* to study MEFs de-differentiation. Following *Garreta et al.*'s work, MEFs were cultured in RAD16-I, and it was detected that they only underwent osteogenesis after osteogenic induction whereas adipogenesis and chondrogenesis occurred with and without adipogenic/chondrogenic induction. Therefore, they concluded that MEFs cultured in 3D lost their fibroblastic phenotype and became chondrocyte-like cells[51]. *Fernandez-Muiños et.al.* continued the study analyzing the influence of matrix on the differentiation process as well as the potential participation of genes involved in early tissue organization. Interestingly, cells only underwent chondrogenic differentiation under certain mechanical conditions, characterized by low stiffness (G' ~ 0.1 kPa)[52]. Also in this area, *Bussmann et. al*. reported the development of chondrocyte-like constructs using human normal dermal fibroblasts (hNDFs)[53]. In parallel, *Genové et. al.* reported the functionalization of RAD16-I to enhance the formation of confluent cell monolayers of human aortic endothelial cells (hAEC)[38], and *Sieminski et. al.* demonstrated the ability of RAD16-I to support robust capillary morphogenesis[48,54]. *Genové et al.* also assessed a new way to culture rat hepatocytes preserving their distinct functionality[55] and *Wu et. al.* demonstrated the capacity of sandwich cultures with modified instructive self-assembling peptides to promote cell-matrix interaction[56]. In addition, recent studies developed by *Alemany-Ribes et.al.* have shown that cells respond differently to photodynamic therapy in 2D and 3D microenvironments based on RAD16-I (the effect in 3D is dramatically lower). Therefore, it

was confirmed that this 3D system aptly reproduces one of the most important factors limiting the efficacy of photodynamic therapy in clinical practice.

These results lead Dr. Semino's laboratory to hypothesize that this 3D-matrix would allow dedifferentiating adult cells into early precursors and/or into other lineages if the surrounding conditions were appropriate. Peptide scaffold provides a favorable microenvironment for normal progenitor cell kinetics and enhances cell differentiation[57]. It was also demonstrated the significance of the mechanical strength of peptides materials, which is proportional to the peptide concentration. Interestingly, collagen type I gel show similar stiffness at these concentrations, suggesting that both materials have similar mechanical properties, so it is possible that cells respond in a similar way growing in both scaffolds[43].

2.1.4 Study of specific factors effect on cell behavior

In vitro studies of cell behavior in different tailored environments may help to improve cell survival under low nutrient and oxygen conditions. In addition, this can enhance cell differentiation[58] in the infarcted tissue[59,60]. In this chapter, 3D systems of RAD16-I with various modifications and distinct chemical inductions are analyzed to evaluate the effect on cell maintenance and differentiation towards the cardiac phenotype.

Matrix modification

Biomaterial science has taken a step forward with designed nanofibers to render more biomimetic scaffolds. In this sense, tailored SAPs have been designed. A novel and promising strategy combines SAPs with functional motifs. These hydrogels have been modified with dextran macromolecules, laminin and collagen motifs, integrin-binding sequence, laminin receptor binding sequence, and heparin-binding sequence. These modifications could be useful to better mimic cardiac environment or even for further *in vivo* implantation to improve cardiac function after MI. It is strongly believed that the attachment of functional motifs to the nanofibers of the engrafted scaffold combined with cell delivery could have a beneficial effect.

Several peptide motifs have been described to improve myogenic activity with the aim to maintain phenotype, allow cell-cell contact, establishment of gap-junctions, as well as cellular viability[38]. The cell-adhesion motif RGD (R: arginine, G: glycine, D: aspartic acid) that derives from fibronectin is, by far, the most characterized and often employed functionalization system. This recognition motif has shown to display high biological activity on cell anchoring, growth, migration, survival, and differentiation of encapsulated cells[61]. Focusing on the obtaining of a functionalized matrix scaffold, RAD16-I peptides were blended with small proportions (1-5 %) of RAD16-I peptides modified to contain the RGD motif. These modified peptides were synthesized by extension of RAD16-I sequence at the amino terminal (RAD-RGD peptide,

Table 2.1-1). Additionally, in order to keep the active sequence free and active, two glycines were added between the main chain and the new sequence.

Table 2.1-1: RAD16-I / RADRGD. Sequences of RAD16-I and RAD16-I modified with RGD.

PEPTIDE	SEQUENCE
RAD16-I	AcN-RADARADARADARADA-$CONH_2$
RADRGD	AcN-GP**RGD**SGY**RGD**S-GG-RADARADARADARADA-$CONH_2$

The binding domains of heparin, that has numerous important biological roles associated with its interaction with diverse proteins, are also interesting motifs to analyze. The presence of heparin can allow better control of local gradients of matrix-binding molecules such as GFs, chemokines or others, which can be maintained in the matrix and later released proteolytically[13,62,63]. Heparin is widely used as an anticoagulant, but its real physiological role remains unclear[64]. It is a linear polydisperse sulphated polysaccharide consisting mainly of repeating units of 1→4-linked pyranosyluronic acid and 2-amino- 2-deoxyglucopyranose (glucosamine) residues. The presence and frequency of these saccharide units vary with the tissue source from which heparin is obtained (Figure 2.1-6). It possesses the highest negative charge density of all known biological macromolecules with an average of 2.7 negative charges per disaccharide provided by sulfonic and carboxyl groups. Consequently, the most common binding interaction between heparin and proteins is through ionic interactions. However, non-electrostatic interactions such as hydrogen bonding and hydrophobic interactions can also contribute to the stability of heparin–protein complexes[65,66]. The sequestering of GFs helps to localize their activity, protect them from degradation, and in some cases enhance their binding to a cell surface receptors[67]. Moreover, heparin can participate in the modulation of various cellular functions such as cell growth, differentiation, morphology, and migration[68]. For this reason, and due to their functional resemble the native ECM polymeric GF delivery systems based on heparin are widely used[69]. Similar strategies report the binding of heparin with other types of materials through covalent interaction with polymers such as alginate, polycaprolactone and collagen or entrapped within chitosan[62,70–73].

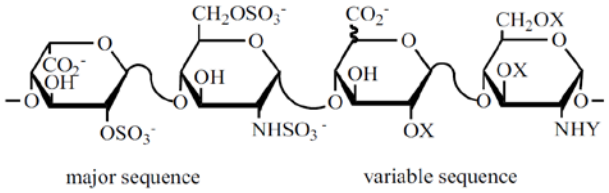

Figure 2.1-6: Heparin structure. Heparin is a linear polysaccharide with variable composition consisting on repeating units of disaccharides with its primary sequence contains an uronic acid residue and a glucosamine residue. Its composition varies depending on the tissue.(X= H or SO_3^-; Y= Ac or SO_3^-). Image adapted from Murugesan et al. 2008 [65].

Chemical and biological induction

Enhancement of cardiomyogenic differentiation has been extensively assessed on different sources of human SCs by exposure to several chemical and biological stimuli[1]. ESCs are capable of spontaneously differentiate into cardiomyogenic lineage *in vitro* (even in the absence of cytokines and GFs)[1]. However, in the case of adult stem cells (ASCs) there is no evidence of differentiation in the absence of stimulation of exogenous cytokines and GFs. However, it has been reported that specific biological activity and interactions can be facilitated through the addition of soluble or insoluble factors and biological domains[14].

The members of transforming growth factors beta superfamily (including TGF-β1 itself, and bone morphogenic protein 2 (BMP-2) and 4 (BMP-4)) have been extensively reported to induce cardiomyogenic differentiation in ESCs. Other GFs implicated in cardiomyogenic differentiation are insulin-like growth factor I (IGF-I), platelet-derived growth factor (PDGF), basic fibroblast growth factor (bFGF), oxytocin, and erythropoietin. They have been reported to regulate cardiac specification of mesodermal progenitors and trigger expression of cardiac proteins. In addition, a number of chemical compounds have been reported to induce cardiomyogenic differentiation *in vitro*. Chemicals result to be less labile, with longer active half-life in solution than proteins, and are easily manufactured. Therefore, they are structurally and chemically more defined compared to proteins. Some of the synthetic chemicals known to promote cardiomyogenic differentiation *in vitro* are 5-azacytidine (5-aza), dimethyl sulfoxide (DMSO), L-ascorbic acid 2-phosphate (Aa 2-P), and retinoic acid (Ra). 5-aza is a nucleoside used as inhibitor of DNA methylation and said to be a potent inducer of cardiomyogenic potential of ESCs and ASCs (in particular bone marrow mesenchymal stem cells (BM-MSCs)). DMSO has shown effective differentiation on ESCs[74,75], the same as Aa 2-P and Ra which are derivatives of vitamin A. Finally, the most effective strategy, reported until now, to enhance the transdifferentiation of SCs is its co-culture with freshly isolated CMs[58].

RECATABI consortia used the protocol described by Smits and coworkers to induce cardiogenesis and CM differentiation *in vitro*. In this protocol, a combination of 5-aza treatment, followed by TGF-β1 and Aa 2-P stimulation was used to achieve a high-differentiation efficiency in 2D cultures of human CM progenitor cells[76]. Recently it has been reported to also induce cardiomyogenic differentiation of adipose-derived stem cells[77]. 5-aza induces the expression of cardiac-specific proteins, but the mechanism by which the expression of these specific markers is increased is unclear. Unfortunately, this treatment is not suitable for further use in patients. Demethylation is not specific for early cardiac genes, but their effects are random. So, this is possible that this treatment leads to tumorigenic cells.

TGF-β1, transforming growth factor-beta 1, is a key molecule in the regulation of the differentiation switch. It simultaneously inhibits adipogenesis and activates myogenesis, enhancing cardiomyogenic differentiation. Aa 2-P, a stable form of vitamin C, increases the expression of muscle-specific glucose and ion transporters. Vitamin C can promote muscle differentiation likely through the increase of myogenic expression, which may in turn regulate muscle differentiation *in vivo*. Both, hormones and GFs are important regulators of myogenic cell differentiation, but little is known about the effect of vitamins on muscle differentiation and development[78].

Induction cardiac medium used was prepared with Iscove's Modified Dulbecco's Medium and HAMF12 Nutrient Mix, GlutaMAX™ supplement. The first one is a highly enriched synthetic media well suited for rapidly proliferating, high-density cell-cultures. The second one contains a wide variety of components (zinc, putrescine, hypoxanthine, and thymidine between others), and it is highly recommended to reduce the serum concentration. The combination of these media was supplemented with insulin-transferrin-selenium (ITS), minimum essential media, alpha (α-MEM), horse serum (HS), TGF-β1 and vitamin C. ITS has been reported to be required for optimal performance of serum-free media: insulin promotes glucose and amino acids uptake, lipogenesis, intracellular transport of proteins and nucleic acids; transferrin is an iron carrier and it may also help to reduce toxic levels of oxygen radicals and peroxide; and selenium, as sodium selenite, is a co-factor for glutathione peroxidase and other proteins, used as an anti-oxidant in media. About HS, it is known to contain twice the protein content and low concentration of trace elements than fetal bovine serum. It has been widely used for CMs maintenance and differentiation. With the aim to increase cell growth and viability, α-MEM was also added to supplement the medium.

This protocol does not reach the high Good Clinical or Manufacturing Practice requirements because of the use of 5-aza. However, the proposed system could provide a framework for clinical adaptation[76]. Our working hypothesis sustains that providing a "non-instructive" 3D microenvironment with the nanometric scaffold RAD16-I would replace the role of 5-aza in the cardiogenic medium. Therefore, we suggest that seeding subATDPCs in a proper 3D environment together with some cardiogenic induction could promote enhancement of cardiac lineage.

2.2 PREVIOUS RESULTS

2.2.1 Combination of RAD16-I and heparin [79]

One of the general aims of the RECATABI European Project was to design and fabricate a new biomaterial nanofiber matrix for controlled release of cell/tissue-inducing factors. This work was developed by Dra. Maria Teresa Fernández-Muiños, and was presented in her thesis entitled "*Effect of the microenvironment in the in vitro chondrogenic and osteogenic differentiation of mouse embryonic fibroblasts*".

Briefly, she evaluated the possibility of combining self-assembling peptide (RAD16-I) with heparin in different blended ratios in order to obtain a new biomaterial composite with good mechanical, structural and biological properties. The chemical and structural stability of the mix were assessed observing the formation of homogeneous hydrogels. Moreover, scanning electron microscopy (SEM) and circular dichroism (CD) results showed that the presence of heparin does not interfere in the nanofiber formation.

Once analyzed the influence of heparin in the self-assembling process and nanofiber formation, it was tested the capacity of the composite to be used as a drug delivery hydrogel. For this purpose, a non-cumulative quantification of the vascular endothelial growth factor 165 ($VEGF_{165}$) angiogenic factor released by the composite and the control RAD16-I self-assembling peptide was performed. Two different kinetics releases were observed for each scaffold. Interestingly, in the case of peptide-heparin composite a gradual release of $VEGF_{165}$ over time was observed during the 36 hours of experiment (Figure 2.2-1b). These results clearly indicate that the self-assembling-heparin hydrogel is a good composite biomaterial to bind and release physiologically significant quantities of $VEGF_{165}$ *in vitro* during the first 24-36h, which could be used to promote a pro-angiogenic effect in an *in vivo* model.

In order to know if the released GF was biologically active, a functional study was performed, with human umbilical vein endothelial cells (hUVECs). The results showed that the released GF have an effect of on hUVECs survival, maintenance and proliferation. Control groups without GF presented high mortality (Figure 2.2-1b). These results confirm that $VEGF_{165}$ maintained their biological activity after being released from the hydrogels. No significant differences, in terms of cell number, were found between the GFs released from RAD16-I or the composite.

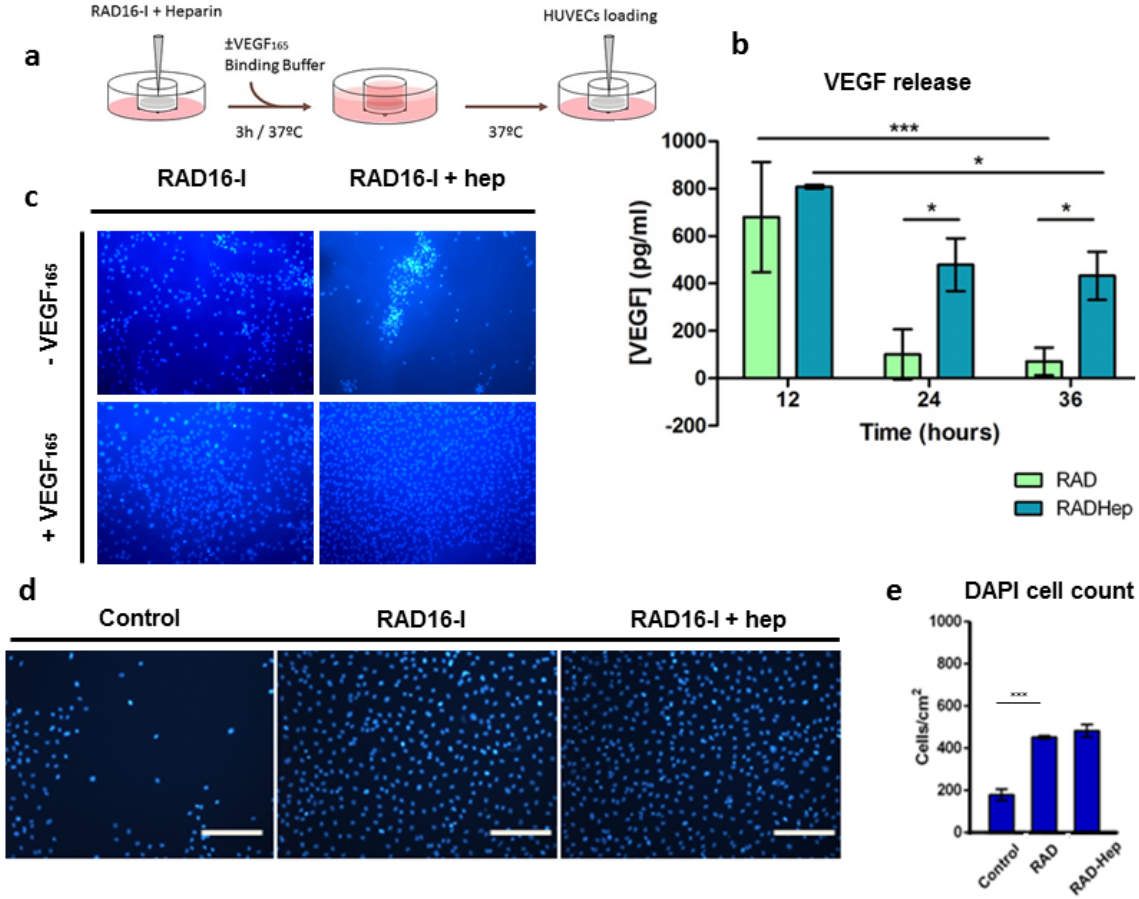

Figure 2.2-1: Analysis of RAD16-I and heparin combination effect. (a) *Schematic process of the binding and release experiments.* Gels were prepared and incubated with $VEGF_{165}$ in binding buffer for 3 hours at 37 ºC. Then, the GF solution was removed, and the gels were incubated with binding buffer to allow the release of $VEGF_{165}$. (b) *Noncumulative release of $VEGF_{165}$.* After taking each sample, all the media was removed, and new media was added to the gels. (c) Effect of heparin and $VEGF_{165}$ in cell proliferation. (d) *Functional study of released $VEGF_{165.}$* $VEGF_{165}$ maintains its biological activity after being released by the gel. (e) DAPI cell count for the functional study *of released $VEGF_{165.}$* Cell number was significantly higher for samples supplemented with the $VEGF_{165,}$ released by the gels.

2.2.2 Cells used in RECATABI project

The cells used in this thesis were the ones designed for the RECATABI European Project. One of the candidates were BM-MSC which are able to transdifferentiate partially into cardiomyogenic lineage, but they were discarded because they rapidly undergo senescence during *in vitro* expansion [80]. As we would need a large cell number, adipose tissue-derived progenitor cells (ATDPC) appear as a possible candidate. These cells have similar surface markers as BM-MSC[81] and can be easily isolated and expanded *in vitro*. Dr. Antoni Bayés-Genís group IGTP isolated ATDPCs from fad pads between skin and sternum from patients undergoing cardiac surgery. These cells were carefully characterized for their superficial antigen profile, proliferative properties, and gene and protein expression. These cells will be referred as subcutaneous ATDPCs (subATDPCs).

SubATDPCs superficial antigen profile and proliferative properties analysis

A standard protocol for subATDPCs isolation and expansion was defined and validated by Dr. Carolina Soler-Botija in *Hospital Germans Tries i Pujol* (IGTP). The protocol was approved by the local Ethics Committee and informed consent was obtained from all patients. The study protocol conformed to the principles outlined in the Declaration of Helsinki.

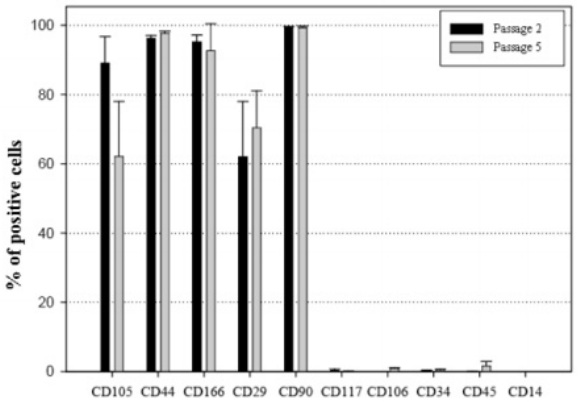

Figure 2.2-2: Subcutaneous ATDPCs superficial antigen profile. SubATDPCs express CD105, CD166, CD29, CD44 and CD90; reveling a mesenchymal stem cell (MSC)-like pattern both at passage 2 and passage 5.

SubATDPCs were characterized using immunophenotipycal analysis to define the cells based on the molecules present on their surface. BM-MSCs were used as control cells. The clusters of differentiation analyzed were: CD105, CD44, CD166, CD29, CD90, CD117, CD106, CD34, CD45, and CD14. Flow cytometry levels of each antigen were defined by the ratio between specific antibody and IgG isotype control (1 = no difference). The results obtained showed that BM-MSCs express CD105, CD44, CD166, CD29, and CD106 (data not shown), while subATDPCs express CD105, CD44, CD166, CD29, and CD90; reveling a MSC-like pattern (Figure 2.2-2). SubATDPCs were also demonstrated to be capable of differentiate towards an adipogenic and osteogenic phenotype as it can be observed in Figure 2.2-3.

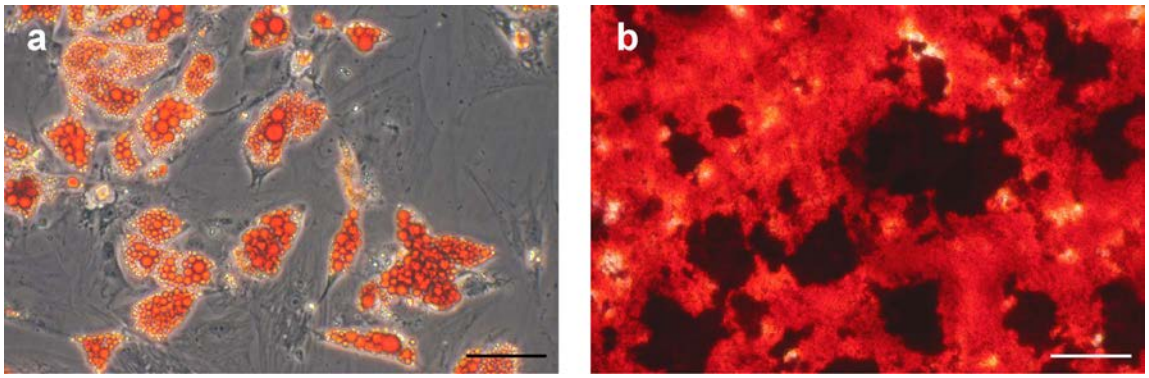

Figure 2.2-3: *In vitro* characterization of subATDPCs cultured in monolayer. (a) Oil Red O staining of subATDPCs cultured in adipogenic differentiation medium showing lipid droplets depositions (red). (b) Von Kossa staining of subATDPCs cultured in osteogenic differentiation medium with the presence of calcium depositions (red). Scale bars 100μm.

On the other hand, proliferative analysis was carried out. The assay was performed in samples from six different patients to confirm reproducibility. The assay revealed subATDPCs duplication time was 3.1 days (Figure 2.2-4).

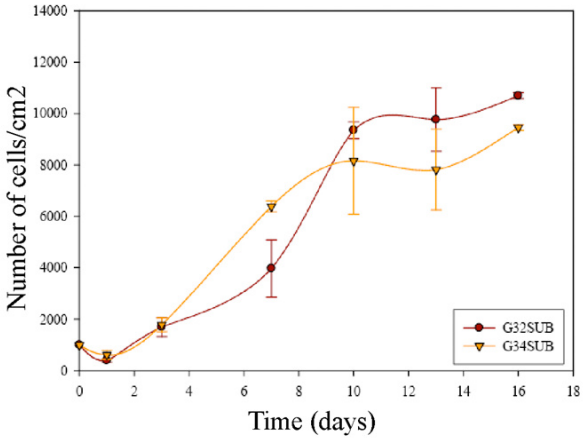

Figure 2.2-4: Subcutaneous ATDPCs duplication time. Cell number per cm^2 of two different pools of subATDPCs.

Compilation of data from cardiac-specific genes, establishment of a gene profile and protein analysis

The cardiomyogenic potential of subATDPCS was assessed by IGTP group. Part of his work was to analyze gene and protein cardiac profile by qRT-PCR, western blot and immunocytofluorescence staining. The expression of sarcomeric α-actinin (ACTN1), Sarcoplasmic/Endoplasmic Reticulum Calcium ATPase 2 (SERCA2), Gap Junction Protein alpha 1 (GJA1 - also known as Connexin-43, Cx43), Transcription Box Transcription Factor 5 (TBX5) transcripts, Myosin Heavy Chain (MHC), cardiac Troponin I (cTnI), Insulin Gene Enhancer protein (ISL1), GATA binding protein 4 (GATA4), and NK2 Transcription Factor Related Locus-5 (NKX-2.5) were analyzed.

The results of qRT-PCR revealed that subATDPCs expressed *ACTN1*, *SERCA2*, *GJA1*, and *TBX5* transcripts, whereas no gene expression of *MHC*, *cTnI*, *ISL1*, *GATA4* and *NKX-2.5* was observed (Figure 2.2-5A). Protein expression was assessed by Western blotting showing expression of ACTN1, SERCA-2, and GJA1 at passage 5 (Figure 2.2-5B). Immunocytofluorescence at passage 5 was also performed to determine cell distribution of the cardiac markers GATA4, SERCA2, cTnI, TBX5, NKX2.5, ACTN1, MHC, and GJA1. Immunostainings were performed with samples from four different patients. The immunocytofluorescence results (Figure 2.2-5C) show expression of ACTN1, SERCA2, and GJA1 as well as a weak signal of TBX5 transcription factor. No expression of GATA4, cTnI, MHC or NKX2.5 was detected.

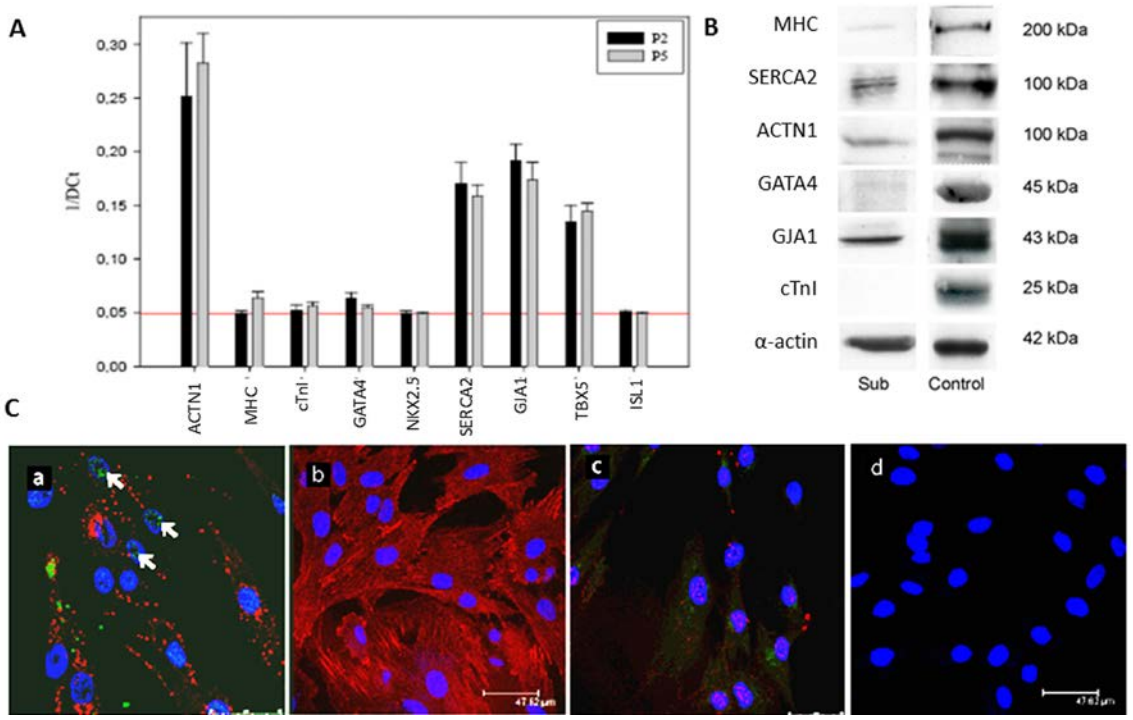

Figure 2.2-5. Study of cardiac specific genes expressed by subATDPCs. (A) SubATDPCs gene expression profile at passage 2 and 5 by qRT-PCR. (B) SubATDPCs cardiac protein expression profile by western blotting. (C) Immunocytofluorescence staining of subATDPCs. (a) TBX5 (green) and GJA1 (red) expression. Arrows indicate nuclear TBX5 signal. (b) ACTN1 (red) expression. (c) SERCA2 (green) and GATA4 (red) expressions. (d) MHC and cTnI immunostaings. Nuclei were counterstained with Hoescht 33342 (blue).

2.3 SPECIFIC AIMS

In vitro models are of great interest to analyze specific factors of human physiology or pathophysiology. These systems provide a simplistic way to examine individual factors as compared to animal models, and better mimic the reality than 2D models. In this sense, the primary objective of this chapter is to better understand subATDPCs behavior when they are encapsulated in a the 3D environment provided by RAD16-I self-assembling peptide. Thus, the specific aims for this chapter are the following:

- To evaluate subATDPCs viability and behavior in the self-assembling peptide scaffold RAD16-I peptide as a function of peptide concentration and cell number. Determine the best conditions to seed these cells in RAD16-I matrix for further analysis (section 2.5.3).

- To study the effect in subATDPCs viability and behavior of RGD motif and heparin polysaccharide modifications in RAD16-I matrix (section 2.5.4 to 2.5.6).

- To assess the potential of subATDPCs to undergo proliferation in RAD16-I 3D cultures prepared with and without RGD and heparin polysaccharide modifications, under different conditions (section 2.5.7).

- To study gene and protein expression of subATDPCs in RAD16-I 3D cultures prepared with and without RGD and heparin polysaccharide modifications, under different conditions (section 2.5.8).

2.4 MATERIALS AND METHODS

2.4.1 Cell culture

Subcutaneous adipose tissue-derived progenitor cells isolation: SubATDPCs were isolated from fat pads between skin and sternum from patients undergoing cardiac surgery by Dr. Antoni Bayés-Genís in Hospital Germans Trias I Pujol (IGTP). Informed consent was obtained from all subjects, and the study protocol conformed to the principles outlined in the Declaration of Helsinki. Adipose tissue biopsy samples were processed as previously described [82,83]. Briefly, samples were rinsed with phosphate buffer saline (PBS - Sigma; D8537-500mL) and cut into small pieces, removing visible blood vessels; thereafter, cells were isolated by collagenase II (Gibco; 17101-015) digestion. Adhered cells were grown under standard conditions (37 °C in 5 % CO_2 humidified atmosphere) in Minimum Essential Medium, alpha (α-MEM - Sigma; M4526) supplemented with 10 % fetal bovine serum (FBS - Lonza; DE14-801F; Lot 1SB003), 1 % (v/v) penicillin-streptomycin (P/S - Labclinics; P11-010), 1 % L-glutamine (Labclinics; M11-004) and 5 µg/mL plasmocin (InvivoGen; ANT-MPT).

Subcutaneous adipose tissue-derived progenitor cells culture: Culture flasks obtained for each patient were maintained for two passages to assure viability, correct growing and mycoplasma contamination. Unlike bacterial or fungal contaminations, mycoplasma contaminations cannot be detected by visual inspection and may not noticeably affect cell culture growth rates. However, mycoplasma infection has been shown to alter DNA, RNA and protein synthesis, introduce chromosomal aberrations and cause alterations or modifications of host cell plasma membrane antigens. For this reason, this step is important for further analysis.

At passage 2, when cell density was about 20,000 cells/cm^2, they were detached using Trypsin-EDTA 0.05 % - 0.02 % (Invitrogen; 25300-062) and pools from 5 different patients were prepared. Each pool was registered with a letter, expanded during 3 more passages, and frozen at passage 5. Each passage was performed when a high level of confluence was reached (90 % approx.). The velocity to reach a confluent culture depends on the cellular type and the passage of the cells (number of cell divisions), in this case, the confluence was obtained after one week of culture. The medium was changed on alternate days.

Subcutaneous adipose tissue-derived progenitor cells freezing and thawing: SubATDPCs (passage 5) were detached using Trypsin-EDTA 0.05 % - 0.02 % (Invitrogen; 25300-062) and counted to be resuspended at a final concentration of 1 million cells/0.5 ml. The freeze medium (used at 4 ºC) was based on FBS with 5 % of dimethyl sulfoxide tissue culture tested (DMSO - Sigma; D2650). DMSO acts as a cryoprotector in order to avoid cellular membrane fracture by reducing the formation of intracellular water crystals. The freezing process was performed slowly by decreasing the temperature of the cells suspended in freezing medium from 4 ºC to

-80 ºC in several hours (24 hours). Aliquots of 0.5 mL per cryotube were prepared. SubATDPCs were maintained at -80 ºC up to a year. On the other hand, the thawing process must be completed quickly. As the cryotube was taken out -80 ºC freezer, it was directly submerged in a bath at 37 ºC until only a little part of cell suspension remained frozen. Then, the cellular suspension was mixed carefully with 10 ml culture medium pre-warmed at 37 ºC. The cells were centrifuged at 1,000 g during 5 minutes, and the supernatant suctioned to eliminate the remaining DMSO. The pellet was resuspended and seeded in T75 flasks. The fast thawing process avoids the osmotic exchanges through the plasmatic membrane between the cells and the medium.

2.4.2 RAD16-I self-assembling peptide preparation

Four different peptide variations of RAD16-I were analyzed: RAD16-I 0.3 % (w/v) without modifications, RAD16-I/RADRGD (95:5) 0.3% (w/v), RAD16-I 0.3% (w/v) with heparin (570:1) and RAD16-I/RADRGD (95:5) 0.3 % (w/v) with heparin (570:1). Shortly, 1 % nanofiber peptide (PURAMATRIX^{TM} - Corning; 354250), was diluted to obtain a solution of 0.3 % RAD16-I in sucrose 10 % (Sigma; S1888) as follows: 300 µL of RAD16-I were combined with 300 µL of sucrose 20 % and 400 µL of sucrose 10 %. In parallel, 30 µL of 1 % water solution RADRGD (synthesized by Peptide 2.0) was combined with 30 µL of sucrose 20 % and 40 µL of sucrose 10 % to obtain a solution of RADRGD 0.3 %. Afterwards, RAD16-I 0.3 % and RADRGD 0.3 % were mixed in a blend ratio of 95:5. To obtain the peptide with heparin, RAD16-I 0.3 % and RAD16-I/RADRGD 0.3 % were mixed with heparin 0.01 % in a blend ratio of 95:5.

2.4.3 Three-dimensional cultures

Assembly using cell culture insert: SubATDPCs pools were thawed at passage 5 and expanded until passage 7. At passage 7, cells were trypsinized, washed with sucrose 10 %, and resuspended in sucrose 10 % to render $1.6 \cdot 10^5$ cells in 40 µL (the experiments with different cell densities were adapted). All 3D cultures (encapsulations) start at passage 8. Three-dimensional constructs for each peptide variation, previously described, were prepared mixing equal volume of the cell suspension and nanofiber peptide obtaining a final cell suspension containing $2 \cdot 10^6$ cells/mL. The mixture was thoroughly mixed by pipetting, and 80 µL were loaded into each 9-mm-diameter cell culture insert (PICM01250, Millipore, Billerica, MA) already placed inside a 6-well culture plates with 500 µL of media outside the insert to wet the membrane[51]. The medium penetrated in the insert from the bottom membrane inducing a bottom-to-top self-assembly of RAD16-I and thus the formation of a gel with cells suspended inside. Medium was added carefully in sequential steps on the top of the hydrogel and allowed to infiltrate, to wash out the remaining sucrose. Finally, 500 µL were loaded inside the insert

and 2.5 mL in the well. On alternate days, 500 µL of medium was discarded from the well and 500 µL of fresh medium was added carefully on the wall of the insert until the end of the experiment. Incubation was performed, in the same way, as in 2D cultures (37 ºC, 5 % CO_2). A scheme of the defined protocol is presented in Figure 2.4-1.

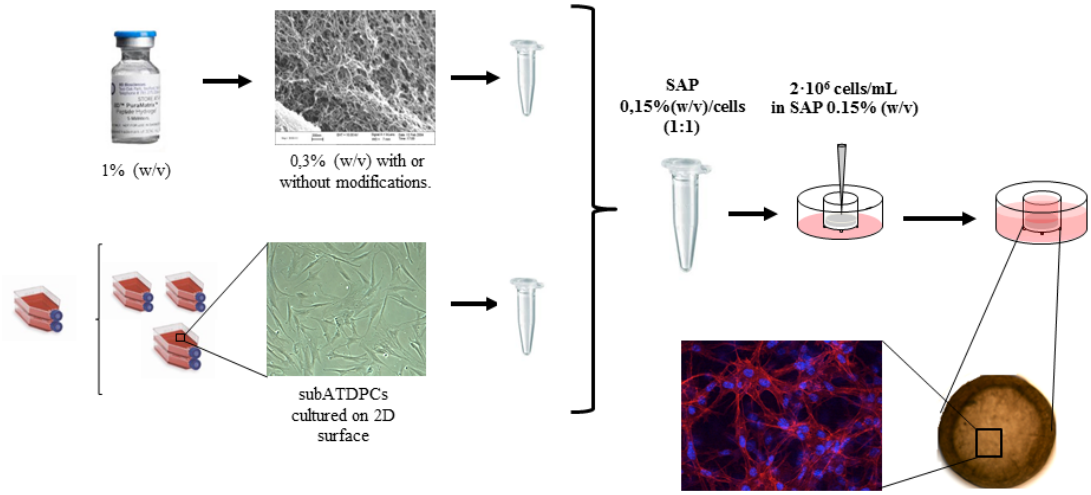

Figure 2.4-1: Three-dimensional cultures assembly scheme. Firstly 2D cultures were trypsinized and expanded until passage 7. RAD16-I 0.3 % was mixed with cell solution ($4 \cdot 10^6$ cells/mL) in a blend ratio of 1:1. The mixture was loaded inside a 9-mm-diameter cell culture insert already placed in 6-well culture plates with 500 µL of media outside the insert to wet the membrane. In the case of the protocol where the assembly was performed without cell culture insert, the mixture was loaded inside 48-well plates previously filled with 150 µL of medium.

Assembly without cell culture insert: With the aim to avoid the use of cell culture inserts, an alternative protocol was established. Previous steps to the loading of the mixture were performed, in the same way, as with cell culture inserts. In this case, cell culture inserts were discarded and instead of 6-well plate, 48-well plates without treatment for cell culture (Labclinics; PAA30048X) were used. Each well was filled with 150 µL of medium, and the mixture of RAD16-I and cells was loaded quickly but carefully in the middle of the well. The viscosity of the RAD16-I and the low volume of medium allow maintaining the two liquid phases immiscible. The ionic strength of the medium induces RAD16-I self-assembling and thus the formation of a gel with cells encapsulated. It is important to load the mixture in one step carefully and assure not to touch the medium with the end of the tip. Medium was added and removed carefully in sequential steps, to wash out the remaining sucrose. Finally, all wells were filled with 800 µL of medium. On alternate days, 400 µL of medium was discarded from the well and 400 µL of fresh medium was added carefully until the end of the experiment. Incubation was performed, in the same way, as in 2D cultures (37 ºC, 5 % CO_2).

3D cultures maintaining: All 3D constructs were maintained in control medium during 4 days, when the medium was completely replaced. Half of the 3D constructs were induced with cardiac induction medium while the other half of the samples was refilled with control medium.

Samples were picked 2 and 4 weeks after induction for their analysis, and cells seeded in 2D cultures were taken as control.

Control medium was based on α-MEM and supplemented with L-glutamine and 10 % FBS. Two formulations of α-MEM were tested: α-MEM from Sigma and α-MEM from Labclinics. The cardiac induction media used was based on the culture media described by A. Smits *et. al.*[76] with slightly differences. Induction cardiac medium was prepared using Iscove's Modified Dulbecco's Medium (IMDM - Gibco; 2198032), and HAMF12 Nutrient Mix, GlutaMAX™ supplement (Gibco; 31765027). The combination of these media was supplemented with ITS (Gibco, 41400-045), α-MEM 100x (Lonza, BE13-114E), HS (Sigma, H1138-100mL), Aa 2-P (Sigma, A4403), and TGF-β1 (Millipore, GF111).

Both media (control and cardiac) were treated for possible contaminations of bacteria or mycoplasma. Penicillin/Streptomycin (P/S) was used to avoid bacterial contamination against gram-positive and gram-negative bacteria. Regarding on mycoplasma contamination Plasmocin™ was added to the medium. This product contains two bactericidal components. The first component acts on the protein synthesis machinery by interfering with the ribosome translation, and the other one acts on DNA replication. These two specific and separate targets are found in mycoplasma and many bacteria, but are entirely absent in eukaryotic cells. In contrast to other anti-mycoplasma compounds, Plasmocin™ is active on both free mycoplasmas and intracellular forms.

The composition of both media is presented in Figure 2.4-2.

CONTROL MEDIUM:	**CARDIAC INDUCTION MEDIUM:**
44 mL αMEM (Sigma; M4526)	23.5 mL IMDM (Gibco; 2198032)
0.5 mL P/S (Labclinics; L11-010)	23.5 mL HAM F12 Nutrient Mix, GlutaMAX™ supplement (Gibco; 31765027)
0.5 mL Glutamine (Labclinics; M11-004)	0.5 mL P/S (Labclinics; L11-010)
5 mL FBS (Lonza; DE14-801F)	0.5 mL αMEM (Lonza; BE13-114E)
10 µL plasmocin (InvivoGen; ANT-MPT)	0.5 mL insulin-transferrin-selenium (Gibco, 41400-045)
	2 mL HS (Sigma; H1138-100ML)
	10 µL plasmocin (InvivoGen; ANT-MPT)
	Freshly add:
	88 µL Ascorbic acid 10mg/mL (Sigma; A4403-100MG)
	50 µL TGF-β1 1µg/mL (Millipore, GF111)

Figure 2.4-2: Culture media. Two culture media were prepared for the *in vitro* experiments. Control medium do not contain induction factors while cardiac induction medium was supplemented with various factors known to induce cardiac differentiation in different cell types. Both media were protected again bacterial and mycoplasma contamination with P/S and Plasmocin™, respectively.

2.4.4 Macroscopic and microscopic analysis of 3D cultures

With the aim to analyze the macroscopic behavior of 3D constructs, all samples were analyzed under Stereoscopic microscope Nikon digital Slight DS-2MV, while network formation was followed using Nikon Eclipse TE2000-1 microscope.

2.4.5 Congo Red staining

Congo Red staining was performed to analyze the presence of the β-sheet structure characteristic of the self-assembling peptide RAD16-I. Samples were incubated with 0.1 % (w/v) Congo Red in water for 5 minutes and washed several times with PBS. Finally, the samples were analyzed under Stereoscopic microscope Nikon digital Slight DS-2MV.

2.4.6 Toluidine Blue staining

Toluidine Blue staining was performed to analyze the presence of highly negative charges provided by the heparin molecules. Briefly, samples were washed with PBS, incubated with Toluidine Blue 0.05 % (w/w) in water during 20 minutes, and washed several times with water. Finally, the samples were analyzed under Stereoscopic microscope Nikon digital Slight DS-2MV.

2.4.7 Live and dead staining (L&D)

The viability of the cells cultured in 3D cultures was assessed using two-colour fluorescence cell viability assay based on intracellular esterase activity and plasma membrane integrity (LIVE/DEAD® Cell Viability Assays, Invitrogen; L-3224). Calcein AM presents an uniform green fluorescence in live cells by detecting intracellular esterase activity while, ethidium homodimer-1 bromide (EtBr) produces a bright red fluorescence by entering in dead cells with damaged membranes and binding to nucleic acids. Shortly, medium was removed, and 3D samples were rinsed with PBS (Labclinics; H15-002). After washing the encapsulations were immersed in PBS containing 1 µL calcein AM and 2 µL EtBr of the stock kits. After 15 minutes the staining solution was removed, and the samples were washed three times with PBS for 30 min. Images were taken with Zeiss AxioVert 200M / ApoTome Microscope.

2.4.8 Dapi and phalloidin staining (D&P)

Cells were double stained using DAPI [4’,6-Diamidino-2-phenylindole] (Sigma; D9542) and Phalloidin–tetramethylrhodamine B isothiocyanate (Sigma; 7418). Briefly, the 3D constructs were fixed for 30 min using 2 % paraformaldehyde (PFA) diluted in PBS followed by 3 washes with PBS. Cell membranes were permeabilized in 0.1 % Triton x-100 (Sigma; X100-500mL) solution with soft shaking during 30 min, followed by 3 PBS washes. The samples were incubated with Phalloidin-TRITC at a final concentration of 1 µg/mL in PBS for 25 min. DAPI solution (1µg/mL in PBS) was added into the previous solution and incubated for 5 minutes to counterstain the nucleus. Samples were carefully washed 3 times with PBS to eliminate the background and examined under Zeiss AxioVert 200M / ApoTome Microscope.

2.4.9 MTT viability assay

MTT [(3-(4,5-dimethylthiazol-2-yl)-2,5-diphenyltetrazolium bromide] assay is a colorimetric test based on the reduction of MTT to formazan crystals, giving purple color. This reaction only takes place when cellular reductase enzymes are active and, therefore; conversion is often used as a measure of viable cells. First, a MTT stock solution (10 mg/mL) was prepared with water, filtered through a 0.2 µm and stored at -20 ºC. Briefly, the medium was aspirated from the culture and MTT reagent (Sigma; M5655-1G) was added to a final concentration of 0.5 mg/mL in culture medium. The samples were incubated for 3 hours at 37 ºC in the dark. After the incubation, the solution was aspirated, and the constructs were lysed using DMSO (Sigma, D8418) to resuspend the formazan crystals. All samples were analyzed in triplicate. The absorbance was read at 550nm using microplate reader, Biotek ELX808.

2.4.10 RNA extraction, purification, and quantification

2D and 3D cultures were washed with PBS. Then, the samples were lysed, and RNA was extracted using PeqGold Total RNA kit (Peqlab; 12-6634-02). Briefly, the lysis was performed using RNA lysis buffer (Peqlab; 12-6834-02) with immediate inactivation of endogenous and exogenous RNases. Samples were disrupted by pipetting up and down with the micropipette (3D constructs growing in control medium) or a pestle (3D constructs growing in cardiac induction medium) and stored at -80ºC. Each 3D sample was constituted by two 3D encapsulations due to limited genetic material. The purification with PeqGold Total RNA kit provided a quick method for total RNA isolation based on the reversible binding characteristics of RNA to Perfect-Bind silica filters in centrifugation columns.

Table 2.4-1: Equations for RNA purity calculation and RNA quantification.

	EQUATIONS
Relationship between nucleic acids and chemical impurities* (range 2-2.4)	A260/A230 = (A260 – A320) / (A230 – A320)
Relationship between nucleic acids and proteins (range 1.8-2.1)**	A260/A280 = (A260 – A320) / (A280 – A320)
RNA concentration	[RNA] / µg·ml-1 = (A260 – A320) x (1/0.025) x dilution factor

*Absorbance at 320 nm corrects light scattering due to dust particles. It provides information about contamination by chemicals: alcohol, phenol and guanidinium from the lysis buffer.
**Absorbance at 280 nm provides information about protein contamination.

RNA amount and purity was determined by measuring samples absorbance at 230 nm, 260 nm, 280 nm and 320 nm with the Helios Alpha UV-Vis Spectrophotometer. The quantification by this technique may be affected by scattering of light and impurities such as protein, phenol or other contaminants that also absorb near 260 nm. For this reason, some correction parameters are introduced (see Table 2.4-1).

2.4.11 cDNA synthesis

The material obtained was used for cDNA synthesis using Quantitect Reverse Transcription Kit (Qiagen; 205311) according to manufacturer's protocols. Briefly, 500 ng of purified RNA was treated with gDNA Wipeout Buffer during 2 min at 42 ºC to eliminate DNA contamination. The treated samples were transcribed to cDNA using Quantiscript Reverse Transcriptase incubated during 15 min at 42 °C. Finally, an inactivation step of 3 min at 95 °C to inactivate the reverse transcriptase was performed. The samples were aliquoted and stored at -80 ºC until gene analysis.

2.4.12 Primers selection

Primers were designed using Primer Blast software from National Center for Biotechnology Information (NCBI). The following parameters were taken into consideration: a melting temperature around 60 ºC, maximum of CG content of 60 % (optimum between 40-50 %), ending with cytosine or guanine bases, maximum of 3-4 dimers and hairpins, 15-30 base pair of primer length and 250-80 base pair of PCR product length. Primers sequences of the designed primers are shown in Table 2.4-2.

Table 2.4-2: Primers for RT-PCR and qRT-PCR. Early and definitive cardiac markers were analyzed

	NAME		SEQUENCE	bp	Tm (ºC)	Fragment
1	*ACTN1*	Fw	GAGAAACTGCTGGAGACCATTGACC	25	63	188bp
		RV	TTGTCGGCATCAGGGAGGGT	20		
2	*GATA4*	Fw	CCTGTCATCTCACTACGGGC	20	60	120bp
		RV	CCTTGTGGGGAGAGCTTCAG	20		
3	*GJA1*	Fw	comercial QT00012684	-	55	92bp
		RV		-		
4	*MEF2C*	Fw	CCATTGGACTCACCAGACCT	20	65	139bp
		RV	AGCACACACACACACTGCAA	20		
5	*MHC*	Fw	TGGGAGATTCGGAGATGGCAGTC	23	64	225bp
		RV	CCTGGTCCTCCTTCACGGTCACTG	24		
6	*NKX2.5*	Fw	AGTGTGCGTCTGCCTTTCCC	20	63	250bp
		RV	AGGTACCGCTGCTGCTTGAAG	21		
7	*TBX5*	Fw	CATGGAGACATCACCCAGTG	20	60	169bp
		RV	GCAGCTGATGTCCTCTAGGC	20		
8	*RPL22*	Fw	TGACATCCGAGGTGCCTTTC	20	60	101bp
		RV	GTTAGCAACTACGCGCAACC	20		

2.4.13 Study of gene expression by RT-PCR

Reverse transcription polymerase chain reaction (RT-PCR) was performed to analyze qualitatively gene expression in 2D and 3D cultures. RT-PCR reaction was carried out using 30 ng of cDNA in a final volume of 25 µL containing 1X ThermoPol Reaction Buffer (stock 10X), 0.42 units of TAQ DNA polymerase (Sigma; D1806), 200 µM of dNTPs (Sigma; DNTP100) and 0.3 µM primers (synthesized by Sigma). The RT-PCR took place under the following conditions: 3 min at 95 ºC (activation) followed by 35 cycles of 20 s at 94 ºC, 30 s of annealing (Tm dependent on primer pair, see Table 2.4-2) and 30 s at 72 ºC. Final extension step was performed at 72 ºC during 15 min. RT-PCR products were size fractionated by 2 or 4 % agarose gel electrophoresis, depending on the expected fragment size.

2.4.14 Study of gene expression by qRT-PCR

Real Time RT-PCR reactions were performed with LightCycler® 480 Real-Time PCR System (Roche), using the iQ™ SYBR® Green Supermix (Bio-Rad;170-8882) as a fluorescent reporter. SYBR® Green binds to double-stranded DNA and upon excitation emits fluorescence.

Real-time RT-PCR was run with the following parameters: 1 cycle of 10 minutes at 95 ^{o}C in order to activate the hot-start iTaq™ DNA polymerase, 50 cycles consisting in 15 seconds at 94 ^{o}C for denaturation of the double stranded cDNA, 15 seconds for primer annealing (Tm dependent on primer pair, see Table 2.4-2), and 15 seconds at 72 ^{o}C for extension. Finally melting curve analyses were performed to test the specificity of PCR products, together with agarose electrophoresis. Relative gene fold variations were all determined by the comparative CT method ($2^{-\Delta\Delta Ct}$) and expression of the target genes was normalized to the housekeeping gene (ribosomal protein 22L, *RPL22*).

2.4.15 Western Blotting for protein analysis

Protein extracts were obtained using RIPA buffer (Sigma; R0278) containing proteinase inhibitor cocktail (Roche; 11836153001) from 2D and 3D cultures of subATDPCs at passage 8. Two 3D cultures constituted each sample for western blotting and they were lysed with the help of pestles to crush the samples. All samples were centrifuged to eliminate the debris and stored at -20 ºC until analysis. Protein content was quantified from the supernatant using Micro BCA™ Protein assay kit (Pierce-Thermo Scientific; 23225). Equal amounts of total protein (5 µg) were denatured with SDS (Sigma; L5750-500G) and β-mercaptoethanol at 95 ºC during 10 min. Subsequently, the proteins were separated by electrophoresis on 10 % SDS–PAGE gels at 150 V during 1 h 30 min. Proteins were blotted onto PVDF membrane (Invitrogen; LC2005) during 2 h at 40 V using wet transference. The membranes were blocked with 5 % non-fat milk buffer during 2 h at room temperature and incubated with rabbit polyclonal anti-GATA4 1 µg/mL (Santa Cruz; sc-9053) or rabbit polyclonal anti-GJA1 1 µg/mL (Santa Cruz; sc-9059) at room temperature during 1h. After 3 short washes with PBST (Phosphate Buffered Saline (Gibco; 18912-014) supplemented with Tween-20 (Sigma; P-1379)) and an overnight PBST wash the blots were incubated with peroxidase-conjugated to rabbit IgG goat polyclonal secondary antibody 1µg/mL (Abcam; ab97051). The protein bands were detected after incubation with SuperSignal® West Pico Chemiluminescent Substrate (Thermo Scientific; 34080) using ImageQuant LAS 4000 mini equipment. Goat polyclonal anti-Actin antibody (Santa Cruz; sc-1615) was used to normalize with peroxidase-conjugated to goat IgG rabbit polyclonal secondary antibody (Abcam; ab97100).

2.4.16 Dynamic mechanical analysis

Viscoelastic properties of 3D constructs were analyzed by dynamic mechanical analysis (DMA). This technique consists of applying a force (stress) to the culture and measure the strain generated by the material when it is displaced. As a result, storage modulus (G') was obtained. Measures were picked at 2 and 4 weeks from subATDPCs cultured in each condition [RAD16-I peptide 0.3 % (w/v) without modifications, RAD16-I/RADRGD (95:5) 0.3 % (w/v), RAD16-I 0.3 % (w/v) with heparin (570:1) and RAD16-I/RADRGD (95:5) 0.3% (w/v) with heparin (570:1)] in control and cardiac induction medium. Four samples of each condition were analyzed. A compression assay with DMA Multi-Frequency-Strain mode and a frequency sweep test was applied to each sample with a DMA Q800 (TA Instruments). The construct was deformed (oscillated) at constant amplitude (strain) over a constant frequency, and the mechanical properties were measured. The conditions of the assay were: Amplitude= 1, Preload force= 0.03 N and Frequency= 1 Hz. Construct diameter and thickness were variable depending on the dimension of the construct. Results were obtained with TA Instrument Explorer software and analyzed with TA Universal analysis software.

2.4.17 Statistics

GrapPad Prism version 5.oo Windows, GraphPad Software, San Diego California USA, www.graphpad.com was used for statistical analysis. The results are presented as mean ± SD as obtained of three independent values per group. Two-way analysis of variance performed comparison of means in qRT-PCR and Western blotting with Bonferroni's posttest. Comparison of assays was made by correlation and linear regression analysis. Differences were considered significant if $p < 0.05$.

2.5 RESULTS AND DISCUSSION

2.5.1 Cell behavior in 2D cultures

SubATDPCs were isolated and expanded by IGTP group, who also defined the basic requirements of these cells in 2D cultures. Figure 2.5-1 shows the general behavior of subATDPCs growing on flat surfaces. As it can be observed, the morphology highly depends on the culture medium. SubATDPCs growing in control medium presented an elongated, individual morphology, but the addition of cardiac induction medium promoted a star-shape morphology and the formation of clusters. On the other hand, proliferation test with MTT assay (Figure 2.5-1b) showed that control medium allowed slow, but constant proliferation. Meanwhile, the cardiac induction medium stopped the proliferation presumably due to a differentiation process.

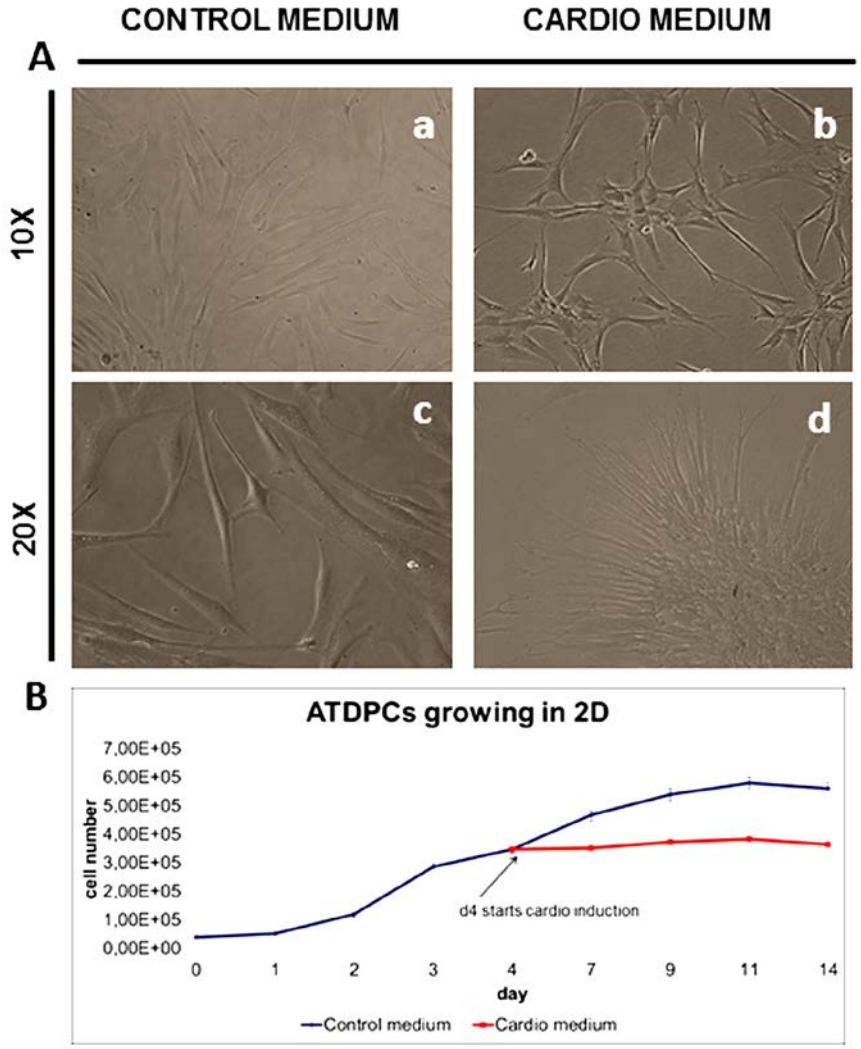

Figure 2.5-1: SubATDPCs growing on flat surfaces. (A) Phase contrast of subATDPCs growing in control medium (a-10X augments and c – 20X augments) and in cardiac medium (b-10X augments and d – 20X augments. (B) MTT assay of 2D cultures growing in control (blue) or cardiac (red) medium.

After assessing the best conditions for 2D cultures, subATDPCs were de-attached from flat surfaces to be embedded in the 3D milieu provided by the self-assembling peptide RAD16-I. Different cell types encapsulated in this material have been reported to be able to migrate and contact one to each other in a truly 3D environment. The first aim of this work was to evaluate subATDPCs viability and behavior in RAD16-I self-assembling peptide as function of peptide concentration and cell number. Therefore, we determined the best conditions (culture media, cell density, and peptide concentration) for subATDPCs to grow in this environment. We based our decisions on cell viability (L&D assay), network formation (D&P staining), and construct diameter reduction (macroscopic analysis). Network structure is intimately related to construct diameter reduction since as denser is the network; more strain is exerted by the cells, thus reducing the overall diameter of the system.

2.5.2 Media selection

The basic component of basal media (used for 2D cultures and control medium for 3D cultures) was α-MEM. The slight differences observed in the formulation of this medium, between two suppliers, lead us to test different media for 3D cultures (constructs) maintenance: α-MEM from LabClinics and α-MEM from Sigma were analyzed. Both media tested were the most enriched α-MEM medium of each supplier, with only slightly differences between their concentrations of amino acids, salts and vitamins. The most important difference lied in the presence of L-glutamine, ribonucleosides, and deoxyribonucleosides in Labclinics medium.

Constructs of subATDPCs encapsulated in 0.15 % RAD16-I (cell density = 2,000 cells/μL, the standard conditions currently used in our laboratory with other cell types) were performed as follows: half of the encapsulations were cultured with α-MEM from LabClinics, and the other half with α-MEM from Sigma. Figure 2.5-2 presents the results obtained after 12 days of culture. Significant differences were found in construct diameter reduction (Figure 2.5-2a) and in the L&D assay (Figure 2.5-2b). A decrease in diameter was observed for the constructs cultured in Sigma medium; however, constructs cultured in LabClinics medium did not show any change in construct diameter. Consequently, the samples cultured with Sigma α-MEM presented a higher condensation after 12 days of culture (nearly 2 mm of diameter) than the samples with LabClinics medium (about 9 mm of diameter). This suggests that Labclinics medium did not allow subATDPCs to properly elongate to form an intricate network. This hypothesis was corroborated by cell viability test that showed more cell density and number of live cells in the construct growing with Sigma medium (Figure 2.5-2b). For all these reasons, thereafter encapsulations with subATDPCs were cultured with α-MEM media from Sigma.

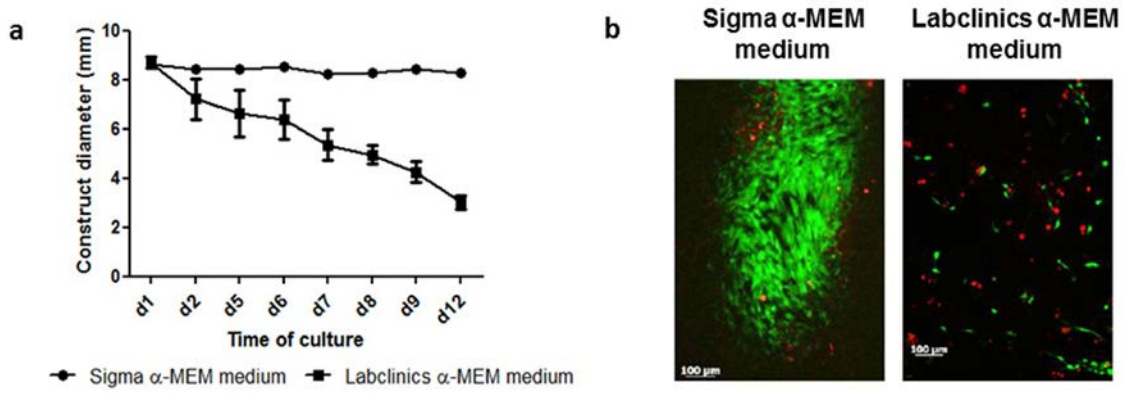

Figure 2.5-2: SubATDPCs behavior depending on α-MEM supplier. (a) Construct diameter reduction progression during 12 days depending on basal media used. (b) L&D staining of 3D cultures using Sigma or Labclinics α-MEM basal media. Live cells stained in green and dead cells in red.

2.5.3 SubATDPCs cultured in a 3D system.

In this chapter, we aimed to analyze subATDPCs behavior in 3D environments, and therefore the first step was to define the best conditions of peptide concentration and cell density for this *in vitro* model.

Regarding cell density, the values must favor cells free movement by allowing an intimal contact between them and the ECM-analog, avoiding overcrowding. Figure 2.5-3 shows the effect of cell density in 3D cultures of RAD16-I 0.15 %. Two cell densities were tested (2,000 cells/µL and 4,000 cells/µL), and construct diameter reduction, cell network and viability were analyzed. No significant diameter reduction was observed independently of cell density, but a clear difference appeared in network formation. The first day cells remained round-shaped (red arrows) in both cases, but after some days of culture cells growing in constructs of 2,000 cells/µL gently started to elongate, to contact one to each other, and to form a cellular network (blue arrows). Constructs of 4,000 cells/µL presented the formation of amorphous clusters (yellow arrows), and L&D staining showed a large number of dead cells. Constructs of 2,000 cells/µL presented high viability and proper network formation after 7 and 9 days of culture. respectively. Therefore, as we were looking for a good 3D environment to analyze subATDPCs behavior *in vitro* we decided to work with a cell density of 2,000 cells/µL.

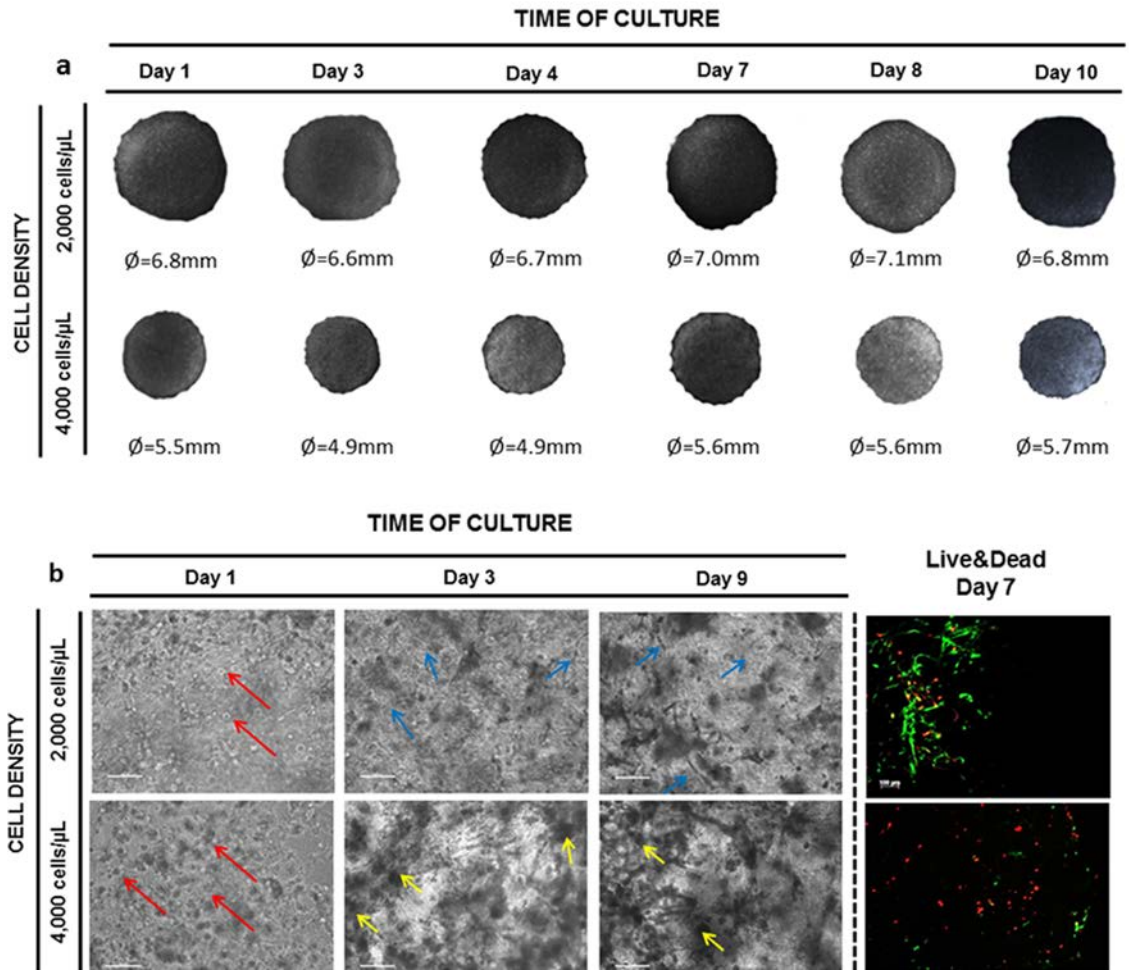

Figure 2.5-3: SubATDPCs at different cell density encapsulated in RAD16-I self-assembling peptide 0.15 %. (a) Macroscopic view of construct diameter reduction depending on cell density during a period of 10 days of culture. (b) Cell network depending on cell density during a period of 9 days of culture (Red arrows point out round shaped cells, blue arrows point out elongated cells, and yellow arrows point out cluster formation) and L&D staining after 7 days of encapsulation. Live cells stained in green and dead cells in red. Scale bar 100µm.

Typically, these 3D structures were prepared using a constant volume of 80 µL, which means that each construct contains 160,000 cells. With the aim to increase cell number for further analysis steps, we prepared 3D constructs doubling their volume. It was known that this would affect medium and oxygen diffusion, so it was important to firstly test how this modification could affect cell behavior in terms of network formation. Figure 2.5-4 shows cell network formed after 5 and 7 days of culture in constructs of 160 µL at different peptide concentration taking as a control subATDPCs growing in RAD16-I 0.15 % at 2,000 cells/µL. The increased construct volume (at same cell density and peptide concentration) led to a poor network formation as compared with the control. After 7 days of culture, construct of 80 µL presented an intricate network, but only some elongated cells could be observed in constructs of 160 µL. Additionally, the increase in peptide concentration was shown to prevent the network formation and less elongated cells could be observed. At the view of these results, we decided to maintain the typical peptide volume (80 µL) and cell density (2,000 cells/µL). Therefore to obtain enough material for further analysis two constructs were used per experimental point.

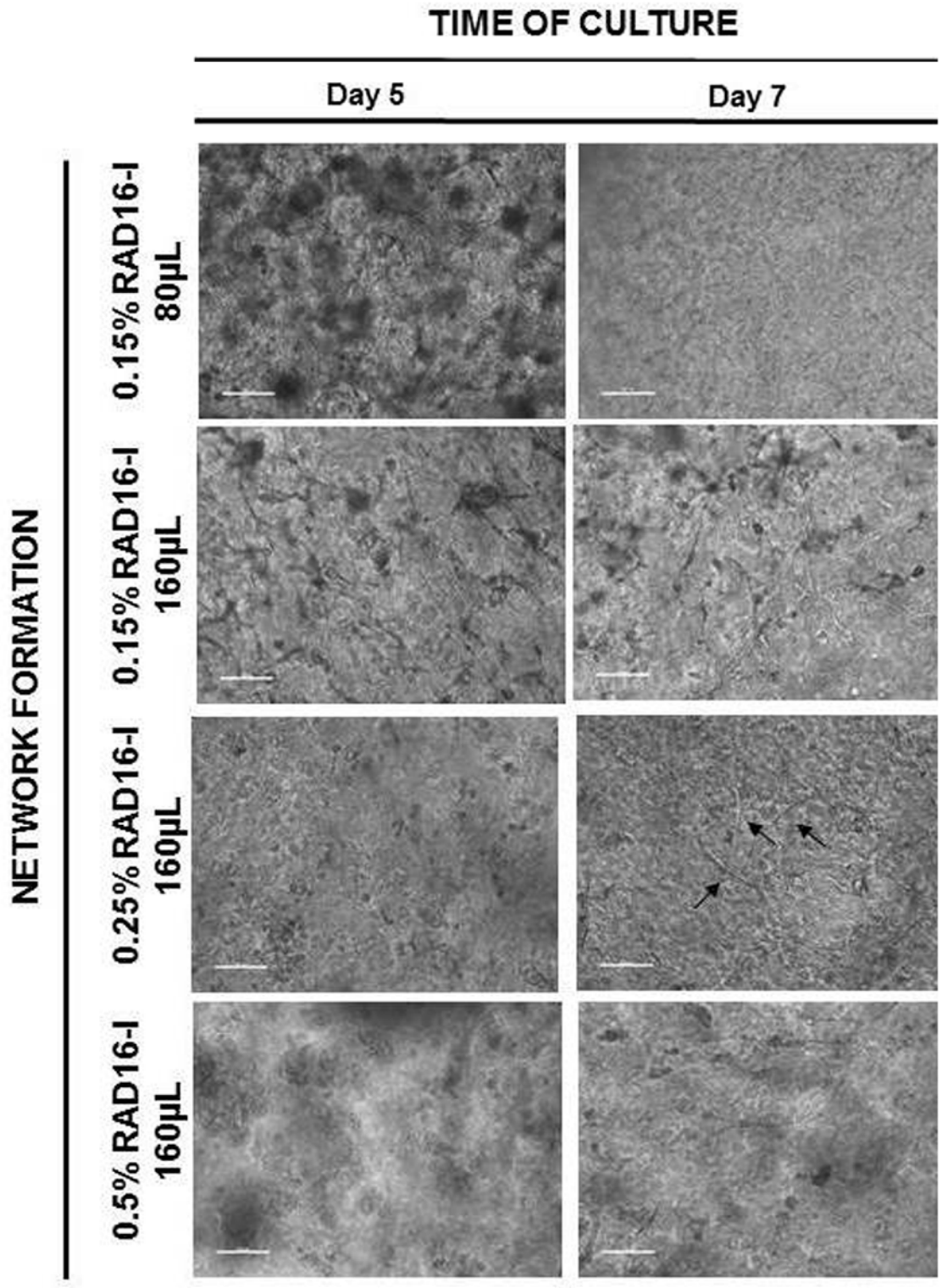

Figure 2.5-4: Effect of construct volume and peptide concentration in the behavior of subATDPCs encapsulated in RAD16-I. Increase of volume of the construct implies a slowing down of the network formation. The increase of peptide concentration worsens the situation.

The final step to decide the best conditions for 3D cultures of subATDPCs in RAD16-I peptide was to test different peptide concentrations, using a cell density of 2,000 cells/µL. Figure 2.5-5 shows cell viability (Figure 2.5-5a) and construct diameter reduction (Figure 2.5-5b) depending

on peptide concentration. Additionally, the effect of the cardiac induction medium (or cardio medium) in the construct morphogenesis and cell viability was analyzed. Cardiac induction medium *in vitro* was used to test the potential of these cells to differentiate towards a cardiac phenotype.

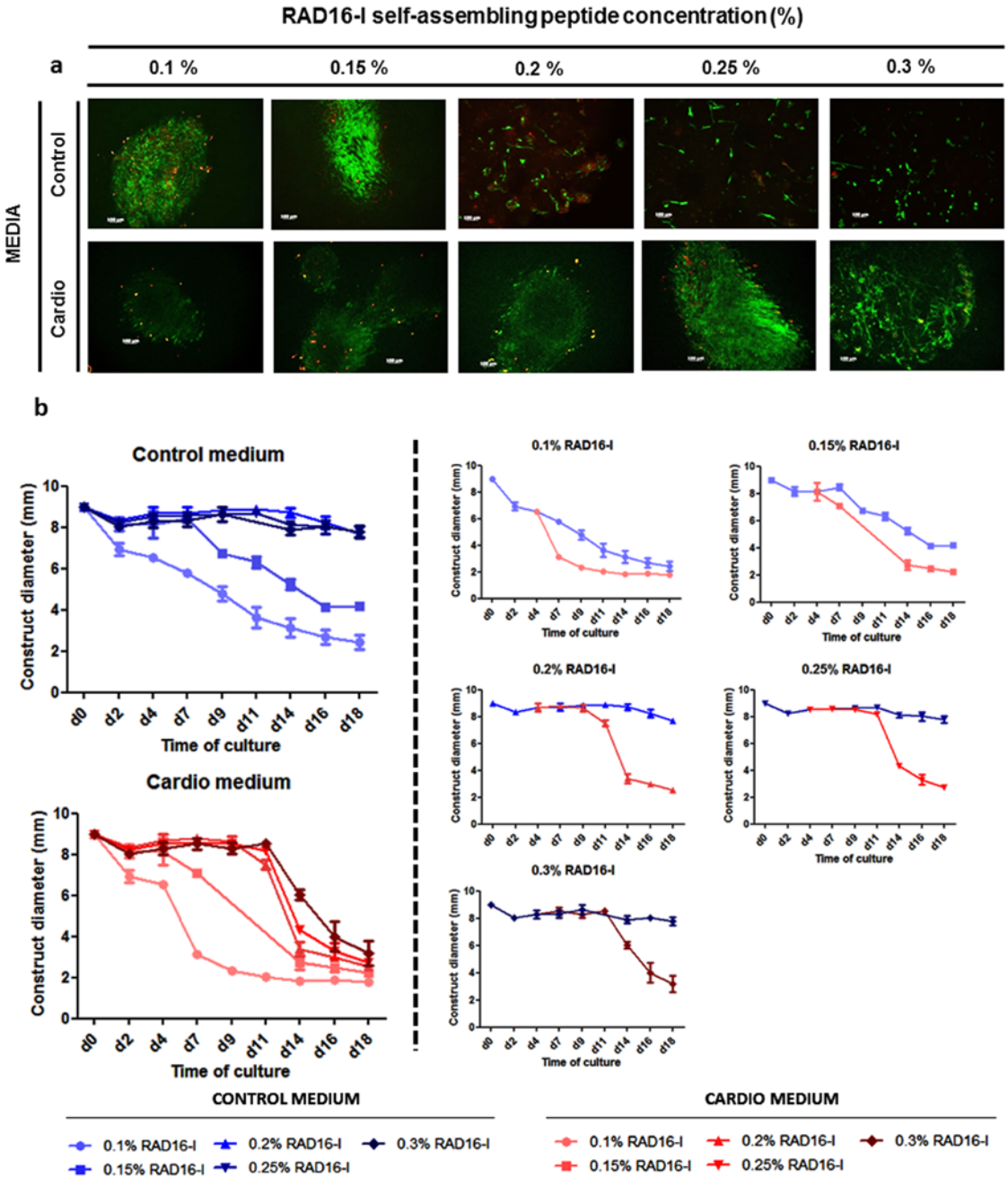

Figure 2.5-5: SubATDPCs growing in different RAD16-I self-assembling peptide concentration. (a) L&D staining of subATDPCs growing in different RAD16-I self-assembling peptide concentration depending on culture medium. Live cells stained in green and dead cells in red. (b) 3D cultures diameter reduction depending on peptide concentration and culture medium.

All peptide concentrations (equally for control or cardiac induction medium) showed a high degree of viability (Figure 2.5-4a). As expected, higher peptide concentration led to a lower

reduction in construct diameter. Interestingly, it was observed that at high concentration of peptide (from 0.2 to 0.3 %) subATDPCs growing in control medium were not able to elongate properly. Therefore, the construct did not condense (all constructs maintained more or less the diameter of 9 mm). On the other hand, the addition of cardiac induction medium allowed the cells to elongate and diminish the diameter of the construct. After 18 days almost all constructs growing in cardiac induction medium, indistinctly of peptide concentration, presented a diameter between 2 and 4 mm. This effect was not observed in constructs growing in control medium.

At the view of all these results, it was concluded that the most appropriate conditions to analyze subATDPCs behavior using RAD16-I to emulate a 3D model *in vitro* were: RAD16-I 0.15 % at cell density of 2,000 cells/µL with α-MEM enriched media from Sigma. In Figure 2.5-6 an overview of subATDPCs behavior in this conditions is presented.

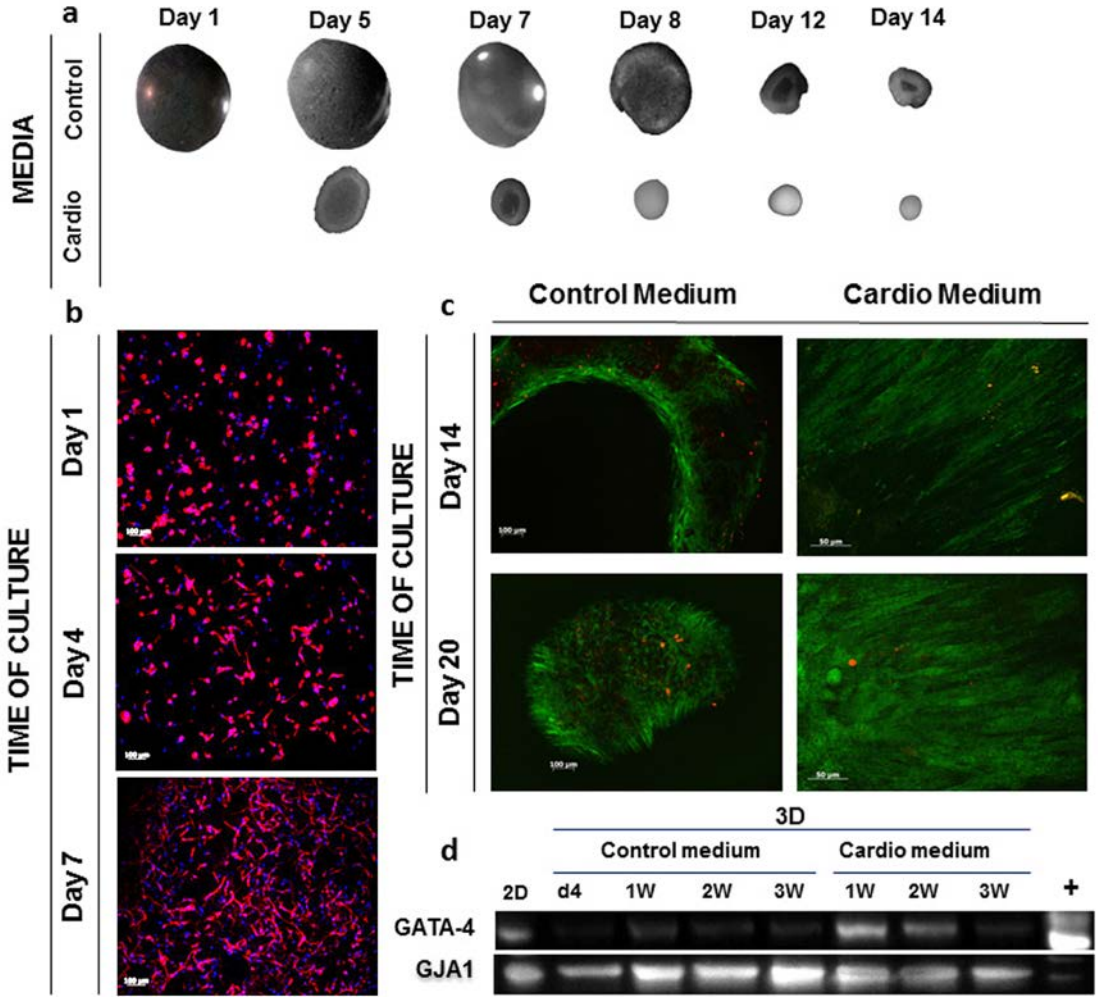

Figure 2.5-6: SubATDPCs growing at a cell density of 2,000 cells/µL in RAD16-I 0.15 %. (a) Macroscopic structure. Construct diameter reduction. (b) D&P staining presenting network formation. Nuclei stained in blue and actin filaments in pink. (c) L&D staining shows the viability after 14 and 20 days of culture depending on culture medium. Live cells stained in green and dead cells in red. (d) GATA4 and GJA1 protein expression after 4 days, 1, 2, and 3 weeks of 3D culture in control, or cardio medium.

After encapsulation, all constructs were maintained in control medium until cells started to elongate at the 4th day of culture (Figure 2.5-6b), then half of the constructs were induced with cardiac induction medium. The morphogenic process of construct diameter reduction was faster for constructs growing in cardiac induction medium, but constructs growing in control medium also displayed this condensation (Figure 2.5-6a). Importantly, cells remained alive in both conditions after 20 days of culture and interestingly, cardiac induction medium induce some kind of cell alignment (Figure 2.5-6c). Finally, protein expression after 4 days, and 1, 2, and 3 weeks of culture were analyzed. It was observed that GATA4 (early cardiac marker) and GJA1 (definitive cardiac marker) were expressed in both control and cardio medium.

2.5.4 RAD16-I self-assembling peptide with RGD and heparin modifications

As explained previously, RAD16-I peptide provides a non-instructive microenvironment, which means that it does not present cues that guide cells to a particular commitment. This fact provides an opportunity to analyze different signals independently, by functionalizing RAD16-I with biologically active motifs that trigger different cells responses. Several peptide motifs have been described to improve myogenic activity. It is, therefore, feasible to prepare a new series of self-assembling peptide carrying functional motifs that activate and maintain myogenic properties. The ECM-analog RAD16-I with heparin-like motifs described in previous results and modified with RGD-based integrin binding domains were tested[84]. Hence, RAD16-I were used as a base to design three new sets of self-assembling peptide scaffolds. RAD16-I modification with heparin was pretended to promote the binding of GFs by naturally interacting with its heparin-like domain for further release. On the other hand, the modification with RGD motif aimed to promote cell maintenance and viability.

Initial efforts in this block of experiments were directed to the preparation of self-assembling peptide with the combination of RADRGD and heparin modifications. RAD16-I self-assembling peptide organize itself into structurally well-defined arrangements as a result of an increase of ionic strength. Therefore, it was important to assure that the proposed modifications did not interfere in the process. The subsequent mixtures were prepared: RAD16-I/RADRGD (95:5), RAD16-I with heparin (570:1), and RAD16-I/RADRGD (95:5) with heparin (570:1). All samples were stained with Congo Red (analysis of β-sheet structures formation), and Toluidine Blue (analysis of heparin binding) using RAD16-I as control.

Congo Red Staining in Figure 2.5-7 shows that all the modifications suggested allow RAD16-I peptide to gel forming β-sheet structures. Toluidine Blue staining show little purple structures inside the gel corresponding to the presence of heparin polysaccharide. Therefore, these nanofiber peptides in principle maintained all the structural features needed to culture subATDPCs even in the presence of RGD motif and heparin polysaccharide. However, first of

all it was necessary to ensure the behavior and viability of these cells encapsulated in the nanofiber peptides.

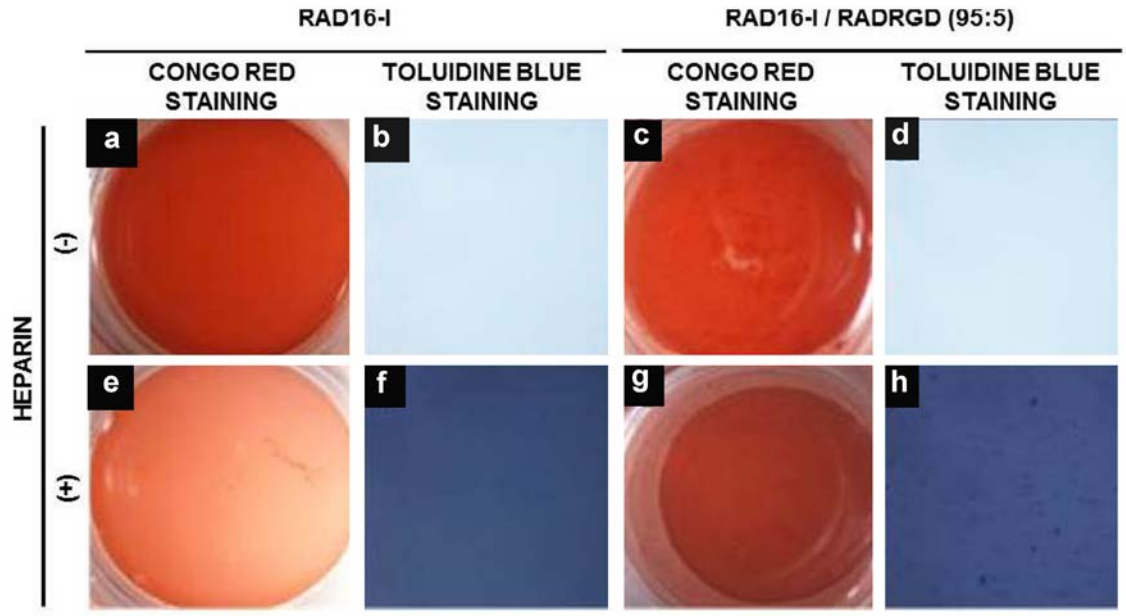

Figure 2.5-7: Analysis of RAD16-I proposed modifications in the self-assembling process. Congo Red Staining stains β-sheet structures and Toluidine Blue staining stains polysaccharides, in this case Heparin. (a) RAD16-I without Heparin – Congo red staining; (b) RAD16-I without Heparin – Toluidine Blue staining; (c) RAD16-I/RGD without Heparin – Congo red staining; (d) RAD16-I/RGD without Heparin – Toluidine Blue staining; (e) RAD16-I with Heparin – Congo red staining; (f) RAD16-I with Heparin – Toluidine Blue staining; (g) RAD16-I/RGD with Heparin – Congo red staining; (h) RAD16-I/RGD with Heparin – Toluidine Blue staining.

2.5.5 SubATDPCs encapsulated in RAD16-I with and without heparin

In the context of RECATABI European project the development of a new biomaterial able to promote vascularization of ischemic areas after myocardial infarction was studied by Fernandez-Muiños *et.al.*[79]. RAD16-I was combined with heparin, which has high GF binding capacity. As a consequence, the RAD16-I peptide-heparin composite (RAD16-I+Hep) could bind soluble GFs localizing their activity into the RAD16-I scaffold, protecting them from degradation, and in some cases, enhancing their binding to cell surface receptors[67]. RAD16-I+Hep was observed to be able to bind and release physiologically significant quantities of $VEGF_{165}$ (chemical signal produced by cells that stimulates the growth of new blood vessels) *in vitro* during the first 24-36h (see *2.2.Preliminary Results*). This system was demonstrated to be a useful tool for drug delivery system for vascularization. In this work, we aim to test its ability to support survival and maintenance of subATDPCs. Additionally, we wanted to analyze the effect of $VEGF_{165}$ presence in the culture media on cell behavior.

3D cultures of subATDPCs were prepared using self-assembling peptide scaffolds of RAD16-I or RAD16-I+Hep (570:1). Half of them were cultured in control medium with $VEGF_{165}$ (Figure 2.5-8a). After five days of culture, D&P staining showed that subATDPCs growing in media containing $VEGF_{165}$ presented higher proliferation and better cell network formation than cells

growing without this GF. The most interesting aspect was that cells encapsulated in RAD16-I+Hep hydrogel presented an aligned growth while the samples that did not contain this polysaccharide showed a disordered pattern (Figure 2.5-8b).

The viability was analyzed using L&D assay. As it can be observed after 13 and 21 days of culture (Figure 2.5-8c and d, respectively), despite there were some dead cells in all samples the most part of them remained alive. Interestingly, after 13 days of culture it could be seen that subATDPCs growing in RAD16-I+Hep scaffolds showed a high ordered pattern regardless of the presence of VEGF growing factor. On the other hand, cells growing without heparin did not show this aligned pattern; instead the cells were completely disordered. The same results could be found after 21 days of culture

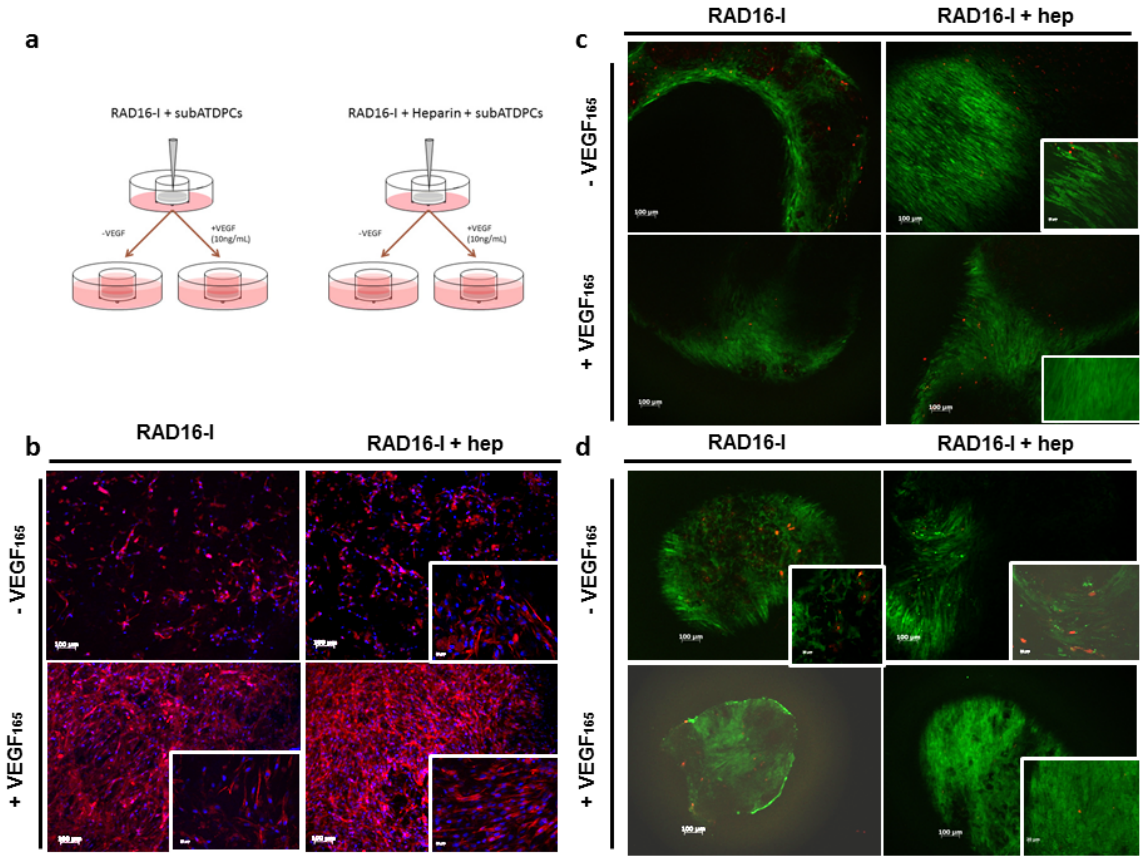

Figure 2.5-8: Effect of heparin in 3D cultures of subATDPCs. (a) Preparation of 3D constructs of RAD16-I with or without heparin. Half of each pool was cultured with VEGF and the other half without VEGF. (b) D&P staining after 5 days of culture. Nuclei stained in blue and actin filaments in pink. (c) L&D staining after 13 days of culture. (d) L&D staining after 21 days if culture. Live cells stained in green and dead cells in red.

.

2.5.6 SubATDPCs encapsulation in RAD16-I with and without peptide modifications

RAD16-I self-assembling peptide containing the motif RGD (RADRGD = AcN-GP**RGD**SGY**RGD**S-GG-$(RADA)_4$) for cell integrin-receptor recognition and signaling was tested to support subATDPCs culture, using the RAD16-I peptide without modifications as control. This new peptide was blended with regular RAD16-I (typically the ratio RAD16-I/RADRGD = 95:5 was used). Behavior and viability of subATDPCs encapsulated in RAD16-I peptide containing RADRGD with or without heparin was analyzed at macroscopic and microscopic level. As it can be clearly seen in the fluorescent images (Figure 2.5-9b) scaffolds composed of RAD16-I/RADRGD motifs presented a higher cell number as compared to RAD16-I peptide alone. Cells encapsulated in RAD16-I constructs resulted to be more isolated and less connected compared to constructs with the modified peptide. So, we suggest that RGD motif was indeed enhancing the connections and migration of the cells. In the case of heparin, we founded different cell behaviors. The combination of heparin with only RAD16-I enhanced the elongation of the cells, but in combination with RGD motif, cells formed more clusters and looser networks. Therefore, from de point of view of cellular network formation, we concluded that heparin could have an adverse effect. In terms of viability, although L&D assay showed some death cells in all conditions, the majority of them were alive. Additionally, in order to assess whether the network correlated with the construct diameter reduction, the diameter of the different constructs was measured. The condensation effect depending on the presence or not of peptide RGD motif and heparin is shown in Figure 2.5-9a. It has to be highlighted that the constructs that presented RGD motifs condensed more than the constructs without it.

On the other hand, as it can be seen in Figure 2.2-1 (see *2.2 Previous Results*) heparin itself could promote the capture of GFs improving their accessibility through heparin binding domains. This behavior could be useful for further *in vivo* applications, therefore heparin modification was not discarded and both RGD motif and heparin polysaccharide will be included in further experiments.

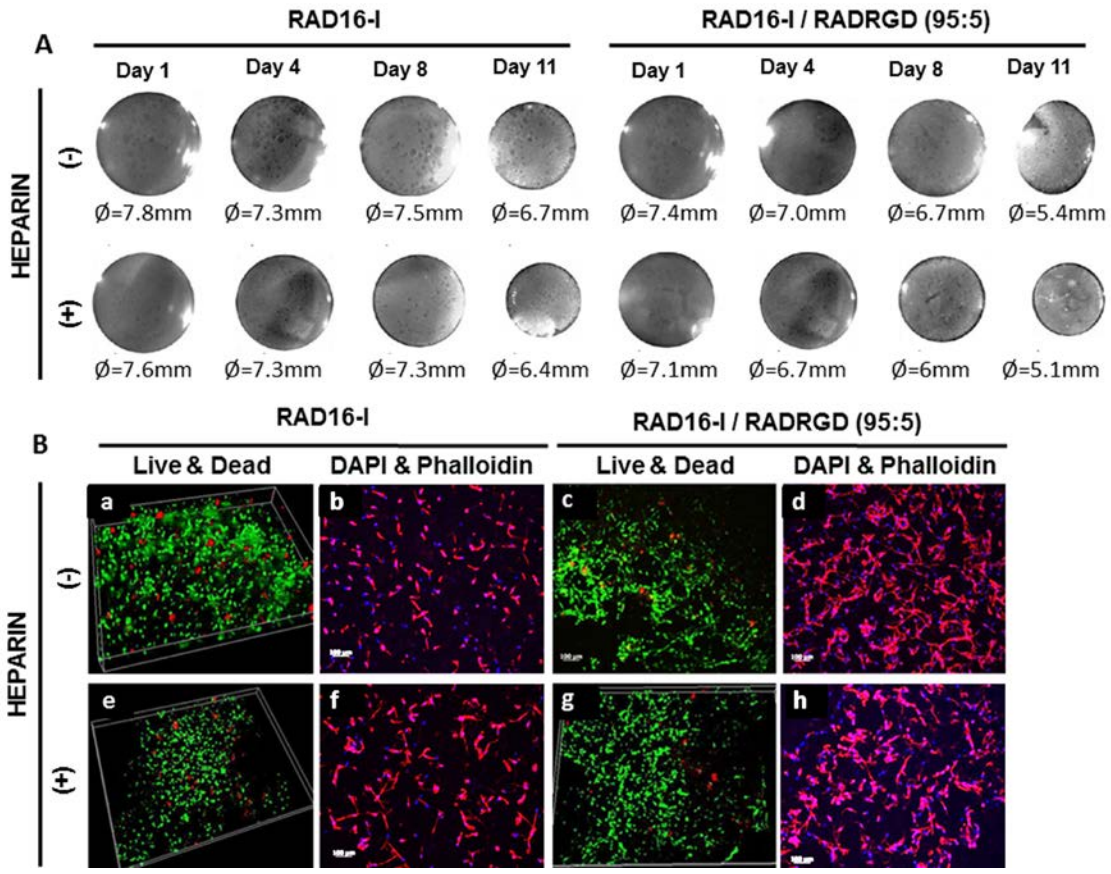

Figure 2.5-9: SubATDPCs encapsulated in RAD16-I nanofiber peptide and RAD16-I with modifications. A) Macroscopic structure of subATDPCs encapsulated in RAD16-I with and without modifications from day 1 to day 11 of culture. B) L&D staining after 11 days of culture (live cells stained in green and dead cells in red) and D&P staining after 9 days of culture (nuclei stained in blue and actin filaments in pink). a) RAD16-I without Heparin – L&D staining; b) RAD16-I without Heparin – D&P staining; c) RAD16-I/RGD without Heparin – L&D staining; d) RAD16-I/RGD without Heparin – D&P staining; e) RAD16-I with Heparin – L&D staining; f) RAD16-I with Heparin – D&P staining; g) RAD16-I/RGD with Heparin – L&D staining; h) RAD16-I/RGD with Heparin – D&P staining.

2.5.7 Proliferation analysis of subATDPCs encapsulated within RAD16-I with and without peptide modifications

MTT assay was used to analyze cell behavior during the first days of culture more accurately. Triplicates of 160,000 cell 3D cultures were prepared for RAD16-I with and without RGD and heparin modificatons. MTT assess cell viability based on the activity of NAD(P)H-dependent cellular oxidoreductases enzymes under defined conditions. These enzymes are capable of reducing MTT to its insoluble formazan. It is important to notice that the reduction of MTT increase with cellular metabolic activity depending on the NAD(P)H flux and therefore assay conditions can alter metabolic activity. Formazan product obtained from the reduction of MTT by oxidoreductases was measured from day 1 until day 14 (see Figure 2.5-10). During the first days of culture, modified peptides showed higher absorbance that cells growing in unmodified peptide, but after four days there were no significant differences. In regard to culture media, no significant difference could be appreciated ($p > 0.05$).

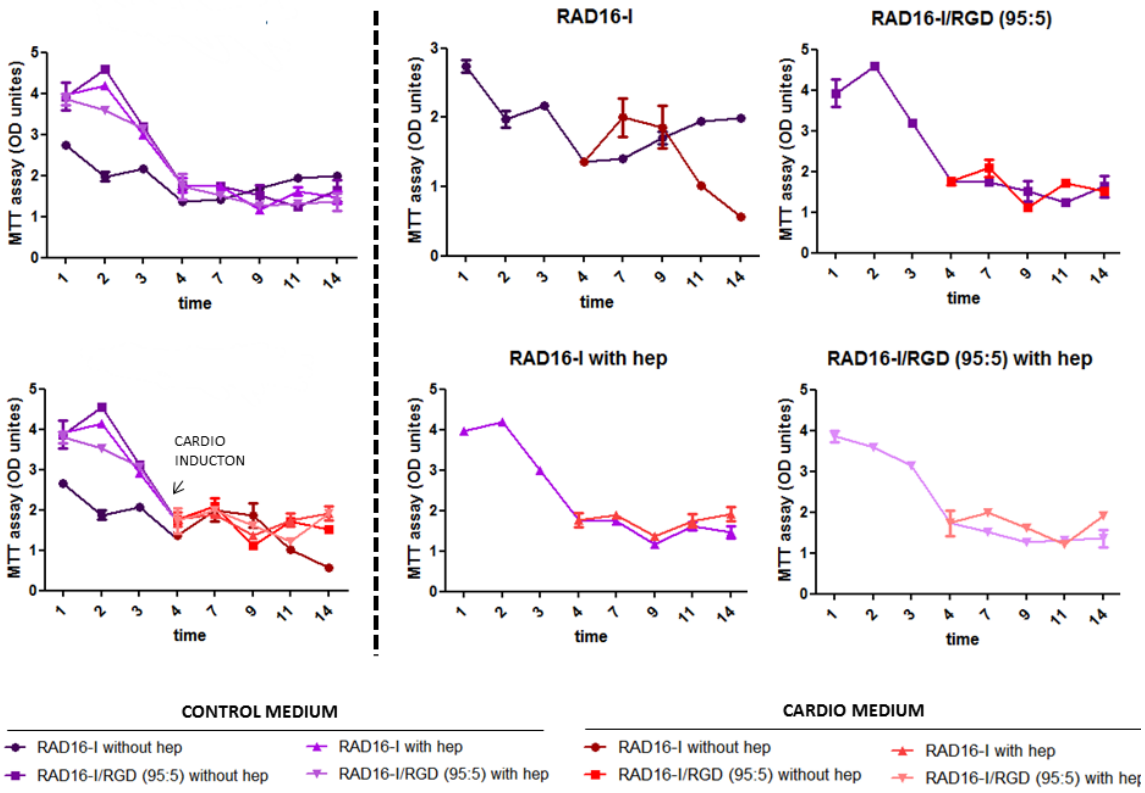

Figure 2.5-10: MTT assay of subATDPCs 3D cultures. SubATDPCs viability was also assessed quantitatively with MTT assay. Purple lines represent cells growing in control medium, and red lines represent their grown in cardiac induction medium. All peptide modifications show a greater absorbance that cells growing in bare RAD16-I peptide until day 4.

It is important to mention that after four days more or less all conditions presented the same pattern of absorbance. However, the cells that grew in RAD16-I bare self-assembling peptide in cardiac induction medium started to decrease their absorbance after 11 days of culture. Careful analysis of subATDPCs growing in RAD16-I peptide in cardiac induction medium after 20 days of culture showed that cells started to migrate outwards of the construct. This effect was also observed for the other conditions when the 3D cultures were considerably condensed. Figure 2.5-11 shows a picture that clearly demonstrates the migration of the cells outwards the construct.

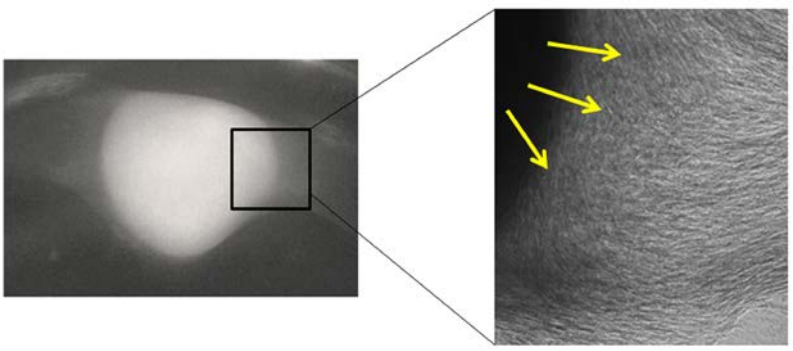

Figure 2.5-11: Macroscopic view subATDPCs 3D culture in RAD16-I. In the left, it can be observed a 3D construct with a blanket covering the whole structure. An amplification in the right part of the picture shows that it is a cape of cells migrating outwards of the construct. Yellow arrows indicate the direction of cells migration.

2.5.8 Nanomaterial evaluation for their effect gene expression

Gene and protein expression of subATDPCs encapsulated in 3D constructs of RAD16-I peptide with and without the presence of RADRGD and heparin modifications were analyzed. Firstly an overview of gene expression at the second week of culture with control and cardiac induction media was assessed by RT-PCR. *TBX5, MEF2C* and *NKX2.5* (early cardiac markers) and *MHC, ACTN1* and *GJA1* (definitive cardiac markers) were analyzed using *RPL22* as internal control (data not shown). *TBX5, MEF2C* and *GJA1* were expressed equally in constructs growing in control and cardiac induction media, but a band of *ACTN1* was only observed when the samples were induced with cardio medium. No expression of *NKX2.5* or *MHC*, was observed. These results encouraged us to quantify *TBX5* and *MEF2C* early cardiac markers, and *ACTN1* and *GJA1* definitive cardiac markers using qRT-PCR. The obtained results were compared with cells growing in flat surfaces with control or cardiac induction media respectively (Figure 2.5-12a).

The obtained results did not present significant differences in terms of gene expression for constructs modified with RADRGD or heparin either in control or cardiac induction media ($p > 0.05$). However, a significant overexpression of *TBX5*, *MEF2C*, *GJA1* and *ACTN1* genes was found when subATDPCs were cultured in 3D environment with chemical cardiogenic induction (*** $p < 0.0001$, ** $p < 0.001$, * $p < 0.01$, ns $p > 0.05$). The combination of 3D environment and chemical induction compared with 2D cultures with chemical induction did not show any significant effect due to the 3D environment itself ($p > 0.05$). On the other hand, as it can be seen in Figure 2.5-12c, the combination of 3D environment with chemical induction caused an overexpression of *TBX5* in all conditions. In the case of *MEF2C* this significant overexpression was only observed in RAD16-I samples ($p < 0.01$ after 2 weeks of culture and $p < 0.0001$ after 4 weeks of culture) and RAD16-I/RADRGD ($p < 0.01$ after 4 weeks of culture). *ACTN1* was highly expressed in all conditions as compared with 2D control medium cultures (between 20 and 60 fold after 2 weeks of culture, and 300 fold in cells cultured on RAD16-I/RADRGD with heparin after 4 weeks of culture). Finally an overexpression of *GJA1* was detected in cells growing in RAD16-I/RADRGD, RAD16-I with heparin and RAD16-I/RADRGD with heparin after 2 weeks of culture and after 4 weeks of culture in cells growing in RAD16-I peptide. It was observed in Figure 2.5-12c that the combination of 3D environment and cardiac induction implied an overexpression of *TBX5, MEF2C* and *GJA1* as compared with the same cells growing in 2D cultures with chemical induction. However, *ACTN1* was much more expressed in these 2D cultures than in the 3D environment.

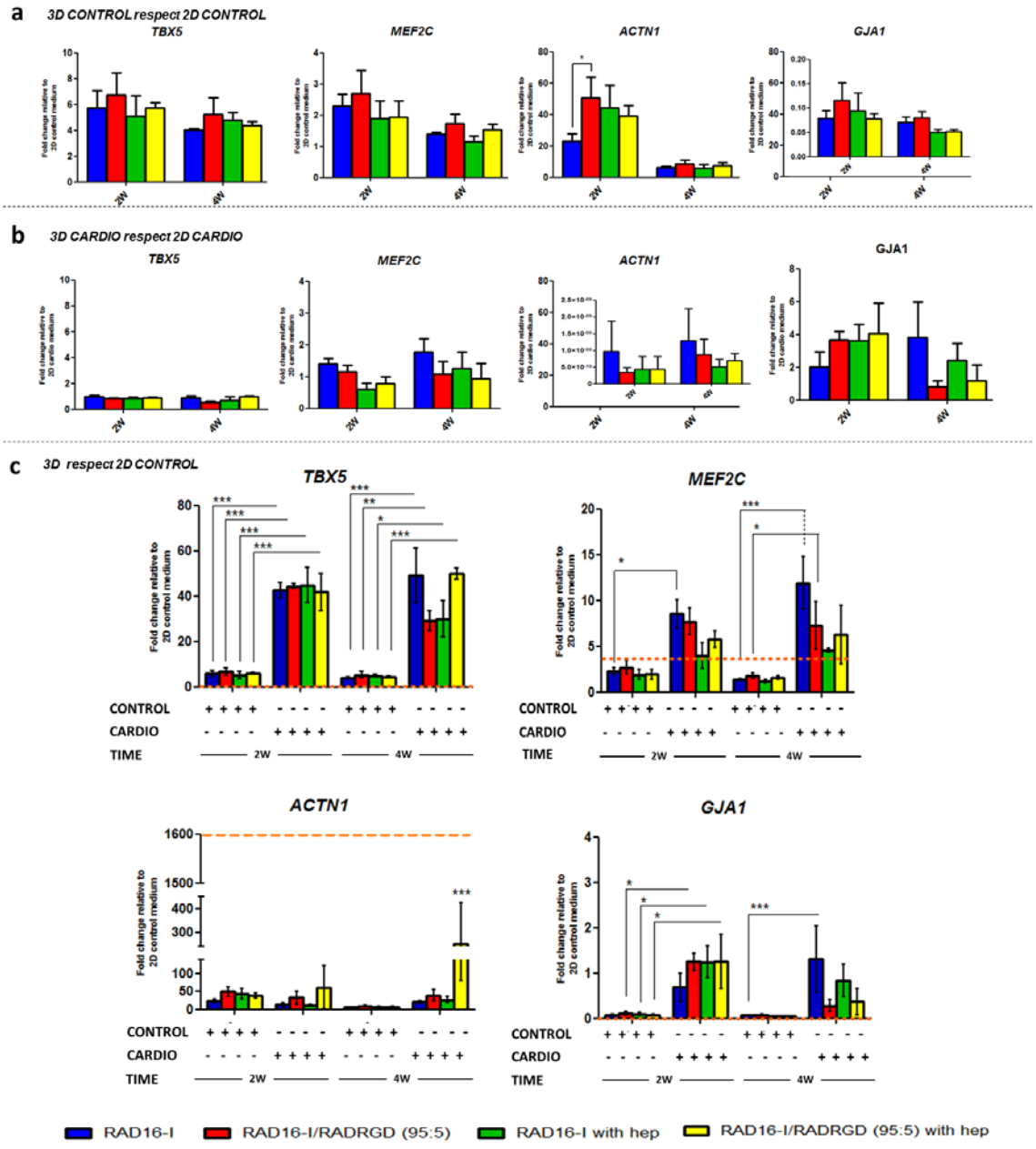

Figure 2.5-12: Early and definitive cardiac markers expression by subATDPCs growing in RAD16-I 0.15 % with and without modification depending on culture media. *TBX5* and *MEF2C* early cardiac markers and *ACTN1* and *GJA1* were quantified by qRT-PCR. The expression of these genes by subATDPCs cultured in four different 3D environment modifications (RAD16-I and RAD16-I/RADRGD with or without heparin) were compared with subATDPCs growing on flat surfaces. (a) 3D cultures growing in control medium were referred to 2D cultures growing in control medium. (b) 3D cultures growing in cardiac induction medium were referred to 2D cultures growing in cardiac induction medium. (c) 3D cultures growing indistinctly in control or cardiac induction medium were referred to 2D cultures with control medium observing a significant effect of the cardiac induction medium (*** $p < 0.0001$, ** $p < 0.001$, * $p < 0.01$, ns $p > 0.05$). The orange dotted lines represent the expression of subATDPCs growing in cardiac induction medium referred to subATDPCs growing in control medium.

At protein level, GATA4 transcription factor and GJA1 (connective protein Cx43) expression were analyzed. Interestingly, we noticed that cardiac induction medium highly increased both GJA1 and GATA4 expression in contrast to control medium. Although, subATDPCs growing in flat surfaces with cardiac induction medium showed expression of GATA4 and GJA1, the environment provided by 3D systems up-regulated it (Figure 2.5-13). Again, it is remarkable

that any either the presence of RGD motif or heparin polysaccharide increased GATA4 or GJA1 expression in comparison with RAD16-I peptide in cardiac induction. Interestingly, only samples containing heparin express GATA4 and only samples without RGD express GJA1 in control medium conditions.

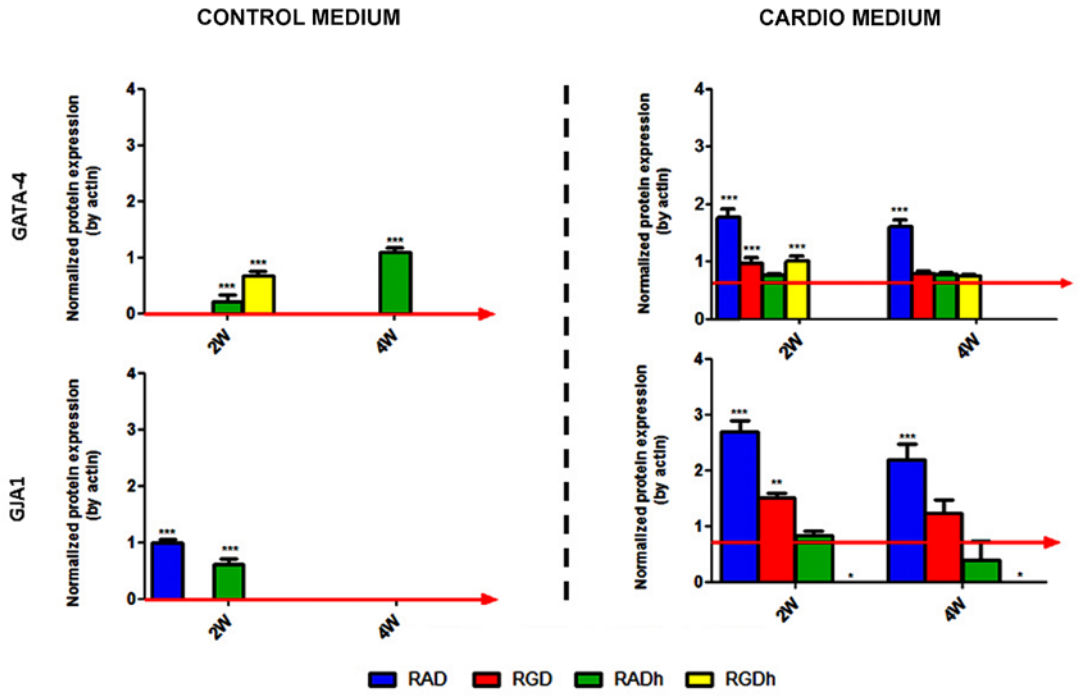

Figure 2.5-13: Protein expression of 3D constructs. (a) GATA4 and GJA1 Western Blot from subATDPCs growing in 3D scaffolds. (b) Quantification of GATA4 and GJA1 expression from subATDPCs growing in 3D scaffolds respect 2D samples in control media and normalization by actin. Red line indicates the normalized protein expression of 2D cultures (by actin). (*** $p < 0.0001$, ** $p < 0.001$, * $p < 0.01$).

2.5.9 Mechanical characterization

Another important aspect to analyze was the stiffness of the matrix where the cells were growing. Viscoelastic properties of 3D constructs were analyzed by dynamic mechanical analysis (DMA). Samples were deformed under an oscillating stress within a range of frequencies and the resultant sinusoidal strain was evaluated. The stress/strain ratio equals the complex viscoelastic modulus (G*) which is defined as $G* = G' + iG''$; where G' is the storage modulus and G" the loss modulus. G' describes the elastic component (measures the stored energy and is related to the stiffness of the sample), and G" represents the viscous component (measures the energy converted to heat and is related to the capacity of the sample to dissipate the energy through molecular motion).

In this case the storage modulus was determined as a measure of the stiffness of the 3D cultures analyzed. It was observed that the proposed modifications did not show differences in storage modulus when the cells were cultured in control medium during 2 weeks. However, the induction with cardio medium promoted an increase of the storage modulus at the same time of

culture (from 4 to 40 KPa). Interestingly, only self-assembling peptides missing heparin and cultured in control medium presented similar storage modulus than constructs cultured with cardiac induction medium (approximately. 40 KPa) after 4 weeks of culture.

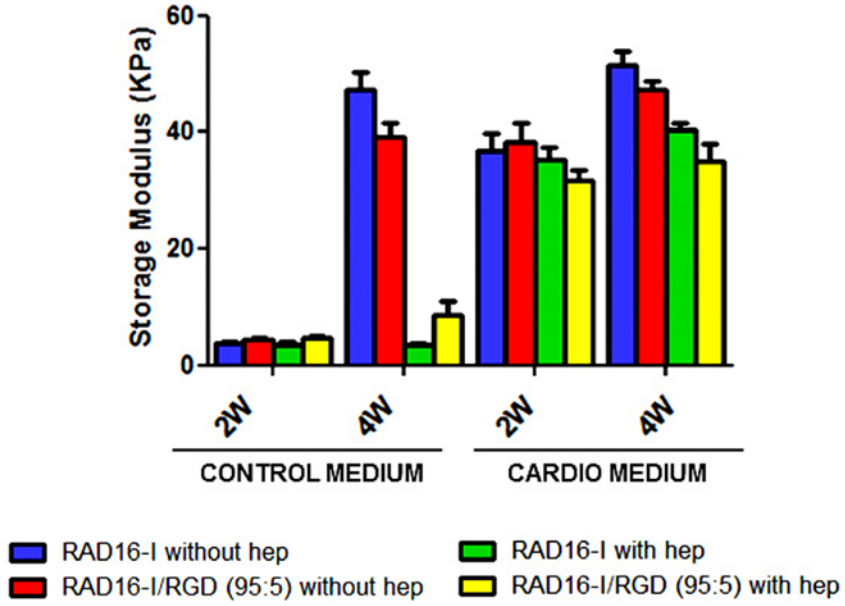

Figure 2.5-14: Dynamic mechanical analysis of subATDPCs encapsulated in RAD16-I with and without modifications (RGD and heparin). Storage modulus of the different matrices was measured in triplicate for each condition

It was suggested that the increase of viscoelastic properties could induce a differential protein expression. Comparing the results obtained by qRT-PCR and DMA it could be stated that the increase of storage modulus lead to an increase of some cardiac genes of subATDPCs. However, the increment in storage modulus in RAD16-I and RAD16-I/RADRGD constructs after 4 weeks of culture in control medium did not show any differential gene expression. Therefore, it could be concluded that in addition to the elasticity of the construct, the signaling provided by the cardiac induction medium is of high importance. It is relevant to remark that in this particular case we were considering the increase of the stiffness effect along the time, but not the initial conditions.

Then, we examined the effect of the material stiffness at the time of the encapsulation (initial conditions). It was previously reported that the increase in nanofiber concentration implies and increase of stiffness (0.15 % RAD16-I corresponds to 120 Pa while 0.2 % RAD16-I to 220 Pa)[85]. SubATDPCs were cultured in RAD16-I and RAD16-I/RADRGD at two different initial stiffness using cardiac induction medium (see Figure 2.5-15). The expression GATA4 (early cardiac marker) and GJA1 (definitive cardiac marker) at protein level were analyzed. As it can be seen in Figure 2.5-15, either initial stiffness conditions as well as matrix modification (RAD16-I/RADRGD) presented a strong effect by down-regulating protein expression ($p <$

0.00001). This effect could be observed clearly at 2 weeks of culture with less significant changes at 4 weeks of culture.

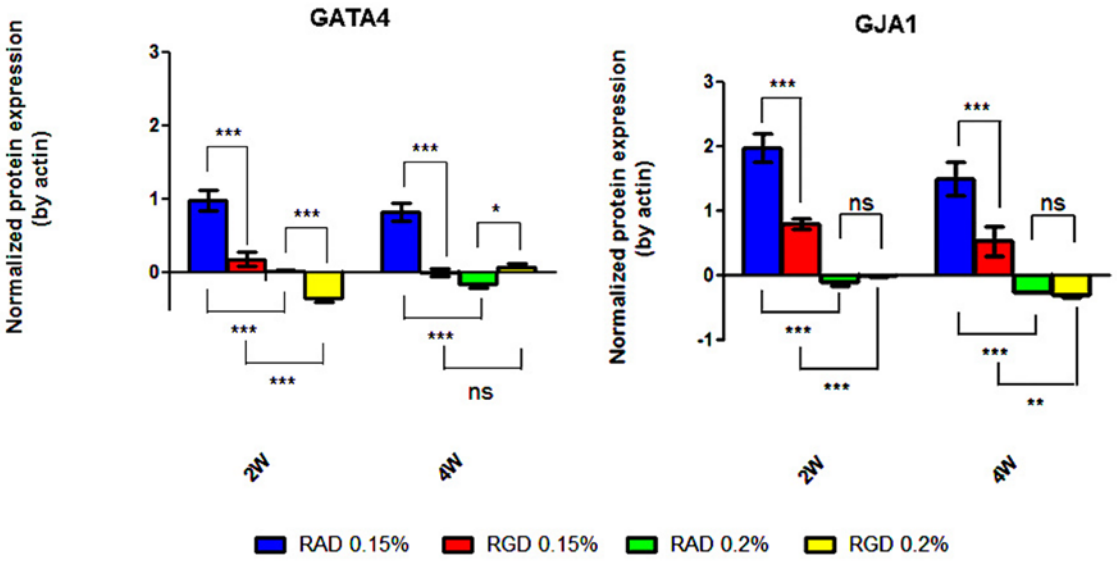

Figure 2.5-15: Protein expression of 3D constructs depending on nanofiber RAD16-I scaffold concentration. **E**ither initial stiffness conditions as well as matrix modification (RAD16-I/RADRGD) present a strong effect by down-regulating protein expression (*** $p < 0.0001$, ** $p < 0.001$, * $p < 0.01$, ns $p > 0.05$). SubATDPCs growing in flat surfaces with cardiac induction medium are taken as control.

GATA4 and GJA1 proteins were significantly down-regulated ($p < 0.0001$) when the initial stiffness of the matrix was 220 Pa as compared with an initial stiffness of 120 Pa ($p < 0.0001$). This pattern was observed after 2 and 4 weeks of culture for RAD16-I matrix except for RGD samples after 4 weeks of cultures where there were no change on GATA4 expression. The addition of RGD motifs in the 3D structure lead to a significant reduction of both proteins expression ($p < 0.0001$) as compared with RAD16-I control matrix. The increase of the stiffness did not show, in the presence of RGD motif a significant effect for GJA1 expression. However, higher stiffness caused GATA4 down-regulation ($p < 0.0001$).

2.6 CONCLUDING REMARKS

Heart is a complex tissue whose behavior is affected by multiple factors. The understanding of the individual effect of each factor can be of great interest for the development of further therapeutic treatments, but the study of all these factors and their combination *in vivo* is extremely difficult[14]. The deconstruction of heart tissue using *in vitro* models can help to elucidate the effect of these factors on healthy or pathologic tissue[86–88]. Different studies in terms of GFs delivery and effect[89–96], gene and protein expression[90,97–110], mechanical properties[111,112], electrical properties[113–118], between others, are nowadays under development.

For the study of all these parameters, different methodologies[15,114,119–124] have been used during the last years with different kind of cells[81,110,125] and materials[8,41,96,122,123,126–132]. 2D cultures allow analyzing cell behavior in a simplistic way and fix some factors before develop a more complex 3D system. Although 2D cultures are the simplest *in vitro* cultures, it is commonly difficult to fix the best parameters for each cell type since they have specific dimensions, behavior, and requirements. For this reason, the isolation of one cell type implies the determination of the best conditions for its culture. In the RECATABI European project, IGTP group defined the basic needs of subATDPCs in 2D cultures. The stipulated conditions (T, gas mixture, and cell growth medium between others) were transferred to 3D cultures.

During last decades, TE has become an important tool for the deconstruction of complex systems using 3D models[14]. Interestingly, combining different materials and different cell types, it is possible to analyze different parameters. Each of these combinations leads to really distinct systems which allow analyzing a wide range of specific parameters[8,122,127,133–135].

In this work, a specific system of subATDPCs entrapped in a 3D matrix of RAD16-I self-assembling peptide with and without integrin-receptor binding (RGD) and heparin binding domains modifications were analyzed. Although the conditions for subATDPCs cultured were previously stipulated, the 3D system itself included additional factors to be taken into account. This 3D model has been widely used with different cell lines, but slight changes such as construct volume, peptide concentration, and cell seeding density must be assessed for each cell type[51,53,56,84,85]. After several analyses, it was concluded that the best working conditions for these cells in 3D cultures of RAD16-I with or without chemical induction were: RAD16-I 0.15 % at cell density of 2,000 cells/μL with α-MEM enriched media from Sigma. The presented results show that slightly differences in 3D cultures conditions highly affect cellular behavior. In this case, a high difference in cell viability and cell network formation was observed with slight changes in culture media. Additionally, cell density, RAD16-I concentration, and construct volume affect cell behavior in terms of network formation. Here, particular attention was focused in cellular connectivity. This concept is really important in cardiac tissue since the

synchronous action of CMs lead to the obtaining of a functional tissue[136]. Therefore, all the commented parameters were switched to obtain a good milieu where the cells could interact forming an intricate network.

Numerous publications are focused on the complete cell differentiation towards a cardiac-like phenotype[134,137–144]. We hypothesize that a complete differentiation for the obtaining of a functional CM-like cells and its further introduction in an ischemic tissue would result in lower cell integration. The final objective of the RECATABI European project was to repopulate the damaged myocardium introducing cells that can differentiate towards CM-like phenotype or promote neovascularization. This may restore contractility and blood supply, and generate favorable atmosphere for native SCs proliferation and differentiation via release of prohomostatic cytokines[145]. We think that *in vitro* cell commitment towards a cardiac phenotype could improve the connectivity, induce further differentiation *in vivo*, and may help to obtain a better functionality. Here, we demonstrated that the 3D environment provided by RAD16-I self-assembling peptide is able to maintain the cardiac commitment of subATDPCs and that chemical induction can induce the overexpression of cardiac markers such as *TBX5*, *MEF2C*, *ACTN1*, and *GJA1*. We hope that these *in vitro* studies provide valuable information for further *in vivo* studies. Interestingly, the viability of subATDPCs encapsulated inside the new nanofiber (with and without the RGD modification and heparin polysaccharide) was completely assessed after 13 and 21 days of culture, which means that a large experiment with mice model could be performed. Additionally, the cell alignment presented in the new nanofiber is a good starting point to obtain cardiomyogenic cells with a degree of organization which indicates their potential spontaneous lineage commitment. Furthermore, cytotoxicity of materials on the stem cells was assessed using MTT assay observing no undesirable results.

Thus it has been demonstrated that RAD16-I nanofiber peptide is a promising material to maintain cells in 3D milieu and analyze the effect of specific cues. Additionally, we propose to use this model to introduce the cells in an infarcted myocardium with the aim to improve the effect of the grafted cells, enhancing their retention and therefore their capability to produce an effect. Nevertheless, this system would not be optimal for *in vivo* implantation since its mechanical behavior is weak and the continuous heart beating has been reported to crush it[146]. Possible alternative is exposed in Chapter 4.

2.7 BIBLIOGRAPHY

1. Heng, B. C., Haider, H. K., Sim, E. K.-W., Cao, T. & Ng, S. C. Strategies for directing the differentiation of stem cells into the cardiomyogenic lineage in vitro. *Cardiovasc Res* **62,** 34–42 (2004).

2. Oberpriller, J. O. & Oberpriller, J. C. Response of the adult newt ventricle to injury. *J. Exp. Zool.* **187,** 249–53 (1974).

3. Laflamme, M. A. & Murry, C. E. Heart regeneration. *Nature* **473,** 326–35 (2011).

4. Institute, H. H. M. Howard Hughes Medical Institute. (2014). at <http://www.hhmi.org/biointeractive/zebrafish-heart-regeneration>

5. Laflamme, M. A. & Murry, C. E. Regenerating the heart. *Nat. Biotechnol.* **23,** 845–856 (2005).

6. Passier, R., van Laake, L. W. & Mummery, C. L. Stem-cell-based therapy and lessons from the heart. *Nature* **453,** 322–9 (2008).

7. Lundberg, M. S. Cardiovascular tissue engineering research support at the National Heart, Lung, and Blood Institute. *Circ. Res.* **112,** 1097–103 (2013).

8. Arnal-Pastor, M., Chachques, J. C., Monleón Pradas, M. & Vallés-Lluch, A. in *Regen. Med. Tissue Eng.* (Andrades, A.) 275–303 (2013). doi:10.5772/56076

9. Baker, M. Why hES cells make teratomas. *Nat. Reports Stem Cells* (2009). doi:10.1038/stemcells.2009.36

10. Hoover-Plow, J. & Gong, Y. Challenges for heart disease stem cell therapy. *Vasc. Health Risk Manag.* **8,** 99–113 (2012).

11. Yamada, K. M. & Cukierman, E. Modeling tissue morphogenesis and cancer in 3D. *Cell* **130,** 601–610 (2007).

12. Pampaloni, F., Reynaud, E. G. & Stelzer, E. H. K. The third dimension bridges the gap between cell culture and live tissue. *Nat. Rev. Mol. Cell Biol.* **8,** 839–45 (2007).

13. Griffith, L. G. & Swartz, M. A. Capturing complex 3D tissue physiology in vitro. *Nat. Rev. Mol. Cell Biol.* **7,** 211–224 (2006).

14. Baker, B. M. & Chen, C. S. Deconstructing the third dimension: how 3D culture microenvironments alter cellular cues. *J. Cell Sci.* **125,** 3015–24 (2012).

15. Castells-Sala, C. *et al.* Current Applications of Tissue Engineering in Biomedicine. *Biochips and Tissue Chips* 0–14 (2013).

16. Smalley, K. S. M., Lioni, M. & Herlyn, M. Life ins't flat: Taking cancer biology to the next dimension. *Vitr. Cell. Dev. Biol.* **42,** 242–247 (2006).

17. Alemany-Ribes, M., García-Díaz, M., Busom, M., Nonell, S. & Semino, C. E. Toward a 3D Cellular Model for Studying In Vitro the Outcome of Photodynamic Treatments: Accounting for the Effects of Tissue Complexity. *Tissue Eng. Part A* (2013).

18. Friedrich, J., Seidel, C., Ebner, R. & Kunz-Schughart, L. A. Spheroid-based drug screen: Considerations and practical approach. *Nat. Protoc.* **4,** 309–24 (2009).

19. Goodman, T. T., Ng, C. P. & Pun, S. H. 3-D tissue culture systems for the evaluation and optimization of nanoparticle-based drug carriers. *Bioconjug. Chem.* **19,** 1951–9 (2008).

20. Griffith, L. G. & Swartz, M. A. Capturing complex 3D tissue physiology in vitro. *Nat. Rev. Mol. Cell Biol.* **7,** 211–24 (2006).

21. Alberts, B. *et al.* in *Biologia Molecular de la Célula* (2011).

22. Rosso, F., Giordano, A., Barbarisi, M. & Barbarisi, A. From cell-ECM interactions to tissue engineering. *J. Cell. Physiol.* **199,** 174–80 (2004).

23. Danen, E. H. J. & Sonnenberg, A. Integrins in regulation of tissue development and function. *J. Pathol.* **201,** 632–41 (2003).

24. Hynes, R. O. Integrins : Bidirectional, Allosteric Signaling Machines. *Cell* **110,** 673–687 (2002).

25. Luo, B.-H., Carman, C. V & Springer, T. A. Structural basis of integrin regulation and signaling. *Annu. Rev. Immunol.* **25,** 619–47 (2007).

26. Ridley, A. *et al.* Cell migration: integrating signals from front to back. *Science.* **302,** 1704–9 (2003).

27. Grashoff, C., Thievessen, I., Lorenz, K., Ussar, S. & Fässler, R. Integrin-linked kinase: integrin's mysterious partner. *Curr. Opin. Cell Biol.* **16,** 565–71 (2004).

28. Guo, W. & Giancotti, F. G. Integrin signalling during tumour progression. *Nat. Rev. Mol. Cell Biol.* **5,** 816–26 (2004).

29. Danen, E. H. J. in *Integrins Dev.* (Landes Bioscience, 2006). at <http://www.landesbioscience.com/curie/chapter/2710/>

30. Science, W. institute of. Gene Cards. *2014* (2014). at <http://www.genecards.org/>

31. Nelson, J. *et al.* The 67 kDa laminin receptor: structure, function and role in disease. *Biosci. Rep.* **28,** 33–48 (2008).

32. Raven, P. H., Johnson, G. B., Mason, K., Losos, J. & Singer, S. in *Biology (Basel).* (Reidy, P., Melde, A. & Weiss, L. A.) 123–140 (2001). at <http://www.mhhe.com/biosci/genbio/raven6b/information/olc/samplechapter.mhtml>

33. Anderson, J. M. & Van Itallie, C. M. Physiology and function of the tight junction. *Cold Spring Harb. Perspect. Biol.* **1,** a002584 (2009).

34. Singapore, M. I., Singapore, N. U., Ministery of Education, S. & Fundation, N. R. MB Info - A modular approach to cellular functions. *2014* (2014). at <http://www.mechanobio.info/modules/go-0007155/02_go-0007155>

35. Goodenough, D. a & Paul, D. L. Gap junctions. *Cold Spring Harb. Perspect. Biol.* **1,** a002576 (2009).

36. Chachques, J. C. Development of bioartificial myocardium using stem cells and nanobiotechnology templates. *Cardiol. Res. Pract.* **2011,** 806795 (2010).

37. Zhang, S. & Altman, M. Peptide self-assembly in functional polymer science and engineering. *React. Funct. Polym.* **41,** 91–102 (1999).

38. Genové, E., Shen, C., Zhang, S. & Semino, C. E. The effect of functionalized self-assembling peptide scaffolds on human aortic endothelial cell function. *Biomaterials* **26,** 3341–3351 (2005).

39. Jun, S. *et al.* Self-assembly of the ionic peptide EAK16: the effect of charge distributions on self-assembly. *Biophys. J.* **87,** 1249–59 (2004).

40. Zhang, S. Fabrication of novel biomaterials through molecular self-assembly. *Nat. Biotechnol.* **21,** 1171–8 (2003).

41. Zhang, S., Ellis-behnke, R. & Zhao, X. *Scaffolding in Tissue Engineering. CHAPTER 15: PuraMatrix : Self-assembling Peptide Nanofiber Scaffolds*. 217–248 (2006).

42. Zhang, S. *et al.* Self-complementary oligopeptide matrices support mammalian cell attachment. *Biomaterials* **16,** 1385–1393 (1995).

43. Semino, C. E. Self-assembling peptides: from Bio-inspired Materials to Bone Regeneration. *J. Dent. Res.* **87,** 606–616 (2008).

44. Ellis-behnke, R. G. *et al.* Nano neuro knitting: Peptide nanofiber scaffold for brain repair and axon regeneration with functional return of vision. *PNAS* **103,** 5054–5059 (2006).

45. Zhang, S. & Rich, A. Direct conversion of an oligopeptide from a beta-sheet to an alpha-helix: a model for amyloid formation. *Proc Natl Acad Sci U S A* **94,** 23–28 (1997).

46. Zhang, S., Holmes, T., Lockshin, C. & Rich, A. Spontaneous assembly of self-complementary oligopeptide to form a stable macroscopic membrane. *Proc. Natl. Acad. Sci. USA* **90,** 3334–3338 (1993).

47. Dégano, I. R. *et al.* The effect of self-assembling peptide nanofiber scaffolds on mouse embryonic fibroblast implantation and proliferation. *Biomaterials* **30,** 1156–65 (2009).

48. Sieminski, a L., Semino, C. E., Gong, H. & Kamm, R. D. Primary sequence of ionic self-assembling peptide gels affects endothelial cell adhesion and capillary morphogenesis. *J. Biomed. Mater. Res. A* **87,** 494–504 (2008).

49. Garreta, E., Genové, E., Borrós, S. & Semino, C. E. Osteogenic differentiation of mouse embryonic stem cells and mouse embryonic fibroblasts in a three-dimensional self-assembling peptide scaffold. *Tissue Eng.* **12,** 2215–27 (2006).

50. Garreta, E., Gasset, D., Semino, C. & Borrós, S. Fabrication of a three-dimensional nanostructured biomaterial for tissue engineering of bone. *Biomol. Eng.* **24,** 75–80 (2007).

51. Quintana, L. *et al.* Early Tissue Patterning Recreated by Mouse Embryonic Fibroblasts in a Three-Dimensional Environment. *Tissue Eng.* **15,** 45–54 (2009).

52. Fernández-Muiños, T., Suárez-Muñoz, M., Sanmartí-Espinal, M. & Semino, C. E. Matrix dimensions, stiffness, and structural properties modulate spontaneous chondrogenic commitment of mouse embryonic fibroblasts. *Tissue Eng. Part A* **20,** 1145–55 (2014).

53. Bussmann, B. M. *et al.* Chondrogenic potential of human dermal fibroblasts in a contractile, soft, self-assembling, peptide hydrogel. *J. Tissue Eng. Regen. Med.* (2013).

54. Sieminski, A. L., Was, a. S., Kim, G., Gong, H. & Kamm, R. D. The Stiffness of Three-dimensional Ionic Self-assembling Peptide Gels Affects the Extent of Capillary-like Network Formation. *Cell Biochem. Biophys.* **49,** 73–83 (2007).

55. Genové, E. *et al.* Functionalized self-assembling peptide hydrogel enhance maintenance of hepatocyte activity in vitro. *J. Cell. Mol. Med.* **13,** 3387–3397 (2009).

56. Wu, J. *et al.* Nanometric self-assembling peptide layers maintain adult hepatocyte phenotype in sandwich cultures. *J. Nanobiotechnology* **8,** 29 (2010).

57. Semino, C. E. Can we build artificial stem cell compartments? *J. Biomed. Biotechnol.* **3,** 164–169 (2003).

58. Liu, J. *et al.* Generation, Characterization and Potential Therapeutic Applications of Cardiomyocytes from Various Stem Cells. *Stem Cells Dev.* **21,** 2095–110 (2012).

59. Li, Z., Guo, X. & Guan, J. A Thermosensitive Hydrogel Capable of Releasing bFGF for Enhanced Differentiation of Mesenchymal Stem Cell into Cardiomyocyte-like Cells under Ischemic Conditions. *Biomacromolecules* **13,** 1956–64 (2012).

60. Baumann, L. *et al.* A novel, biased-like SDF-1 derivative acts synergistically with starPEG-based heparin hydrogels and improves eEPC migration in vitro. *J. Control. Release* **162,** 68–75 (2012).

61. Hersel, U., Dahmen, C. & Kessler, H. RGD modified polymers: biomaterials for stimulated cell adhesion and beyond. *Biomaterials* **24,** 4385–415 (2003).

62. Rajangam, K. *et al.* Heparin binding nanostructures to promote growth of blood vessels. *Nano Lett.* **6,** 2086–90 (2006).

63. Guo, H. *et al.* Sustained delivery of VEGF from designer self-assembling peptides improves cardiac function after myocardial infarction. *Biochem. Biophys. Res. Commun.* **424,** 105–11 (2012).

64. Naderi, H., Matin, M. M. & Bahrami, A. R. Review paper: critical issues in tissue engineering: biomaterials, cell sources, angiogenesis, and drug delivery systems. *J. Biomater. Appl.* **26,** 383–417 (2011).

65. Murugesan, S., Xie, J. & Linhardt, R. J. Immobilization of heparin: approaches and applications. *Curr. Top. Med. Chem.* **8,** 80–100 (2008).

66. Muñoz, E. M. & Linhardt, R. J. Heparin-binding domains in vascular biology. *Arterioscler. Thromb. Vasc. Biol.* **24,** 1549–57 (2004).

67. Sakiyama-Elbert, S. E. & Hubbell, J. a. Development of fibrin derivatives for controlled release of heparin-binding growth factors. *J. Control. Release* **65,** 389–402 (2000).

68. Ono, K., Hattori, H., Takeshita, S., Kurita, A. & Ishihara, M. Structural features in heparin that interact with VEGF165 and modulate its biological activity. *Glycobiology* **9,** 705–711 (1999).

69. Benoit, D. S. W. & Anseth, K. S. Heparin functionalized PEG gels that modulate protein adsorption for hMSC adhesion and differentiation. *Acta Biomater.* **1,** 461–70 (2005).

70. Wissink, M. J. *et al.* Binding and release of basic fibroblast growth factor from heparinized collagen matrices. *Biomaterials* **22,** 2291–9 (2001).

71. Tanihara, M., Suzuki, Y., Yamamoto, E., Noguchi, a & Mizushima, Y. Sustained release of basic fibroblast growth factor and angiogenesis in a novel covalently crosslinked gel of heparin and alginate. *J. Biomed. Mater. Res.* **56,** 216–21 (2001).

72. Singh, S., Wu, B. M. & Dunn, J. C. Y. The enhancement of VEGF-mediated angiogenesis by polycaprolactone scaffolds with surface cross-linked heparin. *Biomaterials* **32,** 2059–69 (2011).

73. Lee, K. W. *et al.* Sustained release of vascular endothelial growth factor from calcium-induced alginate hydrogels reinforced by heparin and chitosan. *Transplant. Proc.* **36,** 2464–5 (2004).

74. Ventura, C. & Maioli, M. Embryonal Pluripotent Stem Cells. *Gene Expr.* (2000).

75. Pandur, P. What does it take to make a heart? *Biol. Cell* **97,** 197–210 (2005).

76. Smits, A. M. *et al.* Human cardiomyocyte progenitor cells differentiate into functional mature cardiomyocytes: an in vitro model for studying human cardiac physiology and pathophysiology. *Nat. Protoc.* **4,** 232–43 (2009).

77. Roura, S. *et al.* Exposure to cardiomyogenic stimuli fails to transdifferentiate human umbilical cord blood-derived mesenchymal stem cells. *Basic Res. Cardiol.* **105,** 419–30 (2010).

78. Mitsumoto, Y., Liu, Z. & Klip, A. A long-lasting vitamin C derivative, ascorbic acid 2-phosphate, increases myogenin gene expression and promotes differentiation in L6 muscle cells. *Biochem. Biophys. Res. Commun.* **199,** 394–402 (1994).

79. Fernández-Muiños, T. *et al.* Bimolecular based heparin and self-assembling hydrogel for tissue engineering applications. *Acta Biomater.* (under submission) (2014).

80. Roura, S. *et al.* Effect of aging on the pluripotential capacity of human CD105+ mesenchymal stem cells. *Eur. J. Heart Fail.* **8,** 555–63 (2006).

81. Cashman, T. J., Gouon-Evans, V. & Costa, K. D. Mesenchymal stem cells for cardiac therapy: practical challenges and potential mechanisms. *Stem Cell Rev.* **9,** 254–65 (2013).

82. Bayes-Genis, A. *et al.* Human progenitor cells derived from cardiac adipose tissue ameliorate myocardial infarction in rodents. *J Mol Cell Cardiol.* **49,** 771–80 (2010).

83. Martinez-Estrada, O., Munoz-Santos, Y., Julve, J., Reina, M. & Vilaro, S. Human adipose tissue as a source of Flk-1+ cells: new method of differentiation and expansion. *Cardiovasc. Res.* **65,** 328–33 (2005).

84. Fernández-Muiños, M. T. Effect of the microenvironment in the in vitro chondrogenic and osteogenic differentiation of mouse embryonic fibroblasts. (2013).

85. Marí-Buyé, N., Luque, T., Navajas, D. & Semino, C. C. E. Development of a three-dimensional bone-like construct in a soft self-assembling peptide matrix. *Tissue Eng. Part A* **19,** 870–881 (2013).

86. Pallua, N. & Suschek, C. V. *Tissue Engineering: From Lab to Clinic*. (2011).

87. Daley, G. Q. Review series introduction Stem cells : roadmap to the clinic. *J. Clin. Invest.* **120,** 8–10 (2010).

88. Prestwich, G. D. *et al.* What Is the Greatest Regulatory Challenge in the Translation of Biomaterials to the Clinic? *Sci. Transl. Med.* **4,** 1–6 (2012).

89. Ferrara, N., Gerber, H.-P. & LeCouter, J. The biology of VEGF and its receptors. *Nat. Med.* **9,** 669–76 (2003).

90. Jamali, M., Karamboulas, C., Rogerson, P. J. & Skerjanc, I. S. BMP signaling regulates Nkx2-5 activity during cardiomyogenesis. *FEBS Lett.* **509,** 126–30 (2001).

91. Claes, F., Vandevelde, W., Moons, L. & Tjwa, M. Another angiogenesis-independent role for VEGF: SDF1-dependent cardiac repair via cardiac stem cells. *Cardiovasc. Res.* **91,** 369–70 (2011).

92. Tang, J.-M. *et al.* VEGF/SDF-1 promotes cardiac stem cell mobilization and myocardial repair in the infarcted heart. *Cardiovasc. Res.* **91,** 402–11 (2011).

93. Chiriac, A., Nelson, T. J., Faustino, R. S., Behfar, A. & Terzic, A. Cardiogenic induction of pluripotent stem cells streamlined through a conserved SDF-1/VEGF/BMP2 integrated network. *PLoS One* **5,** e9943 (2010).

94. Cheng, M., Moretti, M., Engelmayr, G. C. J. & Freed, L. E. Insulin-like Growth Factor-I and Slow, Bi-directional Perfusion Enhance the Formation of Tissue-Engineered Cardiac Grafts. *Tissue Eng Part A* **15,** (2009).

95. Liu, Z. *et al.* WNT signaling promotes Nkx2.5 expression and early cardiomyogenesis via downregulation of Hdac1. *Biochim. Biophys. Acta* **1793,** 300–11 (2009).

96. Puig-Sanvicens, V. & Semino, C. E. Self-assembling peptide scaffolds as innovative platforms for drug and cell delivery systems in cardiac regeneration. *Drug Deliv. Transl. Res.* **3,** 330–335 (2013).

97. Lockhart, M. M. *et al.* Mef2c regulates transcription of the extracellular matrix protein cartilage link protein 1 in the developing murine heart. *PLoS One* **8,** e57073 (2013).

98. Island, M.-L., Fatih, N., Leroyer, P., Brissot, P. & Loreal, O. GATA-4 transcription factor regulates hepatic hepcidin expression. *Biochem. J.* **437,** 477–82 (2011).

99. Wen, X.-Z. Methylation of GATA-4 and GATA-5 and development of sporadic gastric carcinomas. *World J. Gastroenterol.* **16,** 1201 (2010).

100. Schlesinger, J. *et al.* The cardiac transcription network modulated by Gata4, Mef2a, Nkx2.5, Srf, histone modifications, and microRNAs. *PLoS Genet.* **7,** 1–16 (2011).

101. Li, H. *et al.* Paracrine factors released by GATA-4 overexpressed mesenchymal stem cells increase angiogenesis and cell survival. *Am. J. Physiol. Heart Circ. Physiol.* **299,** H1772–81 (2010).

102. Vincentz, J. W., Barnes, R. M., Firulli, B. A., Conway, S. J. & Anthony, B. Cooperative interaction of Nkx2.5 and Mef2c transcription factors during heart development. **237,** 3809–3819 (2008).

103. Oka, T. *et al.* Cardiac-specific deletion of Gata4 reveals its requirement for hypertrophy, compensation, and myocyte viability. *Circ. Res.* **98,** 837–45 (2006).

104. Bisping, E. *et al.* Gata4 is required for maintenance of postnatal cardiac function and protection from pressure overload-induced heart failure. *Proc. Natl. Acad. Sci. U. S. A.* **103,** 14471–6 (2006).

105. Akazawa, H. & Komuro, I. Cardiac transcription factor Csx/Nkx2-5: Its role in cardiac development and diseases. *Pharmacol. Ther.* **107,** 252–68 (2005).

106. Moskowitz, I. P. G. *et al.* The T-Box transcription factor Tbx5 is required for the patterning and maturation of the murine cardiac conduction system. *Development* **131,** 4107–16 (2004).

107. Hiroi, Y. *et al.* Tbx5 associates with Nkx2-5 and synergistically promotes cardiomyocyte differentiation. *Nat. Genet.* **28,** 276–80 (2001).

108. Maynard, S. J., Menown, I. B. & Adgey, a a. Troponin T or troponin I as cardiac markers in ischaemic heart disease. *Heart* **83,** 371–3 (2000).

109. Horb, M. E. & Thomsen, G. H. Tbx5 is essential for heart development. *Development* **126,** 1739–51 (1999).

110. Cyganek, L. Cardiac Progenitor Cells and their Therapeutic Application for Cardiac Repair. *J. Clin. Exp. Cardiolog.* **01,** (2013).

111. Burkhoff, D. & Physiology, C. Mechanical Properties of the heart and its interaction with the vascular system. *Card. Physiol.* 1–17 (2011).

112. Jawad, H., Lyon, A. R., Harding, S. E., Ali, N. N. & Boccaccini, A. R. Myocardial tissue engineering. *Br. Med. Bull.* **87,** 31–47 (2008).

113. Balint, R., Cassidy, N. J. & Cartmell, S. H. Electrical Stimulation : A Novel Tool. *Tissue Eng. Part B. Rev.* **19,** 48–57 (2013).

114. Spadaccio, C. *et al.* In situ electrostimulation drives a regenerative shift in the zone of infarcted myocardium. *Cell Transplant.* **22,** 493–503 (2013).

115. Hronik-tupaj, M. & Kaplan, D. L. A Review of the Responses of Two- and Three-Dimensional Engineered Tissues to Electric Fields. *Tissue Eng. Part B. Rev.* **18,** 167–180 (2012).

116. Huang, G., Pashmforoush, M., Chung, B. & Saxon, L. a. The role of cardiac electrophysiology in myocardial regenerative stem cell therapy. *J. Cardiovasc. Transl. Res.* **4,** 61–5 (2011).

117. Tandon, N. *et al.* Surface-patterned electrode bioreactor for electrical stimulation. *Lab Chip* **10,** 692–700 (2010).

118. Llucià-Valldeperas, A. *et al.* Electrical stimulation of cardiac adipose tissue-derived progenitor cells modulates cell phenotype and genetic machinery. *J Tissue Eng Regen Med.* (2013). doi:10.1002/term.1710.

119. Curtis, M. W. & Russell, B. Cardiac tissue engineering. *J. Cardiovasc. Nurs.* **24,** 87–92 (2009).

120. Kawaguchi, N., Hatta, K. & Nakanishi, T. 3D-culture system for heart regeneration and cardiac medicine. *Biomed Res. Int.* **2013,** 895967 (2013).

121. Le Huu, A., Paul, A., Xu, L., Prakash, S. & Shum-Tim, D. Recent advancements in tissue engineering for stem cell-based cardiac therapies. *Ther. Deliv.* **4,** 503–16 (2013).

122. Ikonen, L. *et al.* 2D and 3D Self-Assembling Nanofiber Hydrogels for Cardiomyocyte Culture. *Biomed Res. Int.* 12 (2013).

123. Shin, S. R. *et al.* Hydrogel Sheets for Engineering Cardiac Constructs and Bioactuators. *ACS Nano* 2369–2380 (2013).

124. Hansson, E. M. & Lendahl, U. Regenerative medicine for the treatment of heart disease. *J. Intern. Med.* **273,** 235–45 (2013).

125. Pawani, H. & Bhartiya, D. Pluripotent stem cells for cardiac regeneration: Overview of recent advances & emerging trends. *Indian J. Med. Res.* **137,** 270–82 (2013).

126. Soler-botija, C. *et al.* Engineered 3D bioimplants using elastomeric scaffold , self-assembling peptide hydrogel , and adipose tissue-derived progenitor cells for cardiac regeneration. *Am. J. Transl. Res.* **6,** 291–301 (2014).

127. Hernandez-Gordillo, V. & Chmielewski, J. Mimicking the extracellular matrix with functionalized, metal-assembled collagen peptide scaffolds. *Biomaterials* **35,** 7363–73 (2014).

128. Fisher, S. a, Tam, R. Y. & Shoichet, M. S. Tissue mimetics: engineered hydrogel matrices provide biomimetic environments for cell growth. *Tissue Eng. Part A* **20,** 895–8 (2014).

129. Marion, M. H. van, Bax, N. A. M., Spreeuwel, A. C. C. van, van der Schaft, D. W. J. & Bouten, C. V. C. Material-based engineering strategies for cardiac regeneration. *Curr. Pharm. Des.* **20,** 2057–68 (2014).

130. Hardy, J. G., Lee, J. Y. & Schmidt, C. E. Biomimetic conducting polymer-based tissue scaffolds. *Curr. Opin. Biotechnol.* **24,** 847–54 (2013).

131. Hashizume, R. *et al.* Biodegradable elastic patch plasty ameliorates left ventricular adverse remodeling after ischemia-reperfusion injury: a preclinical study of a porous polyurethane material in a porcine model. *J. Thorac. Cardiovasc. Surg.* **146,** 391–9.e1 (2013).

132. Vallés-Lluch, A. *et al.* Combining self-assembling peptide gels with three-dimensional elastomer scaffolds. *Acta Biomater.* **9,** 9451–9460 (2013).

133. Herrmann, F. E. M. *et al.* In vitro biological and mechanical evaluation of various scaffold materials for myocardial tissue engineering. *J. Biomed. Mater. Res. A* **102,** 958–66 (2014).

134. Dahlmann, J. *et al.* The use of agarose microwells for scalable embryoid body formation and cardiac differentiation of human and murine pluripotent stem cells. *Biomaterials* **34,** 2463–71 (2013).

135. Gnanaprakasam Thankam, F., Muthu, J., Sankar, V. & Kozhiparambil Gopal, R. Growth and survival of cells in biosynthetic poly vinyl alcohol-alginate IPN hydrogels for cardiac applications. *Colloids Surf. B. Biointerfaces* **107,** 137–45 (2013).

136. Severs, N. J. The cardiac muscle cell. *Bioessays* **22,** 188–99 (2000).

137. Fujikura, J. *et al.* Differentiation of embryonic stem cells is induced by GATA factors. *Genes Dev.* **16,** 784–9 (2002).

138. Roche, S., Richard, M.-J. & Favrot, M.-C. Oct-4, Rex-1, and Gata-4 expression in human MSC increase the differentiation efficiency but not hTERT expression. *J. Cell. Biochem.* **101,** 271–80 (2007).

139. Chen, M. Q. *et al.* Cardiac differentiation of embryonic stem cells with point-source electrical stimulation. *Conf. Proc. IEEE Eng. Med. Biol. Soc.* **2008,** 1729–32 (2008).

140. Boheler, K. R. Differentiation of Pluripotent Embryonic Stem Cells Into Cardiomyocytes. *Circ. Res.* **91,** 189–201 (2002).

141. Planat-Bénard, V. *et al.* Spontaneous cardiomyocyte differentiation from adipose tissue stroma cells. *Circ. Res.* **94,** 223–9 (2004).

142. Gong, J. *et al.* SRC kinase family inhibitor PP2 promotes DMSO-induced cardiac differentiation of P19 cells and inhibits proliferation. *Int. J. Cardiol.* (2012).

143. Huang, Y. *et al.* Effect of cyclic strain on cardiomyogenic differentiation of rat bone marrow derived mesenchymal stem cells. *PLoS One* **7,** e34960 (2012).

144. Serena, E. *et al.* Electrical stimulation of human embryonic stem cells: Cardiac differentiation and the generation of reactive oxygen species. *Cell* **315,** 3611–3619 (2010).

145. Genovese, J. A. *et al.* Cell Based Approaches for Myocardial Regeneration and Artificial Myocardium. *Curr. Stem Cell Res. Ther.* **7,** 121–127 (2007).

146. Dubois, G. *et al.* Self-assembling peptide nanofibers and skeletal myoblast transplantation in infarcted myocardium. *J. Biomed. Mater. Res. B. Appl. Biomater.* **87,** 222–8 (2008).

CHAPTER 3: Set-up of electrical stimulation system for RAD16-I 3D model and preliminary study of its effect on subcutaneous adipose tissue derived progenitor cells

Work presented in Engineering in Medicine and Biology Society (EMBC), 2012 Annual International Conference of the IEEE.

Published by IEEE under the title: Influence of electrical stimulation during cardiac differentiation in 3D-cultures of subcutaneous Adipose Tissue Derived Progenitor Cells (subATDPCs). Castells-Sala *et. al.* (012

3.1 BACKGROUND

3.1.1 Overview

Cardiac muscle participates actively in the contraction of the heart atria and ventricles. This movement causes the rhythmical beating of the heart, which induce the circulation of the blood and its contents throughout the circulatory system of the body. The most exceptional property of this muscle is its capacity to initiate an electrical potential at a fixed rate that spreads rapidly from cell to cell to trigger the contractile mechanism without connection to other parts of the body. This electrical stimuli play pivotal roles in muscle cell function, as cell fate and function are tightly regulated in response to environmental factors and intercellular signals[12]. The generation and precise time distribution of the electrical impulse is initiated by the Pacemaker cells situated in the sinoatrial (SA) node (see Figure 1.1-5). The action potential spreads all over the heart causing depolarization of cellular membranes and activation of the contractile apparatus in cardiomyocytes (CMs)[3]. For the synchronous contraction of the heart muscle itself, it is imperative the tight connection of CMs to enable the propagation of electrical signals all across the heart[4].

After myocardial infarction (MI), adverse remodeling and scar tissue formation due to intracellular signaling and neurohormonal activation actively affects heart contraction. The newly remodeled tissue shows poor cell-cell coupling which results from cell death and loss of gap junctions. Progressively, the wall of the scarred area becomes thinner affecting the systolic function and increasing the wall stress. This fact promotes further adverse remodeling with left ventricle dilatation, apoptosis and necrosis of myocytes, which increase cell disconnection[5]. This fact affects the spread of electrical excitation wave along the plasma membranes of adjoining cardiac muscle cells. In a healthy myocardium, cell connection triggers the release of calcium from an intracellular membrane-bound compartment, the sarcoplasmic reticulum, which increases cytoplasmic calcium and consequently stimulates contraction of the myofibrils[4]. Individual CM must depolarize and contract in a coordinated fashion in order to generate forces for pumping blood. Myocardial ischemia depresses active electrical cell membrane properties, and this generates regional potential differences between normal and ischemic compartments[6].

The emergence of cell grafting as a novel approach for the treatment of heart diseases leads the scientific community to develop diverse methodologies to improve its efficiency. The implanted cells must tolerate the action potential of the native myocardium and at the same time coupling with it. The arrhythmias associated with selective cell therapies are in part attributed to the lack of integration and electrical coupling of the cells with the recipient myocardium. Therefore, in

addition to survival and function, the electrical integration of grafts is a significant challenge to solve. In other terms, electrical signals are present during normal fetal development, and it is thus reasonable to hypothesize that similar stimulus may play a role in the differentiation and integration of cells introduced into a cardiac tissue[3,7]. It is believed that electrical integration can be improved by engineering cardiac tissue constructs *in vitro* before grafting[8].

In this chapter, it will be analyzed the effect of electrical stimulation (ES) in the constructs presented in Chapter 2. Specifically, a new system will be developed to allow the use of ES on RAD16-I three-dimensional (3D) models with the aim to evaluate its effect on the encapsulated cells (subcutaneous adipose tissue derived progenitor cells, subATDPCs). The viability, morphology, and proliferation of subATDPCs encapsulated in the self-assembling peptide under chemical and electrical stimuli will be analyzed.

3.1.2 Myocardial fibers and impulse propagation

As commented in Chapter 1, cardiac muscle is an involuntary striated muscle formed by cylindrically shaped cells called CM with sizes ranging between 80-150 μm in length and 10-20 μm in diameter[9]. CMs are markedly elongated and form layers of tissue with sharply demarcated fiber orientation (see Figure 3.1-1), leading to anisotropic architecture (directionally dependent)[10,11].

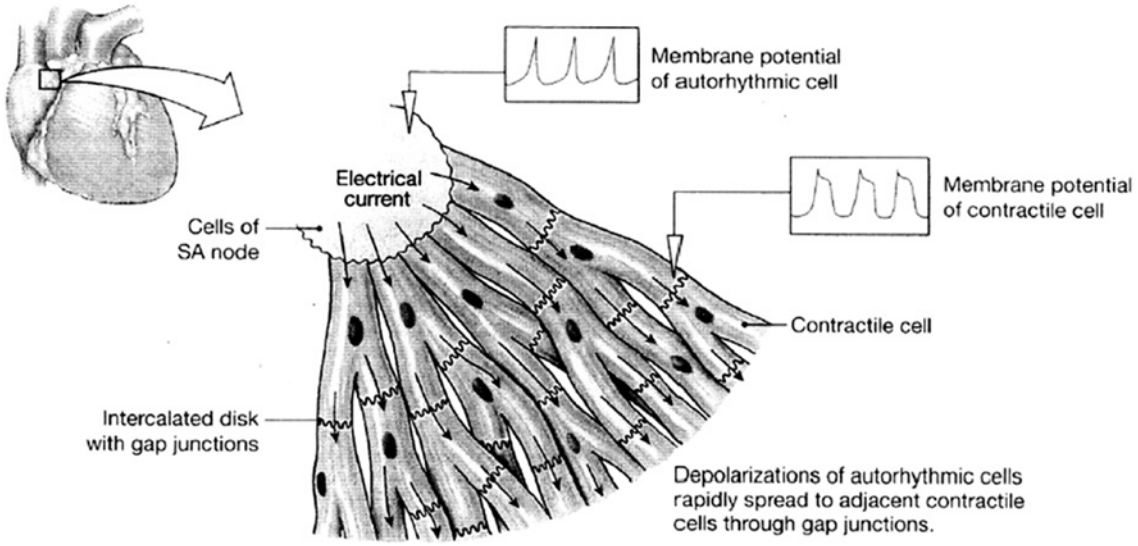

Figure 3.1-1: Myocardial tissue is characterized for an anisotropic architecture. In 1954, it was demonstrated that cardiac tissue is comprised of individual CMs completely bounded by membrane. Subsequently, gap junctions and their distribution as mediators of intercellular communication were described[12].

Tissue anisotropy is a valuable property for normal impulse propagation, because such fiber orientation impacts on directional variations of certain properties, most commonly, conduction velocity[12]. The principal determinant of anisotropic conduction in ventricular muscle is the elongated shape of the cells rather than the junctions distribution. Cell geometry (elongation)

determines the number of junctions per unit space that propagation has to go through in different directions. For example, numerous sites for intercellular current transfer exist in both directions, but because of the elongated shape of the cells, a wave front moving in the transverse direction must cross more intercellular junctions. Thus, the wave fronts would encounter greater resistance and propagate more slowly than wave fronts traveling an equal distance in the longitudinal direction[13].

3.1.3 Electrical synchronism of cardiomyocytes

The CMs are the most physically energetic cell in the body, contracting continuously, without tiring, 3 billion times or more in an average human lifespan[4]. In a CM cytoplasm, known as sarcoplasm, there are numerous mitochondria (40 % of the cytoplasmic volume), which reflects the large energy demands of the heart[14]. An important structure within the CM is the sarcomere, which represents its basic contractile unit. It is formed by myofibrils that run parallel to the long axis of the fiber and are composed of long proteins such as actin and myosin and other proteins that hold them together. These proteins are organized into thin (actin), and thick (myosin) filaments repeated all along the length of the myofibril. CMs are surrounded by a cell membrane called sarcolemma and typically contain one or two nucleus. Additionally, they are surrounded by a delicate connective tissue framework that contains an extensive capillary network that ensures their high metabolic demands of cardiac cells (Figure 3.1-2a).

To produce a heartbeat, the contractile capabilities of the billions of CM that make up the heart have to be mustered in a highly synchronous fashion. This specific assembly requires both an orderly spread of the electrical activation wave and an efficient transmission of contractile force from one cell to another. This issue is faced creating a 3D syncytium with intimate joins of neighboring cells through the membranes. CMs are arranged end-to-end so that a cardiac muscle fiber is composed of individual muscle cells. At their ends, these cells often divide themselves longitudinally before joining to adjacent fibers. This type of division allows cells to form connections with several of its neighbors forming a network of branching fibers. The specialized end-to-end arrangements between adjacent CMs are thickened plasma membranes called intercalated discs that help to hold adjacent cells together and transmit the force of contraction from cell to cell. Intercalated disks integrate the activities of individual cells and provide continuity between adjacent CMs, serving as electrical synapses to allow impulses to pass from cell to cell (Figure 3.1-2b)[15].

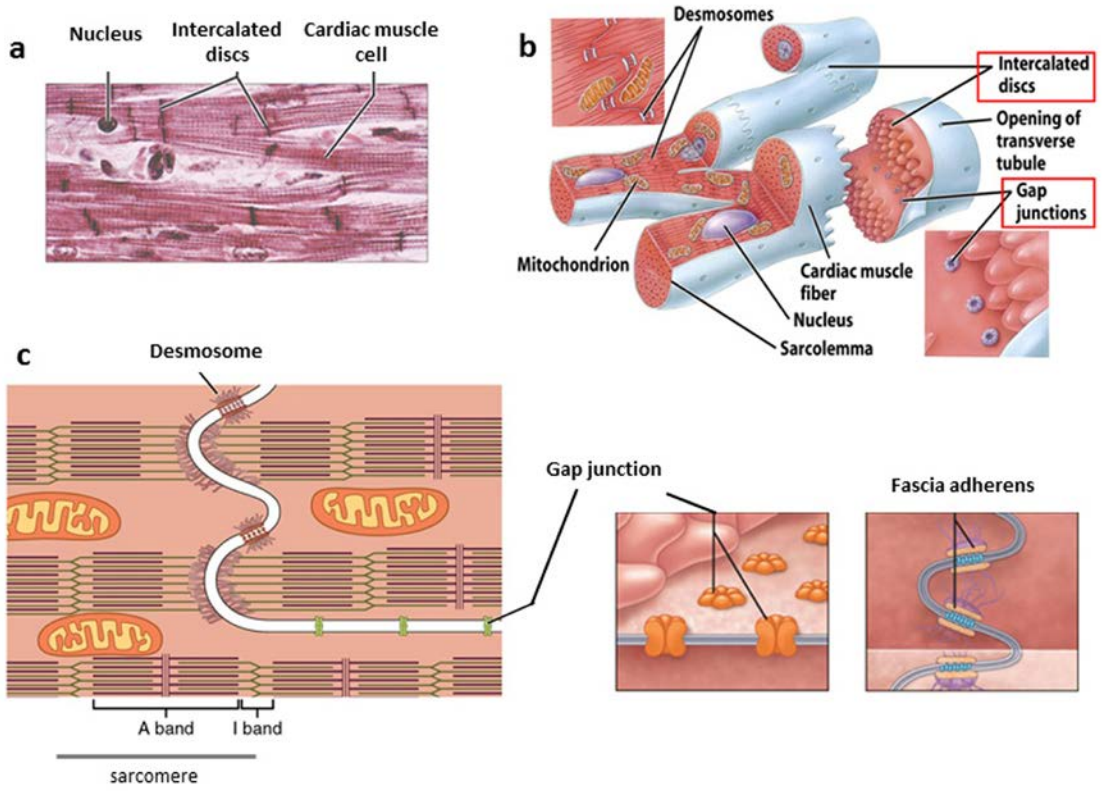

Figure 3.1-2: Structure of cardiac muscle. (a) Photomicrograph of CMs that shows their nuclei and intercalated discs. (b) Schematic view of cardiac muscle fibers and their parts (c) Intercalated disc connects CMs and consists of desmosomes, fascia adherens and gap junctions. Cardiac muscle fibers are formed by myofibrils, which are composed of myofilaments arranged in sarcomeres (c). T tubules are responsible for transmitting the impulse from the sarcolemma (plasma membrane, b) using the energy supplied by mitochondria (b).

Intercalated discs consist of gap junctions, fascia adherens, and desmosomes (Figure 3.1-2c). These junctions serve to hold cells together, to allow ions to pass, and to transmit electrical impulses. Specifically, fascia adherens junctions anchor sites for the actin filaments. Secondly, desmosomes function as strong adhesive binding sites between cardiac cells preventing them from splitting during contractions. Finally, gap junctions are clusters of channels that span the closely opposed plasma membranes, forming cell to cell pathways for rapid conduction of action potential and direct transmission of chemical signals[13].

3.1.4 Electrical stimulation

The use of ES is well established in today's medicine. It is used as bone growth stimulators (implantable and external), for chronic cutaneous wound-healing systems, for functional electrical stimulation devices, and for stimulators for pain relief. Therefore, due to the wide variety of bioelectrical presence and its significant influence within *in vivo* tissues, it has been subject of study for the past years[5,7,16–21]. In this context, several *in vitro* studies have already shown the ability of the electrical field to influence the behavior of a variety of cell types[22].

ES can be defined as a safe physical method to induce different changes in cell behavior. Here, we will apply ES to induce physical changes in the cells, but further studies can be directed to trigger biochemical changes moving towards cardiac phenotype. Several potential advantages of this type of stimulus have been described[21,23]:

1. Absence of toxic chemicals. This type of stimulation represents a safe alternative to drugs such as 5-azacytidine (5-aza) and chemical cytokines[24].
2. Absence of the immunogenic response in the host tissue.
3. Less expensive than growth factors (GFs) and chemicals. It offers a cheap, simple, and flexible way to deliver GFs by inducing the cells themselves to produce these materials through natural pathways[22].
4. Use of simple equipment designed with basic theoretical understanding of electromagnetism.
5. Requirement of little cell handling and processing of tissue engineered constructs.
6. It can be used synergistically with other techniques[22].

Endogenous electric fields play an essential role in the functioning of all living organisms. It is well-known their effect in the action potentials of nerves and muscles, but it has also been said to control cellular functions, such as morphology, elongation, gene expression, proliferation, and migration[22]. ES aims to mimic the electrical environment of electroactive muscle cells and help to regulate cell-cell and cell-ECM interaction[21]. It has been shown that ES alters several properties of engineered tissues, including cell differentiation, proliferation, morphology, adhesion, migration, and function[23]. It has been also demonstrated that different stimulation parameters affect different sets of tissue characteristics. Direct current (DC) field stimulation typically directs cell orientation, alters cell morphology, and directs cell migration, while alternating current (AC) fields enhance cell differentiation and increase tissue function[23]. Despite its great potential, its role in tissue regeneration and its ability to influence cell behavior, ES has rarely been considered in tissue engineering (TE)[22]. The utilization of external electrical stimuli holds promise to gain greater control over cellular growth, maturation, adhesion, and orientation. Its early use in TE has been reported to improve contractile and

conductive properties of cardiac constructs, enhance proliferation and differentiation of stem cells (SCs), and increase cell alignment and length of neurite outgrowth[22].

In other terms, electrical propagation through cardiac tissue is primordial for proper heart function. Therefore, electromechanical coupling between the engineered constructs and host myocardium for simultaneous beating is required. So, the engineered cardiac patch should connect to the electrical syncytium of the existing myocardium, rather than having spontaneous contractile activity. Cells distribution at the nanometer scale in an engineered cardiac tissue must be coupled by functional gap junctions and be capable of propagating electrical impulses to prevent arrhythmia upon implantation. At the millimeter scale, the tissue should consist of elongated myofibers aligned to facilitate the synchronous contractions. In this context, the main challenge is to provide the appropriate electromechanical stimulation during *in vitro* cell culture. The difficulty is to establish a functional excitation–contraction machinery of individual CM and to find regimes of electrical or mechanical stimulation, (or both) that result in cell coupling[25]. Therefore, the use of electrical field stimulation as a pre-training method for inducing synchronous construct contractions is currently under development within different platforms[23,26].

Radisic and co-workers reported, using a 3D model of neonatal rat ventricular myocytes, that the effects of ES depend strongly on the time of its initiation[16]. They found that after cell disaggregation by enzyme digestion, cells were transiently incapable of transmitting electrical signals and contract in response to pacing (Figure 3.1-3; Phase 1). After cell isolation, all the connections between cells were disrupted. They hypothesize that during Phase 1 cells began to recover from the adverse treatment synthesizing and assembling the lost proteins. At the same time, they recovered surface channels and receptors. At this point, ES had an inhibitory role, and it was convenient to delay it until the cells were fully recovered. When cells started to connect one to each other, cultivation with an electrical field could be performed (Figure 3.1-3; Phase 2). It was described that the application of ES to 3D constructs induces hyperpolarization at the anode end of the cell and depolarization at the cathode end of the cell. The cells aligned with the electrical field lines were subjected to the largest voltage difference and were likely the first ones to generate action potentials and contract. Processes formed at the cells' ends promoted the establishment of gap junctions, propagation of pacing signals, and generation of action potentials that induced synchronous macroscopic contractions. As the contractions began, they could drive the organization of sarcomeres and thereby increased the contractile force in response to electrical stimuli. Therefore, ES could enhance the development of ultrastructural and contractile properties of the individual cells and increase the number of functionally coupled cells engaged in synchronous contractions of the constructs[16].

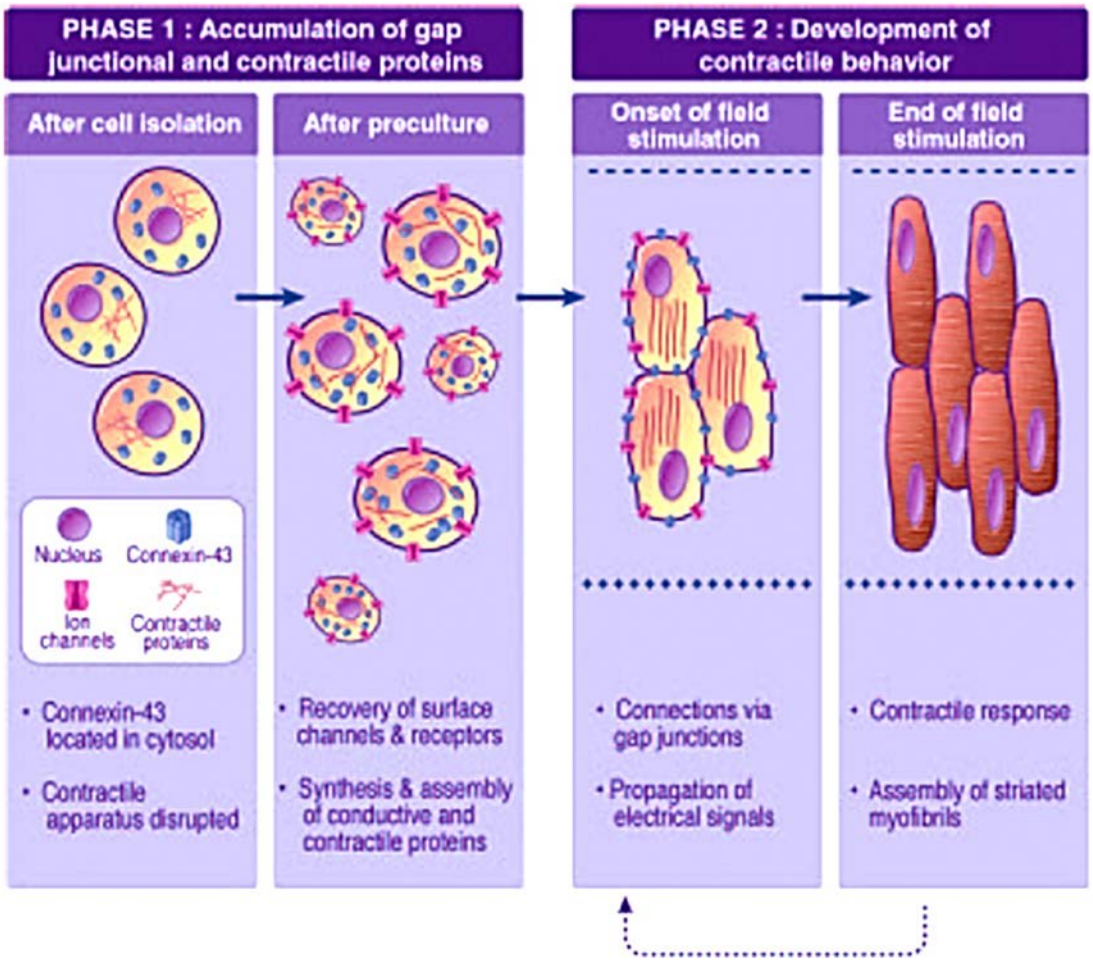

Figure 3.1-3: Progressive development of conductive and contractile properties of cardiac constructs cultured *in vitro*. Phase 1 pre-culture without ES. Phase 2: cultivation with ES. The cells oriented in the direction of the electrical field will be the first ones to elongate and establish gap junctions with neighboring cells. Reproduced from Radisic *et. al.* 2004[16]

Methods of electrical stimulation

Electrical stimuli can be applied in the form of monophasic or biphasic signals, such as sinusoidal, saw tooth or square wave signals, in the form of pulses, pulse bursts, or continuously. These signals can be generated easily by low-cost integrated chips, signals generators, or dedicated therapeutic systems[22].

Different methodologies to deliver an electrical stimulus have been developed (see Figure 3.1-4). With direct stimulation (Figure 3.1-4a), the electrodes are in direct contact with the cell culture media or implanted into the patient or laboratory animal. Indirect stimulation is a contactless approach used in many therapeutic devices and *in vitro* experimental setups. Three indirect techniques are used: capacitive, inductive, and combined (Figure 3.1-4b-d). Specifically, capacitive stimulation is generated between the two plates that serve as electrodes, following the same principle as in a capacitor. Inductive coupling uses controlled electromagnetic fields produced by coils placed around the cell culture to induce an electrical

field. Finally, combined coupling method is a combination of a magnetic field and an alternating current generated by a transient electromagnetic field[22].

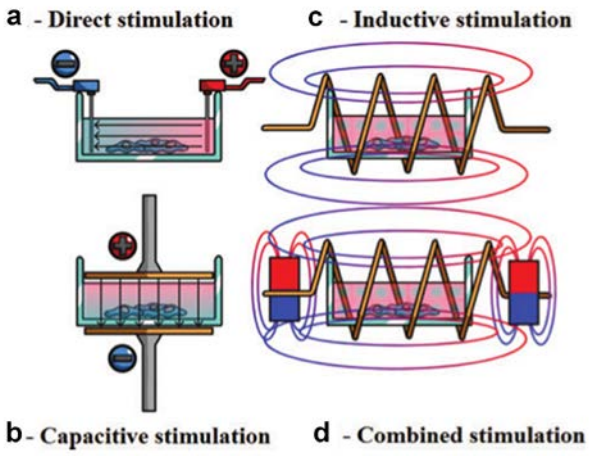

Figure 3.1-4: Methods to deliver an electrical stimulus *in vitro*[22]. These methods can be divided into direct (direct contact with the cell culture) and indirect (there is not direct contact). Indirect methods can be divided into capacitive (b), inductive (c) and combined (d) methods. Image adapted from Balint et. al. 2013.

3.2 PREVIOUS RESULTS

In the work performed by Llucià-Valldeperas *et. al.*[27], the effect of ES on the cardiac differentiation potential of two different types of ATDPCs obtained from patients undergoing cardiac surgery was studied. Cardiac adipose tissue biopsy samples were obtained from fat pads surrounding the cardiac groove, near the base of the heart and around the aortic root[28]. Subcutaneous samples were taken from fat pads between skin and sternum from the same patients[29].

The protocol reported consisted of 2 ms monophasic square-wave pulses of 50 mV/cm at 1 Hz, which is similar to the native heart, over 14 days as it is presented in Figure 3.4-1B.

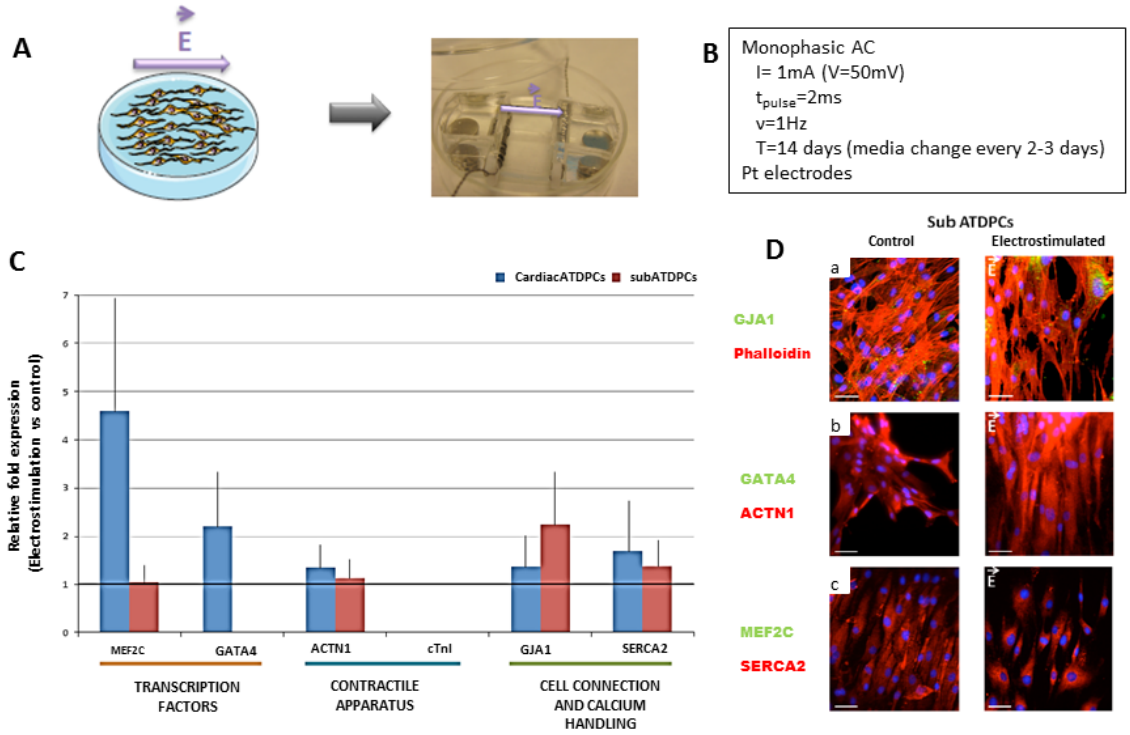

Figure 3.2-1: Effect of electro-stimulation on subATDPCs growing in 2D cultures. (A) Scheme and picture of the system used to electro-stimulate subATDPCs in 2D cultures[i] (B) ES program used in 2D cultures (C) Real-time PCR for the analysis of cardiomyogenic genes in cardiac and subcutaneous ATDPCs. Relative fold expressions of cardiomyogenic markers in electro-stimulated vs. non-treated controls are shown in both cardiac and subcutaneous ATDPCs. Cardiac Troponin I (cTnI) transcripts were not detected in either cell type. Values were normalized to GAPDH expression and are shown as mean ± SEM for six independent experiments, performed in duplicate; *$p \leq 0.05$ vs. subcutaneous ATDPCs group. (D) Protein expression subATDPCs detected by immunofluorescence on a vertical patterned surface: (a) Phalloidin staining (red) and GJA1 expression (green); (b), sarcomeric α-actinin (red) and GATA-4 (green) expression; and (c) SERCA2 (red) and MEF2 (green) expression. Nuclei were counterstained with Hoechst 33342. Scale bars=50mm. Reproduced from Llucià-Valldeperas *et. al.* 2013[27]

Cells were cultured on biocompatible patterned surfaces. Cardiomyogenic differentiation was examined by qRT-PCR (for cardio and subcutaneous ATDPCs) and by immunocytofluorescence (for subcutaneous ATDPCS) as it can be observed in Figure 3.4-1C

[i] System custom made by Electronic and Biomedical Instrumentation Group, Departament Enginyeria Electrònica, Universitat Politècnica de Catalunya (UPC).

and D. qRT-PCR results (Figure 3.4-1C) showed a significant up-regulation of *MEF2C* ($p = 0.05$) and *GATA4* ($p = 0.03$) at day 14 for cardiac ATDPC after stimulation. On the other hand, subcutaneous ATDPCs only exhibited an increase of *GJA1* expression (2-fold). Imunocytofluorescence also showed that, in response to ES, subATDPCs became aligned following the linear surface pattern of the construct (Figure 3.4-1D)[27].

These results lead our group to inquire how this type of stimulus can affect cells growing in 3D systems.

3.3 SPECIFIC AIMS

Tissue engineering (TE) as a new discipline open the window for a wide variety of studies. These studies are predicted to be more relevant than traditional 2D cultures in the context that 3D systems can mimic the *in vivo* environment in a more realistic way. However, these novel systems are technically tricky. The protocols already stipulated for general 2D cultures are needed to be redefined for their use in these models and, usually, each system needs a specific protocol. For this reason, although during the last decades much research has been focused in this area; nowadays a lot of work is still needed.

In the previous chapter, subATDPCs behavior in the 3D milieu provided by self-assembling peptide RAD16-I was tested. The effect of chemical induction was also analyzed. In this chapter, ES will be applied in the 3D system developed in Chapter 2 with the aim to analyze the behavior of the encapsulated cells in terms of viability, morphology and proliferation. The general aim is to imitate, as well as possible, the conditions that the cells would find *in vivo* and analyze their response to the stimulus.

Therefore, the specific objectives of this chapter are:

- To set the protocol for the electrical induction of cells cultured in 3D scaffolds based on RAD16-I and test the hypotheses that subATDPCs in RAD16-I self-assembling peptide scaffolds are able survive under electrical conditions similar to the native heart (section 3.5.1 and 3.5.2).

- To assess the potential of subATDPCs to undergo proliferation in 3D cultures, under electrical or chemical induction (section 3.5.3).

- To study subATDPCs behavior under the combination of the 3D environment provided by RAD16-I with electrical and chemical stimuli (section 3.5.4).

3.4 MATERIALS AND METHODS

3.4.1 Cells used in this chapter

Human normal dermal fibroblasts (hNDF) adherent cells, isolated from the skin of anonymous adult patients, were kindly provided by Dr. Jesús Otero Hernández from "Hospital Universitario Central de Asturias". They were seeded in T75 flasks using Dulbecco's Modified Eagle Medium (DMEM - Labclinics, E15-099) supplemented with 10 % (v/v) fetal bovine serum (FBS - Lonza, DE14-801F), 1 % (v/v) penicillin/ streptomycin (P/S - Labclinics, 011-010), and 2 mM Glutamine (Labclinics, M11-004) at 37 ºC in 5 % CO2 humidified atmosphere. Initially, $5 \cdot 10^5$ cells were seeded in T75 flask. When cells density was about 3,000 cells/cm^2, they were detached using Trypsin-EDTA 0.05 % - 0.02 % (Invitrogen, 25300-062) and expanded until there were enough cells to start 3D cultures (encapsulations).

Subcutaneous adipose tissue derived progenitor cells, obtained from cardiac surgery, were provided by IGTP group from ICREC Research Program, "Hospital Universitari Germans Trias i Pujol", and treated as explained in Chapter 2. Shortly, pools of 5 patients were prepared and adhered cells were grown in control medium under standard conditions (37 °C in 5 % CO_2 humidified atmosphere). Control medium consisted on: Minimum Essential Medium, alpha (α-MEM - Sigma; M4526) supplemented with 10 % FBS (Lonza; DE14-801F; Lot 1SB003), 1 % (v/v) P/S (Labclinics; P11-010), 1 % L-glutamine (Labclinics; M11-004), and 5 µg/mL plasmocin (InvivoGen; ANT-MPT)

3.4.2 Control three-dimensional cultures

Assembly: SubATDPCs pools were thawed at passage 5 and expanded until passage 7. At passage 7, cells were trypsinized, washed with sucrose 10 %, and resuspended in sucrose 10 % to render $1.6 \cdot 10^5$ cells in 40 µL. All 3D cultures started at passage 8. The constructs were prepared mixing equal volume of the cell suspension and RAD16-I self-assembling peptide (PURAMATRIX™ – Corning, 354250) obtaining a final cell suspension which contained $2 \cdot 10^6$ cells/mL. The mixture was carefully mixed by pipetting, and 80 µL were loaded into each 9-mm-diameter cell culture insert (PICM01250, Millipore, Billerica, MA) previous wet with medium. Medium was added carefully in sequential steps on the top of the hydrogel and allowed to infiltrate, to wash out the remaining sucrose. Finally, 500 µL were loaded inside the insert and 2.5 mL in the well. On alternate days, 500 µL of medium was discarded from the well and 500 µL of fresh medium were added carefully on the wall of the insert until the end of the experiment. Incubation was performed, in the same way, as in flat surfaces (37 ºC, 5 % CO_2). A scheme of the defined protocol is presented in Figure 2.4-1.

Assembly of 3D cultures attached to the membrane: The preparation of the 3D constructs was conducted in the same way as explained, obtaining a final cell suspension of RAD16-I self-assembling peptide containing $2 \cdot 10^6$ cells/mL. The cell-peptide mixture was carefully mixed by pipetting, and 80 µL were loaded into on a dry 9-mm-diameter cell culture insert membrane (PICM01250, Millipore, Billerica, MA). Using this procedure, the peptide solution penetrates into the porous of the membrane and the subsequent self-assembling, by media loading, stacks the gel on the surface of the membrane. Two different final peptide concentrations were used: 0.15 % and 0.2 %.

3D cultures maintaining: All 3D cultures were maintained during four days in control medium. After this interval of time, the medium of all samples was entirely replaced. The constructs were covered with cardiac induction medium or control medium again (see Figure 2.4-2). The cardiac induction medium was prepared using Iscove's Modified Dulbecco's Medium (IMDM - Gibco; 2198032), and HAMF12 Nutrient Mix, GlutaMAX™ supplement (Gibco; 31765027). The combination of these media was supplemented with insulin-transferrin-selenium (ITS - Gibco, 41400-045), α-MEM (100x, Lonza, BE13-114E), horse serum (HS - Sigma, H1138-100mL), Ascorbic acid 2-phosphate (Aa 2P- Sigma, A4403), and Transforming growth factor beta 1 (TGF-β1 - Millipore, GF111). 1 % (v/v) P/S (Labclinics; P11-010), and 5 µg/mL plasmocin (InvivoGen; ANT-MPT) (see Figure 2.4-2) were also added.

3.4.3 Electrical stimulation studies

Electrical stimulator set-up: The stimulation unit set-up used was custom made by "*Electronic and Biomedical Instrumentation Group, Departament Enginyeria Electrònica, Universitat Politècnica de Catalunya (UPC)"* by Dr. Benjamin Sanchez (see Figure 3.4-1).

The set-up consists of a combination of a monophasic programmable electrical device, a printed circuit board (PCB) (FR-4 plastic laminate designed with Ultiboard Circuit Design, National Instruments) that enabled electrical stimulation of up to six petri dishes (10x35 mm), and two Platinum-Iridium wire electrodes (0.5 mm diameter) per culture plate and insert (0.4 m pore, 12 mm external diameter, 9 mm internal diameter Millipore, cat PICM01250) (Figure 3.4-1)[18]. After the customization of the inserts with the electrodes, both were sterilized by ethylene oxide. Before starting a culture in the proposed system, the whole system was treated with ethanol and ultraviolet light overnight.

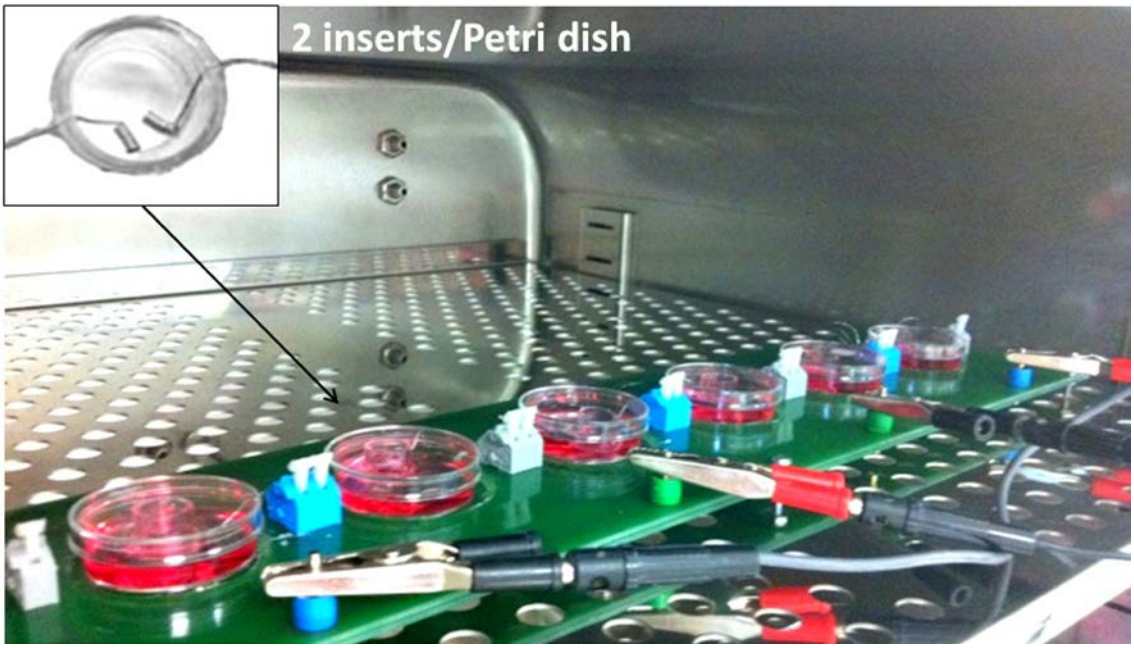

Figure 3.4-1: The electrical stimulation set-up inside the cell culture incubator. The Printed Circuit Board (PCB) (in green), cultures plates with media and detail of an insert with the stimulation electrodes (left top).

Electro-stimulation conditions: For a given electric field amplitude applied to the cells using two stimulation electrodes, a fraction of the electric field is lost near the electrodes due to the electrode impedance. This effect results from the medium-electrode interface and as a consequence, the effectiveness of the applied electric field is variable from the point of view of the cells. The variability of the field depends on the electrode material, the electrodes, the effective stimulation area and the medium volume. To mitigate this effect and increase the electrodes' surface, the electrodes were twisted at the end (Figure 3.4-1, top and Figure 3.4-2a and b). Furthermore, the experimental protocol conditions were modified according to the measured effective electric field applied to the cells. The conditions were verified within a set of experimental validation measurements.

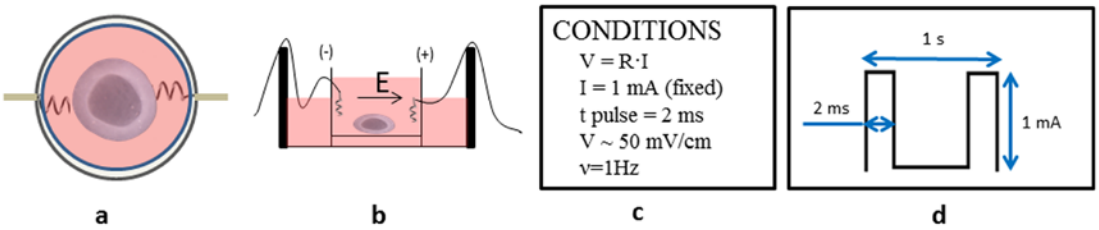

Figure 3.4-2: Electro-stimulation protocol. (a) Top-view of one insert prepared for ES. (b) Cross-section of one insert prepared for ES. The electric field always follows the same direction. (c) Conditions stipulated for the ES set-up. (d) Trains of electrical pulses (rectangular, monophasic, 2 ms time duration, amplitude 50 mV/cm, frequency 1 Hz).

At the other end, each of the electrodes was connected to the connector provided by the PCB and to the electrical stimulator through an isolator stage to prevent DC stimulation (outside incubator). As for the electrical connection between corresponding culture plates, three of the

culture plates were in parallel and in series with the other three. With this connection, a sample could be removed without the need to stop the experiment[18].

Electrical stimulation protocol: With the aim to electro-stimulate cells growing in a 3D milieu, the assembly of the constructs was performed in inserts previously start ES. Each insert was custom made with two platinum electrodes which free ends were connected to the stimulator. Two custom made electrodes were placed in a Petri dish, and one construct was prepared in each insert. Cell encapsulation was performed as control 3D cultures (see section 3.4.2) but in this case petri dishes were filled with 3 ml of culture medium instead of 2.5 ml. Constructs were pre-cultured without ES during 2 or 7 days depending on the experiment. Trains of electrical pulses (rectangular, monophasic, 2 ms time duration, at 50 mV/cm and 1 Hz) were applied continuously for an additional 14 days (Figure 3.4-2c and d). Constructs cultured without electrical stimulation under identical conditions were used as controls.

3.4.4 Macroscopic and microscopic analysis of 3D cultures

With the aim to analyze the macroscopic behavior of 3D constructs, all samples were analyzed under Stereoscopic microscope Nikon digital Slight DS-2MV, while network formation was followed using Nikon Eclipse TE2000-1 microscope.

3.4.5 Live and dead staining (L&D)

The viability of the cells cultured in 3D cultures was assessed using two-colour fluorescence cell viability assay based on intracellular esterase activity and plasma membrane integrity (LIVE/DEAD® Cell Viability Assays, Invitrogen; L-3224) as it has been explained in Chapter 2, section 2.4.7. Images were taken with Zeiss AxioVert 200M / ApoTome Microscope.

3.4.6 Dapi and phalloidin staining (D&P)

Cells were double stained using DAPI [4',6-Diamidino-2-phenylindole] (Sigma; D9542) and Phalloidin–tetramethylrhodamine B isothiocyanate (Sigma; 7418) as it has been explained in Chapter 2, section 2.4.8. The samples were examined under Zeiss AxioVert 200M / ApoTome Microscope.

3.4.7 MTT viability assay

MTT was used to analyze cell viability as it has been explained in Chapter 2, section 2.4-9. Briefly, each analyzed day, the culture media were aspirated, and MTT reagent (Sigma; M5655-1G) was added to a final concentration of 0.5 mg/mL in culture media covering the samples. The samples were incubated for 3 hours at 37 ºC. At the end of the incubation period, the solution was removed, and the constructs were lysed using dimethylsulfoxide (DMSO – Sigma, D8418) to lyse the cells and resuspend the formazan crystals. All samples were analyzed in

triplicate. The absorbance was read at 550 nm with a BIOTECH ELX 800 spectrometer using DMSO as a blank.

3.4.8 Study of gene expression by RT-PCR

Reverse transcription polymerase chain reaction (RT-PCR) was performed to analyze gene expression. The samples were lysed and RNA was extracted with PeqGold Total RNA kit (Peqlab; 12-6834-02), followed by cDNA synthesis using Quantitect Reverse Transcription Kit (Qiagen; 205311) according to manufacturer protocol (detailed information about these steps is reported in Chapter 2, sections 2.4-10 and 2.4-11). RT-PCR reaction was carried out using 30 ng of cDNA in a final volume of 50 μL containing: 1X ThermoPol Reaction Buffer (stock 10X), 0.4 units of Deep Vent DNA polymerase (New England Biolabs; M0258S), 200 μM of dNTPs and 0.3 μM primers. The RT-PCR took place under the following conditions: 3 min at 95 ºC (activation) followed by 35 cycles of 20s at 94 ºC, 30 s of annealing (Tm dependent on primer pair, see Table 3.4-1) and 30 s at 72 ºC. Final extension step was performed at 72 ºC during 15 min. Commercial primers were used for GATA4 gene (Qiagen; QT00031997), cardiac troponinI (Qiagen; QT00084917), and GJA1 also known as Connexin43 (Qiagen; QT00012684) (see Table 3.4-1). Synthetic primers were used for human 18S housekeeping gene amplifying a fragment of 245 bp: h18S forward 5'-GCTACCACATCCAAGGAAGGCAG-3' and h18S reverse 5'-CGCTCCCAAGATCCAACTACGAG-3'. RT-PCR products were size fractionated by 2 or 4 % agarose gel electrophoresis, depending on the expected fragment size.

Table 3.4-1: Primer information provided by Qiagen.

Official symbol	GATA4	cTnI	GJA1
Official name	GATA binding protein 4	Troponin type 3 (cardiac)	Gap junction, alpha 1, 43 KDa
Species	Human (homo sapiens)	Human (homo sapiens)	Human (homo sapiens)
Detected transcript	NM 002052	NM 00363	NM 00165
Length of detected transcript (bp)	3419	866	3130
Amplicon length (bp)	81	113	92

3.4.9 Statistical analysis

The means and standard deviations were calculated for the recorded data.

3.5 RESULTS AND DISCUSSION

3.5.1 Set-up electro-stimulation system

The first efforts within this chapter were focused on the preparation of an ES system. It must be able to induce ES to the cells growing in the 3D constructs developed in the previous chapter, as it has been done with 2D cultures[27] (see previous results). It consisted of the components presented in Figure 3.5-1: the monophasic programmable electrical device and the isolator stage (Figure 3.5-1a), the Printed Circuit Board (PCB - Figure 3.5-1b), two inserts with Platinum-Iridium wire electrodes per petri dish and six petri dishes per PCB (Figure 3.5-1c). The maximum capacity per PCB was twelve inserts.

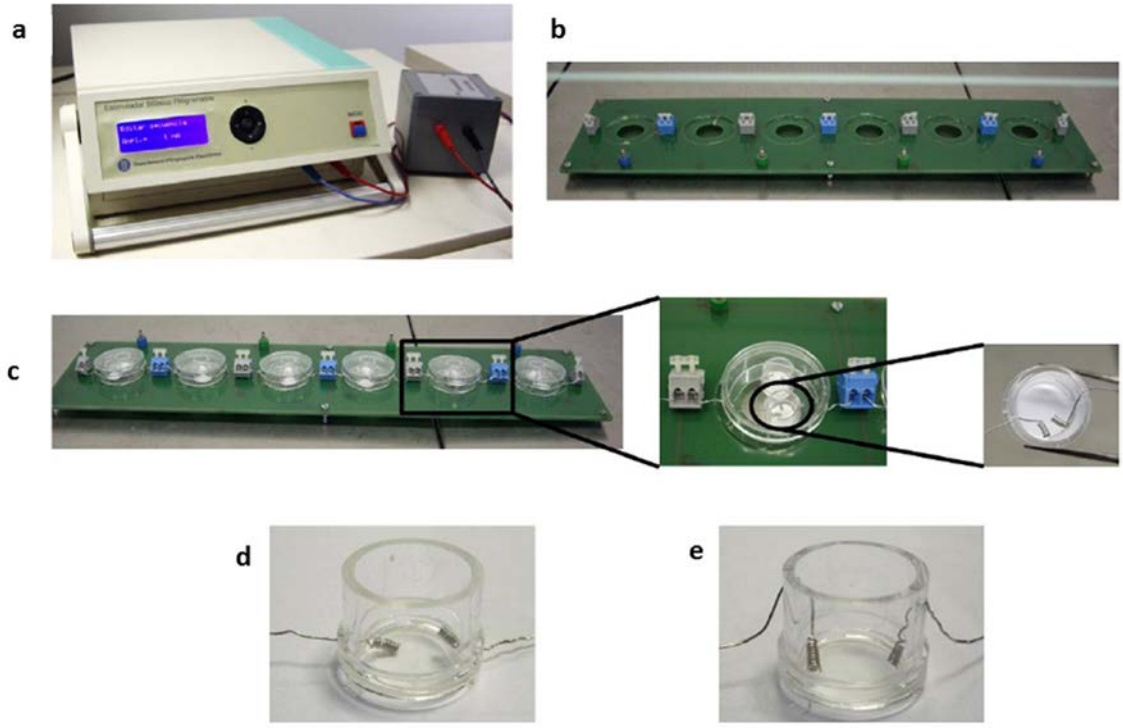

Figure 3.5-1: Components of the electrical stimulation system. (a) Electrical stimulator and isolator stage. (b) Printed circuit board (PCB). (c) PCB with the six petri dishes containing two inserts per petri dish. Detail of the inserts in the petri dish. (d) Modified insert with the electrodes at the bottom. (e) Modified insert with the electrodes at the top.

Cell culture inserts to electrically stimulate 3D systems were adapted to allow the passage of current introducing Platinum-Iridium wire electrodes. The electrodes were included in the inserts in two different ways:

Insert with the holes at the bottom part (Figure 3.5-1d)

The constructs could not be directly prepared in this insert since the peptide-cells mixture could spread out through the holes. Consequently, constructs were performed into regular inserts and pre-cultured without ES during 7 days. Generally, at day 7, the structures had condensed and

had enough consistency to enable their transference into the adapted inserts. Then, ES was initiated.

Inserts with the holes at the top part (Figure 3.5-1e)

In this case, encapsulation and ES were performed in the same insert without the need of transferring the 3D construct. It was important to assure to twist down the electrodes as shown in the picture. In this way, they were medium-coated during the experiment and the circuit was closed enabling the pass of the current.

The PCB with the petri dishes containing the modified inserts was located inside the incubator in order to provide the right conditions to the cell culture (temperature of 37 ºC and 5 % CO_2 in humidified atmosphere). The monophasic programmable electrical device and the isolator stage were placed outside the incubator. The electrical pulses were generated by the electrical stimulator, and the electric field passes through the PCB thanks to the connectors that allow the connection of the inserts electrodes.

3.5.2 Preliminary studies

Setting of electro-stimulation protocol using hNDFs

hNDF were used to set the ES protocol. This cellular type were easy available and gave us the opportunity to adjust the parameters, become familiar with the system, and understand the equipment function. Additionally, hNDFs grew faster and were more studied in our laboratory than subATDPCs.

As mentioned, for modified inserts with the electrodes at the bottom, the encapsulation assembly was carried out in normal inserts. After 7 days of culture, the constructs were transferred into modified inserts in order to start the electrical stimuls. hNDFs constructs were quite condensed at this time point (see Figure 3.5-2a) and a good cellular network was formed at day 5 compared to the rounded shape of the cells one day after encapsulation (see Figure 3.5-2c). This macroscopic morphology allowed the simple transference from the standard insert to the modified one. Two weeks after starting electrical stimuli, all the constructs (both electro-stimulated and non-electro-stimulated) reached at a similar construct diameter reduction: 0.27 cm the electro-stimulated construct and 0.24 cm the no electro-stimulated (total time of culture 21 days). The high condensation of the 3D culture, at the final point of the experiment, did not allow visualizing the cellular network properly. Interestingly, L&D assay at days 15 and 21 (Figure 3.5-2b), confirmed that most of the cells remained alive under this electrical conditions, which are similar to the native heart ones. After 8 days of being subjected to electrical pulses (day 15) and at the end of the culture, after 14 days of electrical stimulation (day 21) most part of the cells were alive (green) and only some of them died (red).

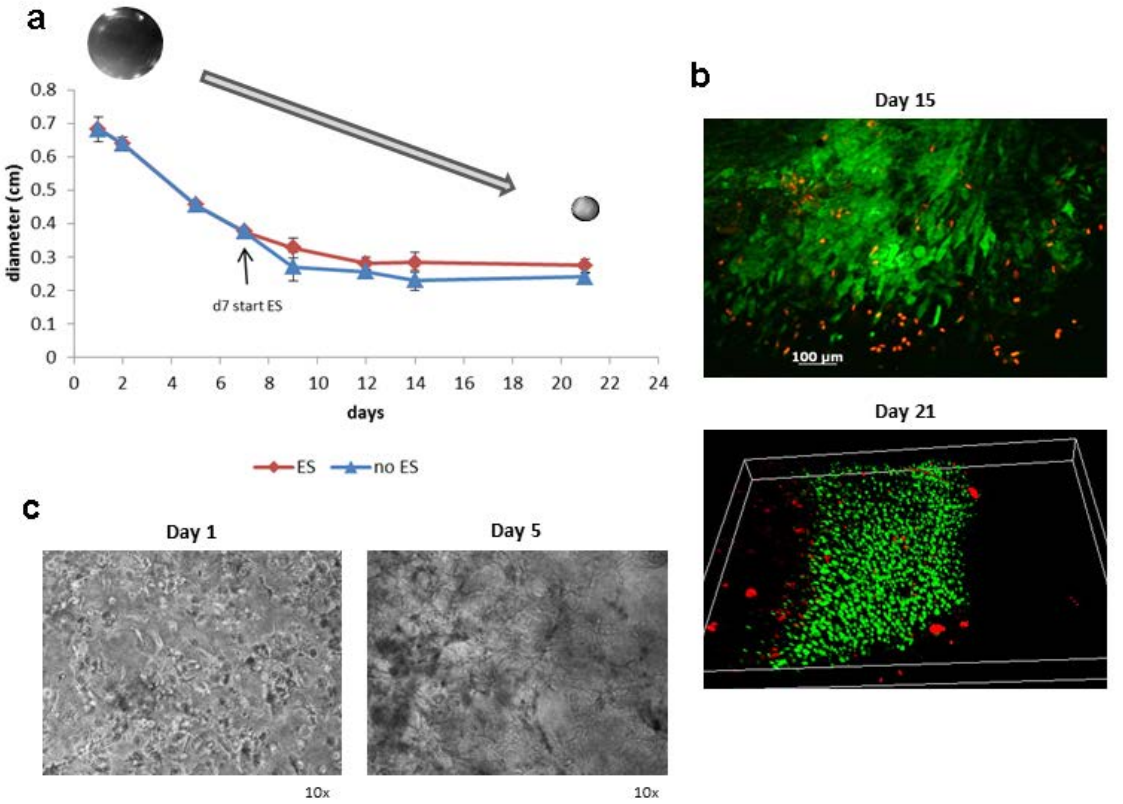

Figure 3.5-2: Effect of electro-stimulation on 3D constructs of hNDF in RAD16-I 0.15 %. Cells were encapsulated in 0.15 % RAD16-I and cultured with control medium with and without ES. ES started at day 7. (a) Condensation graphic for 3D constructs with and without ES. (b) Cell viability of electro-stimulated hNDF within the self-assembling peptide hydrogel at days 15 and 21 (live cells stain green and dead cells, red). 3D reconstruction images were obtained from several optical sections taken with Zeiss ApoTome system. (c) Pictures of cell morphology after 1 and 5 days of culture with a 10x objective under the contrast phase microscope.

Analysis of electro-stimulation of subATDPCs

SubATDPCS are pretended to be implanted in an infarcted tissue to assist myocardial regeneration. For this reason, it is of high interest to analyze their behavior under electrical conditions similar to the ones of the native heart. The developed system allowed analyzing this issue. SubATDPCs in the 3D environment provided by 0.15 % RAD16-I presented good viability and construct diameter reduction (see Chapter 2), both in control and cardiac induction media. For this reason, the analysis of the effect of ES was carried out in both conditions.

First of all, the effect that ES could cause on subATDPCs behavior growing in control media was evaluated, considering as controls samples not treated with ES and cultured with the same medium. The first important observation was that subATDPCs had slower response in terms of cellular network formation and construct diameter reduction when compared with hNDF. No significant construct diameter reduction was observed after 7 days of culture (Figure 3.5-3a). Thus, the constructs were not stiffer enough, and some samples broke during the process of transference to the modified inserts. Broken samples were discarded (2 of a total of 8).

After starting ES protocol, the construct diameter reduction was similar in both electro-stimulated and non-electro-stimulated samples. No notable differences were observed and after 4 days of ES, the diameter size of electro-stimulated and non-electro-stimulated samples was approximately 0.4 cm (Figure 3.5-3a).

The formation of the network started before the ES as it can be visualized in Figure 3.5-3b. Importantly, L&D assay (Figure 3.5-3c) showed high cell viability of the electro-stimulated constructs after 14 and 20 days. Thus, it can be concluded that ES did not affect negatively subATDPCs maintenance in RAD16-I self-assembling peptide in terms of construct diameter reduction, network generation, and viability. These results are of high interest for further *in vivo* implantation since we can conclude that the cells would tolerate the electrical conditions found *in vivo*.

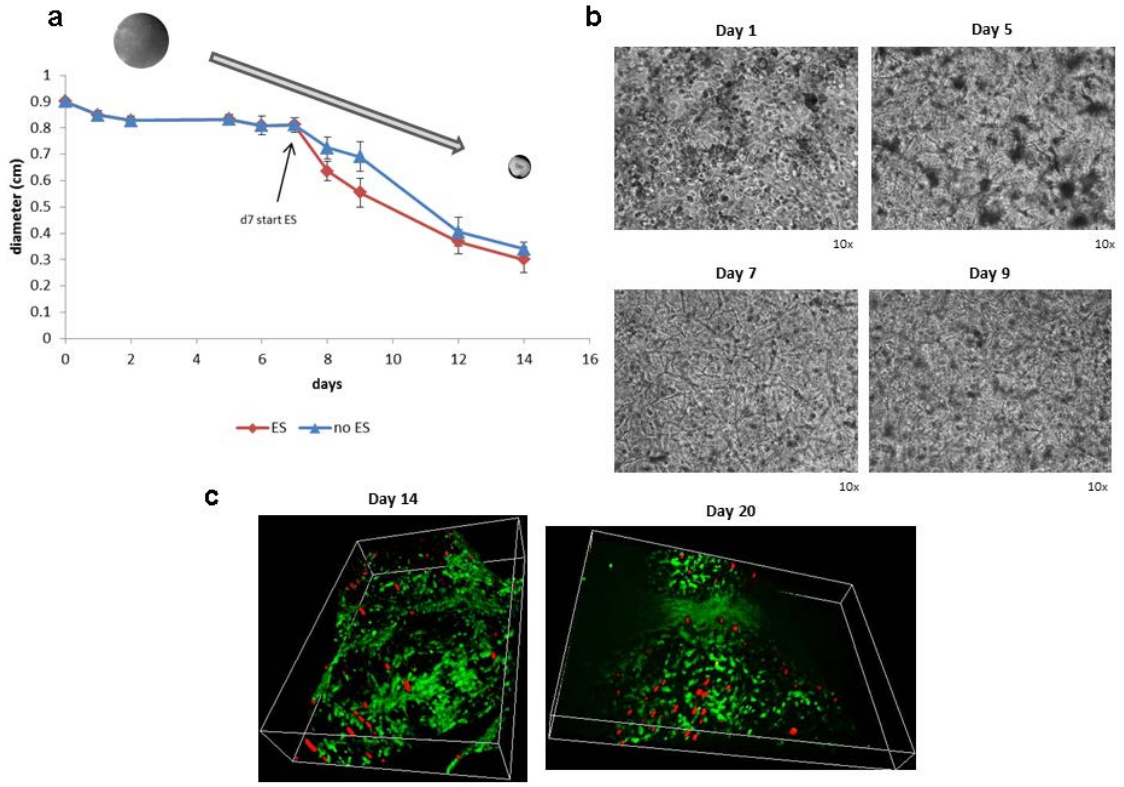

Figure 3.5-3: Effect of electro-stimulation on 3D constructs of subATDPCs in RAD16-I 0.15 %. Cells were encapsulated in 0.15 % RAD16-I and cultured with control medium with and without ES. ES started at day 7. (a) Condensation graphic for 3D constructs with and without ES. (b) Contrast phase pictures of cell morphology at days 1, 5, 7 and 9 of culture. (c) Cell viability of electro-stimulated subATDPCs within the self-assembling peptide hydrogel at days 14 and 20 (live cells stain green and dead cells, red). 3D reconstruction images were obtained from several optical sections taken with Zeiss ApoTome system.

Additionally, some samples from electro-stimulated and non-electro-stimulated 3D constructs at different days were analyzed by RT-PCR. As it can be observed in the corresponding agarose gel electrophoresis (Figure 3.5-4), at day 20, the electro-stimulated sample showed the expression of cTnI and also GATA4 and GJA1 although fainted. GJA1 was highly expressed after 7 days of ES but its expression decrease one week later. These preliminary results, with a

slight expression of early and late cardiac markers, were promising, but further analyses are required to make a definitive statement.

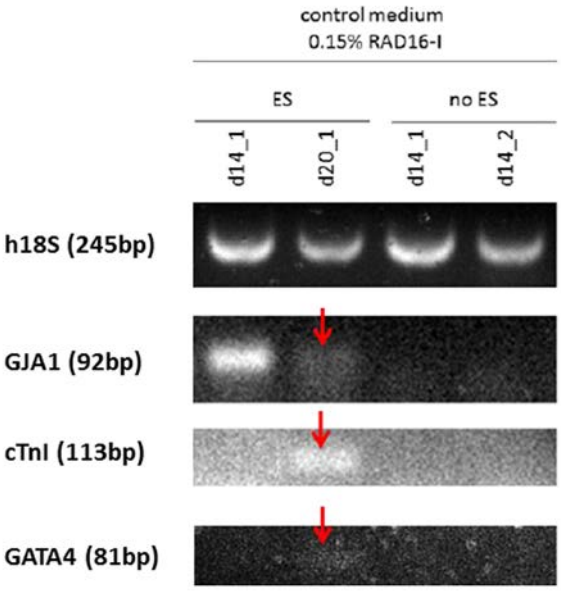

Figure 3.5-4: RT-PCR of subATDPCs growing in control media under electrical induction as compared with samples without this stimuli. Expression analyses of subATDPCs growing in 0.15 % RAD16-I in control medium, electro-stimulated (ES) and non-electro-stimulated (no ES). Samples were taken at day 14 (d14) and day 20 (d20)**.** The analyzed genes were h18S (245 bp), gap junction protein, alpha 1 (92bp), cardiac troponinI (113bp), and GATA4 (81bp). Agarose gel 4 %.

With the aim to improve the technical issues of the protocol previously discussed, a new strategy was addressed in order to avoid the transference of the constructs from standard inserts to modified inserts during the culture. For this purpose, modified inserts with the electrodes at the top were used (Figure 3.5-1e). Thereby, the encapsulation was performed in the same insert where it was electro-stimulated, avoiding the transference. This new approach allowed us to start ES at the second day of encapsulation, when the network started to be formed but before it was completely structured. This procedure was conceived with the aim to force the cells to form a network with anisotropic architecture. As Milica *et. al.* reported, it is important to allow cells to recover from trypsinization, but it is also indispensable to obtain a degree of organization to assure the better conditions for electric impulse propagation[16].

For this reason, we thought it could be interesting to force the electrical field to always affect the constructs in the same direction, to induce some order within the cellular growth. With this objective, the encapsulations were fixed at the bottom of the culture insert. In order to achieve this goal, the cell-peptide mixture was loaded on a dry insert membrane. In this way, the peptide solution wet the membrane penetrating into the porous. The subsequent self-assembling, by medium loading, stacks the gel on the surface of the membrane. Therefore, construct attached onto the membrane could not float when medium was added. Also, with the aim to maintain the

constructs attached on the insert membrane, the peptide concentration was increased to 0.2 % RAD16-I to slow down the condensation process (see Figure 2.5-5b).

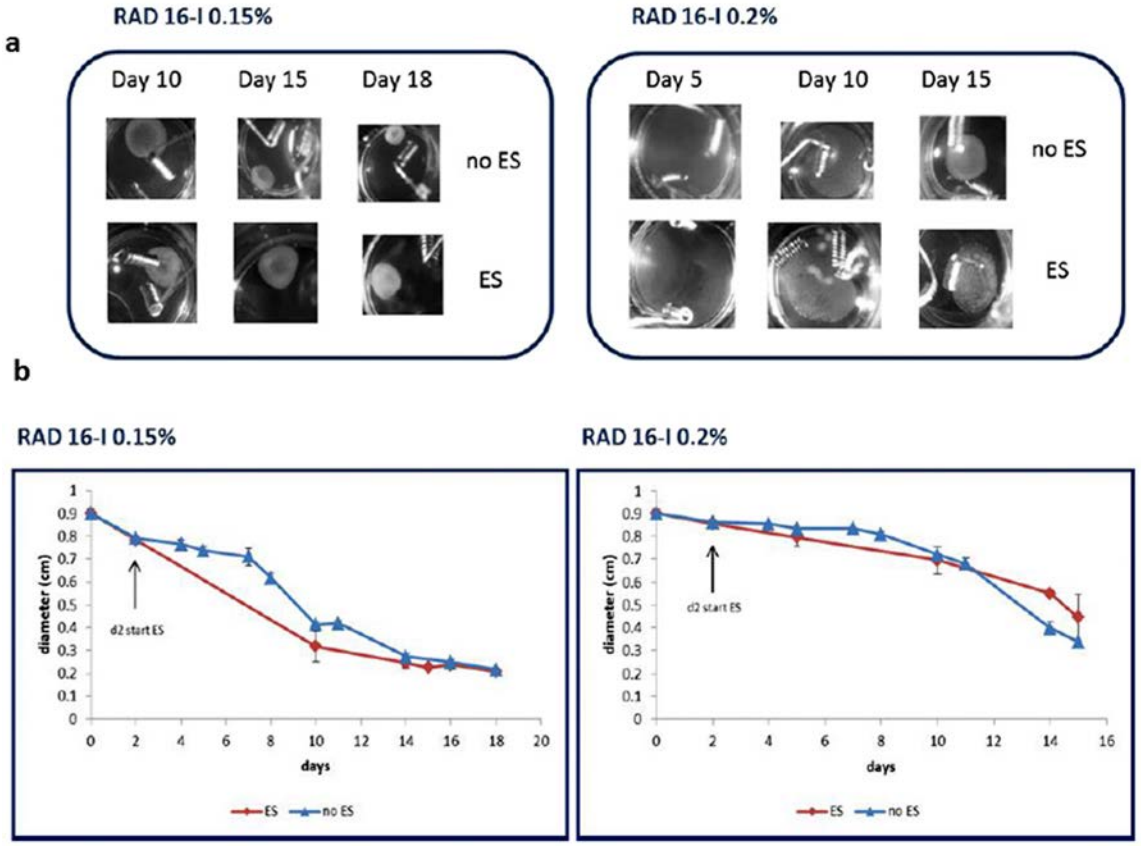

Figure 3.5-5: Effect of electro-stimulation on 3D constructs of subATDPCs in RAD16-I immobilized on the insert membrane. Cells were encapsulated in 0.15 % and 0.2 % RAD16-I and cultured with control medium with and without electro-stimulation (ES and no ES respectively). ES starts at day 2. (a) Contrast phase constructs pictures at days 5, 10, 15 and 18 under the magnifier. (b) Condensation graphic for 3D constructs. The diameter of three samples for each condition was measured to obtain a standard deviation.

Accordingly, subATDPCs were encapsulated in 0.15 % and 0.2 % RAD16-I and cultured in control medium during 18 and 15 days respectively, starting the ES at the second day of culture. The macroscopic images and the condensation process tendency for both peptide concentrations are shown in Figure 3.4-5a and b. Although 0.2 % RAD16-I constructs were initially stuck onto the membrane, from day 10 on, most encapsulations detached from the bottom of the insert and started to condense. For this reason, and regarding the directionality of the electric field, as this protocol did not ensure the immobilization of the construct, it was not possible to achieve any conclusion. The condensation obtained with the ES protocol was similar to that the one obtained without it in both peptide concentration conditions.

A preliminary gene analysis was performed by RT-PCR as it is presented in Figure 3.5-6. The early cardiac marker GATA-4 and definitive cardiac marker GJA1 were analyzed. GJA1 was detected in all conditions while GATA4 was not amplified in any of the samples. It was hypothesized that subATDPCs in this conditions are not dedifferentiating into an early cardiac

precursor but evolving into a CM-like phenotype with good interconnection between them. Nevertheless, it was only a preliminary data that needs to be further explored.

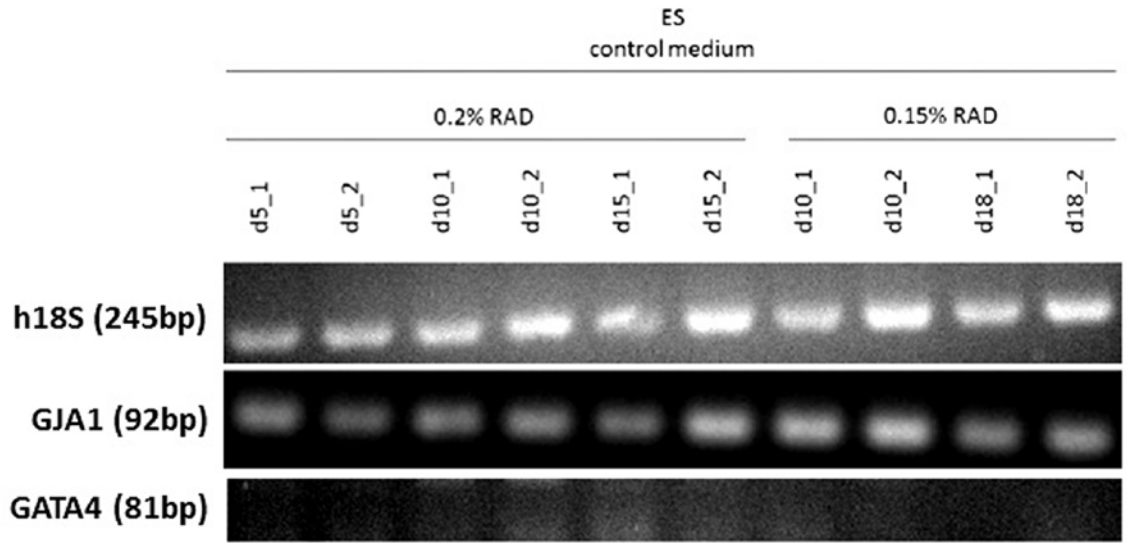

Figure 3.5-6: RT-PCR of subATDPCs growing in control media under electrical stimulation at two different RAD16-I self-assembling peptide concentrations. The analyzed genes were h18S (245 bp),gap junction protein, alpha-1 (92 bp) and GATA4 (81 bp). Analysis of subATDPCs expression growing in 0.15 % and 0.2 % RAD16-I using electro-stimulation (ES) and control medium. The samples were analyzed at days 5 (d5), 10 (d10), 15 (d15) and 18 (d18) of culture. Agarose gel 4 %.

The impossibility to fix the construct using the previously described protocol leads us to change the strategy. Agarose bed was selected to be added on the top of the 3D constructs to keep them fixed on the bottom of the culture inserts. At day 7, the entire medium of the culture inserts was removed, and 80 µL of cell culture agarose was loaded on the construct. Agarose adhered the construct in the insert assuring that it would not change the position, and the electrical field would always affect it in the same direction[18]. Once the agarose was gelled (20 minutes at room temperature) inserts and petri dishes were refilled with the appropriate media. A preliminary study using different concentrations and volumes of agarose was performed (data not shown). The best condition to enable the diffusion of the medium and to maintain the position of the construct was 80 µl of 0.75 % agarose. This protocol will be used in the next experiments.

3.5.3 Proliferation studies of subATDPCs in a 3D environment with chemical and electrical stimulation

Numerous methods can monitor cell health. Plasma membrane integrity, DNA synthesis, DNA content, enzyme activity, presence of ATP, and cellular reducing conditions are known indicators of cell viability or cell death. Assays that measure metabolic activity are suitable for analyzing proliferation, viability, and cytotoxicity. The reduction of tetrazolium salts such as MTT, MTS and XTT between others or the reduction of resazurin only occurs in metabolically active cells. Actively proliferating cells increase their metabolic activity while cells exposed to toxins, typically decrease their activity.

The effect of both inductive stimuli (chemical and electrical) in terms of cell proliferation and construct macroscopic behavior was analyzed. MTT proliferation assay was performed with samples under chemical and electrical induction separately. In each case the results were compared with cells growing in 3D environment without stimulation. SubATDPCs were cultured into the soft nanofiber scaffold RAD16-I in presence of control and cardiac induction media (Figure 3.5-7). As observed in Figure 3.5-7a, the evolution of constructs diameter reduction was dependent on the culturing medium. After 14 days of culture the diameter of constructs cultured in cardiac induction medium measured 0.19 cm while in control medium measured 0.52 cm (see Figure 3.5-7a and e).

At the same time, the cellular metabolic activity (related to mitochondrial oxidoreductase activity) was measured (Figure 3.5-7f). After induction with cardiac induction medium, at days 7 and 9, the metabolic activity of cells cultured of both conditions were similar. However, from day 11 to 14 each condition showed a different profile. Control cultures profile showed a slight increase of oxidoreductase activity, while chemically induced cultures presented a decreasing tendency. Initially, we thought that this effect was due to cell dead associated to the high condensation of chemically induced cultures. Nevertheless, by looking at the constructs in detail we observed a consistent mass of cells leaving out the scaffolds (see Figure 3.5-7c). As MTT assay was performed only for the cells growing inside the constructs, but not for the remaining cells in the tissue culture insert, we sub-estimated the total number of cells in the chemically induced samples.

We hypothesize that cells do not have enough space in such condensed environment to fulfill the nutrient and oxygen requirements and start to migrate outwards the construct. This movement could be an advantage for future therapeutic applications of cell delivery into an infarcted heart. However, this should be further studied in order to understand the underlying causes entirely.

Moreover, to assess whether the cells were alive, L&D assay was performed at day 10 of culture with cardiac induction medium (Figure 3.5-7b). Although some dead cells were observed (in red) the majority remained alive (green). Surprisingly, the cells growing inside the 3D cultures induced with cardiac induction medium presented a highly aligned pattern. This alignment was again confirmed at day 14 of culture with the pictures of D&P staining (Figure 3.5-7d). The whole construct was captured (Figure 3.5-7d left) and magnification (Figure 3.5-7d right) showed the aligned pattern of the cells. This alignment could be due to an efficient spatial disposition since cell density increases in a highly condensed construct.

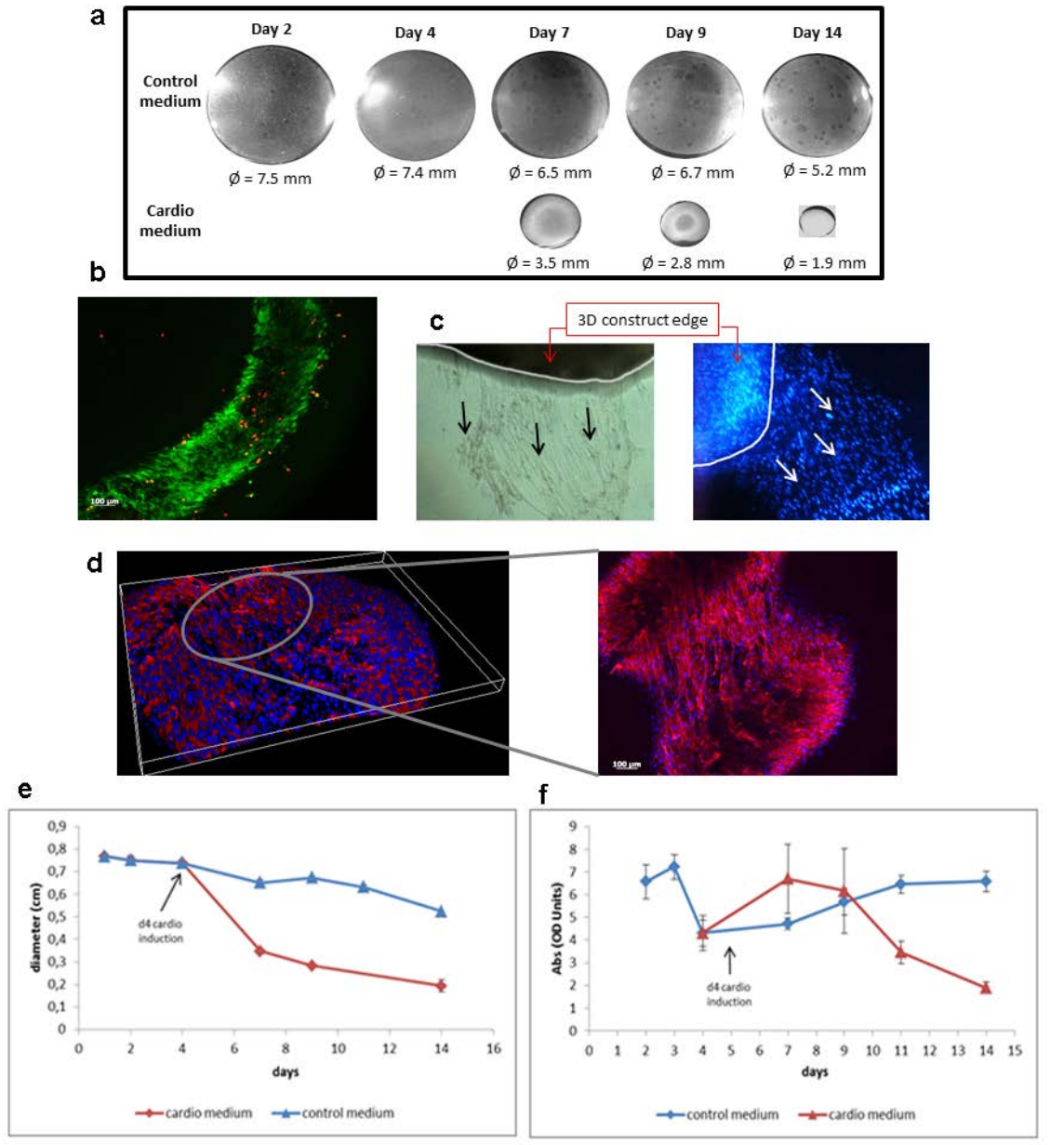

Figure 3.5-7: Behavior, growth and survival of subATDPCs into RAD16-I cultured in control vs cardiac induction medium. Cells were encapsulated in 0.15 % RAD16-I and cultured with cardio and control media during 14 days. The induction with cardiac induction medium starts at day 4. (a) Constructs pictures at different days under the magnifier. (b) L&D assay of a 3D construct cultured with cardiac induction medium at day 10 (live cells stain green and dead cells, red). (c) Contrast phase picture (left) and DAPI staining picture (right) of cells leaving from a 3D construct cultured with cardiac induction medium at day 14. The white line marks the 3D construct. (d) D&P staining of the 3D construct cultured with cardiac induction medium at day 14. 3D reconstruction images were obtained from several optical sections taken with Zeiss ApoTome system. (e) Condensation graphic of samples cultured with control and cardiac induction media. The diameter of three samples for each condition was measured to obtain a standard deviation. (f) Proliferation graphic of samples cultured with control and cardiac induction media. The cell number was measured with MTT assay. The samples were measured in triplicate to obtain a standard deviation.

This analysis was also performed for electrically induced cells. The results obtained are shown in Figure 3.5-8. Using ES the condensation process was not observed as compared with chemical induction (Figure 3.5-8a and c), and no major differences existed between the diameter of electro-stimulated and non-electro-stimulated constructs.

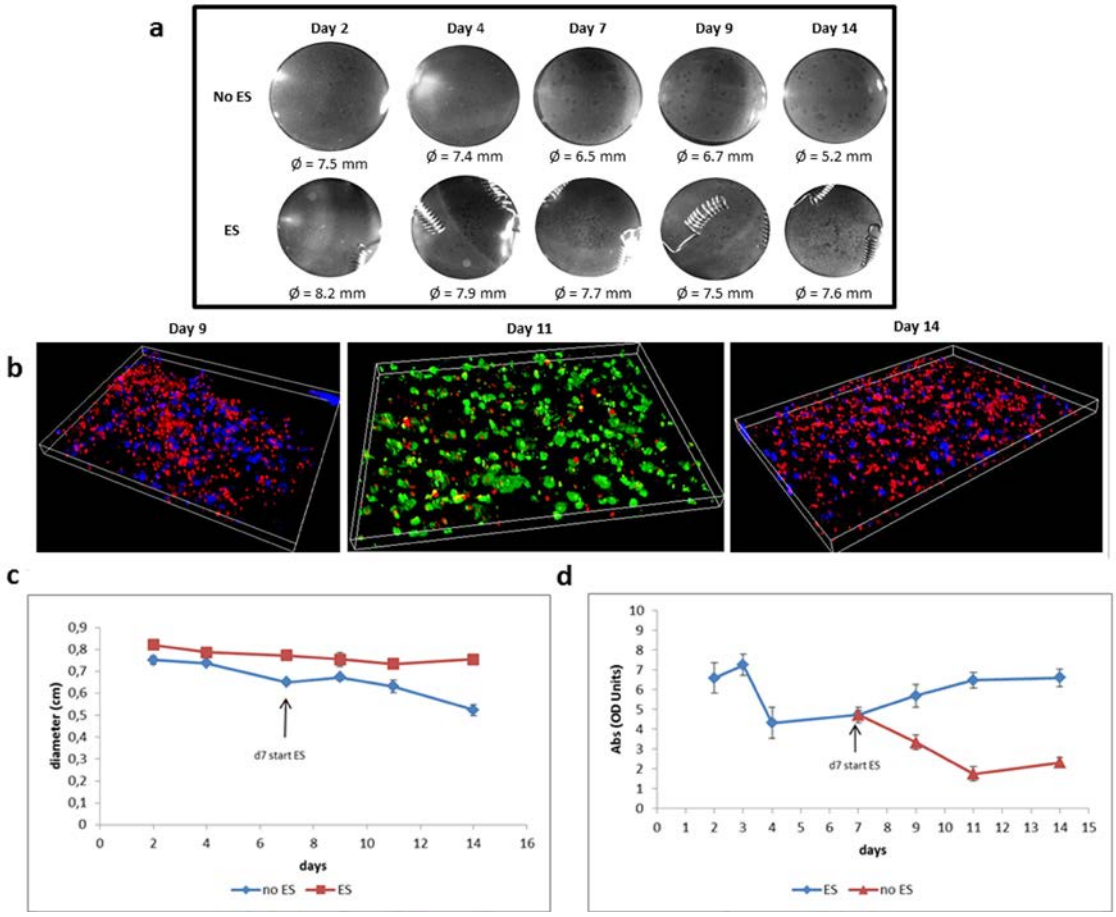

Figure 3.5-8: Behavior and survival of subATDPCs into RAD16-I under electrical stimulation. Cells were encapsulated in 0.15 % RAD16-I, cultured with control medium and electro-stimulated up to day 14. (a) Constructs pictures at different days under the magnifier. (b) Fluorescence pictures of electro-stimulated 3D constructs at different days. Days 9 and 14 D&P staining (nuclei stain in blue and cytoskeletal filaments in pink) and day 11 L&D assay (live cells stain green and dead cells, red) were performed. 3D reconstruction images were obtained from several optical sections taken with Zeiss ApoTome system. (c) Condensation graphic of electro-stimulated (ES) and non-electro-stimulated (no ES) samples. The diameter of three samples for each condition was measured to obtain a standard deviation. (d) Proliferation graphic of ES and no ES samples. The cell number was measured with MTT assay. The samples were measured in triplicate to obtain a standard deviation.

The cell morphology was analyzed by contrast phase microscopy (data not shown) and by fluorescence staining (Figure 3.5-8b), and no cellular network could be noticed. This fact confirmed one of our hypotheses that only when cells form network and inter-connect one to each other, stretch all together allowing the construct condensation process to occur.

The proliferation assay (Figure 3.5-8d) showed a decrease in the metabolic activity of the electro-stimulated 3D constructs, similarly to what was observed in chemically induced samples (see Figure 3.5-7). L&D assay was performed 4 days after starting the ES, and the majority of the cells were alive. Unfortunately, in this case we could not elucidate if this effect was due to cell death, end of proliferation in combination of cell death, or migration outwards of the construct (as observed before for cardiac induced samples). We speculate that maybe the cells were also leaving out the scaffold due to the influence of the electro-stimulation, but since the constructs did not condense we could not reach any conclusion.

3.5.4 SubATDPCs growing in a 3D culture based in RAD16-I peptide combining chemical and electrical stimuli

Next step of these proof of concept studies consisted in combining the chemical and electrical induction in order to analyze subATDPCs behavior. Thus, cardiac induction medium was added at day 4 of culture, and as the stimulus was pretended to be increased gradually, ES started at day 7. Agarose beds were used to fix the 0.15 % RAD16-I construct, and all the encapsulations were electro-stimulated until day 18, but using different media.

The construct morphology and construct diameter reduction can be observed in Figure 3.5-9a and b, respectively. Just before started ES, the chemically induced constructs showed a diameter of 0.52 cm while the constructs maintained in control media gave a diameter of 0.77 cm. In fact, at the end of the culture there was a difference of 0.49 cm in the diameter of the constructs. As it has been suggested in Chapter 2, induction with cardiac induction medium enhances the cell interactions and consequently, the condensation. Cell morphology was analyzed at the end of the culture under the fluorescence microscope.

Again, D&P staining of an electro-stimulated construct with control medium revealed no network formation at day 18, (rounded shape cells, Figure 3.5-9c). This absence of connection correlates with the fact that the constructs were not able to condensate (Figure 3.5-9a). On the contrary, electro-stimulated constructs cultured with cardiac induction medium condensate and the cells interacted one to each other forming an intricate network. In Figure 3.5-9d it can be observed the whole construct after L&D assay (left) and by D&P staining (center). A close up of the construct (right) showed the elongation of the cells and their intricate network.

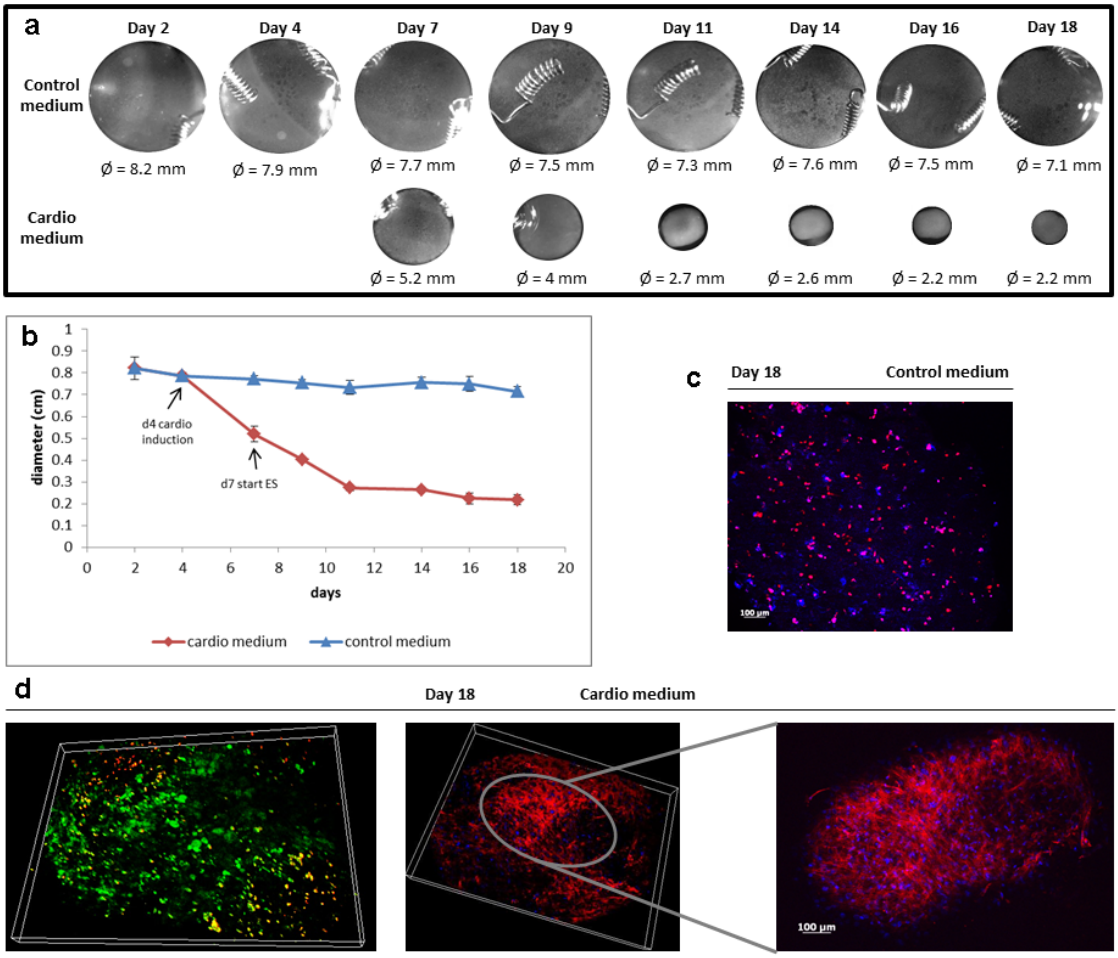

Figure 3.5-9: Effect of chemical and electrical stimulation combination on 3D constructs of subATDPCs in RAD16-I. Cells were encapsulated in 0.15 % RAD16-I, half of them cultured with control and the other half with cardio media and all electro-stimulated. At day, 4 cardio medium was added to the corresponding samples and at day 7 the electro-stimulation started. (a) Constructs pictures at different days under the magnifier. (b) Condensation graphic of 3D constructs electro-stimulated growing in control or cardio medium. (c) D&P staining of electro-stimulated sample growing with control medium at day 18. (d) Live and dead assay (left) (live cells stain green and dead cells, red) and D&P staining (center and right) of samples electro-stimulated with cardio medium at day 18. 3D reconstruction images were obtained from several optical sections taken with Zeiss ApoTome system.

At the end of these studies it is important to compare the results obtained in this chapter and the ones obtained in Chapter 2. It was observed a differential network formation and therefore construct diameter reduction when subATDPCs were cultured in control medium without stimuli. Figure 2.5-2, Figure 2.5-5, Figure 2.5-6 and Figure 3.5-3 show the formation of an intricate network with the subsequent construct diameter reduction. On the other hand, Figure 3.5-7, Figure 3.5-8 and Figure 3.5-9 do not present the formation of this network. This fact was attributed to the cell pool used. Although the aim of combining cells of different patients is to avoid at the maximum extent experimental variability we observed that at least 5 patients were not enough to homogenize the results.

3.6 CONCLUDING REMARKS

Heart is a complex integrated system that leverages mechanoelectrical signals to synchronize CM contraction and push blood through the body[30]. *In vivo*, the correct magnitude, timing, and distribution of these signals are critical for proper functioning. Indeed, aberrant signals can lead to acute incidents, long term pathologies, and even death[30]. For the thorough investigation of the specific factors that deeply affect cardiac function *in vitro* models are emerging as engaging tools. Nonetheless, the complex and intricate set of signals that trigger heart function are hard complicated to replicate accurately and fully in an *in vitro* model[30].

Progenitor cells have the ability to differentiate into various cell types, which can be achieved by extrinsic physical stimuli (mechanical[31–34] or electrical[2,19,27,35,36]), chemical stimuli (cytokines and effector molecules)[37–41], biological/genetic stimuli (cell co-cultures[42,43], genetic manipulations[41]), and even environmental effect[34,44–46]. It has been reported that endogenous electric fields play an essential role in the functioning of all living mechanisms. It is thought that the use of external electrical stimuli may lead to gain greater control over cellular growth maturation, adhesion, and orientation[22]. Additionally, ES is a safe method to induce changes in progenitor cells towards cardiac phenotype, avoiding more harmful agents such as demethylation agents[47] or viral vectors[48]. In this chapter, we have studied the effect of an applied electrical field on subATDPCs using the *in vitro* model developed in Chapter 2, and combining it with the chemical induction previously described. At this point, we have obtained an evidence of the viability of the presented system. However, further studies could lead us to replicate *in vivo* environment in a more feasible way and analyze specific cell responses before *in vivo* implantation.

A direct stimulation methodology was chosen to electrically stimulate the *in vitro* models developed in Chapter 2. Methodologically, direct stimulation is the simplest electrical stimulation method. However, it may carry some disadvantages such as insufficient biocompatibility of electrodes, changes in pH, reduced levels of molecular oxygen, and the generation of dangerous Faradaic byproducts (reactive oxygen species in the culture medium)[22]. All these factors were demonstrated not to be harmful in this type of cultures as it has been observed in viability assays of hNDF and subATDPCs, after 2 weeks of ES.

In our study, the approach was to evaluate the effect that ES has on subATDPCs seeded in RAD16-I scaffold combined or not with chemical induction. In this framework, macroscopic morphology, viability, and proliferation of subATDPCs growing in the 3D structures were analyzed. Interestingly, the cells remained alive and were able to proliferate in the stipulated conditions, which were similar to those found in the native heart.

ES was suggested as a promising tool for solving various cardiovascular related problems[22]. Its galvanotactic property (movement of an organism or any of its parts in a particular direction in response to an electric current) could be crucial in better controlling angiogenesis. This effect can improve cell viability inside 3D structures that would be implanted in an ischemic heart. Additionally, from the point of view of Cardiac Tissue Engineering, electricity could help to overcome the challenge of insufficient alignment and differentiation or even better coupling between cells that can lead to improved contractile and conductive properties[16]. With this preliminary study, we wanted to lay the foundations for further ES studies using this 3D *in vitro* model (RAD16-I). More systematic analysis (more times and samples) would be needed to better assess the platform.

The lack of gap junctions due to the absence of electrophysiological connection between donor and host cells has been reported to lead to failed cell integration into the myocardium[24]. What is interesting is that although subATDPCs do not present the desired alignment, do express GJA1 with and without ES in control medium. This fact implies good cell-cell connection and leads us to think that this property would benefits cell integration after their implantation within the appropriate environment. In further steps with longer ES times, it would be interesting to control field direction using the agarose bed to help cell alignment and improve cell connectivity. In this way that could lead to better conductive properties[5,16,49].

3.7 FURTHER STEPS

This Chapter gives an overview of the possibilities of the developed 3D *in vitro* model to analyze specific factors that could have a significant effect on cellular behavior. Specifically, here we deal with the effect that the electrical stimulus would have on subATDPCs that are planned to be used for clinical purposes. In this Ph.D. Thesis only a preliminary studies that helped us to set the ES protocol and to analyze subATDPCs behavior was assessed. Further studies are needed before concluding the effect of ES in subATDPCs growing in 3D environment:

- Analyze different ES conditions.
- Determine when it is better to start the electrical stimulus. As it was described by Milica *et. al.*[16] the effect of ES would change if it is introduced before the cells synthesize and assemble the lost proteins while recover surface channels and receptors.
- Analyze the effect of ES alone at short times at gene and protein level.
- Analyze the effect of ES alone after long culture times at gene and protein level (data previously reported that MSCs take at least 1 to 4 weeks to complete their differentiation into CM within heart).
- Determine the better combination in terms of time for the joining of chemical and electrical stimulus.
- Analyze the effect of ES in combination with chemical induction at short times at gene and protein level.
- Analyze the effect of ES in combination with chemical induction after long culture times at gene and protein level.

The analysis of this parameters and their combination may help to understand better the behavior that these cells could have *in vivo* after their implantation in an ischemic heart with the hope to improve its function. Additionally, it may help to improve the methodology to obtain better results.

In other terms, the developed system might also be useful for cell training before their *in vivo* implantation. After the complete characterization of the cells, it could be interesting to culture the cells at different times of ES and implant the construct in an *in vivo* model to study their coupling capacity.

3.8 BIBLIOGRAPHY

1. Van den Akker, N. M. S., Caolo, V. & Molin, D. G. M. Cellular decisions in cardiac outflow tract and coronary development: an act by VEGF and NOTCH. *Differentiation.* **84,** 62–78 (2012).

2. Genovese, J. a *et al.* Electrostimulation induces cardiomyocyte predifferentiation of fibroblasts. *Biochem. Biophys. Res. Commun.* **370,** 450–5 (2008).

3. Tandon, N. *et al.* Alignment and elongation of human adipose-derived stem cells in response to direct-current electrical stimulation. *Conf. Proc. IEEE Eng. Med. Biol. Soc.* **2009,** 6517–21 (2009).

4. Severs, N. J. The cardiac muscle cell. *Bioessays* **22,** 188–99 (2000).

5. Huang, G., Pashmforoush, M., Chung, B. & Saxon, L. a. The role of cardiac electrophysiology in myocardial regenerative stem cell therapy. *J. Cardiovasc. Transl. Res.* **4,** 61–5 (2011).

6. Cinca, J. *et al.* Passive transmission of ischemic ST segment changes in low electrical resistance myocardial infarct scar in the pig. *Cardiovasc. Res.* **40,** 103–12 (1998).

7. Chen, M. Q. *et al.* Cardiac differentiation of embryonic stem cells with point-source electrical stimulation. *Conf. Proc. IEEE Eng. Med. Biol. Soc.* **2008,** 1729–32 (2008).

8. Zimmermann, W. *et al.* Cardiac Grafting of Engineered Heart Tissue in Syngenic Rats. *Online* **106,** I151–7 (2002).

9. Walker, C. A. & Spinale, F. G. The structure and function of the cardiac myocyte: A review of fundamental concepts. *J. Thorac. Cardiovasc. Surg.* **118,** 375–382 (1999).

10. Salazar, Y., Bragos, R., Casas, O., Cinca, J. & Rosell, J. Transmural versus nontransmural in situ electrical impedance spectrum for healthy, ischemic, and healed myocardium. *IEEE Trans. Biomed. Eng.* **51,** 1421–7 (2004).

11. Steendijk, P., van der Velde, E. T. & Baan, J. Dependence of anisotropic myocardial electrical resistivity on cardiac phase and excitation frequency. *Basic Res. Cardiol.* **89,** 411–26

12. Valderrábano, M. Influence of anisotropic conduction properties in the propagation of the cardiac action potential. *Prog. Biophys. Mol. Biol.* **94,** 144–168 (2008).

13. Kanno, S. & Saffitz, J. E. The role of myocardial gap junctions in electrical conduction and arrhythmogenesis. *Cardiovasc. Pathol.* **10,** 169–77 (2001).

14. Ruiz-Meana, M., Fernandez-Sanz, C. & Garcia-Dorado, D. The SR-mitochondria interaction: a new player in cardiac pathophysiology. *Cardiovasc. Res.* **88,** 30–9 (2010).

15. Gallik, S. & HistologyOLM. Cardiac Muscle. *Retrieved April 20* (2013). at <http://histologyolm.stevegallik.org/node/146>

16. Radisic, M. *et al.* Functional assembly of engineered myocardium by electrical stimulation of cardiac myocytes cultured on scaffolds. *Proc. Natl. Acad. Sci. U. S. A.* **101,** 18129–34 (2004).

17. Tung, L., Sliz, N. & Mulligan, M. R. Influence of electrical axis of stimulation on excitation of cardiac muscle cells. *Circ. Res.* **69,** 722–30 (1991).

18. Castells-Sala, C. *et al.* Influence of electrical stimulation during cardiac differentiation in 3D-cultures of SUBcutaneous Adipose Tissue Derived Progenitor Cells (subATDPCs). *Conf Proc IEEE Eng Med Biol Soc* 3–6 (2012).

19. Spadaccio, C. *et al.* In situ electrostimulation drives a regenerative shift in the zone of infarcted myocardium. *Cell Transplant.* **22,** 493–503 (2013).

20. Serena, E. *et al.* Electrical stimulation of human embryonic stem cells: Cardiac differentiation and the generation of reactive oxygen species. *Cell* **315,** 3611–3619 (2010).

21. Ahadian, S. *et al.* Electrical stimulation as a biomimicry tool for regulating muscle cell behavior. *Organogenesis* **9,** 87–92 (2013).

22. Balint, R., Cassidy, N. J. & Cartmell, S. H. Electrical Stimulation : A Novel Tool. *Tissue Eng. Part B. Rev.* **19,** 48–57 (2013).

23. Hronik-tupaj, M. & Kaplan, D. L. A Review of the Responses of Two- and Three-Dimensional Engineered Tissues to Electric Fields. *Tissue Eng. Part B. Rev.* **18,** 167–180 (2012).

24. Haneef, K. *et al.* Development of bioartificial myocardium by electrostimulation of 3D collagen scaffolds seeded with stem cells. *Heart Int.* **7,** e14 (2012).

25. Vunjak-Novakovic, G. *et al.* Challenges in cardiac tissue engineering. *Tissue Eng. Part B. Rev.* **16,** 169–87 (2010).

26. Tandon, N. *et al.* Electrical stimulation systems for cardiac tissue engineering. **4,** 155–173 (2009).

27. Llucià-Valldeperas, A. *et al.* Electrical stimulation of cardiac adipose tissue-derived progenitor cells modulates cell phenotype and genetic machinery. *J Tissue Eng Regen Med.* (2013).

28. Büscher, D., Bayes Genis, A., Roura Ferrer, S., Farré Crespo, J. & Prat Vidal, C. POPULATION OF ADULT STEM CELLS DERIVED FROM CARDIAC ADIPOSE TISSUE AND USE THEREOF IN CARDIAC REGENERATION. (2012).

29. Bayes-Genis, A. *et al.* Human progenitor cells derived from cardiac adipose tissue ameliorate myocardial infarction in rodents. *J Mol Cell Cardiol.* **49,** 771–80 (2010).

30. Simmons, C. S., Petzold, B. C. & Pruitt, B. L. Microsystems for biomimetic stimulation of cardiac cells. *Lab Chip* **12,** 3235–48 (2012).

31. Girão-Silva, T. *et al.* Short-term mechanical stretch fails to differentiate human adipose-derived stem cells into cardiovascular cell phenotypes. *Biomed. Eng. Online* **13,** 54 (2014).

32. Amin, S. *et al.* Comparing the effect of equiaxial cyclic mechanical stimulation on GATA4 expression in adipose-derived and bone marrow-derived mesenchymal stem cells. *Cell Biol. Int.* **38,** 219–27 (2014).

33. Hazeltine, L. B. *et al.* Temporal impact of substrate mechanics on differentiation of human embryonic stem cells to cardiomyocytes. *Acta Biomater.* **10,** 604–12 (2014).

34. Arshi, A. *et al.* Rigid microenvironments promote cardiac differentiation of mouse and human embryonic stem cells. *Sci Technol Adv Mater* **14,** 1–14 (2014).

35. Haneef, K. *et al.* Development of bioartificial myocardium by electrostimulation of 3D collagen scaffolds seeded with stem cells. *Hear. Int.* **7** e14

36. Shafy, A. *et al.* Association of electrostimulation with cell transplantation in ischemic heart disease. *J. Thorac. Cardiovasc. Surg.* **138,** 994–1001 (2009).

37. Song, Y.-H. *et al.* VEGF is critical for spontaneous differentiation of stem cells into cardiomyocytes. *Biochem. Biophys. Res. Commun.* **354,** 999–1003 (2007).

38. Takahashi, T. *et al.* Ascorbic acid enhances differentiation of embryonic stem cells into cardiac myocytes. *Circulation* **107,** 1912–6 (2003).

39. Cao, N. *et al.* Ascorbic acid enhances the cardiac differentiation of induced pluripotent stem cells through promoting the proliferation of cardiac progenitor cells. *Cell Res.* **22,** 219–36 (2012).

40. Minami, I. *et al.* A small molecule that promotes cardiac differentiation of human pluripotent stem cells under defined, cytokine- and xeno-free conditions. *Cell Rep.* **2,** 1448–60 (2012).

41. Wu, X., Ding, S., Ding, Q., Gray, N. S. & Schultz, P. G. Small molecules that induce cardiomyogenesis in embryonic stem cells. *J. Am. Chem. Soc.* **126,** 1590–1 (2004).

42. Mummery, C. *et al.* Differentiation of human embryonic stem cells to cardiomyocytes: role of coculture with visceral endoderm-like cells. *Circulation* **107,** 2733–40 (2003).

43. Gaustad, K. G., Boquest, A. C., Anderson, B. E., Gerdes, A. M. & Collas, P. Differentiation of human adipose tissue stem cells using extracts of rat cardiomyocytes. *Biochem. Biophys. Res. Commun.* **314,** 420–427 (2004).

44. Guan, J. *et al.* The stimulation of the cardiac differentiation of mesenchymal stem cells in tissue constructs that mimic myocardium structure and biomechanics. *Biomaterials* **32,** 5568–80 (2011).

45. Li, Z., Guo, X. & Guan, J. An oxygen release system to augment cardiac progenitor cell survival and differentiation under hypoxic condition. *Biomaterials* (2012).

46. Cell, S. *et al.* Biomimetic Three-Dimensional Anisotropic Geometries by Uniaxial Stretch of Poly(E-Caprolactone) Films for Mesenchimal Stem Cell Proliferation, Alignment, and Myogenic Differentiation. *Tissue Eng. Part C. Methods* **19,** 538–549 (2013).

47. Paquin, J., Danalache, B. a, Jankowski, M., McCann, S. M. & Gutkowska, J. Oxytocin induces differentiation of P19 embryonic stem cells to cardiomyocytes. *Proc. Natl. Acad. Sci. U. S. A.* **99,** 9550–5 (2002).

48. Gallo, P. *et al.* A lentiviral vector with a short troponin-I promoter for tracking cardiomyocyte differentiation of human embryonic stem cells. *Gene Ther.* **15,** 161–70 (2008).

49. Robinson, K. R. The responses of cells to electrical fields: a review. *J. Cell Biol.* **101,** 2023–7 (1985).

CHAPTER 4: Development of bioactive implant for ventricular function restoration after myocardial infarction

Vallés-Lluch, A *et. al*. 2013 Combining self-assembling peptide gels with three-dimensional elastomer scaffolds *Acta Biomaterialia*. **9** 9451–60

Soler-botija C, *et. al*. 2014 Engineered 3D bioimplants using elastomeric scaffold, self-assembling peptide hydrogel, and adipose tissue-derived progenitor cells for cardiac regeneration *Am. J. Transl. Res.* **6** 291–301

Castells-Sala C *et. al* (under submission) Development of bioactive patch for maintenance of implanted cells at the myocardial infarcted site

Castells-Sala C *et al*. (under submission). Bioimplant development to assist myocardial infarct using elastomeric scaffolds filled with peptide gel and adipose tissue-derived progenitor cells

Martínez-Ramos C. *et al* (under preparation). PCLMA based bioactive implant development to assist myocardial infarction.

4.1 BACKGROUND

4.1.1 Overview

As commented in the previous chapters, although the treatments for myocardial infarction (MI) have been improved during the last decades, the death of cardiac muscle remains an issue. Due to the benefits reported for cardiomyoplasty, cells-based therapies give new hope in regenerative medicine and are undergoing experimental and clinical trials. Unfortunately, until now, cell transplantation has not achieved clear hemodynamic benefits for myocardial diseases[1,2]. It has been estimated that a cell number on the order of one billion would need to be replaced in patients with heart failure[3]. Moreover, they are needed to survive, differentiate, and have mechanical and electrical cell-cell contacts between them and the host[4]. The main obstacle for the grafted cells is that the ischemic event is followed by inflammatory reaction, and cytokines and growth factors (GF) secretion. Therefore, the transplantation of unprotected cells into this environment results in a significant cell death. Additionally, the constant beating (human heart beats normally over 2 billion times and pumps over 150 million liters of blood in a life span which stimulate cell wash out[5]) leads to low bioretention and engraftment. In this context, it seems suitable to provide a safe environment (niche) to maintain the cells in the affected zone and aid their proliferation and differentiation[2].

After MI, the changes not only affect the contractile elements of the myocardium, but also the extracellular matrix (ECM), that gives structural strength, is pathologically modified (collagen type I decrease from 80 % to 40 %). Therefore, both cardiomyocyte (CM) death and scar formation modulate cardiac remodeling, which refers to the changes in size, shape, structure, and physiology of the heart. The regional structural changes lead to global left ventricular (LV) geometric change (dilated cardiomyopathy), altering fiber direction and diminishing function. All these events lead to an increase in LV wall stress and mitral valve regurgitation. This process may progress inducing heart dilatation, a negative symptom in the evolution of heart failure patients, related with morbidity and mortality[2,6]. Kelley *et. al.* first demonstrated that restraining infarct expansion preserved LV geometry and prevents a decline in cardiac function. As, clinical studies have confirmed the effectiveness of LV restrain in humans, it is possible that biomaterials could be used *in situ* to increase the wall thickness, restore the geometry, and provide structural support of an injured LV[7].

In this context RECATABI consortium proposed an approach to address both, the death of CM, and the remodeling of the heart muscle, with the final aim to avoid heart failure. Basically, the strategy consisted in the development of a bioactive implant containing three components: (1) an elastomeric microporous membrane, to provide biomechanical support, (2) a self-assembling peptide (SAP) nanofiber gel, to provide an adequate microenvironment within the membrane's

pores, and (3) subcutaneous adipose tissue derived progenitor cells (subATDPCs)[8] as a cell component. Figure 4.1-1 presents the initial scheme of the bioactive implant proposed by RECATABI consortium, which included inside the elastomeric porous membrane a mixture of RAD16-I SAP with subATDPCs. With this approach the cells would remain adhered to the implanted zone preventing cell loss and providing more directed repair mechanism[3].

4.1.2 Materials used for cardiac tissue engineering during the last years[9]

During the last years, the study of many scientists has been and still is focused in the design of scaffolds. The issue remains in obtaining a scaffold with the appropriate characteristics to provide to the cells a suitable milieu where they can grow in three-dimensional (3D) configuration that closely mimic heart native architecture[10,11]. In addition, the scaffold may work as a vehicle for cell delivery. The main purpose is to replicate the biological and mechanical function of the native ECM allowing cells to grow and migrate out of the synthetic niche in order to colonize the affected zone. Parameters such as topography, charge, roughness, hydrophilicity, and hydrophobicity are known to be essential to enhance cell attachment, differentiation, and viability.

One of the first materials used for Cardiac Tissue Engineering (CTE) was based on hydrolytically degradable biocompatible polymers composed of polylactic acid (PLA), polyglycolic acid (PGA), or their copolymer poly(lactic-co-glycolic) acid (PLGA). Subsequently, researchers realized that the mechanical properties of the material used needed to be adapted to the elastic properties of the heart tissue[12]. Several studies have been performed in this specific field working with various natural or synthetic biomaterials. Between natural biomaterials collagen, fibrin, gelatin, and alginate have been extensively investigated for CTE[13]. Additionally, chitosan has been widely used due to their intrinsic characteristics as a soft material for myocardial repair and their anti-oxidative properties[14,15]. Interestingly, the poor mechanical properties of this material were improved reinforcing the hydrogel with chitosan fibers[10]. Other natural materials like elastin, fibroin, fibronectin, laminin, and vitronectin with diverse structural and biological features are suitable for CTE approaches[15–26]. Moreover, cross-linked matrices of low and high molecular weight maltodextrins obtained an adequate stiffness grade material[27]. In parallel, lots of efforts have been focused in the use of artificial materials. Different kinds of polymers have been used for these purposes. Due to their elastic properties, elastomers such as poly(glycerol sebacate) (PGS), poly(ester urethane urea) (PEUU), poly(L-lactic acid)-co-poly-(3-caprolactone) (PLCL), and poly(1,8-octanediol-co-citrate) (POC), resulted to be interesting materials. For instance, blending POC and PLCL produced an elastomeric nanofibrous scaffold with mechanical properties (tensile strength and Young's Modulus) comparable to the native cardiac tissue[28]. Other materials that have recently attracted

attention due to their excellent mechanical properties (especially fatigue resistance) are poly(aliphatic/aromatic-ester)s (PED). PEDs are thermoplastic elastomers that can be tailor made to have stress-strain curves typical of elastomers or to have a higher toughness typical of thermoplastics[29]. On the other hand, spherical beads of PLGA have also been used as a platform for delivery, improving the post-infarcted cardiac function[30].

Besides cell repopulation and ventricle dilatation, it is clear that there are other issues in the necrotic heart tissue that need to be solved. One of these properties is electrical conductivity which presents decreased performance. Dvir *et. al.* proposed to incorporate gold nanowires (NWs) within alginate scaffolds which can improve electrical communication between adjacent cardiac cells [31]. Moreover, materials especially resistant to the formation of fibrous capsule, such as polyethylene glycol (PEG), are suitable candidates for CTE[32–37].

In terms of clinical applicability, an important criterion for the choice of one biomaterial is its methodology of application. Trying to maximize cell retention and survival in the ischemic area during cell delivery; injectable extracellular matrices have been widely studied as vehicles for cell injection. Due to their properties, hydrogels seem to be ideal materials for injectable scaffolds. They are highly hydrated and possess ECM-like viscoelastic and diffusive transport characteristics. Although injectable cell therapies are desirable to avoid invasive chirurgic procedures, they present two main challenges: (1) the material needs to be liquid until the moment of injection and then solidify quickly after delivery *in vivo*, and (2) the continuous contraction-relaxation cycles of heart tissue, makes difficult the integration of the material within the host muscular, vascular, and connective tissue compartments. Therefore, although different studies have demonstrated that the use of injectable matrices enhances the beneficial effect of intramyocardial cell injection, their poor mechanical properties remain a handicap and previously assembled patches appeared as an alternative[21].

4.1.3 RECATABI concept

The primary goal of European Consortium RECATABI (**R**egeneration of **Ca**rdiac **T**issue **A**ssisted by **B**ioactive **I**mplants)[38,39] was to develop a bioengineered platform to support cell survival after implantation. Additionally, this platform should allow cell mobilization into the ischemic tissue to promote slow progressive tissue remodeling and tissue replacement with minimal ventricle dilatation. These objectives were faced by the fabrication of nanoscale-engineered biomaterials and scaffolds to match the biological, biomechanical, and biophysical requirements of the implanted tissue.

The chemical and biophysical cues of ECM *in vivo* are essential elements for the regulation of cell fate and function[40]. Synthetic and natural hydrogels possess many properties to those of the

ECM, which makes them suitable candidates for engineered cellular niches (see Chapter 2). RECATABI platform proposed the use of RAD16-I, which was proved to have biomimetic characteristics, with the purpose to display structural and functional properties (after the addition of specific motifs) similar to ECM. As commented, from the clinical point of view these types of materials are appropriate candidates for non-invasive techniques, but unfortunately they cannot meet the demanding mechanical requirements of heart tissue, which greatly limits their use. RECATABI consortia propose to include RAD16-I inside of a porous scaffold with microscopic pores. The microporous scaffold would be able to act as a vehicle and protect mechanically the cells into the soft nanofiber scaffold, creating cell niches[2]. Additionally, the proposed scaffolds would be able to provide mechanical strength and geometrical definiteness to the heart. Therefore, the microporous scaffolds were designed to function as carriers to implant the cells into the infarcted myocardium and to be able to sustain the cyclic mechanical deformation of heart beating. Elastomeric membranes were introduced as principal candidates since they are capable of recovering from deformation and represent a feasible substrate from the mechanical perspective. The developed implant presented in Figure 4.1-1 combines self-assembling peptide[41], newly designed elastomeric membranes, and subcutaneous adipose tissue derived progenitor cells (subATDPCs)[8,9,40,42].

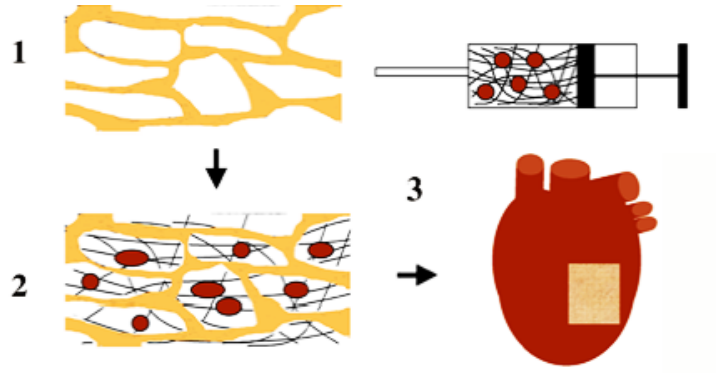

Figure 4.1-1: RECATABI therapeutic concept: Regeneration of cardiac tissue assisted by a bioactive implant. Elastomeric microporous membrane scaffolds (with mechanical properties similar to cardiac tissue) were filled with a self-assembling peptide nanofiber (a synthetic ECM analog) containing stem cells (1) in order to obtain a bioactive implant (2). The membrane acts as a carrier but most importantly, protects mechanically the cells growing into the soft nanofiber scaffold. Additionally it was designed to act as a LV restrainer.

The scaffolds designed and synthesized by the Center of Biomaterials and Tissue Engineering group of UPV for the RECATABI project were: a non-degradable polymeric porous membrane of ethyl acrylate (EA) and a partially degradable polymer of caprolactone methacryloxyl ethyl ester (CLMA) membranes. Mechanical support properties of biodegradable materials would be lost along the time which could derivate in LV dilation, complicating to avoid tissue loss function. Both materials, which are described in section 4.2 (*Previous Results*), were filled with RAD16-I to obtain two different bioactive implants. The combination of RAD16-I with

elastomeric membrane would be referred as composite henceforth. Cell addition into the composite will be referred as a bioactive implant.

In terms of ventricle remodeling, one of the principal mechanisms by which cellular therapy could bring functional benefits would be that the implant should provide a supporting scaffolding effect. This result would limit the spread of the infarcted area, preventing the excessive remodeling and dilatation of the ventricle which may reduce the risk of heart failure progression and the indication for heart transplantation. This approach takes advantage of the ability of an elastomeric material to serve as flexible patch. Here the consortium proposes that, a permanent scaffold would contribute to the regeneration but also act as a permanent mechanical restraint to limit ventricular dilatation[3,43]. Additionally, it was expected that within this approach the cells would remain in the implanted site preventing cell loss.

4.1.4 Clinical Translation, a gap to bridge

Advanced-therapy medicinal products (ATMPs) are medicines based on gene therapy, somatic-cell therapy or tissue engineering that wants to offer new insights for the treatments of diseases that right now have not available solution. During the last decade, the biology of stem cells has been presented together with expressions such as “promise”, “rapid progress” and “future therapies”. This lead to a growing concern about its possible future clinical use. The lack of an EU-wide regulatory framework in the past led to divergent national approaches which hindered the access to these products[44]. The regulatory framework for ATMPs was established by Regulation (EC) No 1394/2007 on advanced therapy medicinal products and the European directives 2003/63/EC and 2009/120/EC[45]. The aim of this regulation is to ensure the free movement of these medicines within the European Union (EU) and to facilitate their access to the EU market. Moreover, it could foster the competitiveness of European pharmaceutical companies in the field while guaranteeing the highest level of health protection for patients.

Typical regulatory concerns surrounding the use of cellular components are product safety, cell characterization and control, and characterization of their manufacturing process. With regard to safety, cell donors must be carefully screened. Additionally, once the cellular product is expanded in Good Manufacturing Practices (GMP) production facilities, it must be checked by several standardized tests such as viability, sterility, adventitious agents, genetic stability/tumorigenicity, pyrogenicity, mycoplasma infection, etc. Additionally, it is required to test biological activity and toxicity in a relevant animal model according to Good Laboratory Practice (GLP). Finally, in order to guarantee respect for human subject rights, ensure data quality, and steer clear of avoidable errors is mandatory. European Directives 2001/20/EC and 2005/28/EC on Good Clinical Practice (GCP), and associated guidelines must be followed. Likewise, and specifically for the clinical translation of stem cells (SCs), the International

Society for Stem Cell Research Guidelines (ISSCR Guidelines) offer an adequate starting point. In conclusion, a medicinal product development, from discovery to marketing authorizations, is thus a costly, lengthy, highly regulated, and high-risk process[46].

Although still today, a clear statement on cell therapy efficacy cannot be made, and the experimental basis of myocardial cell therapy is incomplete, several clinical trials have already been initiated[5,47]. Significant findings for cellular cardiomyoplasty, show an enhanced contractile and systolic function, improvement in LV remodeling parameters and a decrease of LV end-systolic volume[11,34,48,49]. Despite many cell types have been analyzed, most clinical trials have worked with autologous bone marrow mononucleated cells (BM-MNC) delivered using different methodologies such as intracoronary injection, stop-flow balloon catheter, and angioplasty balloon catheter among others [50]. Interestingly, several experimental studies showed the benefits of engineered materials charged with SCs for ischemic models. The first clinical trial for the use of CTE was the MAGNUM Clinical Trial (**M**yocardial **A**ssistance by **G**rafting a **N**ew bioartificial **U**pgraded **M**yocardium)[51]. In this approach, a collagen type I matrix was seeded with autologous BM-MNC and grafted onto the LV wall. The cell-seeded collagen matrix increased the thickness of the infarct scar with viable tissue and helped to normalize cardiac wall stress in injured regions, thus limiting ventricular remodeling and improving diastolic function. The main limitations of collagen scaffolds for heart repair are their low mechanical properties and its complete bio resorption and degradation at mid-term. Clinical studies are also under way to investigate the safety and feasibility of cell implantation in patients[32].

Moreover, some of the remaining questions before cell transplantation could be safely translated to clinic are optimal timing for cell transplantation, ideal cell type and number, long-term survival, application route, and terminal differentiation post-implantation[52]. The identification of the migration, differentiation, and regeneration mechanisms is also of great interest. In addition, even though cell component is the main analyzed factor, it is also important to analyze patient selection, concomitant procedures, cell transplantation, cell survival, cell tracking, dose, age, regulatory issues, and funding[34,53]. In conclusion, despite significant technical advancements, there is still a definite need for further refinements before CTE concepts could be translated into clinical practice.

4.2 PREVIOUS RESULTS

This Chapter is focused in the *in vitro* work developed by the European RECATABI project in Dr. Semino's laboratory. The five groups mentioned in the introduction worked during 3 years side by side to direct the investigation. At the beginning of the project, the cells and the biomaterials to be used along the project were defined. To make this decision all the efforts were focused on the stipulation of the most favorable source of cells and materials to be applied in future therapeutic protocols[54–56]. In one side, Dr. Bayés-Genís group isolated, and characterized the cell candidate (subcutaneous Adipose Tissue Derived Progenitor Cells (subATDPCs), as it is explained in Chapter 2). On the other hand, Dr. Monleón Pradas group designed, synthesized, and characterized the biomaterials to be tested during the project. The basic properties that the biomaterial must to accomplish were: (1) high porosity with controllable porous size and interconnectivity; (2) elastomeric at body temperature; (3) low swelling to avoid dimensional changes while maintaining mechanical properties; and (4) low degradation to content ventricle dilatation.

4.2.1 Microporous scaffolds used as cell vehicle and ventricle dilatation contention in RECATABI project

Biomaterials-based artificial matrices are designed to provide structural and functional support to cells for organizing into effective tissues. Synthetic polymers can alleviate the complexities of processing, purification, immunogenicity, and pathogen transmissions usually associated with natural polymers. A scaffold for Tissue Engineering (TE) should have mechanical properties matching the host tissue at the site of implant[57]. In the context of CTE, the intrinsic dynamic mechanical environment requires biomaterials designed to match the tissue modulus and to recover from the mechanical strains[58]. In this project, elastomeric materials were proposed as principal candidates for heart regenerative applications, since they allow better flexibility for cell-scaffold integration[57]. The biostable elastomer poly(ethyl acrylate) - PEA - and the semidegradable one poly(caprolactone methacryloyloxyethyl ester) - PCLMA - were found to be suitable candidates for the intended application due to their physical and mechanical properties and their reported capacity to maintain different type of cells[59–68]. The advantage of using elastomeric materials has not been definitely shown, but there is a strong reason to believe that mechanical properties of the match material matter[6]. Previous studies showed an improvement in LV function due to an augmented elastin network; therefore elasticity and distensibility in the infarcted LV appeared as an advantage[6].

Cell adhesion to synthetic materials is a complex phenomenon critical for biomedical and biotechnical applications. It can be controlled by guiding the wettability, charge, chemistry,

roughness, and stiffness of such scaffolds. Additionally, it has been reported that biomaterial surface chemistry modulates cell responses (both *in vitro* and *in vivo*) such as cell survival, cycle progression, and phenotype expression[69]. The molecular mechanisms of all these cues remain poorly understood, but the effect of the biomaterials in cell responses is generally attributed to the material-dependent capacity to absorb different type of protein species, at a specific concentration, and with or without biologically activity[70,71]. Also morphological interactions (biomaterial topography) affect this interaction. On the other hand, in the absence of specific cell adhesion domains, positive surface charges play an important role in cell attachment[72]. The density of charges is highly important for cell attachment. Moderate densities of positive charges, which support a slight increase of hydrophilicity, can improve cell adhesion. However, high densities of charges render the surface very hydrophilic, which then diminishes cell adhesion. In other terms, microporous scaffolds have the same order of magnitude that cells size and therefore, they are not capable to reproduce properly the 3D environment found *in vivo*.

Previous studies showed that PEA and PCLMA (both hydrophobic and with null charge) elastomeric membranes are good candidates for cell adhesion. They were chosen as main candidates for RECATABI European project.

Material samples of copolymer composition determined as suitable candidates to match mechanical and degradation requirements

Polymer films based on the combination of ethyl acrylate (EA) and caprolactone methacryloyloxyethyl ester (CLMA) were synthesized in different mass proportions, intended to serve as basic chemistries for the elastomer scaffold membranes (monomeric structures are presented in Figure 4.2-1). The EA monomer yields PEA, biostable and elastomeric at body temperature. It was chosen because of the wide expertise of UPV group using it with different architectures and several cell types: keratocytes, chondrocytes, neural cells, endothelial cells or dental pulp stem cells[59,60,62,63].On the other hand, the CLMA monomer yields PCLMA, also elastomeric with a biostable skeleton and a biodegradable lateral chain of caprolactone. It was previously proved to have outstanding biological behavior, and was also tested with different architectures and several cell types: chondrocytes, bone marrow stem cells, and osteoblasts[66–68].

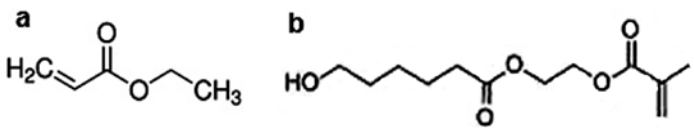

Figure 4.2-1: Monomers used for the synthesis of the elastomeric membranes employed in RECATABI Project. (a) Ethyl acrylate (EA), and (b) Caprolactone methacryloyloxyethyl ester.

PEA scaffolds were designed with interconnected cylindrical orthogonal or spherical interconnected pores and PCLMA scaffolds with spherical interconnected pores. PEA and PCLMA scaffolds were 0.8 mm-thick and were cut into samples having 5 mm in diameter. Porous size of both elastomeric membranes was about 120 microns. The architecture of developed scaffolds was analyzed by scanning electron microscopy (SEM) in a frontal view and cross section (Figure 4.2-2). Cylindrical interconnected orthogonal pores of PEA scaffold were clearly observed in a cross section image (Figure 4.2-2a). Different layers of cylindrical crossed pores in parallel and perpendicular planes could be also visualized (Figure 4.2-2b). On the other hand, interconnected spherical pores of PCLMA scaffold were readily appreciated leaving a trabecular regular aspect to the scaffolds (Figure 4.2-2c and d).

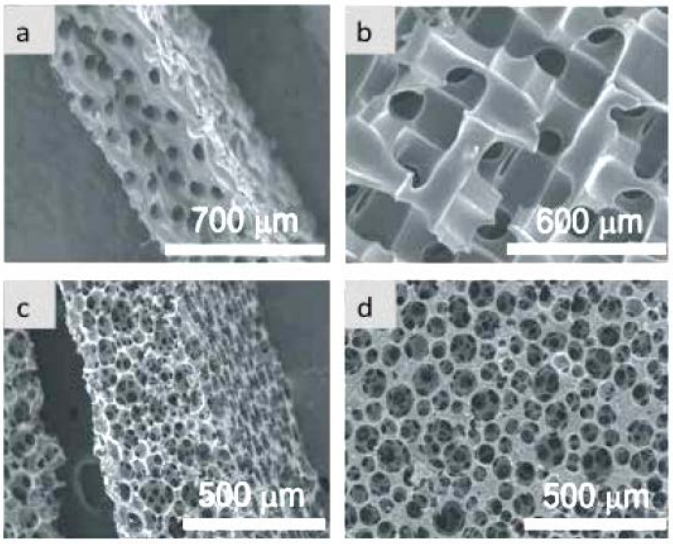

Figure 4.2-2: Scanning electron microscopy images of the designed microporous membranes. (a, b) PEA scaffolds with cylindrical orthogonal pores and (c, d) PCLMA scaffolds with spherical pores: (a, c) cross-section, (b, d) surface. PEA with spherical pores is not shown.

Mechanical properties of poly(ethyl acrylate-co- caprolactone methacryloyloxyethyl ester), P(EA-co-CLMA), copolymers in different proportions of EA and CLMA were tested (Figure 4.2-3). Both homopolymers and their copolymers were hydrophobic as it can be concluded from their equilibrium water content (EWC) (Figure 4.2-3c). Additionally, both were elastomeric at body temperature as it could be deduced from the results of Young Modulus, Breaking Strength, and Strain at Break (Figure 4.2-3a and b). The degradation of PEA and PCLMA homopolymers was followed by immersion in phosphate buffer saline (PBS), and in an aqueous medium at pH 3.5. At different times up to 60 days the weight loss of both biomaterials was determined. The biostable PEA did not degrade, whereas PCLMA lost 15 % of its mass by hydrolysis in the acid medium (Figure 4.2-3d and e).

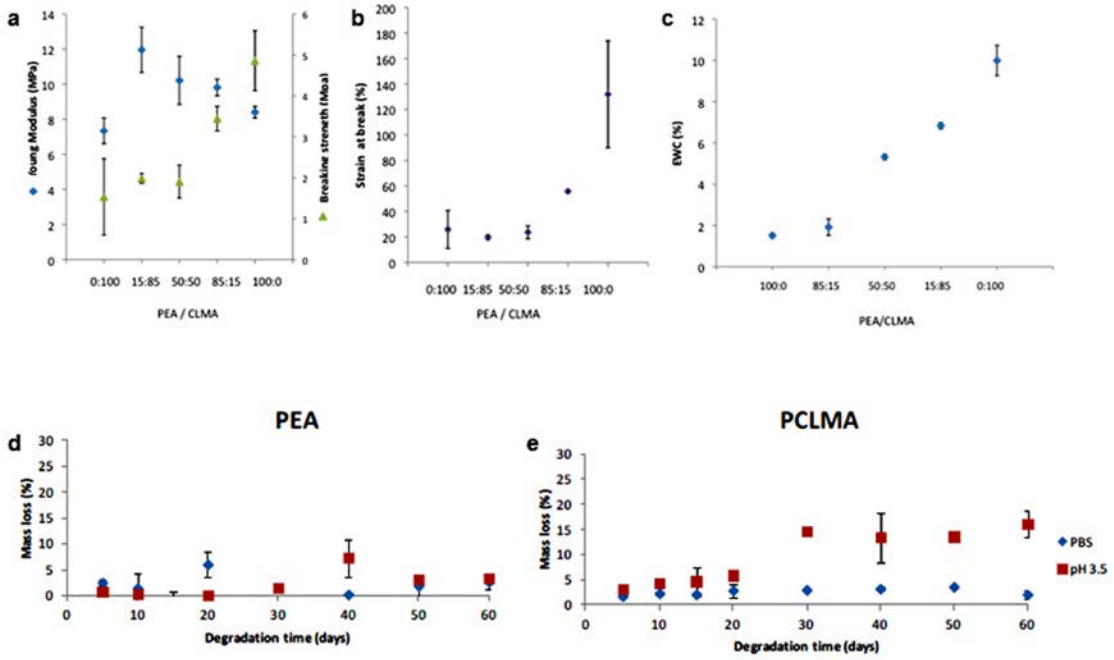

Figure 4.2-3: Mechanical and degradation features of the designed elastomeric membranes. (a) Young moduli obtained as the slope of the stress-strain curves and breaking strength performed on P(EA-co-CLMA) copolymers with different proportions of their homopolymers. (b) Strain at break obtained from the tensile measurements performed on P(EA-co-CLMA) copolymers with different proportions of their homopolymers. (c) Equilibrium water content, defined as the ratio of the mass of absorbed water at equilibrium to the mass of the dry material. The mass of absorbed water was measured after immersion of P(EA-co-CLMA) copolymers with different proportions of their homopolymers in PBS at 37 ºC until equilibrium. (d) Weight loss versus degradation time in acid medium and PBS for PEA elastomeric membrane. (e) Mass loss versus degradation time in acid medium and PBS for PCLMA elastomeric membrane.

4.3 SPECIFIC AIMS

Tissue death after blood supply restriction is only the beginning of a host of deleterious events that lead to an impasse that could conclude with heart failure. Nowadays, the recovery of heart function after MI to avoid this no exit way is a notable concern. While immediately intervention is focused on the cause to avoid damage at the maximum extend, new efforts are focused on the consequence.

In vitro analysis is of great interest for the deconstruction of complex organ systems such as the heart with the final aim to analyze specific factors. All the knowledge obtained from this kind of models is useful for its application in the obtaining of tissue substitutes that could repair a damaged tissue. The final aim of RECATABI European project was to obtain a patch capable of restoring ventricular function after MI. This thesis is mainly focused in the *in vitro* work of RECATABI project. In Chapter 2 and Chapter 3, *in vitro* models to analyze specific cues were developed; in this Chapter the preparation of bioactive implants and its *in vitro* analysis are presented. The main objectives of this chapter are:

- To define a methodology to assemble the bioactive implant consisting of elastomeric membranes filled with RAD16-I self-assembling peptide and subATDPCs (section 4.5.1 and 4.5-2).

- To establish and verify a proof of concept for the maintenance of implanted cells at the myocardial infarcted site using a bioactive implant based on PEA or PCLMA elastomeric membranes (section 4.5.3).

- To study the properties of the bioactive implant prepared with PEA elastomeric membrane in terms of cell viability, growth, distribution, and protein and gene expression (section 4.5.4).

- To study the properties of the bioactive implant prepared with PCLMA elastomeric membrane in terms of cell viability, growth, distribution, and protein and gene expression (section 4.5.5).

Additionally, and only as an overview, a summary of the most relevant results of the *in vivo* analysis developed by IGTP and CardioMonde groups are presented.

4.4 MATERIALS AND METHODS

4.4.1 Culture of cells used to establish RECATABI concept protocol.

Two different cell types were used to establish the RECATABI concept protocol: human normal dermal fibroblasts (hNDF) and mouse fibroblasts cell line (L929). Once established, the cells used were subcutaneous adipose tissue derived progenitor cells (subATDPCs)

Human normal dermal fibroblasts (hNDF) adherent cells, isolated from the skin of anonymous adult patients, were kindly provided by Dr. Jesús Otero Hernández from "Hospital Universitario Central de Asturias". hNDF were seeded in T75 cm^2 flasks using Dulbecco's Modified Eagle Medium (DMEM - Labclinics, E15-099) supplemented with 10 % (v/v) fetal bovine serum (FBS - Lonza, DE14-801F), 1 % (v/v) penicillin/ streptomycin (P/S - Labclinics, 011-010), and 2 mM Glutamine (Labclinics, M11-004) at 37 ºC in 5 % CO2 humidified atmosphere.

Mouse fibroblast cell line L929 from subcutaneous connective tissue, areolar and adipose (Sigma Aldrich, 04102001-1VL) at passage 10 were seeded and expanded with DMEM - high glucose (Sigma, D-6546). The media was supplemented with 10 % FBS (Lonza, DE14-801F), 1 % P/S (Labclinics, 011-010), and 2 mM L-glutamine (Sigma, G7513). Cultures were maintained at 37 ºC in 5 % CO2 humidified atmosphere.

Subcutaneous adipose tissue-derived progenitor celli: SubATDPCs, obtained from cardiac surgery as explained in Chapter 2, were provided by IGTP group from ICREC Research Program, "Hospital Universitari Germans Trias I Pujol"[73,74]. Informed consent was obtained from all subjects, and the study protocol conformed to the principles outlined in the Declaration of Helsinki[75]. SubATDPCs were treated as explained in Chapter 2 (See *2.4.1. Cell culture*). Adhered cells were grown under standard conditions (37 °C in 5 % CO_2 humidified atmosphere) in Minimum Essential Medium, Alpha (α-MEM - Sigma; M4526) supplemented with 10 % FBS (Lonza; DE14-801F; Lot 1SB003), 1 % (v/v) P/S (Labclinics; P11-010), 1 % L-glutamine (Labclinics; M11-004) and 5 µg/mL plasmocin (InvivoGen; ANT-MPT).

4.4.2 RECATABI concept

SubATDPCs pools were thawed at passage 5 and expanded until passage 7. Parallel, 1 % RAD16-I (PuraMatrix 1% (w/v) – Corning, 354250) was diluted, in two steps, with 20 % sucrose and 10 % sucrose to obtain a solution of 0.3 % RAD16-I. Then, cells at passage 7 were trypsinized, washed with sucrose 10 % and resuspended in sucrose 10 % to render the double of the desired final concentration. Equal volume of the cell suspension and RAD16-I 0.3 % was mixed to render the final cell suspension in 0.15 % RAD16-I. When the mixture was prepared

[i] Kindly provided by Dr. Carolina Soler-Botija, Hospital Germans Trias i Pujol, Badalona

and mixed correctly by pipetting, different methodologies were tested to introduce it inside the porous elastomeric membranes as it will be explained in results and discussion section.

4.4.3 Plasma treatment

The elastomeric membranes were placed in a cylindrical Pyrex reactor equipped with a copper coil that generates plasma under vacuum conditions (0.02 mbar). A mixture of argon with different oxygen percentages (0 – 40 %) was fed into the chamber increasing the final pressure up to 0.06 mbar. The samples were then submitted to plasma at 50-100 W for 10 min. This work was performed by Dra. Núria Marí-Buyé.

4.4.4 Preparation of the elastomeric membrane pre-filled with RAD16-I self-assembling peptide nanofiber scaffolds (composite)

The self-assembling peptide RAD16-I was loaded inside the elastomeric membranes scaffolds' pores before the addition of the cells. Prior to its use, RAD16-I was placed in a bath sonicator (Bandelin) for 30 min at 25 ºC applying 30 W to decrease its viscosity and diluted to 0.15 % (w/v)[42]. The mixture was vortexed (Elmi SkyLine) to ensure homogenization. Each elastomeric membrane was submerged in a RAD16-I nanofiber peptide 0.15 % solution and with the help of the vacuum the solution was forced to penetrate in the microporous structure of the hydrophobic scaffolds. Next, an increase of the ionic strength with PBS or culture medium was used to induce the self-assembly[42]. The efficient filling and gelling was assessed by SEM and Congo Red Staining after 30 min gelling. Materials to be used for cell culture were previously sterilized with gamma radiation.

4.4.5 Structural, mechanical and electrical characterization of the elastomeric membranes and its composite

Morphology: The porosity of the bare scaffolds, π (pore volume fraction), was obtained through the specific volume of PEA (reciprocal of 1.13 $g \cdot cm^{-3}$)[76] or PCLMA, respectively, v, the weight, m, and apparent (geometric) volume, V, of the scaffolds as: $\pi = V^{pores}/V = 1 - mv/V$. The specific volume of PCLMA was previously obtained as follows: dry pieces of PCLMA films were weighed in air, m, and immersed in n-octane (95 %, Fluka, $\rho_{n\text{-octane}}$ = 0.703 g cm^{-3}), m', at room temperature. Specific volume was calculated as the volume of n-octane displaced, obtained as $V_{displ} = (m - m')/\rho_{n\text{-octane}}$, divided by the mass of the sample: $v = V_{displ}/m$. Mettler AX 205 balance (Mettler-Toledo Inc., Columbus, OH, USA) with a sensitivity of 0.01 mg, equipped with a Mettler ME 33360 density accessory kit, was used. This work was performed by Maria Arnal in *"Universitat Politècnica de València"* (UPV).

Surface wettability: The wettability of the elastomeric membranes was measured using a Drop Shape Analysis System DSA100 (KRÜSS, Deutschland). Briefly, water drops were deposited

on the membranes and the contact angle between each drop, and the surface of the membrane was measured.

Swelling and tensile properties: To quantify the swelling of the scaffolds, 5 mm-diameter pieces of PEA and PCLMA films were dry weighed and after different times of immersion in PBS at 37 ºC until equilibrium was confirmed[42]. The EWC was obtained as the ratio of the mass of water absorbed at equilibrium to the mass of dry polymer: $EWC=(m_{wet}-m)/m$. Pieces of PEA and PCLMA scaffolds and their films were cut into 0.5 x 3 cm^2 pieces. Then, tensile tests were performed in a Microtest SCM3000 95 (Microtest SA, Madrid, Spain) device at a deformation rate of 0.2 mm/min until fracture. The tensile modulus was obtained in each case as the average of the slope in the strain-stress plots. This work was performed by Maria Arnal in UPV.

Study of the impedance: The electrical impedance of the membranes filled with hydrogel and submerged in α-MEM medium was measured at 10 kHz using a commercial impedance meter (Autolab, PGSTAT128N). Membranes filled with physiologic serum (ρ =0.625 Ωm) were also measured to normalize the membranes filled with hydrogel impedance values (Ω) to resistivity units (Ω·m). Platinum electrodes (0.5 mm diameter) were used for measurements performed at room temperature (25 ºC). The electrodes were introduced in parallel to the membrane plane and separated by a distance of 5 mm. This work was performed in collaboration with Dr. Benjamin Sanchez from "*Universitat Politècnica de Catalunya*" (UPC).

4.4.6 Cell seeding in elastomeric membrane/self-assembling peptide composites

SubATDPCs pools were thawed at passage 5 and expanded until passage 7. Before cell seeding, RAD16-I 0.15 % was introduced inside the bare elastomers pores as described in section 4.4.4. Once filled with the solution, elastomers of 8 mm diameter were placed in 48-well plates and 5 mm diameter ones in 96-well plates. Then, subATDPCs passage 7 were trypsinized and divided into two solutions at a final concentration of 10,000 cells/µL and 5,000 cells/µL in sucrose 10 %. The first suspension was injected (using a Hammilton syringe) inside 8 mm diameter scaffolds for gene and protein profile analysis and inside 5 mm diameter scaffolds for image analysis. The second suspension was injected in 5 mm scaffolds for viability studies. After injection, the samples were incubated with soft shake during 30 min allowing the cells to migrate slightly into the construct. Finally 800 µL and 350 µL of fresh media were added in 48- and 96- well plates respectively allowing the peptide to gel. Samples were cultured under standard conditions (37 ºC and 5 % CO_2 in humidified atmosphere) during 1 and 7 days, and half of the media was changed daily. The same procedure was performed with bare elastomers prefilled with PBS (see Figure 4.4-1).

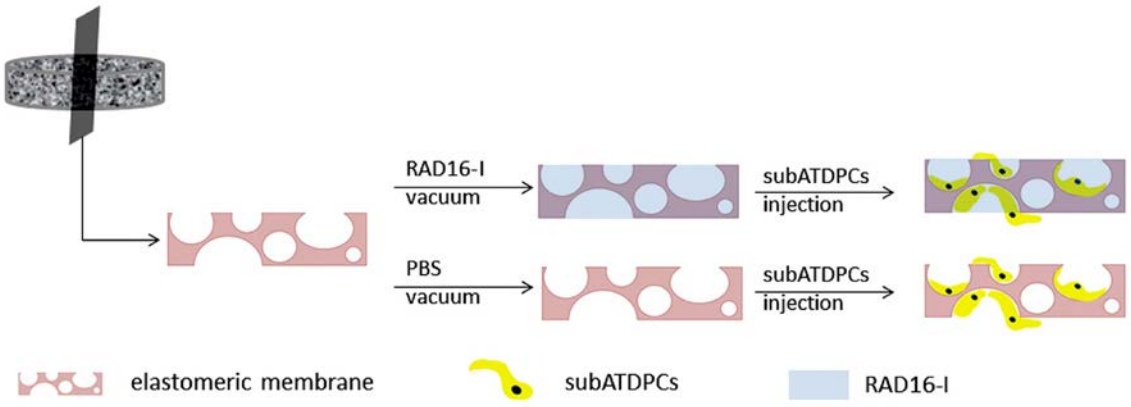

Figure 4.4-1: Bioactive patch preparation: methodology scheme. Elastomeric membranes were polymerized leaving interconnected pores. Here a section of a scaffold with spherical pores is taken as an example. The scaffolds were filled with RAD16-I (composites) or PBS (bare PEA) using vacuum. Finally, subATDPCs were injected inside the scaffolds. Scaffold size and cell number were dependent on the analysis but cell density was maintained (625 cells/μL).

4.4.7 Congo Red staining

Congo Red staining was performed to stain the β-sheet structure characteristic of the self-assembling peptide RAD16-I inside the pores of elastomeric membranes. Samples were incubated with 0.1 % (w/v) Congo Red in water for 5 minutes and washed several times with PBS. Finally, the samples were analyzed under Stereoscopic microscope Nikon digital Slight DS-2MV.

4.4.8 Live and dead staining (L&D)

The viability of the cells cultured in 3D cultures was assessed using two-color fluorescence cell viability assay based on intracellular esterase activity and plasma membrane integrity (LIVE/DEAD® Cell Viability Assays, Invitrogen; L-3224) as it has been explained in Chapter 2, section 2.4.6. Images were taken with Zeiss AxioVert 200M / ApoTome Microscope.

4.4.9 Dapi and phalloidin staining (D&P)

Cells were double stained using DAPI [4',6-Diamidino-2-phenylindole] (Sigma; D9542) and Phalloidin–tetramethylrhodamine B isothiocyanate (Sigma; 7418) as it has been explained in Chapter 2, section 2.4.7. The samples were examined under Zeiss AxioVert 200M / ApoTome Microscope.

4.4.10 MTT viability assay

Cell viability was analyzed in 5 mm diameter scaffolds using MTT assay. Shortly, 250,000 cells were seeded in each scaffold. After 1 and 10 days, the culture media was aspirated and MTT reagent (Sigma, M5655) was added to a final concentration of 0.5 mg/mL in culture medium. The samples were incubated for 3 hours at 37 ºC and formanzan crystals were dissolved by soaking the samples about 10 min in 300 μl of dimethylsulfoxide (DMSO – Sigma; D8418)

with shaking. All samples were analyzed in triplicate and controls of the scaffolds without cells were also analyzed. The absorbance was read at 550 nm with a BIOTECH ELX 800 spectrometer.

4.4.11 Study of gene expression by RT-PCR

Reverse transcription polymerase chain reaction (RT-PCR) was performed to analyze gene expression in two-dimensional (2D) cultures and bioimplant cultures. The samples were lysed, and RNA was extracted with PeqGold Total RNA kit (Peqlab; 12-6634-02). Before lysis the samples were cut in small pieces to better extract the material filing the elastomeric membrane porous. Following, cDNA synthesis was performed using Quantitect Reverse Transcription Kit (Qiagen; 205311) according to manufacturer protocol and as it has been explained in Chapter 2, sections 2.4.10 and 2.4.11. RT-PCR reaction was carried out using 30 ng of cDNA in a final volume of 25 μL containing 1X ThermoPol Reaction Buffer (stock 10X), 0.42 units of TAQ DNA polymerase (Sigma; D1806), 200 μM of dNTPs (Sigma; DNTP100), and 0.3 μM primers (synthesized by Sigma). The RT-PCR took place under the following conditions: 3 min at 95 ºC (activation) followed by 35 cycles of 20 s at 94 ºC, 30 s of annealing (Tm dependent on primer pair, see Table 4.4-1) and 30 s at 72 ºC. Final extension step was performed at 72 ºC during 15 min. RT-PCR products were size fractionated by 2 or 4 % agarose gel electrophoresis, depending on the expected fragment size.

4.4.12 Study of gene expression by qRT-PCR

Real Time reactions were performed with LightCycler® 480 Real-Time PCR System (Roche), using the iQ™ SYBR® Green Supermix (Bio-RAD; 170-8882) as explained in Chapter 2, section 2.4.14. Briefly, the samples were lysed, and RNA was extracted with PeqGold Total RNA kit (Peqlab; 12-6634-02), followed by cDNA synthesis using Quantitect Reverse Transcription Kit (Qiagen; 205311) according to manufacturer protocol (detailed information about these steps is reported in Chapter 2, sections 2.4.10 and 2.4.11). Before lysis the samples were cut in small pieces to better extract the material filing the elastomeric membrane porous. Relative gene fold variations were all determined by the comparative CT method (2-ΔΔCt) and expression of the target genes (TBX5 as early cardiac marker and GJA1as definitive cardiac marker) was normalized to the housekeeping gene (ribosomal protein 22L, RPL22). Primers used are defined in Table 4.4-1.

Table 4.4-1: Primers for RT-PCR and qRT-PCR. Early and definitive cardiac markers were analyzed. Additionally, E-cadherin (CDH1) and its natural repressor SNAI1 were studied.

	NAME		SEQUENCE	bp	Tm (ºC)	Fragment
1	*ACTN1*	Fw	GAGAAACTGCTGGAGACCATTGACC	25	63	188bp
		RV	TTGTCGGCATCAGGGAGGGT	20		
2	*GJA1*	Fw	comercial QT00012684	-	55	92bp
		RV		-		
3	*MEF2C*	Fw	CCATTGGACTCACCAGACCT	20	65	139bp
		RV	AGCACACACACACACTGCAA	20		
4	*MHC*	Fw	TGGGAGATTCGGAGATGGCAGTC	23	64	225bp
		RV	CCTGGTCCTCCTTCACGGTCACTG	24		
5	*NKX2.5*	Fw	AGTGTGCGTCTGCCTTTCCC	20	63	250bp
		RV	AGGTACCGCTGCTGCTTGAAG	21		
6	*TBX5*	Fw	CATGGAGACATCACCCAGTG	20	60	169bp
		RV	GCAGCTGATGTCCTCTAGGC	20		
7	*RPL22*	Fw	TGACATCCGAGGTGCCTTTC	20	60	101bp
		RV	GTTAGCAACTACGCGCAACC	20		
8	*cTnT*	Fw	AGAGGCTGAGACCGAGGAGACCA	23	64	207bp
		RV	TGCAACTCATTCAGGTCCTTCTCCA	25		
9	*CDH1*	Fw	AGCCAAAGAGAGAGCGGAAC	20	60	216bp
		RV	AAGCAGGCACTTGGGGATTC	20		
10	*SNAI1*	Fw	TAGCGAGTGGTTCTTCTGCG	20	60	164bp
		RV	AGGGCTGCTGGAAGGTAAAC	20		

4.4.13 Western Blotting for protein analysis

Bioimplants of 8 mm diameter were cut in small pieces and lysed with the help of pestles to crush the samples using RIPA buffer (Sigma; R0278) containing proteinase inhibitor cocktail (Roche; 11836153001). 2D samples growing on PEA or PCLMA films were taken as control. Protein content of the supernatant was determined using Micro BCA™ Protein assay kit (Pierce-Thermo Scientific; 23225). Equal amounts of total protein (10 µg) were denatured using SDS (Sigma; L5750-500G) and β-mercaptoethanol at 95 ºC during 10 min. The whole lysate was separated by electrophoresis on 10 % SDS-PAGE gels at 150 V during 1 h 30 min and transferred using wet transference on PVDF membrane (Invitrogen; LC2002) during 2 h at 40 V. The membranes were blocked with 5 % milk buffer during 2 h at room temperature. Then, they were incubated with rabbit polyclonal anti-GATA4 1 µg/mL (Santa Cruz; sc-9053), rabbit polyclonal anti-GJA1 1 µg/mL (Santa Cruz; sc-9059) or rabbit polyclonal anti-TBX5 1 µg/mL (Santa Cruz, sc-48782) at room temperature for 1 h. After 3 short washes with Phosphate Buffered Saline (PBS - Gibco; 18912-014) complemented with Tween-20 (Sigma; P-1379) (PBST) and an overnight PBST wash, the blots were incubated with peroxidase-conjugated to rabbit IgG goat polyclonal secondary antibody 1µg/mL (Abcam; ab97051). The protein bands were detected after incubation with SuperSignal® West Pico Chemiluminescent Substrate (Thermo Scientific; 34080) using ImageQuant LAS 4000 mini equipment. Goat polyclonal anti-Actin antibody (Santa Cruz; sc-1615) was used to normalize using peroxidase-conjugated to goat IgG rabbit polyclonal as secondary antibody (Abcam; ab97100).

4.4.14 Immunocytochemistry

After seven days of *in vitro* culture, composites were fixed for 20 min with paraformaldehyde 4 % (PFA – Sigma, 158127) and the expression of ACTN1 and F-actin (for PEA samples) and Vimentin and F-actin (for PCLMA samples) was examined. Briefly, composites were washed with PBS (Sigma, P4417) and permeablized during 60 min with PBS-1 % bovine serum albumin (BSA – Sigma; A2153) (PBSA). Afterwards, PEA were incubated overnight at 4 ºC with Monoclonal Anti-sarcomeric α-actinin Clone EA-53 (Sigma, A7782) diluted in PBSA at a dilution rate of 1:100 and PCLMA samples in Monoclonal Anti-Vimentin Clone V9 (Sigma, V6630) diluted in PBSA at a dilution rate of 1:40. Subsequently, samples were exposed to the secondary antibody goat anti-mouse 488 (DakoCytomation; Z0420). Additionally, it was used a marker for selective F-actin staining (Alexa Fluor Phalloidin 647 – Invitrogen, A22287) at a dilution of 1:200 in 0.1 % PBSA for 2 h at room temperature. Nuclei were counterstained with DAPI (Sigma; D9542) at a final concentration of 1µg/mL. Finally, samples were cryoprotected by immersion in phosphate buffer (PB) 0.1 M containing 30 % sucrose for 1 day and included in optimal cutting temperature (OCT) embedding compound. Sections of 100 µm were obtained by using a cryostat (Leica, CM 1900) and evaluated by confocal microscopy (Olympus FV1000). This work was performed in collaboration with Dr. Cristina Martínez-Ramos in UPV.

4.4.15 Scanning electron microscopy

Composites and bioactive implants were treated using standard procedures in order to evaluate the morphology by SEM. Samples were fixed with 2.5 % Glutaraldehyde in PB 0.1 M for 60 minutes at 37 ºC. After that, samples were treated with 1 % osmium tetraoxide for 2 h, followed by dehydration using increasing concentrations of ethanol for 10 min each wash (30º, 50º, 70º, 96º, 100º). Finally, samples were air dried and sputtered with gold before study in a Hitachi (S-4800) microscope. Imaging of samples was performed using 15 kV of voltage. This work was performed in collaboration with Dr. Cristina Martínez-Ramos in UPV. In parallel, some samples also dehydrated in subsequent steps and coated with gold were examined using NovaNano SEM 230 model (FEI, The Netherlands).

CryoSEM images of the composites were also obtained using a JSM5410 (JEOL Ltd., Tokyo, Japan) device equipped with a cryounit (Oxford CT 1500) to confirm the uniform filling of the scaffolds with the peptide gel. Cross sections were previously obtained by immersion of the samples in liquid nitrogen. Water within the peptide gel was sublimated at -70 ºC in the cryogenic unit for 15 min in vacuum. Samples were gold-sputtered and observed at 15 kV and 15 mm of working distance in a Hitachi (S-4800) microscope.

4.4.16 Genetic labelling of subATDPCs

Cells were transduced using CMVp-RLuc-mRFP1 lentiviral vector (2 x 106 transducing units/mL, MOI = 21, 48 h) to express the Renilla luciferase (Rluc) control reporter labelled with red fluorescent protein (RLuc-RFP) under the control of the cytomegalovirus (CMV) promoter, a reporter of cell number. Additionally, to monitor cardiomyogenic lineage differentiation, positively transduced cells expressing RLuc-RFP were selected by fluorescence-activated cell sorting and transduced with lentiviral vector hcTnIp-PLuc-eGFP to express the promoter-less Luciferase (PLuc) reporter construct labelled with enhanced green fluorescen protein (PLuc-eGFP) under the regulation of human cardiac Troponin I promoter (hcTnIp)[75,77]. Dr. Juli Bagó kindly performed this transduction. Doubly transduced cells were loaded into the bioactive implant which was delivered onto the infarcted area of a MI model[75].

4.4.17 Myocardial infarction model[ii]

The study was performed on 8 female severe combined immunodeficiency (SCID) mice (20 to 25 g; Charles River Laboratories, inc.). Myocardial infarction was created as previously described[78] occluding the left anterior descending (LAD) coronary artery which provoke and acute infarct. The animals were randomly assigned to one of the following groups: (1) PEA-bioimplant implantation and no MI induction (the PEA sham group, n=2), (2) MI induction and PEA-bioimplant implantation (n=2), (3) PCLMA-bioimplant implantation and no MI induction (the PCLMA sham group, n=2), and (4) MI induction and PEA-bioimplant implantation (n=2). The bioimplants were implanted immediately after occlusion[75].

4.4.18 Assembly and transplantation of the bioimplant

The bioimplants were cultured in standard conditions for 24 h before implantation onto the healthy or the infarcted myocardium of mice. The fixation of the implant was made making use of synthetic surgical glue (Glubran®2) to fix their edges to the tissue and avoid sliding. Three days post-implantation hearts were arrested in diastole with arrest solution (68.4 mM NaCl, 59 mM KCl, 11.1 mM Glucose, 1.9 mM NaHCO3, 29.7 mM BDM (2,3-butanedione monoxime), 1000U Heparin). Then the samples were excised, fixed, cryopreserved in 30 % sucrose in PBS, embedded in OCT (Sakura; 4583), and snap-frozen in liquid nitrogen-cooled isopentane. Tissue blocks were stored at -80°C until sectioning[75].

[ii] All *in vivo* bioactive implant implantation in small animal models and subsequent analysis were performed by Dr. Carolina Soler-Botija of IGTP group.

4.4.19 Non-invasive bioluminescence imaging of luciferase activity from bioimplant

Anesthetized mice, bearing a bioimplant seeded with PLuc expressing cells, were intraperitoneally injected with 150 µl of luciferin for *in vivo* BLI (16.7 mg/mL in physiological serum) (Caliper, Hopkinton, MA). Mice were monitored right after implantation and before sacrifice. Quantification and analysis of photons recorded in images was performed using the Caliper image analysis software (Caliper, Hopkinton, MA).

4.4.20 Histology and immunohistochemistry

Mouse heart cryosections were stained with Masson's trichrome (collagen: blue, myocardium: red) and photographed using a TL RCI^{TM} stereoscope (Leica) for morphology evaluation. Additionally, sections were incubated with the primary antibodies against cTnI (2 µg/mL) (Abcam) and RFP (2 µg/mL) (Abcam) to enhance cells detection. Actin fibres were stained with Phalloidin Alexa568 (1:40, Invitrogen). Nuclei were counterstained with Hoechst 33342 and results analysed with Leica TCS SP2 mycrosystem.

4.4.21 Statistical analysis

GraphPad Prism version 5.00 Windows, GraphPad Software, San Diego California USA, www.graphpad.com was used for statistical analyses. The results are given as mean ± SD as obtained of three independent experiments per group. Two-way analysis of variance performed comparison of means in proliferation and qRT-PCR assays with Bonferroni's posttest. Comparison of assays was made by correlation and linear regression analysis. Differences were considered significant if p-value < 0.05.

4.5 RESULTS AND DISCUSSION

4.5.1 Set the protocol

The first approach of RECATABI concept was to introduce a mixture of cells and RAD16-I self-assembling peptide inside the porous of elastomeric microporous membranes. The final aim was to obtain a patch with mechanical properties similar to heart tissue (provided by the elastomeric membrane) and, at the same time, provide a 3D milieu where the cells could grow and migrate (provided by RAD16-I). The idea was to mix the cells with RAD16-I peptide (as it has been presented in Chapter 2, section 2.4.3) and load the mixture inside the pores of the elastomeric membranes designed by Dr. Monleón group at UPV (Figure 4.5-1).

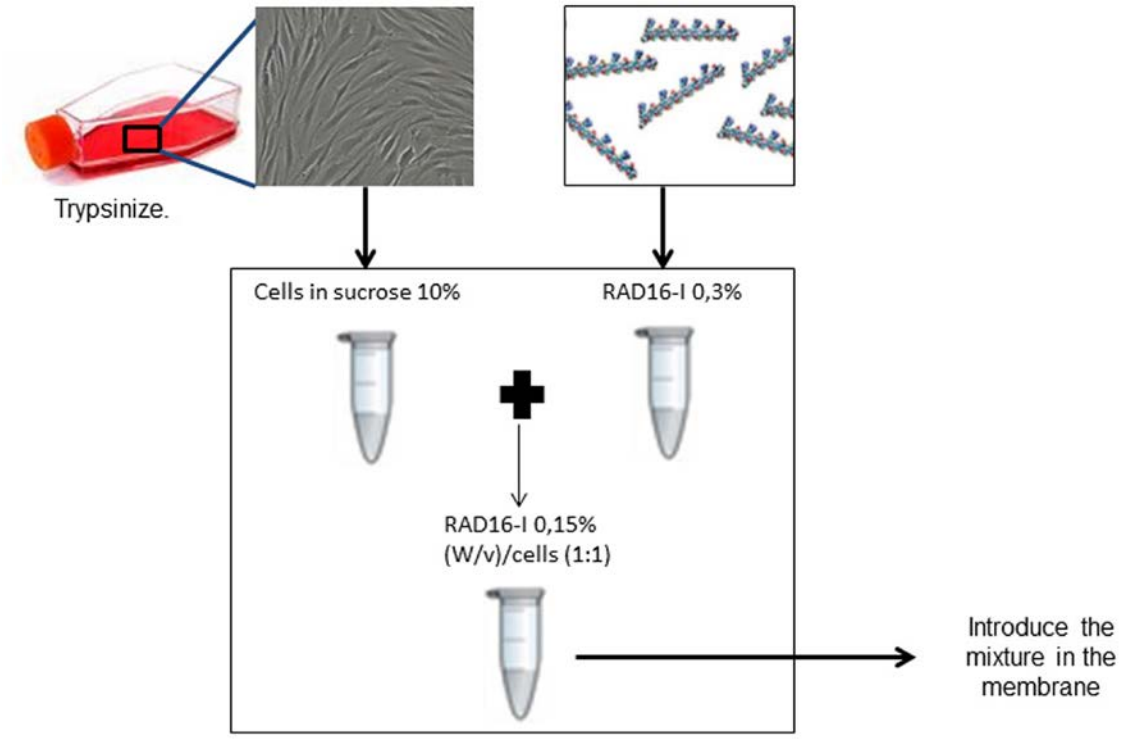

Figure 4.5-1: RECATABI methodology concept. The first approximation for the assembly of bioactive implant consisted in the introduction of a mixture of RAD16-I with subATDPCs inside the porous structure of the microporous elastomeric membranes provided by Dr. Monleón Pradas group.

During the progression of the project various elastomeric membranes with different chemical and structural characteristics were designed and fabricated. The first membrane to be tested was the one composed by ethylene acrylate (EA), which has been widely used by Dr. Monleon Pradas group in various applications[59,60,62,63]. Here, the possibility of using it for the development of the proposed bioactive implant was tested. PEA is a hydrophobic polymer, therefore its copolymerization with more hydrophilic monomers has been used to improve wettability[79]. As commented above, the protocol suggested pretends to introduce an aqueous solution inside the porous membrane, but the high hydrophobicity of the developed membrane

makes it difficult. For this reason, it was proposed to slightly increase the hydrophilicity of PEA elastomeric membrane including hydroxyl groups in the molecular structure. As it was previously reported that high hydrophobicity of this material improves cell adhesion[59], only a slight increase of the hydrophilicity, trying to introduce the aqueous solution easily inside the pores, was tested. A copolymer of poly(ethyl acrylate) and poly (hydroxyl ethyl acrylate) (PEA/PHEA) in a blending ratio of 90:10 was prepared. PEA elastomeric membrane and PEA/PHEA (90:10) were tested for the delivery of the aqueous solution inside their pores. As it can be observed in Figure 4.5-3a, although the addition of hydrophilic residues, both PEA and PEA/PHEA (90:10) membranes were highly hydrophobic.

An alternative proposal was to set up the elastomeric membranes with the aim to eliminate the air inside the pores. This approach was hoped to facilitate the diffusion of the aqueous solution composed of RAD16-I and cells. The first step was to force a sucrose 10 % solution to penetrate inside the elastomeric membrane porous with the help of the vacuum. Subsequently, the membranes were dried to moist and then the aqueous solution was loaded on the top (see Figure 4.5-2).

Figure 4.5-2: Microporous elastomeric membranes pre-conditioning protocol. The proposed elastomeric membranes were highly hydrophobic as it can be observed in (Figure 4.5-3a). The first attempt to facilitate the penetration of the aqueous mixture inside the elastomeric membranes pores was to fill the pores with PBS with the aim that this facilitates the difusion of the mixture. Firstly the membranes were sterilized with EtOH 70 % and carefully dried. PBS was forced to penetrate into the pores of the elastomeric membrane pores using vacuum, and then it was substituted by sucrose 10 % to avoid RAD16-I peptide gel. Once the sucrose 10 % were filling the pores the elastomeric membrane was dried to moist. At this step, the membranes were prepared for the loading of cells + peptide mixture.

After the pre-conditioning protocol, RAD16-I was loaded on the membrane and the gel process was immediately induced. The samples were stained with Congo Red to assure the formation of β-sheet structures. Figure 4.5-3a (C and D) show that the pre-conditioning protocol allowed the aqueous solution to get inside the porous and that the gel process was conducted successfully. PEA/PHEA (90:10) presented lower Congo Red staining what may mean that a lowest quantity of mixture was retained inside the elastomeric membrane pores.

It is well known that each cell type would have different behavior inside each biomaterial. However, the mechanistic of the cell introduction at short times will depend mostly on porosity, interconnectivity and wettability of the material, and the cell size. Here, first seeding tests were performed with hNDF cells with the aim to set the protocol. L&D staining (Figure 4.5-3b) showed a high concentration of live cells on the top of both elastomeric membranes, but not

inside. Some of the cells seeded on PEA membrane were able to diffuse inside the porous but PEA/PHEA (90:10) showed no cells inside its structure (Figure 4.5-3b). Additionally, the loading of only hNDF without the self-assembling peptide was compared with the loading of the mixture. DAPI staining results in Figure 4.5-3C showed that PEA/PHEA (90:10) presented no cells inside his structure regardless on the SAP presence. On the other hand, PEA contained higher number of cells when they were introduced in combination with RAD16-I. These results suggested PEA as a better membrane to be used for the preparation of the bioactive implant proposed. However, it would be harder needed to increase the seeding efficiency.

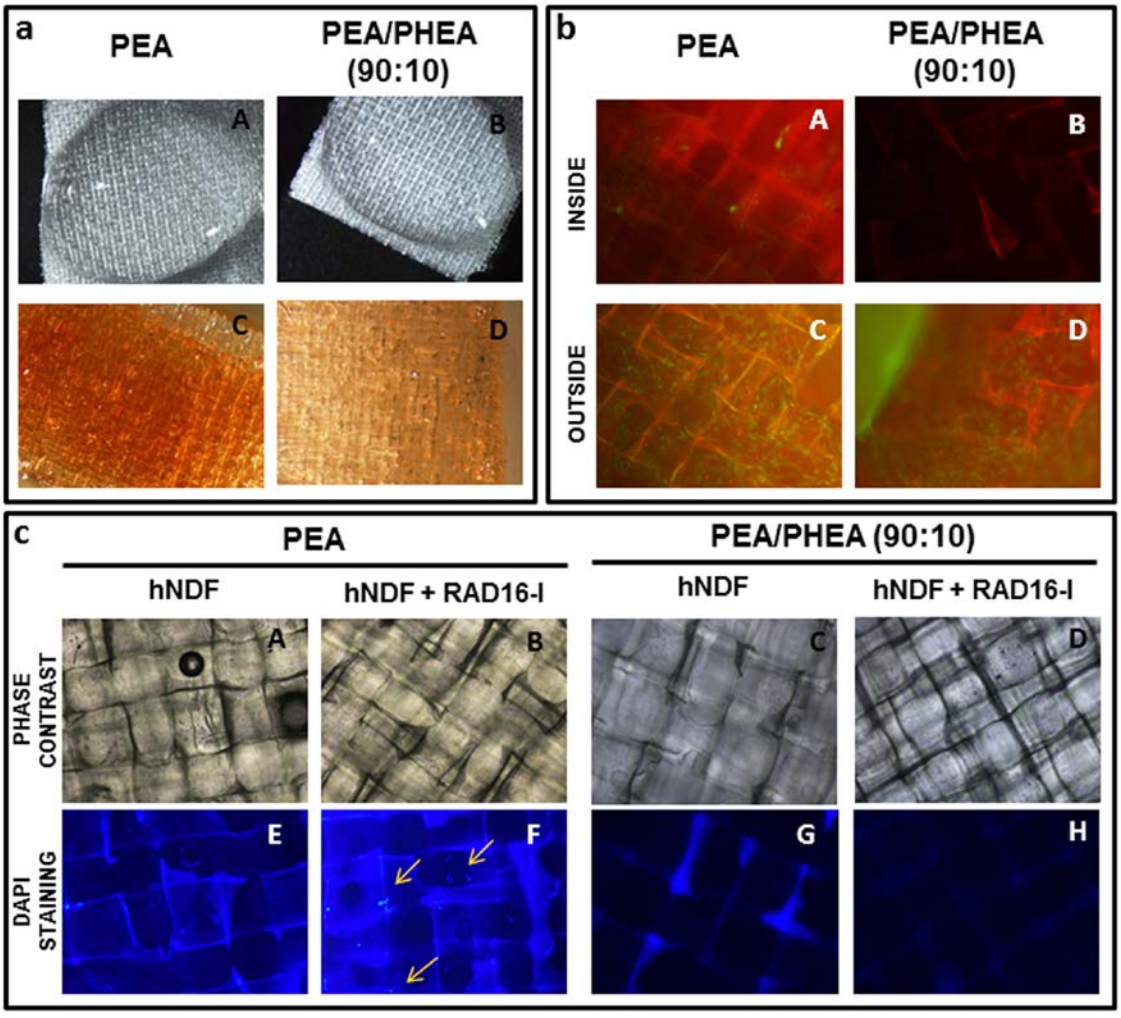

Figure 4.5-3: Mixture of cells and RAD16-I loading on PEA and PEA/PHEA (90:10) membrane after pre-conditioning protocol. (a) Macroscopic view of the hydrophobic behavior of PEA and PEA/PHEA (90:10) elastomeric membranes (A, B). RAD16-I introduction and subsequent self-assembling by increasing salt charge (C, D). The correct formation of β-sheet was assessed by Congo Red Staining. (b) L&D assay of PEA and PEA/PHEA bioactive implants after RAD16-I + hNDFs mixture loading and subsequent self-assembly of RAD16-I. Live cells are stained in green and dead cells in red. Inside and outside sections are presented. (c) Contrast phase (A-D) pictures and DAPI staining (E-H) imaging of hNDF cells loaded with or without RAD16-I on PEA and PEA/PHEA membranes.

It was proposed that the low seeding efficiency inside the structure could be caused by: (1) the hydrophobic nature of the biomaterial which avoids the solution to infiltrate inside the pores or (2) the pores size. It is crucial to design an optimized scaffold that would improve nutrient and

cell transfer to the center of the scaffold, both *in vitro* and *in vivo*. Scaffold porosity[iii] in particular controls the key processes of nutrient supply to cells, metabolite dispersal, local pH stability, and cell signaling[69]. The size of the pores can affect how close the cells are at the initial stages of cultivation (cell-cell communication), but also influences the amount of space the cells have for 3D organization in the later stages of tissue growth. In this work all the elastomeric membranes tested had a pore size of approximately 120 µm where cells would be able to contact intimately one to each other and have enough space for achieve a 3D organization.

With the aim to overcome the hydrophobic issue, both membranes were treated with physical plasma, modifying the surface properties to allow the aqueous solution to diffuse, but without modifying the bulk properties (see Figure 4.5-4).

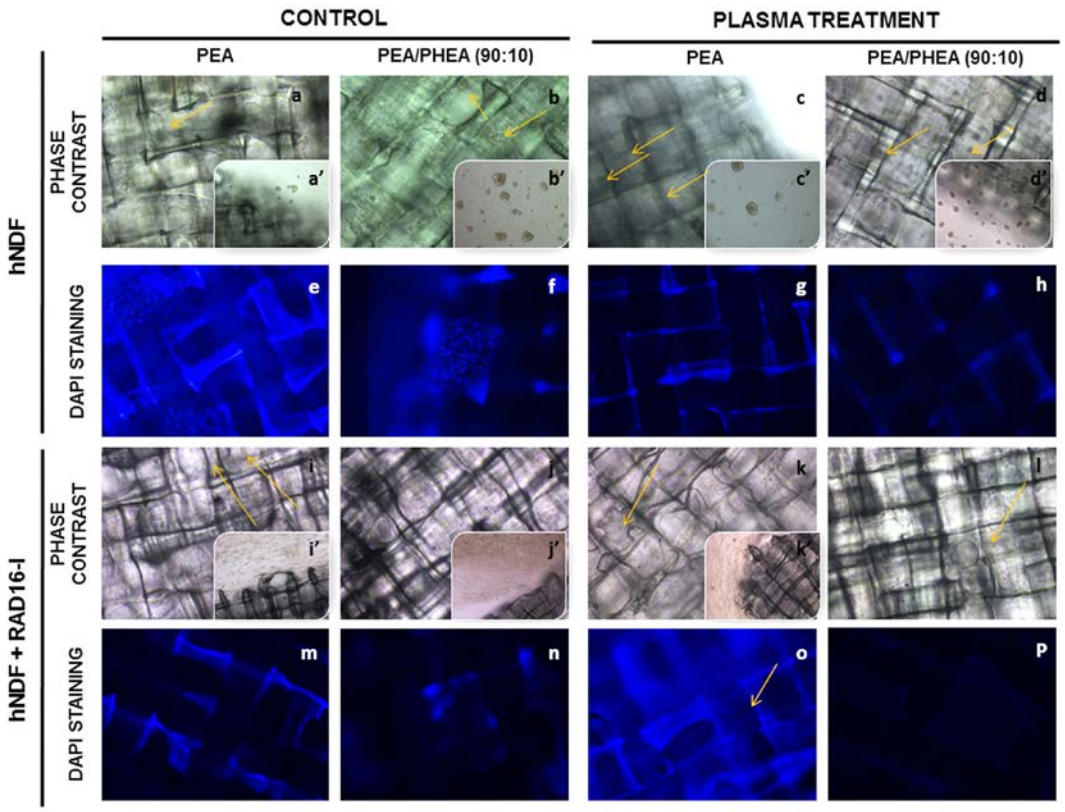

Figure 4.5-4: Mixture of cells and RAD16-I loading on PEA and PEA/PHEA modified with plasma treatment. (a-d) Contrast microscopy images of hNDF cells cultured in PEA and PEA/PHEA (90:10) elastomeric membranes without RAD16-I using plasma treatment (c, d) and without it (a, b). (e-h) DAPI staining images of hNDF cells cultured in PEA and PEA/PHEA (90:10) elastomeric membranes without RAD16-I using plasma treatment (g, h) and without it (e, f). (i-l) Contrast microscopy images of hNDF cells cultured in PEA and PEA/PHEA (90:10) elastomeric membranes with RAD16-I using plasma treatment (k, l) and without it (i, j). (m-p) DAPI staining images of hNDF cells cultured in PEA and PEA/PHEA (90:10) elastomeric membranes with RAD16-I with plasma treatment (o, p) and without it (m, n).

[iii] *In vivo* tissues have a hierarchical structure that varies over length scales of 0.1-1mm. The subcellular structures (1-10µm) control cell-cell inter-relationships and supracellular scale structures (100-1000µm) build the essential functional units of the tissue[69].

Different plasma conditions were tested (data not shown), and elastomeric membranes presenting high hydrophilicity were obtained, but in cell seeding efficiency terms, no significant improvement were observed. This outcome was mainly caused because most part of the aqueous solution run through the porous and no cells could remain neither on the top nor inside the elastomeric membrane. Additionally, it is possible that plasma treatment produced an extreme surface hydrophilicity that avoids cell adhesion through previous protein adhesion. Moreover, after subsequent tests it was observed that plasma modification (at least with the specific conditions applied) was time dependent, which would make it difficult to transfer the procedure to the clinic. Consequently, plasma treatment was discarded. On the other hand, the results presented in Figure 4.5-3 and Figure 4.5-4 for PEA/PHEA (90:10) elastomeric membrane showed the formation of clusters and in general less cell number as compared to PEA elastomeric membrane. Therefore, it was concluded to discard PEA/PHEA (90:10) elastomeric membrane, which do not present a special improvement for the proposed protocol.

Continuing with the aim to increase cell number inside the elastomeric membrane pores, PEA elastomeric membrane pre-conditioned with the protocol given in Figure 4.5-2 was loaded with different cellular densities. Two different mixtures of RAD16-I self-assembling 0.15 % peptide containing 160,000 cells or 500,000 cells were prepared for the loading. L&D and D&P assays were used for the analysis.

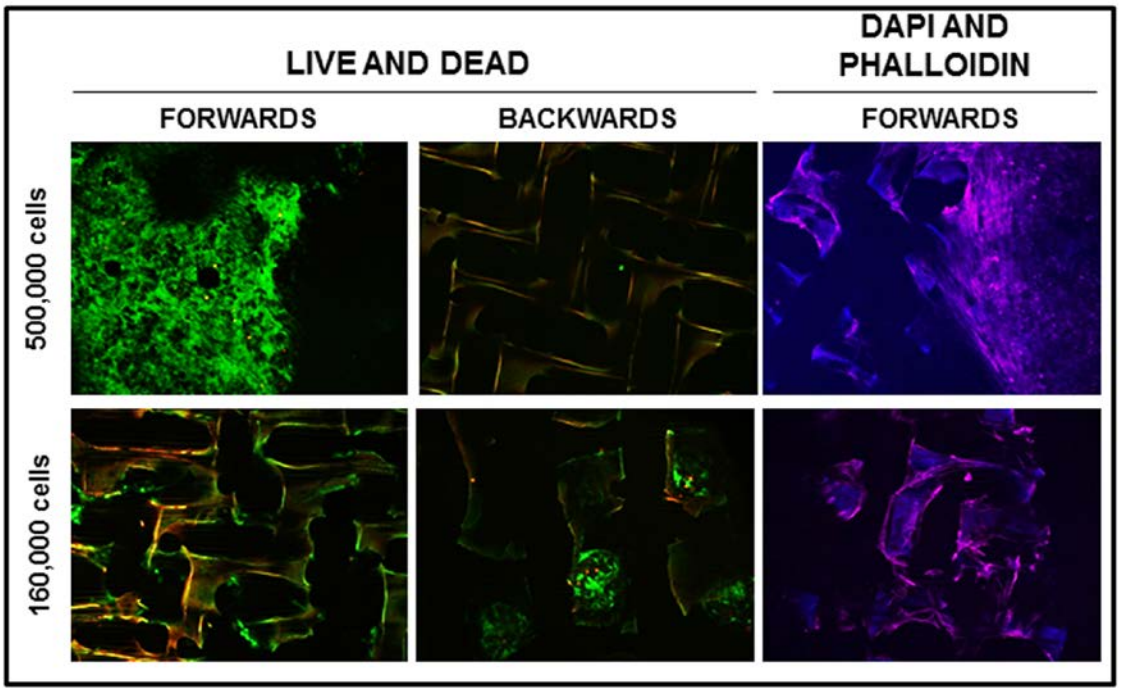

Figure 4.5-5: Analysis of cell density effect for the preparation of the bioactive implant. Two different cell densities combined with RAD16-I were loaded on PEA elastomeric membrane. L&D assay (green for live cells and red for dead cells) and D&P staining (blue for nuclei and pink for actin filaments) were used to analyze cell viability and morphology, respectively. Pictures of the top and bottom of the bioactive implant were taken to assure if the cells were able to diffuse through the pores.

In this case, little pressure applied with the tip in the moment of the loading was used. As it can be observed in Figure 4.5-5, when 500,000 cells were loaded they remained on the top of the membrane. Instead, when 160,000 cells were loaded some cells where found inside the pores. We hypothesize that, presumably due to an increase of solution density; higher cell density would not be able to diffuse inside the pores. Interestingly, in both cases cells were alive and formed a good network.

At this point it was noticed that natural diffusion was not enough to fill the scaffolds with the aqueous solution (peptide + cells) due to their hydrophobic nature. Therefore, an alternative loading procedures such as the application of pressure or even centrifugation to force the solution to penetrate into the pores were tested[42]. These procedures yielded heterogeneous filling of the elastomeric membranes pores, therefore, these methods were not further considered and the idea to introduce the RAD16-I peptide and cells in one step was substituted by two subsequent steps procedure.

4.5.2 Combination of self-assembling peptide gel with 3D elastomeric scaffolds and cell seeding methodology[iv]

The technical impossibility to obtain a homogeneous distribution of RAD16-I peptide and cells inside the pores of PEA elastomeric membrane in one step method, lead the consortium to redefine the parameters and a new protocol of two steps was assessed.

The first action of this two steps procedure was to fill the elastomeric pores with the self-assembling peptide using pressure and obtaining the composite. As it was not desired to subject the cells to a process that can negatively affect their viability and performance, they were seeded afterwards. The procedure described in Materials and Methods Section (*4.4.4 Preparation of the elastomeric membrane pre-filled with RAD16-I self-assembling peptide nanofiber scaffolds (composite)*) allowed the homogeneously filling of the scaffold pores with the RAD16-I solution as it can be observed in Figure 4.5-6. Again, Congo Red staining assure the correct gel of the hydrogel within the pores.

[iv] This work has been performed in close collaboration with UPV and published in Acta Biomaterialia Journal: Vallés-Lluch A, Arnal-Pastor M, Martínez-Ramos C, Vilariño-Feltrer G, Vikingsson L, Castells-Sala C, Semino C E and Monleón Pradas M 2013 Combining self-assembling peptide gels with three-dimensional elastomer scaffolds *Acta Biomater.* **9** 9451–60.

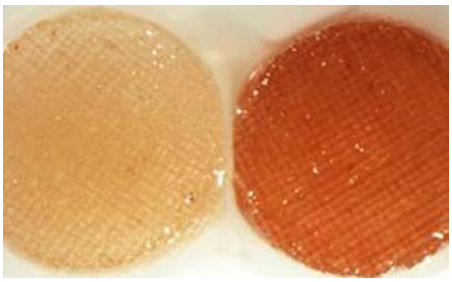

Figure 4.5-6: Congo red staining of PEA-composite. The introduction of RAD16-I peptide by pressure inside the elastomeric membranes was assessed by the staining of β-sheet structure formed by the SAP after gel. PEA elastomeric membrane filled with PBS (left) and with RAD16-I (right).

After confirm the correct introduction of RAD16-I inside the pores, cell seeding on the composite was tested. Four conditions were analyzed using PEA elastomeric membranes: PEA was filled with PBS or RAD16-I and static or dynamic seeding was used. L929 fibroblasts (10^5 cells) in sucrose 10 % were loaded in a droplet on bare scaffolds filled with PBS or RAD16-I solution. The cells were allowed to diffuse inside the composite with or without smoothly shaken and after 30 min medium was added to induce RAD16-I to gel. As it can be observed in Figure 4.5-7 and Figure 4.5-8, cells colonized the scaffolds filled with RAD16-I easily, and consequently after 7 days they were able to proliferate and occupy all the pores. Comparison of the images obtained from scaffolds seeded statically and dynamically clearly indicates that the dynamic seeding favors the migration of the cells inside the pores[42].

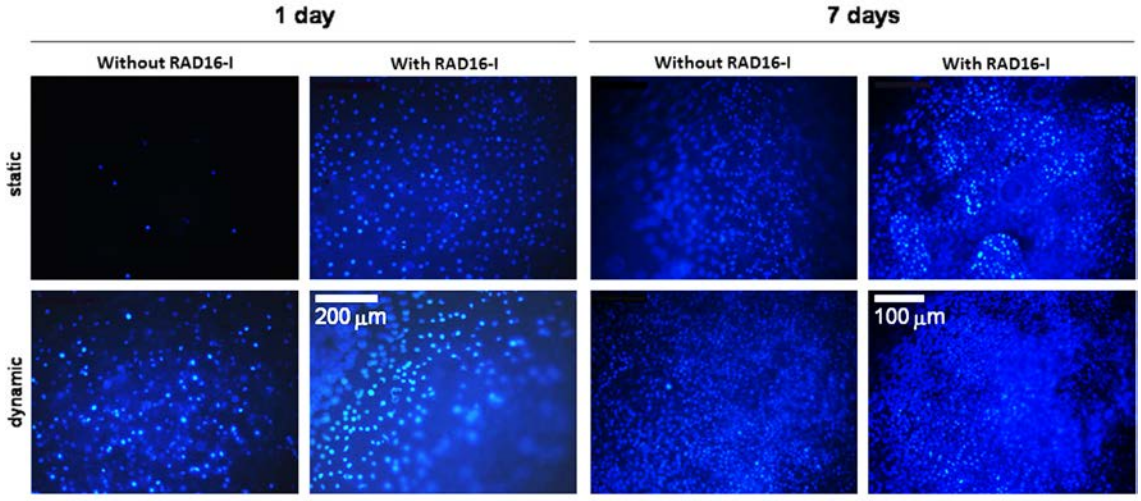

Figure 4.5-7: Seeding of L929 cells on PEA elastomeric membranes using different cell-seeding methodologies. Fluorescence microscopy images of the PEA elastomeric membranes surfaces (with and without RAD16-I self-assembling peptide within their pores) seeded with L929 fibroblasts (statically and dynamically). Samples were fixed after 1 day (scale bar 200 μm) and 7 days (scale bar 100 μm) of culture and stained with DAPI (nuclei in blue).

One day after cell loading, dynamic cell seeding for scaffolds containing RAD16-I gel led to a uniform distribution of the cells throughout the scaffold (Figure 4.5-7). The cells seemed to be leaning on the polymeric trabeculae at this culture time, and after 7 days they appeared invading completely the lumen of the pores (the area occupied by the scaffold is clearly seen in dark)[42] (see Figure 4.5-8).

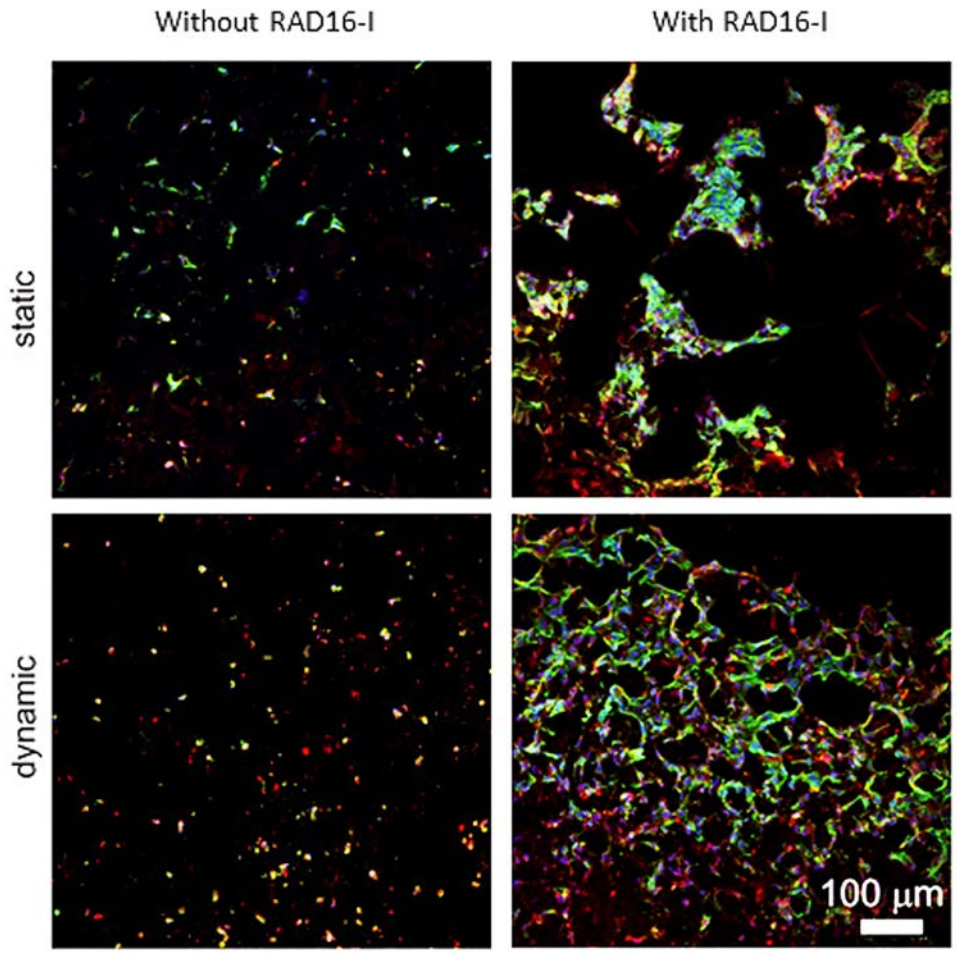

Figure 4.5-8: Cross-section of L929 cells seeded statically and dynamically in PEA elastomeric membranes with and without RAD16-I peptide in their pores. DAPI stain for nuclei (blue), phalloidin stain for actin (green) and vimentin stain for cytoskeleton (red). Images correspond to 100 µm thick internal slices after 7 days of culture. Scale bar 100 µm.

From the point of view of the cells, the presence of RAD16-I within the pores improved fibroblasts colonization in terms of cell number and distribution (Figure 4.5-7). Interestingly, after 7 days of culture, the cells proliferated much more when the pores were filled with the self-assembling peptide gel. The dynamic seeding conditions achieved the best results in terms of cell density and uniformity within the pores. We hypothesize that RAD16-I increase the diffusion speed of the cells. PEA is a hydrophobic polymer onto which most cells are willing to adhere and spread, thus delaying their progress through the structure. Swimming through the peptide solution seems a faster way of colonization than creeping on the scaffold's pores surfaces. In these experiments, the cells were seeded with the minimum amount of medium, and cultured as a droplet onto the composite; this procedure avoids their spilling out of the scaffold and optimizes cell seeding. RAD16-I was gelled later, consequently entrapping the cells inside the pores.

The same protocol was tested using PCLMA elastomeric membranes (Figure 4.5-9). After filling the pores by pressure with RAD16-I, L929 cells were seeded as a droplet on the top of the membrane and dynamic seeding was used. As it can be observed, most part of the cells remains on the surface of the porous of the elastomeric membrane, but do not inside the trabeculae.

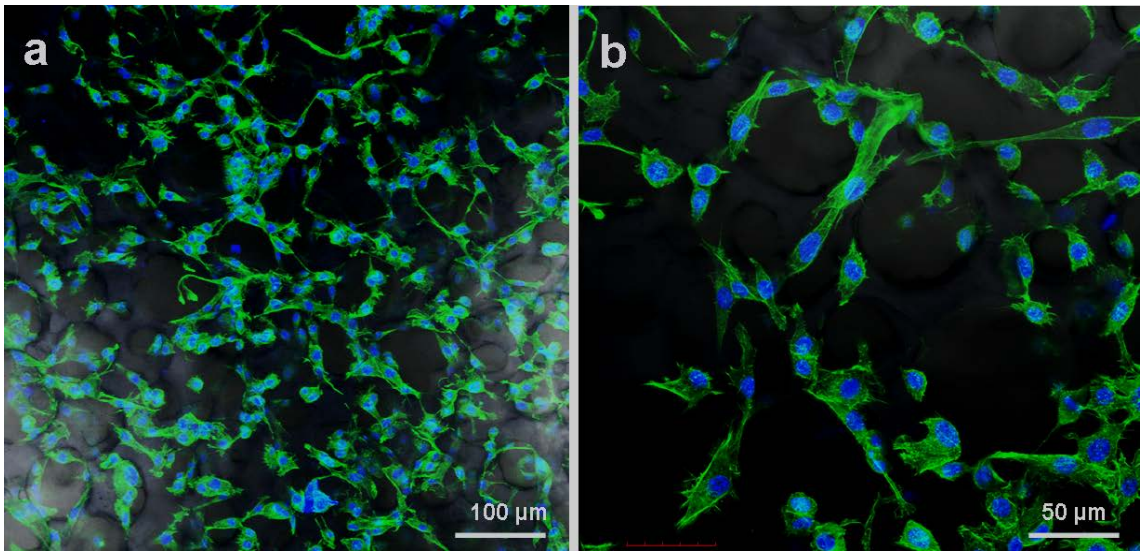

Figure 4.5-9: Cross-section of L929 cells seeded dynamically in PCLMA elastomeric membranes with RAD16-I peptide in their pores. DAPI stain for nuclei (blue), phalloidin stain for actin (green). Images correspond to 100 µm thick internal slices after 7 days of culture. Scale bars: 100 µm (a) and 50 µm (b).

These results showed that it was feasible to combine elastomeric hydrophobic scaffolds with RAD16-I to prepare a composite. The obtained composite have some of the distinctive advantages of both materials. It can act as a vehicle for cell seeding and cell supply with unique properties: a cell-friendly and ECM-like microenvironment that facilitates efficient and uniform cell colonization of the scaffolds. At the same time shape stability, mechanical consistency and strength was provided. In terms of mechanical properties, the composite represents an improvement respect the 3D system provided by the nanofibers. RAD16-I has the rheological properties of soft gels, and thus negligible resistance to shearing and tensile stresses and to manipulation in general. Its combination with elastomeric membranes represents an improvement of several orders of magnitude: from module values typical of soft hydrogels (10 to 80 Pa) to values typical of an elastomer (order of 1 MPa). Therefore, a manageable construct, able to withstand tractions, compressions and shears to the extent that a typical elastomer scaffold does, were obtained[42].

4.5.3 Proof of concept of the bioactive implant development for maintenance of implanted cells at the myocardial infarcted site using PEA and PCLMA elastomeric membranes[v]

The first step of the project was to provide a proof of concept of the viability of the proposed bioimplants using both suggested elastomeric membranes. Since the architecture and composition are different it was not pretended to select a definitive elastomeric membrane, but analyze the strengths and weaknesses of each one.

Composite development (elastomeric membrane + RAD16-I self-assembling peptide)

The architecture of developed scaffolds was analysed by SEM in a frontal view and cross section (Figure 4.5-10). Cylindrical interconnected orthogonal pores of PEA scaffold can be clearly observed in a cross section image (Figure 4.5-10b). Additionally, different layers of cylindrical crossed pores in parallel and perpendicular planes can be visualized (Figure 4.5-10a). On the other hand, interconnected spherical pores of PCLMA scaffolds can be readily appreciated providing a trabecular regular aspect (Figure 4.5-10c and d). Again the correct filling and gel of RAD16-I self-assembling peptide inside the pores of elastomeric membranes was assessed using Congo Red staining and SEM imaging. The positive Congo red staining (Figure 4.5-10c and g) indicated that the formation of the gel leads to a β-sheet structure. In parallel, the cryoSEM images (Figure 4.5-10d and h) confirmed that the scaffolds' pores were uniformly filled with the peptide gel. The hydrogel was shown as a honeycomb-like structure after sublimation of water. Although the quantity of RAD16-I cannot be quantified the complete filling of the porous was assessed.

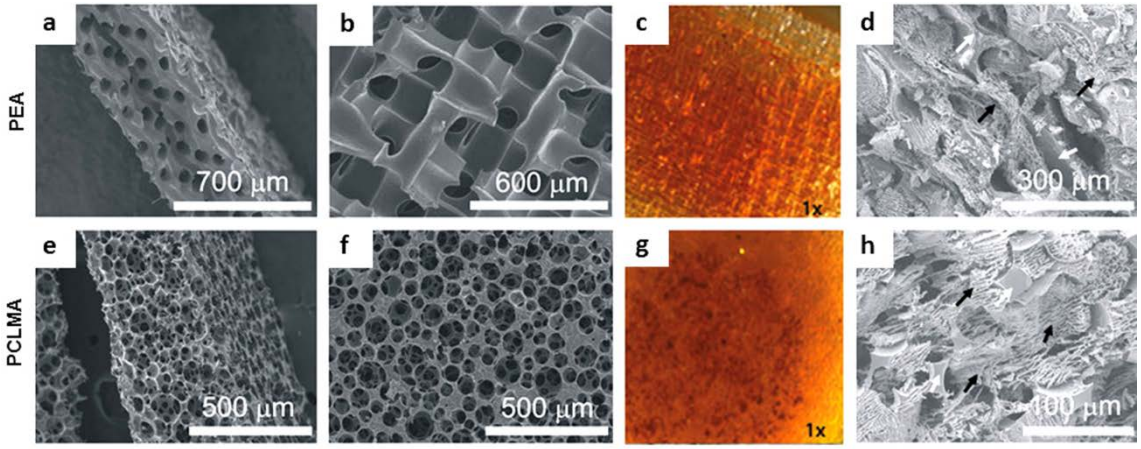

Figure 4.5-10: Characterization of PEA and PCLMA bare membranes and composites. Microscopic images of the (a-d) PEA scaffolds with cylindrical orthogonal pores and (e-h) PCLMA scaffolds with spherical pores. (a, e) SEM images, cross section, (b, f) SEM images, surface. (c, g) Congo Red staining and (d, h) cryoSEM images of the scaffolds loaded with 0.15% RAD16-I and gelled with PBS, surface. White arrows point out the elastomeric membrane while the black ones point out the self-assembling peptide structure after gel.

[v] This work was performed in close collaboration with UPV and IGTP groups from Valencia and Badalona respectively.

For the obtaining of the elastomeric membranes with the desired architecture a porogenic template was used. Due to the characteristics of each monomer used (stable PEA and semidegradable PCLMA), different types of porogenic template were employed depending on the stability of the monomers: a nylon mesh for PEA with subsequent wash with HNO_3 and sinterized microspheres of poly(methyl methacrylate) for PCLMA with a more softly wash with acetone. Therefore, although each elastomeric membrane has its specific architecture, both present high porosity and interconnectivity where the cells can achieve a good interconnection.

The measured porosities of both types of scaffolds, swelling in PBS and their apparent tensile moduli (together with the tensile moduli of the bulk respective samples) are listed in Table 4.5-1.

Table 4.5-1: Structural and mechanical parameters of the elastomeric membrane. Morphological parameters (porosity, π, equilibrium water content in PBS, *EWC*, and Young modulus, *E*) of PEA scaffolds with cylindrical orthogonal pores and PCLMA scaffolds with spherical pores. Young modulus between brackets corresponds to the bulk PEA and PCLMA polymers.

	π (%)	*EWC* (%)	*E* (MPa)	Contact Angle (°)
PEA	76.4±6.1	1.14±0.16	0.04±0.02 (0.84±0.08)	115±0,95
PCLMA	89.0±1.0	10.00±0.73	0.40±0.08 (0.73±0.07)	123,46±1,5

In general, the values obtained for PCLMA scaffolds are slightly higher than those for PEA, but it can be stated that both structures are highly porous, have a hydrophobic character and elasticity typical of elastomeric polymers. Since they differ in their chemical composition and architecture (sizes and shape of pores and interconnectivity), their biological performances will likely be different. Nonetheless, it can be safely stated that the stiffness of both proposed cardiac bioactive implants would closely match the values reported for the heart muscle of mice after dissection (0.06 MPa) and the ones of rat or human (0.14 or 0.2-0.5 MPa, respectively at the end of diastole)[13,32,80]. The hydrophobic nature is again demonstrated in Table 4.5-1 (none of them swells more than 10 % in PBS) and Figure 4.5-11.

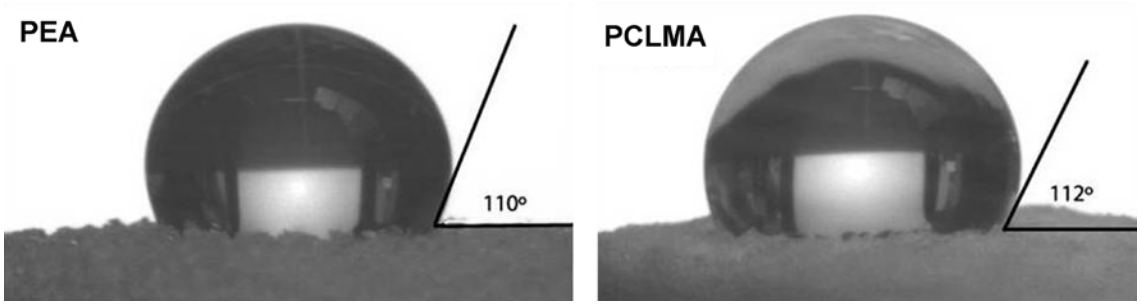

Figure 4.5-11: Wettability of PEA and PCLMA elastomeric membranes. Contact angle images of PEA and PCLMA scaffolds. Both elastomeric membranes showed an acute angle corresponding to a high hydrophobic material.

Electrical resistivity of the composites

The electrical resistivity (ρ) of the composites was also analyzed, and data were normalized. Electrical resistivity of 53.0 ± 8.5 Ωm was obtained for PEA membrane while 52.8 ± 5.5 Ωm was obtained for PCLMA (Table 4.5-2). By comparing PEA and PCLMA membranes, it can be observed that both membranes studied present similar electrical resistivity and both of them below the resistivity of transmural and non-transmural infarcted myocardium.

Table 4.5-2: Electrical parameters of PEA and PCLMA composites. Electric impedance values at 10 KHz for PEA and PCLMA scaffold previous filled with RAD16-I 0.15 % self-assembling peptide and healed transmural and non-transmural myocardium.

	ρ (Ωm)
PEA	53.0 ± 8.5[a]
PCLMA	52.8 ± 5.5[a]
Infarcted non-transmural myocardium	122 ± 27[b]
Infarcted transmural myocardium	104 ± 31[c]

[a] In work / [b] Cinca *et. al.* 1998 and Salazar *et. al.* 2004[81,82] / [c]Salazar *et. al.* 2004[82]

From an electrical standpoint, it is well-known that the electrical resistivity is lower and less frequency dependent in necrotic than in healthy myocardium[83,84]. According to the values reported in Table 4.5-2 it can be observed that the resistivity values for the composites are below to infarcted non-transmural and transmural myocardium resistivity, but the resistivity value of normal myocardium is larger compared to infarcted myocardium (250 Ω·cm at 10 kHz) [81]. We think that the resultant equivalent resistance coming from the parallel combination of the infarcted tissue and the scaffold will actually benefit the electrical coupling with native myocardium tissue. Based on the simple circuit theory principle, which confirm that the equivalent resistance of two resistances in parallel is equal or lower than the lowest resistance, the scaffold will provide a low-resistance pathway that should contribute to facilitate the electrical signal propagation from the native heart tissue into the scaffold. Thus, we speculate that both composites, which have similar electrical resistivity, will equally facilitate the propagation of electrical pulses throughout the contact area between the composites and the infarcted zone.

Bioimplant preparation (elastomeric membrane + RAD16-I self-assembling peptide + subATDPCs)

Once assessed the correct introduction of RAD16-I nanofiber peptide inside both elastomeric membrane, subATDPCs suspended in the medium were loaded on the constructs. While shaking, the cells were allowed to diffuse while the high ionic strength of the media induced the self-assembly of RAD16-I. After 1 and 4 days of *in vitro* culture, the bioimplants were removed from the well plate, and gene expression was analyzed. The morphology of the cells after 7 days

of *in vitro* culture can be observed in Figure 4.5-12. Cells were growing mostly at the surface of the construct for both types of elastomeric membranes, which indicated that they were unable to invade the scaffolds completely, *in vitro*. The surfaces were, though, entirely covered by cells after this culture time. D&P staining in Figure 4.5-12g to h shows how some cells have been able to migrate inside the construct during the first days of culture, but most part remain on the surface.

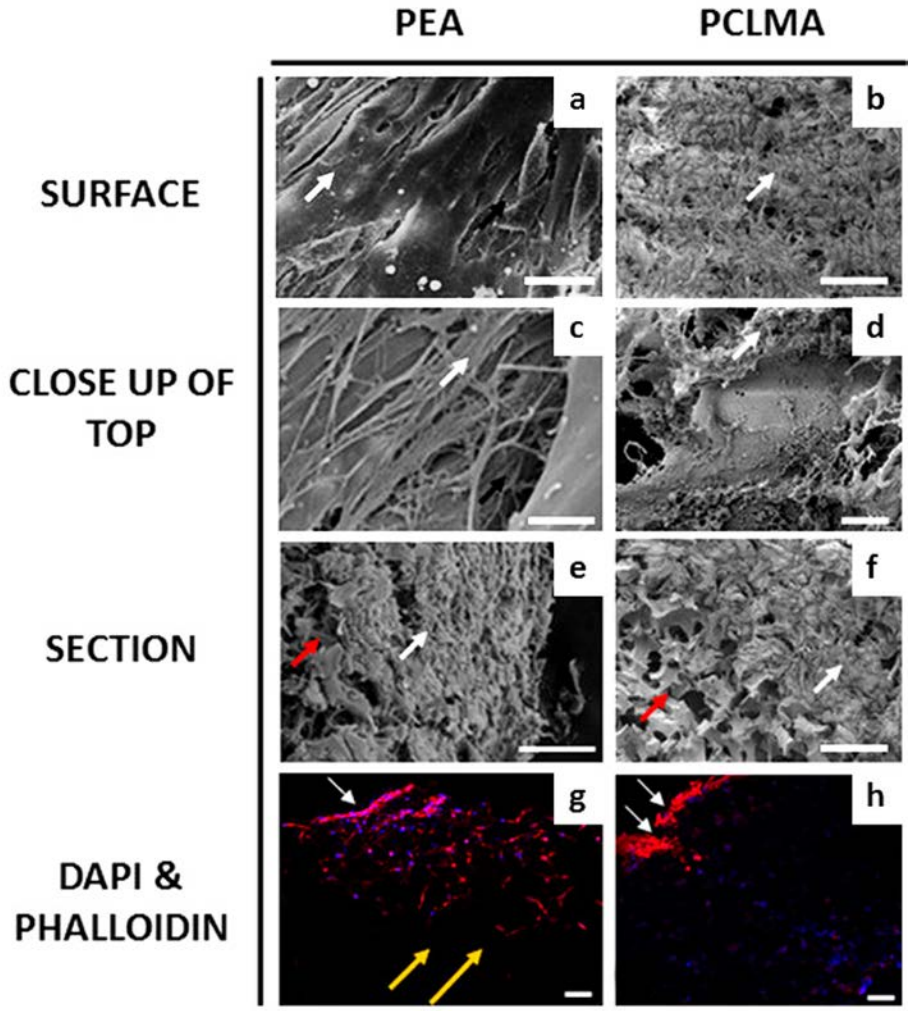

Figure 4.5-12: PEA and PCLMA bioactive implants characterization. Microscopic images of subATDPCs growing in the developed composite after 7 seeding days. (a) Surface of PEA bioactive implant; (b) surface of PCLMA bioactive implant; (c, d) close up of top PEA, and PCLMA scaffold respectively; (e) PEA scaffold cross section; (f) PCLMA scaffold cross section; and (g, h) D&P staining of subATDPCs in PEA and PCLMA bioactive implant. In images a o f white arrows show the cells growing in the bioactive implant, black arrows note the nanofibers of self-assembling peptide RAD16-I, and red arrows signalize the structure of porous elastomeric membrane. White arrows in image g and h indicate scaffolds surface while yellow arrows indicate cells migrating inside the composite. Scale bars: a 30µm; b, e-h 100µm; c 3 µm; and d 5 µm.

Study of gene expression by RT-PCR

RT-PCR analysis was performed to assess the possible cardiac gene expression of the cells after 1 and 4 days (Figure 4.5-13) of culture. Day 1 samples showed gene expression before implantation of the bioactive implant in mice, and day 4 presents gene expression of the bioactive implant cultured *in vitro* for 4 days, which coincides with the length of the *in vivo*

experiments (1 day of pre-culture and 3 days of follow-up after implantation). Interestingly, expression of early cardiac markers such as *TBX5* (T-box transcription factor 5), *MEF2C* (Myocyte Enhancer Factor 2C) and some definitive cardiac markers such as *ACTN1* (Actinin, alpha1), *cTnT* (Troponin T2) and *GJA1* (Gap Junction, alpha 1) could be observed. Additionally, expression of *CDH1* (E-Cadherin) and *SNAI1* (Snail Family Zinc Finger 1, a natural repressor of CDH1) were analyzed.

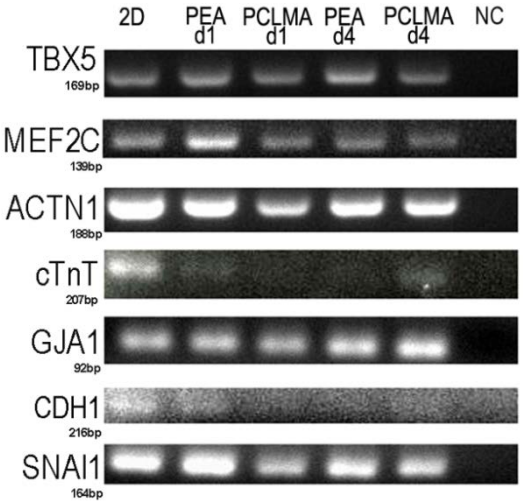

Figure 4.5-13: Expression of cellular markers in the developed bioactive implants by RT-PCR. Cardiac and general markers expressed by subATDPCs cultured in the developed implant of PEA and PCLMA after 1 (d1) and 4 (d4) days of culture *in vitro* compared to 2D cultures. NC: Negative control (PCR without template).

No significant differences were detected between day 1 and day 4 on gene expression except for *cTnT*, which was down-regulated in the composite but was up-regulated again in PCLMA at 4 days of culture. In addition, the expression of *CDH1* in both composite-systems was down-regulated, but SNAI1 repression factor was maintained. CDH1 and GJA1 genes encode for cell connection proteins. CDH1[85] is an anchoring junction involved in mechanisms regulating cell-cell adhesions, mobility and proliferation while GJA1 is a communicating junction that provides a route for the diffusion of low molecular weight materials from cell to cell having a crucial role in the synchronized contraction of the heart. *CDH1* down-regulation could be translated as a decrease of subATDPCs interconnection, which could mean that they were able to migrate as the results in Figure 4.5-14 suggest. *In vivo* results showed a migration either inside the membrane or to the infarcted area after implantation. *GJA1* expression was maintained which could facilitate the assembly of the low molecular route once cells contact one to each other. In conclusion, it seemed that subATDPCs were maintaining their gene profile, which indicates that they tend to preserve their cardiogenic potential lineage, at least *in vitro*.

In vivo implantation

The *in vitro* model gives an overview of the bioactive implant potential, but in any case these results could be extrapolated to the *in vivo* scenario. Here, a proof of concept of short time

points was developed to analyze the bioactive implant feasibility in terms of integration and cell viability. Both bioactive implants were implanted as a proof of concept in small animal models (mice) and analyzed 3 days after implantation. With the intention of monitoring cell survival and distribution of the implanted cells after the bioactive implant *in vivo* implantation, a non-invasive bioluminescence imaging (BLI) system was used. Cells within the bioimplant were previously labelled with CMVp-Rluc-mRFP1 reporters for BLI and fluorescence detection.

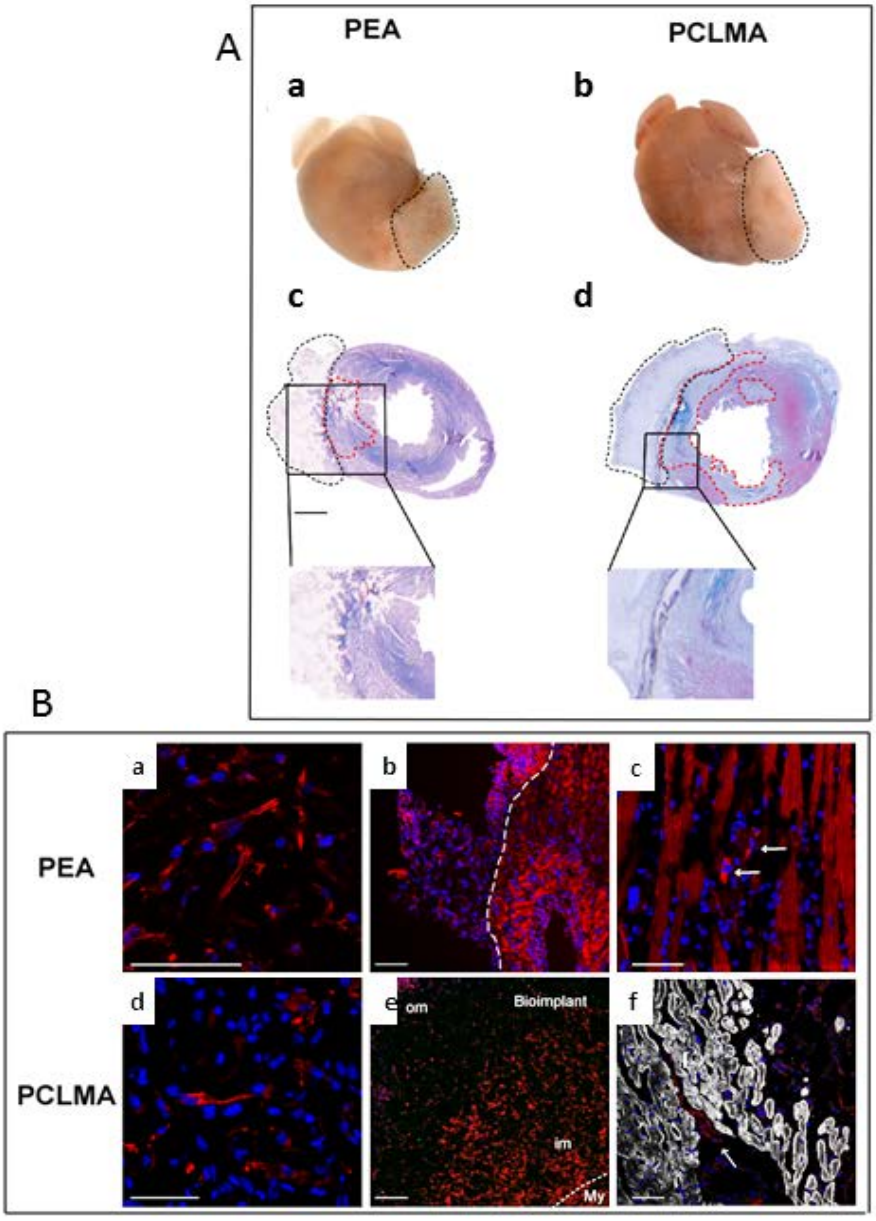

Figure 4.5-14: General view of the PEA and PCLMA bioactive implants on mice heart after 3 days of implantation. A) W*hole heart excision and macroscopic examination*. (a and b) Macroscopic view of mouse heart and bioactive implant (outlined) at 3 days post-implantation, and (c and d) Masson's trichrome staining of heart cross with bioactive implant. The dotted zone in black corresponds to the bioactive implant and the dotted red area to the infarcted zone. B*) Microscopic view of the bioactive implant.* (a and d) Detail of elongated subATDPCs (red) inside the PEA (a) and PCLMA (d) bioactive implants; (b and e) views of the PEA (b) and PCLMA (e) bioactive implants attached to the myocardium (implant and myocardium are limited by dotted lines (Phalloidin staining in red); and (c and f) migration of the subATDPCs (white arrows) to the myocardium (cTnI staining in white) in PEA (c) and PCLMA (f) groups. Constitutive expression of RFP (red) in subATDPCs. Nuclei were counterstained with Hoescht 33342 (blue). Scale bars 1 mm (A, a to d), 50 µm (a-d and f), and 100 µm (e).

Photon counts quantification showed human subATDPCs survival and thoracic location three days post-implantation of PEA and PCLMA bioimplants (data not shown). Interestingly, it was noticed that both bioactive implants intimately attach to the myocardium. Moreover, the whole heart excision and histology examination demonstrated that both remained in the position at the infarction area where they were placed suggesting some resilience to the heart mechanical forces (Figure 4.5-14A a to d).

Although both bioactive implants were attached to the myocardium, the PCLMA bioimplants showed greater cell immobilization and better integration in the infarcted area than the PEA ones. Three days after implantation, subATDPCs within the PEA bioimplant were homogeneously distributed acquiring some of them an elongated shape (Figure 4.5-14B, a). On the other hand, PCLMA bioimplant cells were mainly distributed in the borders of the myocardium (My) or inner membrane (im). Only few cells were found in the outer membrane (om) (Figure 4.5-14B, e). Few cells already started migration to the damaged myocardium Figure 4.5-14B, c and f).

We did not expect to observe profusely cell migration at such short time assay, but we speculate that the cells might start to contribute to a paracrine effect by secreting specific factors; phenomena previously reported using mesenchymal stem cells (MSC) and CM in rat and mice models, respectively [20,86,87]. Importantly, in previous studies an increase of vascularization and a reduction of infarct size after ATDPCs injection was reported[73]. Therefore, their better retention onto the infracted tissue using this platform might lead to positive benefits by the stimulation of vessel formation.

After assessing the viability of the proposed bioactive implant through the presented proof of concept, the preparation of the bioactive implant was tried to be improved. We decided to focus our attention to obtain bioactive implants completely filled with cells, increasing cell number. Cell loading on the composite, was substituted by cell injection with a syringe as described in section 4.4.7:*"Cell seeding in elastomeric membrane/self-assembling peptide composites"* (see Figure 4.4-1). *In vitro* studies of the obtained composites with PEA and PCLMA membranes are presented in the next sections.

4.5.4 Analysis of subATDPCs injected in PEA elastomeric membrane and the designed composite

Characterization of bare PEA scaffolds and composites

The RAD16-I peptide solution was successfully loaded and gelled inside the PEA scaffolds' pores using the protocol described previously[42]. The obtaining of the desired composites was confirmed by SEM imaging (Figure 4.5-15). Figure 4.5-15a presents an overview of the bare PEA and in Figure 4.5-15b it can be appreciated the walls of the microporous completely empty. The loading of self-assembling peptide solution gives rise to a nanofiber network distributed all along the PEA scaffold pore (Figure 4.5-15c and d). This nanofiber structure does not appear when scaffolds were loaded with PBS.

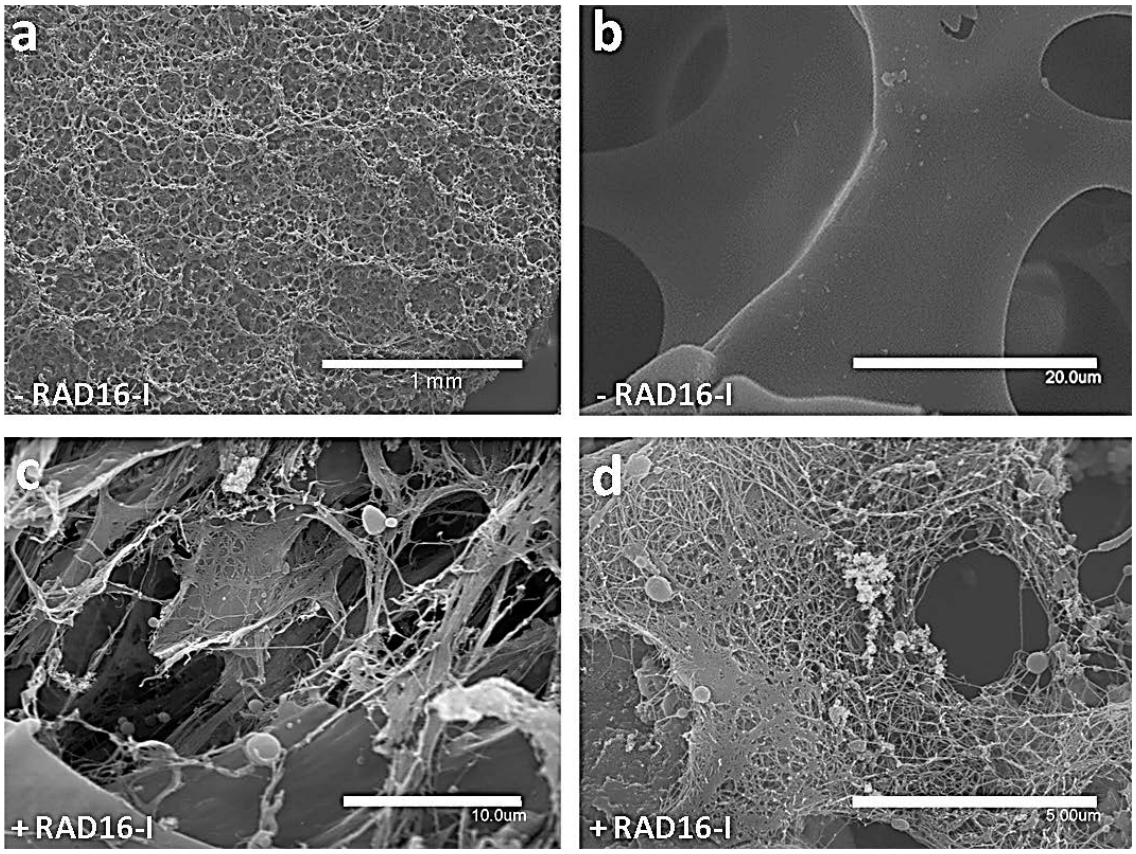

Figure 4.5-15: Assessment of PEA-composite formation. SEM images of surface (a) and sections of bare (b) and RAD16-I filled PEA scaffolds (c). (d) Detail of RAD16-I nanofibers. Scale bare: 1 mm (a), 20 µm (b), 10 µm (c), and 5 µm (d).

SubATDPCs layout in bare scaffolds or composites

For the examination of cell distribution in scaffolds, general cell staining with D&P was assessed after 7 days of culture. Composites showed much more uniform cell distribution than bare PEA scaffolds (Figure 4.5-16). SubATDPCs displayed a more elongated morphology around the pores of bare scaffolds; covering the PEA trabeculae as compared to composites

where cells showed a compact cell network (they were close one to each other and exhibited a spread out morphology).

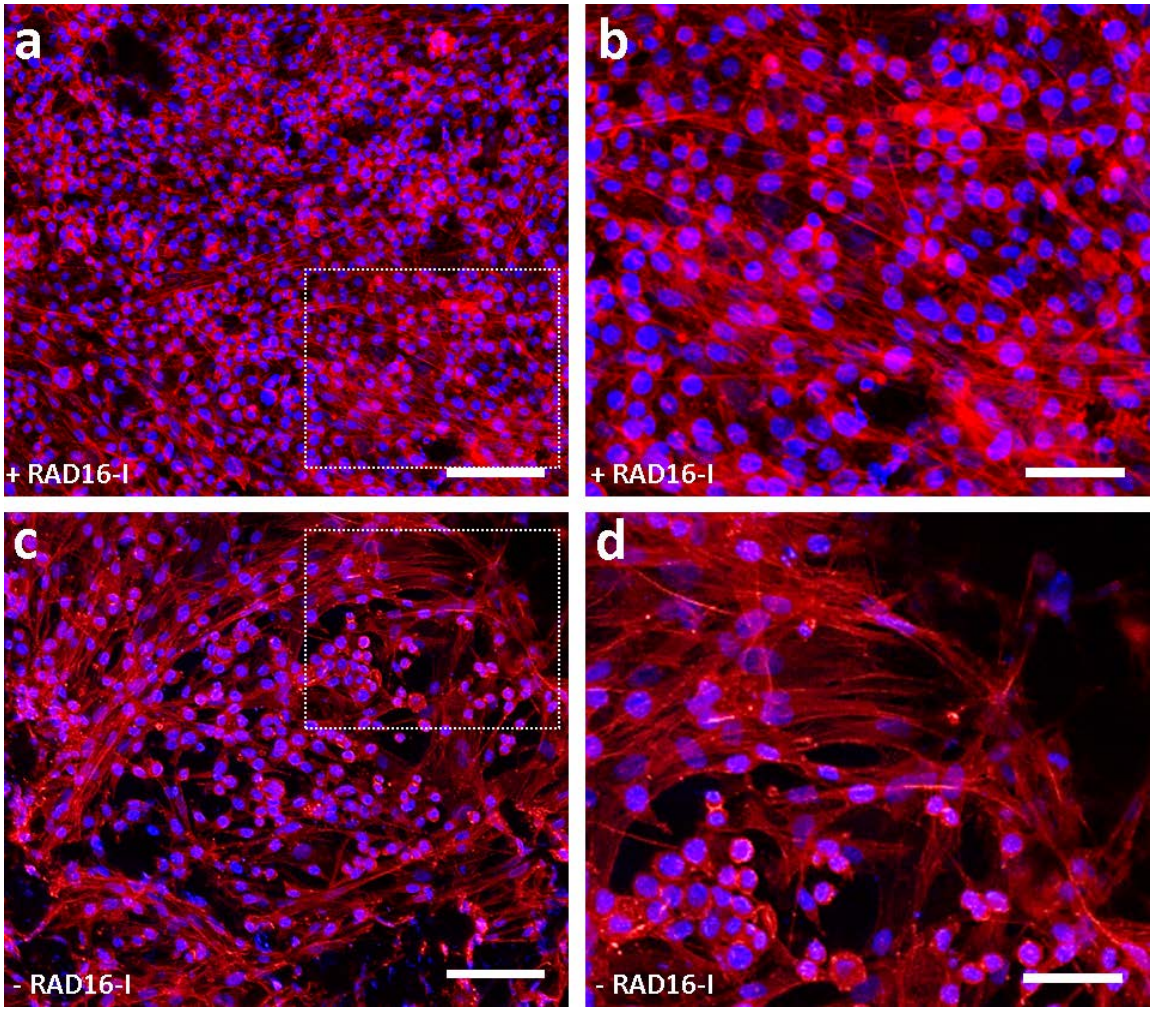

Figure 4.5-16: Surface confocal laser scanner microscopy images of cultured composites and bare PEA scaffolds. Phalloidin (red) staining of subATDPCs growing in the pores of composites (a and b) and bare PEA scaffolds (c and d). DAPI staining for nuclei (blue). Scale bar: 100 µm (a and c) and 50 µm (b and d).

Samples were also labeled with ACTN1 marker, which recognizes α-skeletal muscle actinin and α-cardiac muscle actinin (Figure 4.5-17). ACTN1 seemed to be expressed more homogeneously across the composite than in bare PEA scaffolds (Figure 4.5-17). Within the composite, subATDPCs presented ACTN1 in an elongated layout (Figure 4.5-17a and b), but the absence of RAD16-I this protein appeared surrounding the nuclei but did not elongate.

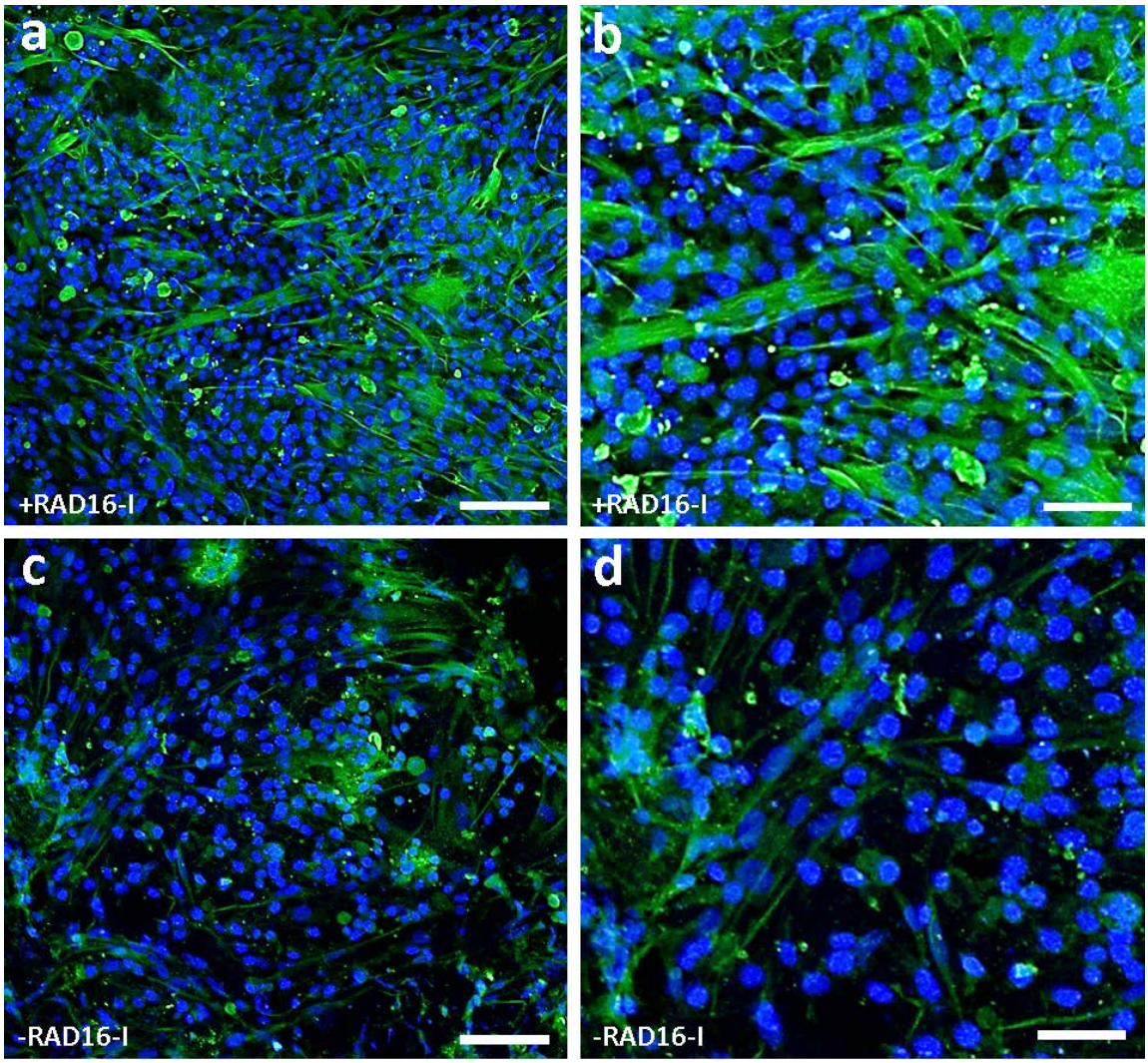

Figure 4.5-17: Surface confocal laser microscopy images of cultured composites and bare PEA scaffolds. ACTN1 (green) staining of subATDPCs growing in pores of composites (a and b) and bare PEA scaffolds (c and d). DAPI staining for nuclei (blue). Scale bar: 100 µm (a and c) and 50 µm (b and d).

In both cases, a significant fraction of cells resided on the top of the scaffolds. SEM imaging proved that subATDPCs were able to cover bare PEA and composites' surfaces (Figure 4.5-18). Significantly, subATDPCs growing in composites were uniformly distributed covering the surface after 7 days of culture entirely, whereas, on bare PEA scaffolds, a heterogeneous layout was observed. Moreover, subATDPCs cultured on composites' surfaces were organized in a well-ordered pattern, which would facilitate cell-cell contact (Figure 4.5-18b). In contrast, subATDPCs growing on bare PEA scaffolds exhibited a disorganized distribution adhered to PEA trabeculae and maintaining pores empty (Figure 4.5-18e).

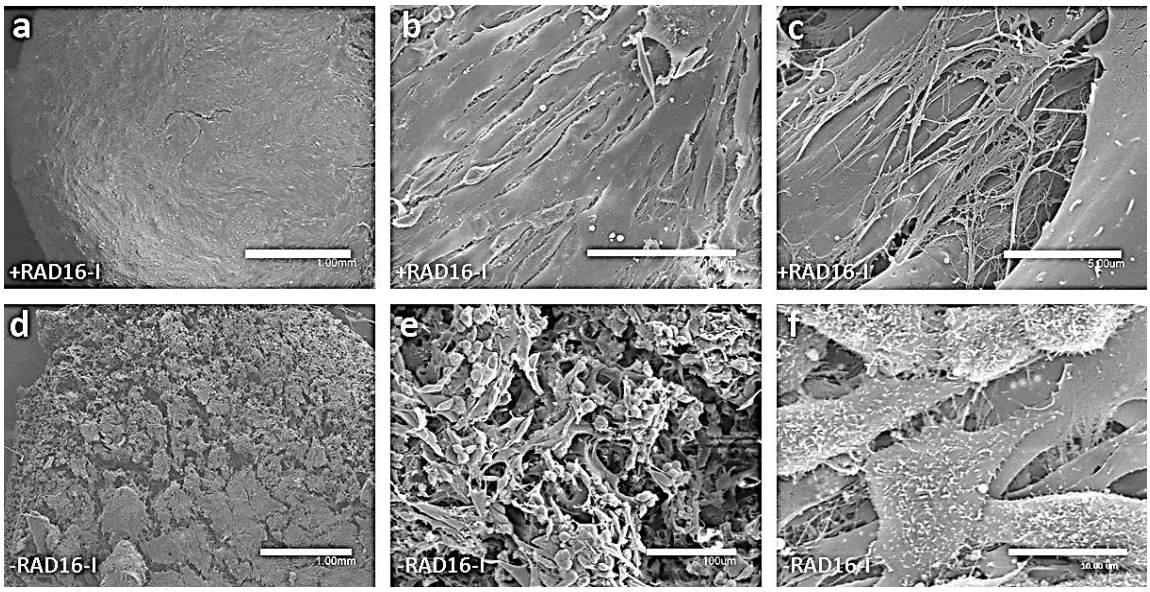

Figure 4.5-18: Cell morphology analysis on bare PEA or composite by SEM after 7 days of culture. Overview of composite (a) and bare PEA (d) seeded with subATDPCs. Close up of the surface of PEA-composite (b and c) and the surface of bare PEA seeded with subATDPCs (e and f). Scale bar represents 1 mm (a and d), 100 µm (b and e), 10 µm (c) and 5 µm (f).

Viability, growth and distribution of subATDPCs inside PEA bare scaffolds or composites

SubATDPCs' viability inside bare and gel-filled scaffolds was monitored after 1 and 10 days of culture by MTT colorimetric assay (Figure 4.5-19). The MTT test revealed that there were no significant differences in terms of viability between cells growing in bare PEA membranes and those cultured in the composites containing the self-assembling peptide RAD16-I (Figure 4.5-19a). In both structures, cell growth was observed at the same extent.

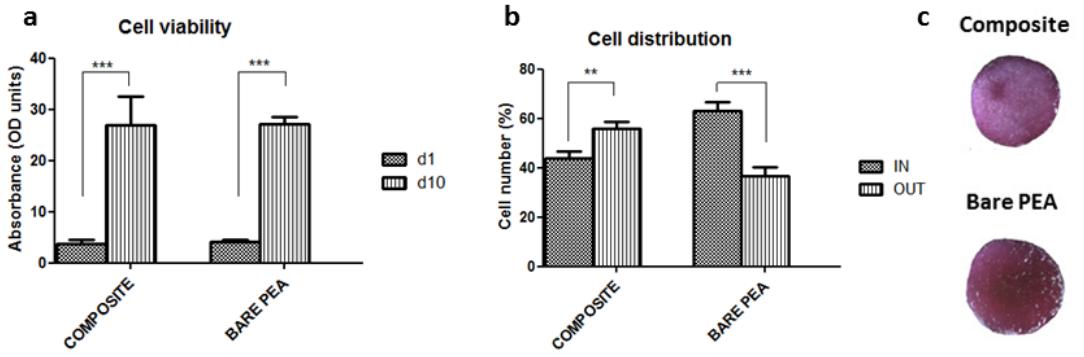

Figure 4.5-19: MTT viability assay of subATDPCs growing inside bare PEA scaffolds and composites. (a) SubATDPCs proliferation from day 1 to day 10 within both structures. (b) Cell distribution inside the structures and on the culture plate at day 10 of culture. (c) Coloration of both structures owing to the formation of formazan crystals (** $p < 0.01$ and *** $p < 0.001$).

Interestingly, it was noticed that after 10 days of culture a significant fraction of the cells did not remain in the inner pores of the PEA scaffolds migrating outwards to end adhered on the surface of the well (data not shown). This effect was found to be enhanced in the case of the composite with 53 % of the total cells detected on the surface of the well (Figure 4.5-19b). Instead, 36 %

of seeded cells in bare PEA membranes were detected outside the scaffold. It can also be appreciated in Figure 4.5-19c that the purplish intensity from formazan crystals ws stronger in bare scaffolds than in the composites. These results indicate that cell mobilization is enhanced in the case of composites, which suggest that it is a good platform to assure cell delivery to the affected tissue.

Protein and gene expression of cells cultured in PEA bare scaffolds and composites

With the aim of characterizing subATDPCs growing in the scaffolds protein and gene expression of early and definitive cardiac markers were analyzed, using cells growing on 2D PEA surfaces as controls. Here, the expression of early cardiac markers such as GATA4 (GATA binding protein 4), TBX5 (T-box transcription factor 5), NKX2.5 (NK2 homeobox 5), and MEF2C (Myocyte Enhancer Factor 2C); as well as some definitive cardiac markers such as ACTN1 (α-actinin), cTnT (Troponin T2, Tropomyosin-binding subunit in troponin complex), GJA1 (Gap Junction protein, alpha-1), and MHC (myosin, heavy chain) were examined.

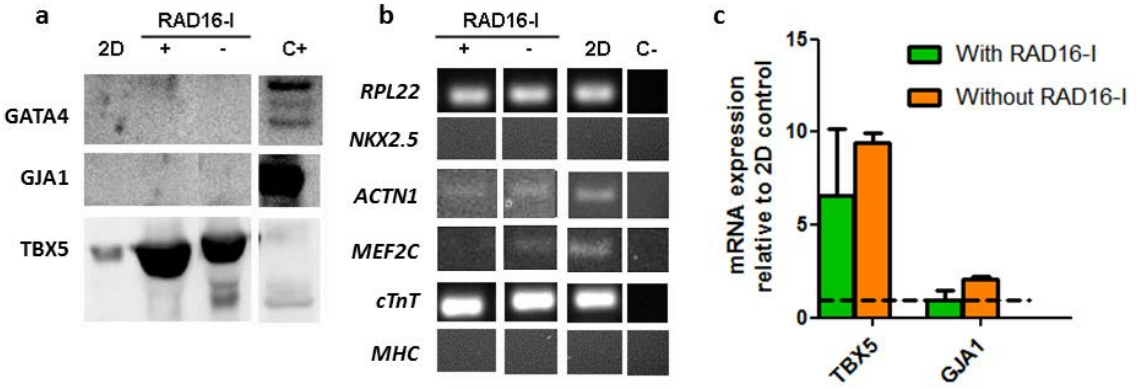

Figure 4.5-20: Protein and gene expression of cells cultured in bare PEA scaffolds and composites. *a) Western blotting.* Protein expression of cells cultured on 2D PEA compared to cells cultured in bare PEA scaffolds (RAD16-I -) and composites (RAD16-I +). C+ stands for the positive control for each protein. *b) RT-PCR.* Gene expression of cells cultured on 2D PEA compared to cells cultured in bare PEA scaffolds and composites. C- stands for the negative control used. *c) qRT-PCR.* The expression of *TBX5* and *GJA1* were assessed by Real Time RT-PCR experiments, establishing the base line through conventional monolayer cultures on PEA surfaces. No significant differences were observed between bare PEA and composites ($p > 0.05$)

The expression of TBX5 early cardiac marker was found both at protein and gene levels (Figure 4.5-20a and c, respectively). Real time RT-PCR showed no significant ($p > 0.05$) difference between subATDPCs cultured in bare PEA or in composites. This early cardiac marker has been reported to be critical in heart development, and has been shown to interact with NKX2.5, GATA4 and MEF2C to synergistically activate target genes expression in CM[88]. A light band of *MEF2C* was detected by RT-PCR (Figure 4.5-20b). This gene has been reported to play a key role in myogenesis[89] and has long been associated with the regulation of myocardial-expressed genes[90]. The expression of GATA4 and *NKX2.5*, also early cardiac markers, was not detected, which was not surprising at this early time point considering that at least 1 to 4 weeks have been

reported to be needed for implanted MSC to reach differentiation into CM within heart[91]. In addition, definitive cardiac markers were evaluated. GJA1, which is the major gap junction protein in the heart and therefore has a crucial role in the synchronized contraction, was analyzed at protein and gene levels (Figure 4.5-20a and c). No significant ($p > 0.05$) increase in gene expression (respect to 2D cultures) was detected by qRT-PCR (Figure 4.5-20c). Additionally, at protein level, GJA1 was not detected in any tested condition (Figure 4.5-20a). Moreover, *MHC, ACTN1,* and *cTnT,* at gene level were studied. *MHC* gene expression was not detected, but *ACTN1* and *cTnT* were identified (Figure 4.5-20b). Finally, ACTN1 expression was detected at gene and protein levels and cTnT at gene level in all conditions (Figure 4.5-20b and Figure 4.5-17).

4.5.5 Analysis of subATDPCs growing in PCLMA elastomeric membrane and the designed composite

Characterization of bare PCLMA and composite

RAD16-I self-assembling peptide was introduced by pressure inside the porous of PCLMA elastomeric membrane and after gel their fiber appeared covering all the trabecular structure as it can be seen by the SEM imaging (Figure 4.5-22).

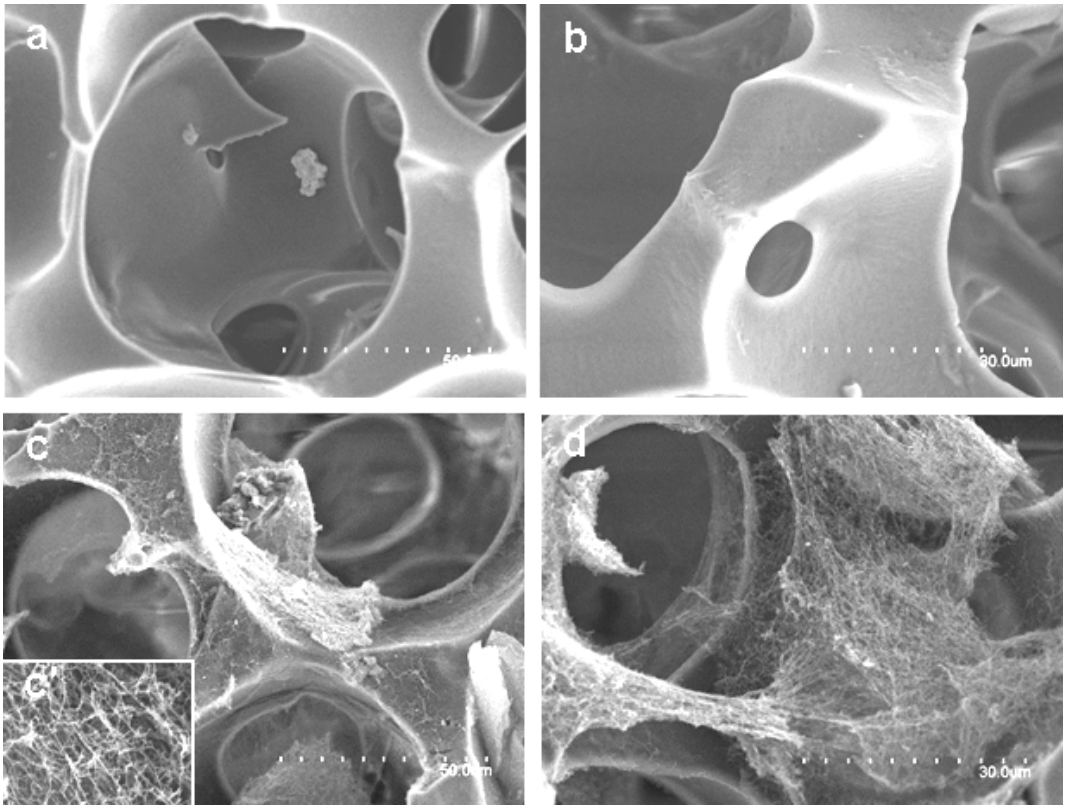

Figure 4.5-21: Assessment of PCLMA-composite formation. SEM images of bare (a, b) and RAD16-I filled PCLMA scaffolds (c, d). (c') Detail of RAD16-I nanofibers. Scale bare: (a, c), 50 µm and (b, d), 30 µm.

Figure 4.5-22a and b show the bare PCLMA porous and Figure 4.5-22c and d the elastomeric membrane filled with RAD16-I. The nanofiber of self-assembling peptide did not fill the microporous but remain on the surface of the trabeculae. Figure 4.5-22c' shows an amplification of the nanofiber structure. In this case, it seemed that RAD16-I self-assembling peptide nanofibers remained on the surface of the porous but did not fill them completely. To better analyze the deposition of RAD16-I self-assembling peptide, images from 30 µm to 500 nm were analyzed. In Figure 4.5-22a, it cannot be clearly observed the presence of self-assembling peptide, but Figure 4.5-22b shows a coarse surface. Subsequent amplifications (Figure 4.5-22c to d) demonstrated the presence of nanofibers deposited on the top of the wall pores. Herein, it could be concluded that RAD16-I peptide introduced inside the microporous of PCLMA scaffold do not provide a 3D environment filling completely the elastomeric membrane pores, but appeared to be deposited on the porous surface.

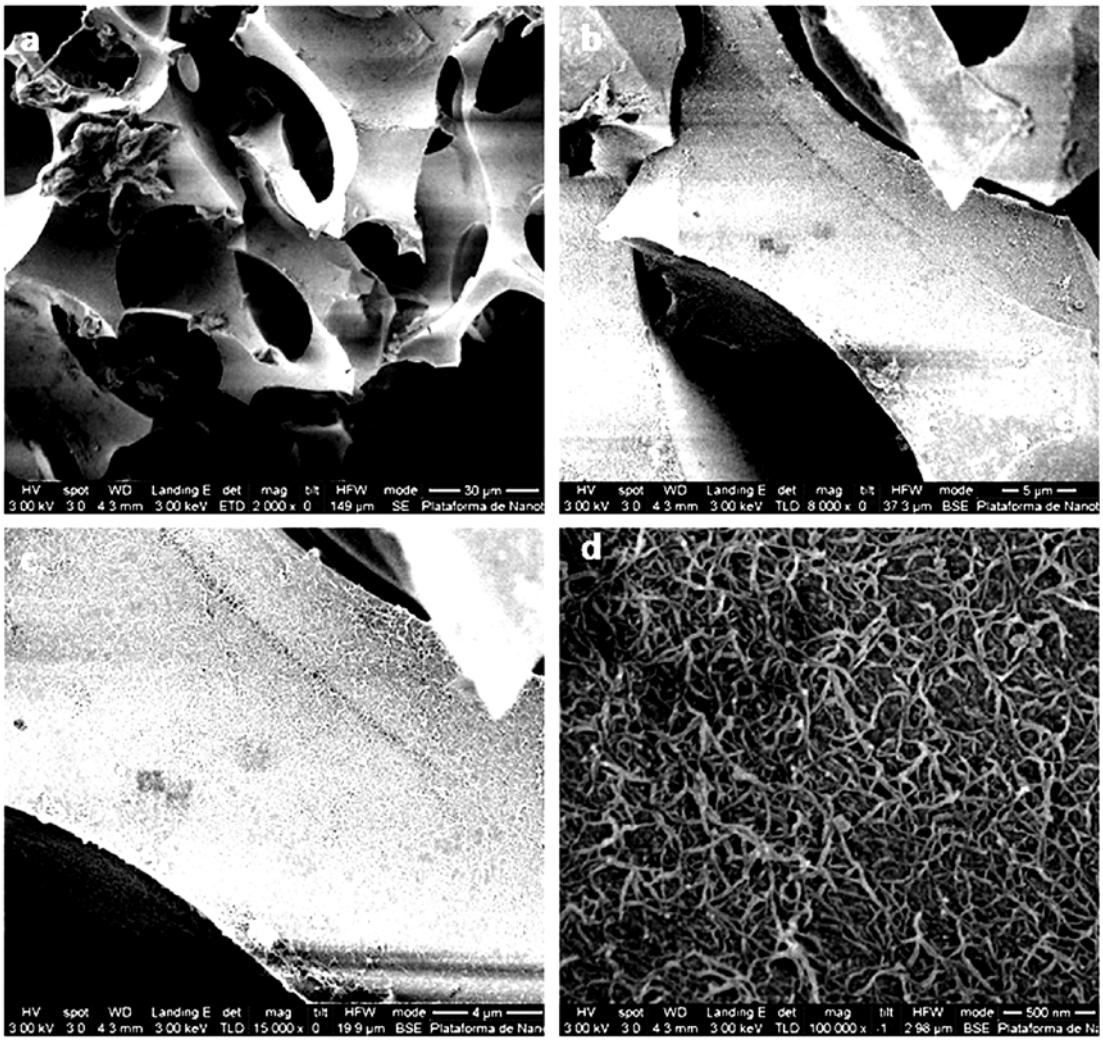

Figure 4.5-22: Analysis of RAD16-I self-assembling peptide deposition of PCLMA wall pores. The subsequent amplification of PCLMA filled with RAD16-I show the deposition of the self-assembling peptide on the elastomeric membrane surface (a) 2000X (b) 8000X (c) 15000X (d) 100000X

SubATDPCs layout in bare scaffolds or composites

For the examination of cell distribution in scaffolds, general cell staining with D&P was assessed after 7 days of culture. An uniform distribution of subATDPCs was observed for PCLMA-composite (Figure 4.5-23a and b). Additionally, the PCLMA-composite was also stained with Vimentin, a type III intermediate filament found in various non-epithelial cells, especially in MSC (Figure 4.5-23c and d). Vimentin is attached to the nucleus, endoplasmatic reticulum and mithocondria.

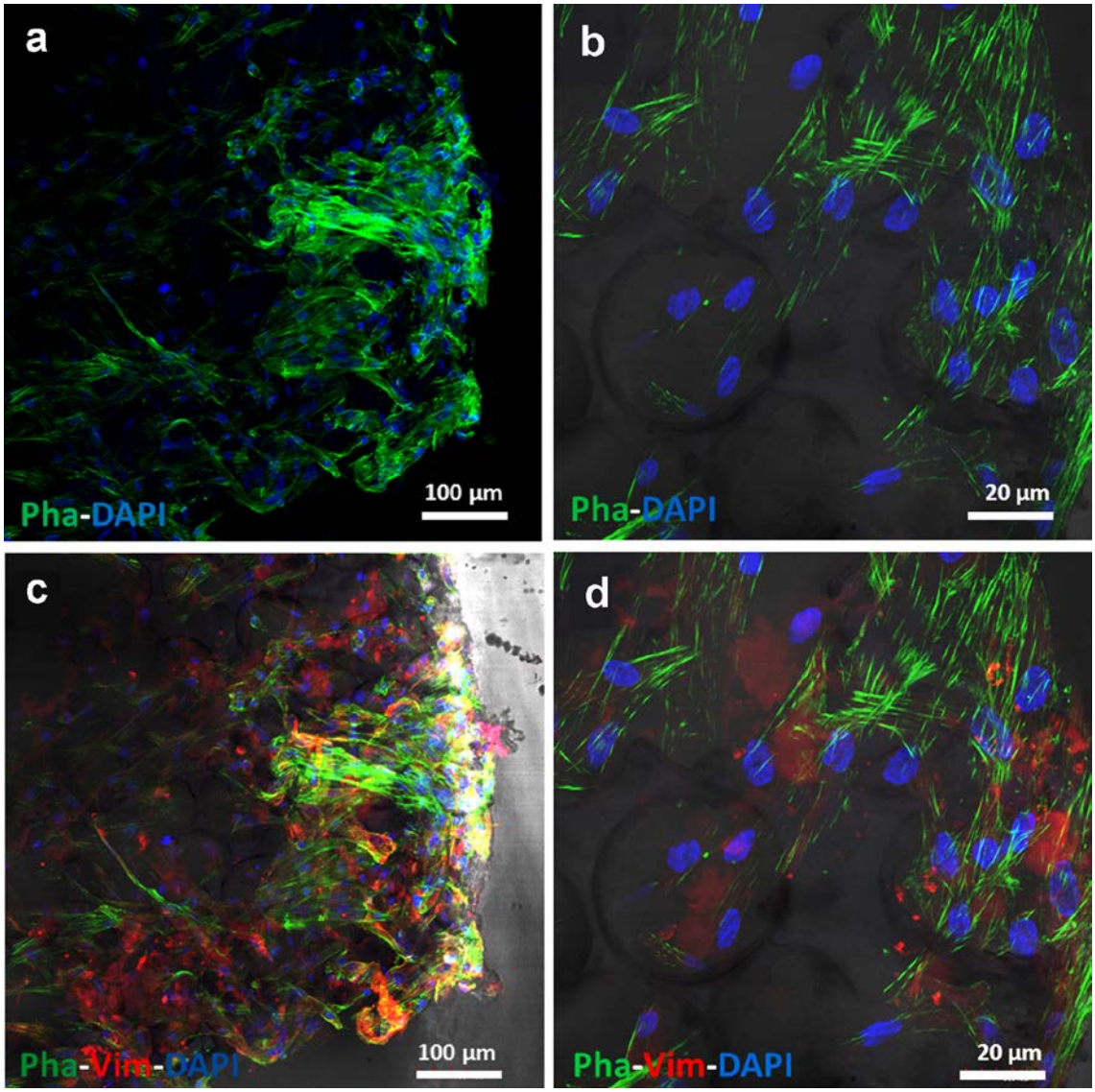

Figure 4.5-23: Surface confocal laser scanning microscopy images of PCLMA composites. (a, b) Phalloidin staining of subATDPCs growing inside PCLMA composite at different magnifications. (c, d) Phalloidin and Vimentin staining of subATDPCs growing in PCLMA composite at different magnifications. Scale bar (a, c) 100 µm and (b, d) 20 µm. Nuclei are counterstained with DAPI (blue).

Additionally, bare and composite PCLMA elastomeric scaffolds were analyzed by SEM imaging (Figure 4.5-24). As it occurred for PEA elastomeric membrane, a significant fraction of cells resided on the top of the scaffolds covering the surface. Again cell distribution depended

on the presence of RAD16-I self-assembling peptide. SubATDPCs growing in composites were uniformly distributed covering the surface after 7 days of culture entirely, whereas, on bare PCLMA scaffolds, a heterogeneous layout was observed. Therefore, although RAD16-I was not providing a 3D environment within PCLMA pores, it aids subATDPCs to grown in an ordered arrangement.

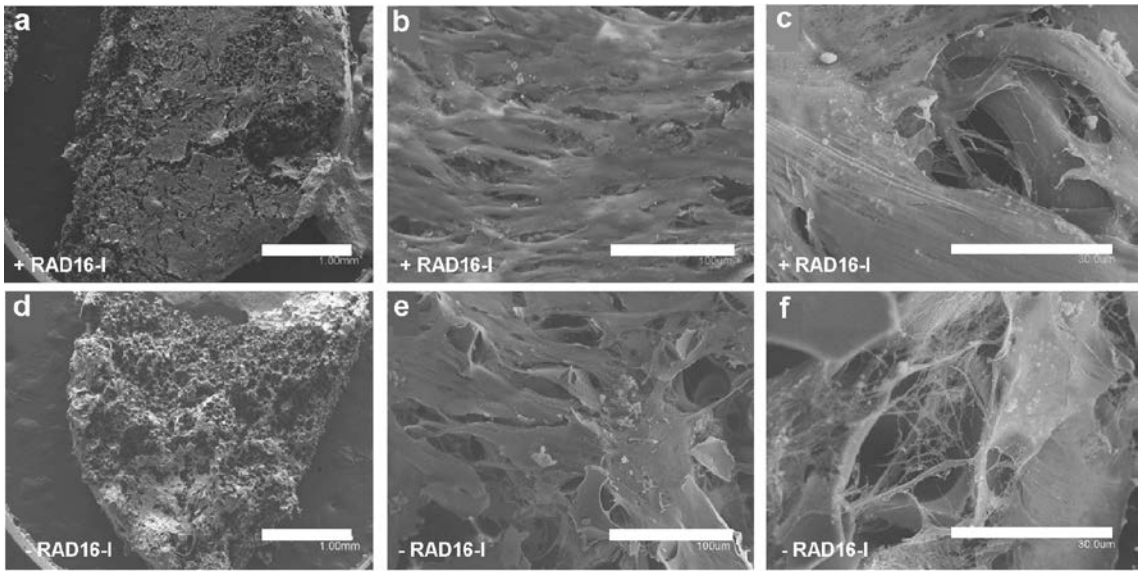

Figure 4.5-24: Cell morphology analysis on bare PCLMA or composite by SEM after 7 days of culture. Overview of composite (a) and bare PCLMA (d) seeded with subATDPCs. Close up of the surface of PCLMA composite (b and c) and the surface of PCLMA-composite seeded with subATDPCs (e and f). Scale bar represents 1 mm (a and d), 100 µm (b and e), 30 µm (c and f).

Viability, growth and distribution of subATDPCs inside PCLMA bare scaffolds or composites

SubATDPCs viability inside the PCLMA bare elastomer and the composite was monitored after 1 and 10 days of culture by MTT colorimetric assay (Figure 4.5-25). As revealed by the MTT test, there was no significant differences ($p > 0.05$) in cell viability between cells growing in bare PCLMA membrane and cells cultured in the composite containing the self-assembling peptide RAD16-I (Figure 4.5-25a). In addition, after 10 days of culture no significant increase on cell number could be observed. In this case, most part of subATDPCs remained inside the scaffolds instead of migrating outwards (Figure 4.5-25c). In contrast with PEA elastomeric membranes, the migration of subATDPCs in PCLMA membranes was much lower (about 22 % for PCLMA and more that 50 % for PEA elastomeric membrane). No significant difference could be observed after the addition of RAD16-I inside the elastomeric membrane pores. We hypothesize that this could be caused by the lack of a 3D nanofiber network filling the microporous of the PCLMA elastomeric membrane. At day 1 the cells adhered on the surface covering the trabeculae, but the lack of the diffusion media provided by the 3D nanofiber environment avoided their mobility outwards. We hypothesize that this lack of mobilization

caused an early fill of the elastomeric membrane surface which did not leave space for cell proliferation.

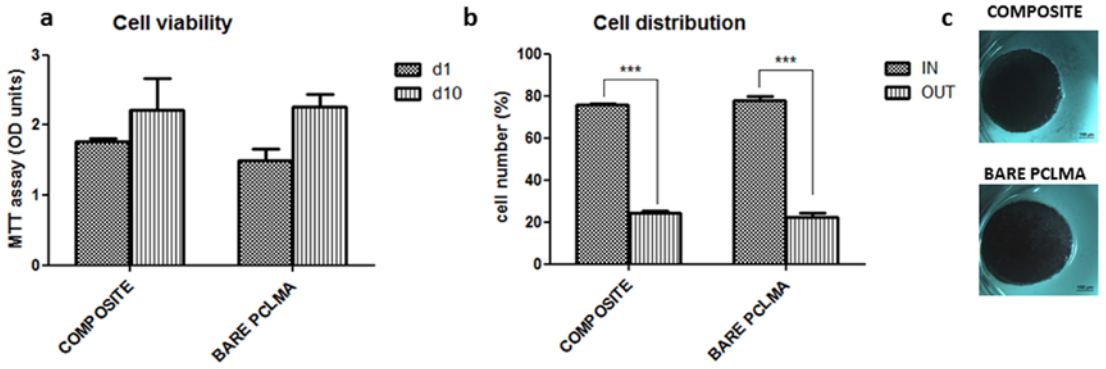

Figure 4.5-25: MTT viability assay of subATDPCs growing inside bare PCLMA scaffold and composite. (a) SubATDPCs proliferation from day 1 to day 10 inside the composite and bare PCLMA (b) Cell distribution inside the structures and on the culture plate at day 10 of culture. (c) Coloration of both structures owing to the formation of formazan crystals (*** $p < 0.001$).

Protein and gene expression of cells cultured in PCLMA bare scaffolds and composites

The characterization of subATDPCs growing in the scaffolds was conducted by protein and gene expression of early and definitive cardiac markers, using cells growing on 2D PCLMA surfaces as controls. The expression of early cardiac markers such as GATA4, TBX5, NKX2.5, and MEF2C; as well as some definitive cardiac markers such as ACTN1, cTnT and GJA1 were examined.

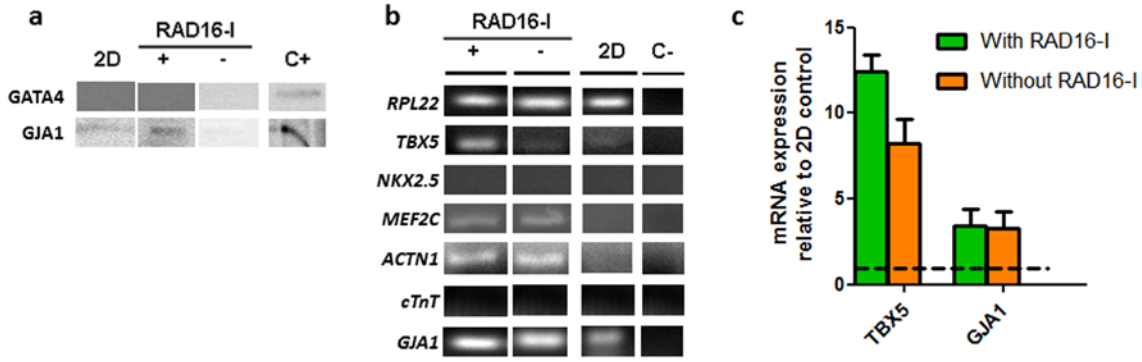

Figure 4.5-26: Protein and gene profile of cells cultured in bare PCLMA scaffolds and composites. *a) Western blotting.* Protein expression of cells cultured on 2D PCLMA compared to cells cultured in bare PCLMA scaffolds (RAD16-I -) and composites (RAD16-I +). C+ stands for the positive control for each protein. *b) RT-PCR.* Gene expression of cells cultured on 2D PCLMA compared to cells cultured in bare PCLMA scaffolds and composites. C- stands for the negative control used. *c) qRT-PCR.* The expression of *TBX5* and *GJA1* were assessed by Real Time RT-PCR experiments, establishing the base line through conventional monolayer cultures on PEA surfaces. No significant differences were observed between bare PEA and composites ($p > 0.05$).

The expression of early cardiac markers *TBX5* and *MEF2C* were detected at gene level (Figure 4.5-26b) in both bare PCLMA and composite structures. However *NKX2.5* was not detected in any condition. Real time qRT-PCR showed no significant ($p > 0.05$) difference on *TBX5* expression between subATDPCs cultured in bare PCLMA or in composites, but presented a 10-

fold up-regulation respect to 2D cultures (Figure 4.5-26c). Additionally, GATA4 was not detected at protein level (Figure 4.5-26a). The expression of *TBX5* and *MEF2C* has been reported to synergistically activate target genes expression in CMs and specifically *MEF2C* expression has been related with the expression of genes such as *ACTN1* and *MHC*[88–90]. In parallel, the evaluation of definitive cardiac markers showed expression of *ACTN1* and *GJA1* at gene level, but *cTnT* was not detected in this case (Figure 4.5-26b). Real time RT-PCR showed no significant ($p > 0.05$) difference on *GJA1* expression between subATDPCs cultured in bare PCLMA or in composites (Figure 4.5-26c). However, at protein level GJA1 was detected in composites but not in bare PCLMA (Figure 4.5-26a). This lead us to hypothesize that the presence of RAD16-I inside the pores of PCLMA elastomeric membranes improve cell interconnection, in agreement to what it was observed by cell distribution into the scaffolds (see Figure 4.5-25).

It is important to notice that experiments conducted with PEA and PCLMA elastomeric membranes used different subATDPCs pools (each pool was obtained from 5 different patients). This leads to different gene expression at 2D level, which means that only internal comparisons could be stated. However, in both cases it can be concluded that the combination of RAD16-I with this elastomeric membranes leads to the obtaining of a non-cardio-conductive biomaterial which is able to maintain the phenotype of the seeded cells.

4.5.6 *In vivo* studies

RECATABI European project combines the work of interdisciplinary groups of scientists as it has been stated. After *in vitro* work, more intensive *in vivo* studies were performed using small animal models (work developed by IGTP group in Badalona) and large animal models (work developed by Cardio-Monde group in Hôpital Européen Georges-Pompidou, Paris). Here some of the obtained results are reported.

Small animal models (mice)[vi]

In terms of performance, it was noticed that PEA elastomeric membrane was too rigid to be implanted in the small mice hearts, and long term studies were only performed using PCLMA elastomeric membranes with this animal model. In these experiments, it was sought to monitor cardiomyogenic lineage differentiation and the survival of subATDPCs.

[vi] Experiments performed by IGTP group and published in: Soler-botija C, *et. al*. 2014 Engineered 3D bioimplants using elastomeric scaffold, self-assembling peptide hydrogel, and adipose tissue-derived progenitor cells for cardiac regeneration *Am. J. Transl. Res.* **6** 291–301

The cells obtained from fat pads undergoing cardiac surgery were isolated (as explained in Materials and Methods) and double transduced to report the cell number (CVM-RLuc-RFP reporter) and to monitor cardiomyogenic lineage differentiation (hcTnIp-PLuc-eGFP reporter). These cells were used for the preparation of the bioactive implant with PCLMA elastomeric membrane as described in section 4.4.7. *"Cell seeding in elastomeric membrane/self-assembling peptide composites"* (see Figure 4.4-1). The bioimplant was placed onto the healthy or the infarcted myocardium of mice and non-invasive BLI imaging was used to monitor luciferase activity. A scheme of the whole procedure is presented in Figure 4.5-27.

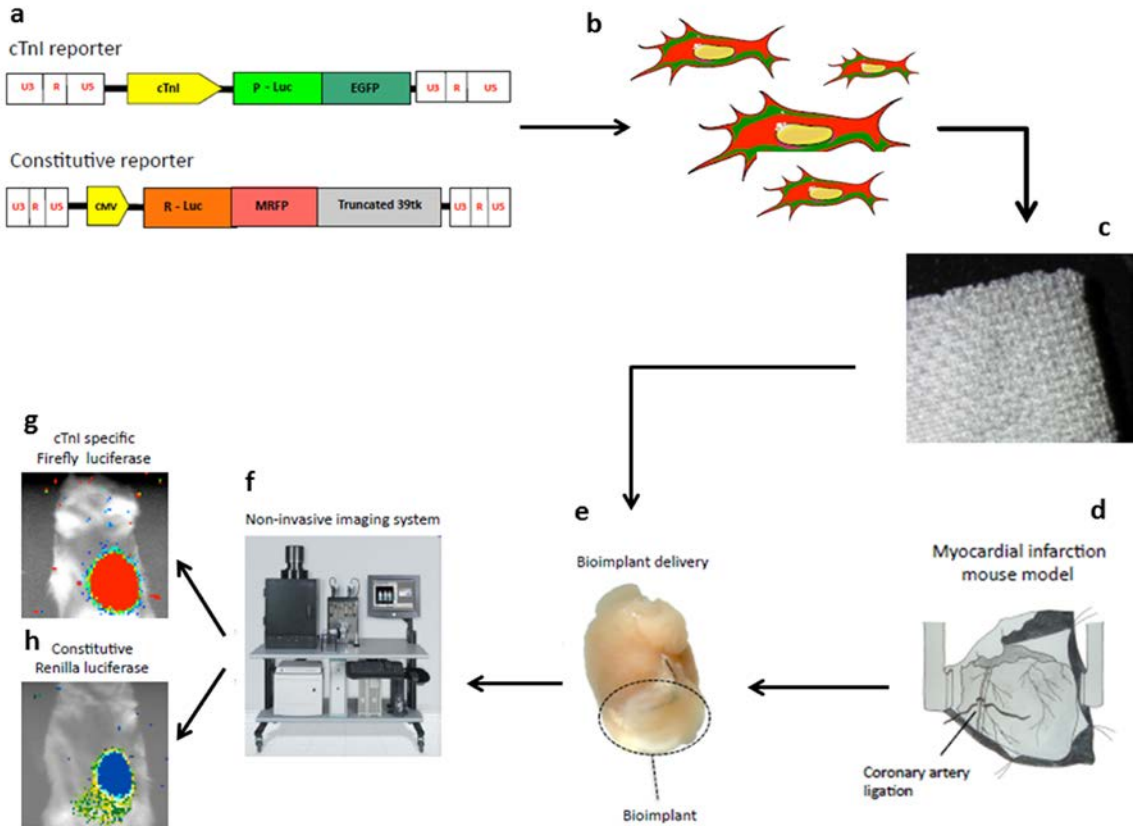

Figure 4.5-27: *In vivo* studies procedure used for small animal models. (a) Cells transduction with CMVp-RLuc-mRFP1 and hcTnIp-PLuc-eGFP lentiviral vector. Transduced cells (b) were introduced in PCLMA elastomeric membrane (c). (d) MI was induced using coronary artery ligation as previously described[78] and subsequently bioactive implants were implanted using surgical glue (Glubran®2). (f) Mice were monitored immediately after implantation and at 1, 2, and 3 weeks post-implantation by BLI. Fluorescence was also detected from the excised hearts immediately after sacrifice. Quantification and analysis of photons recorded and fluorescence in images were performed using non-invasive BLI imaging system. All animals were analysed for (g) cTnI specific firely luciferase and (g) constitutive Renilla luciferase expression (modified from Soler-Botija *et.al.*)[75].

A total of 25 female SCID mice (20-25 g; Charles River Laboratories, Inc.) were used for this study. The animals were randomly assigned to one of the following four groups: (1) bioimplant implantation (PCLMA+RAD16-I+subATDPCs) and no MI induction (the sham group, n=6), (2) MI induction and no bioimplant (the control- MI group, n=5), (3) MI induction and scaffold (PCLMA) implantation (the MI-scaffold group, n=5), and (4) MI induction and bioimplant implantation (the MI-bioimplant group, n=9)[75].

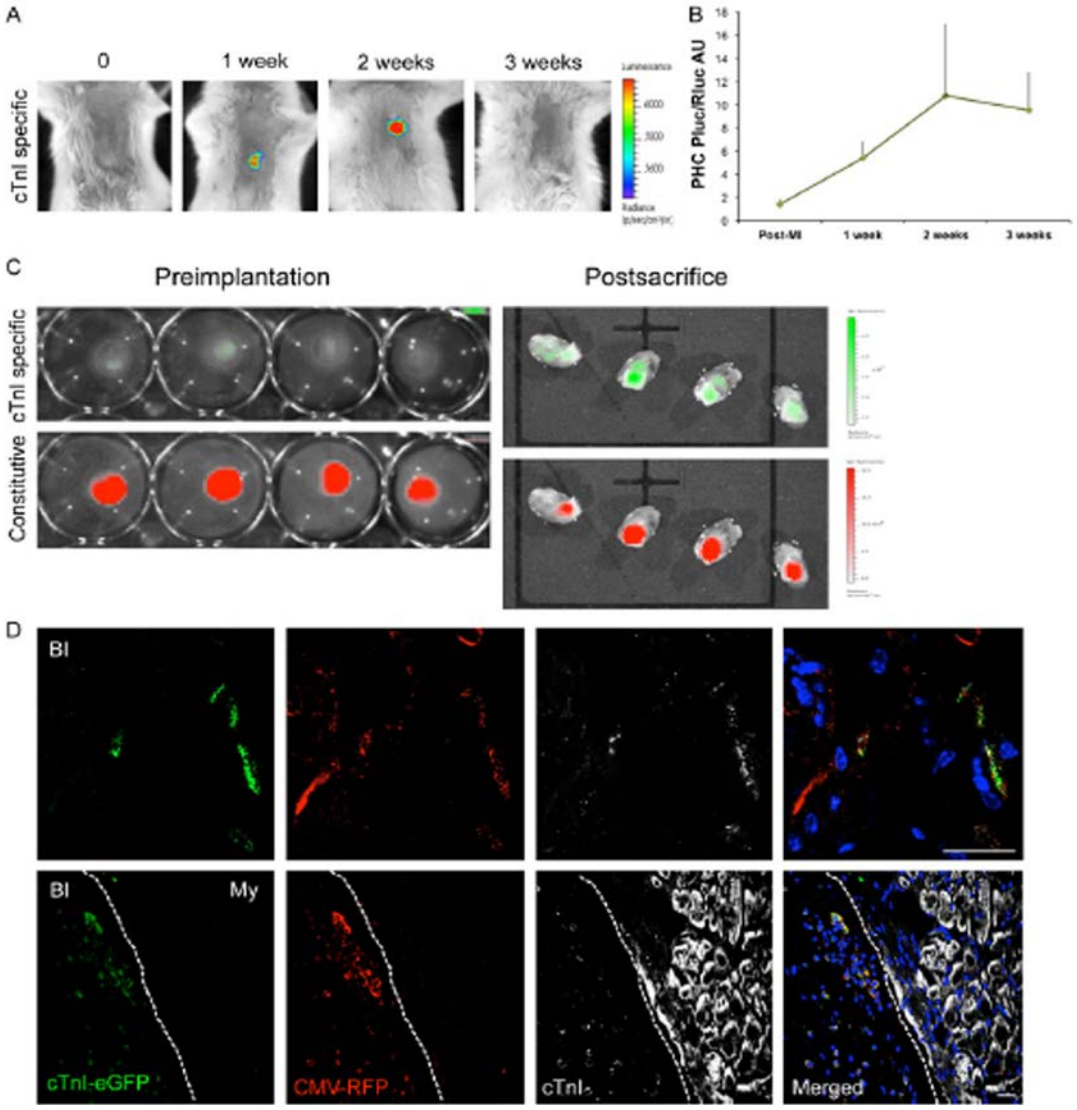

Figure 4.5-28: BLI and fluorescent evaluation of cTnI expression and survival of PCLMA bioactive implant placed over the mouse infarcted myocardium. A) Representative BLI of labeled subATDPCs within the bioactive implant displays the luciferase signal from the cell differentiation reporter (PLuc-eGFP) that is regulated by the hcTnI promoter. Images of the hcTnI-specific reporter are superimposed on black-and-white dorsal images of the recipient animal. Color bars illustrate relative light intensities from PLuc. B) Histograms of the PLuc/RLuc ratio calculated from photon fluxes recorded via BLI from bioactive implant-treated infarcted animals. C) Representative fluorescence images from subATDPCs within the bioactive implant pre-implantation and post-sacrifice over the excised hearts. Upper images show fluorescence from the cell differentiation reporter (PLuc-eGFP) regulated by hcTnIp (green). Bottom images are representative of constitutive fluorescence from the cell-number reporter (CMVp-RLuc-mRFP1; red). Color bars illustrate the relative fluorescence intensities from eGFP (green) and RFP (red). D) Immunofluorescence staining of mouse heart cross-sections shows the bioactive implant filled with human subATDPCs. Transplanted cells were detected via RFP immunostaining (red), and cTnI expression was detected with anti-eGFP (green) and anti-cTnI (white) antibodies. (BI, bioactive implant; My, myocardium). Scale bars, 20 μm Image obtained from Soler-Botija *et.al.*[75].

As it can be observed in Figure 4.5-28A and B, BLI photon counts revealed an increase in the ratio between hcTnIp-regulated PLuc and CMV-regulated RLuc activities in infarcted and sham-infarcted animals (data not shown). hcTnI was expressed *de novo* as early as one week post-implantation, with expression increasing up to 9-fold at 3 weeks. Interestingly, an important RFP signal was detected in excised hearts, indicating the retention and local presence of the implanted cells after sacrifice (Figure 4.5-28C). In concordance with BLI, GFP was also

detected, indicating hcTnI expression at the time of sacrifice. Comparisons of the GFP/RFP ratio pre-implantation and at sacrifice demonstrated a 16-fold increase in hcTnI expression.

Immunodetection of RFP in histological analyses of excised heart cross-sections revealed the presence of subATDPCs in the bioactive implant up to 4 weeks after implantation in all analyzed groups (Figure 4.5-28D). Additionally, to relate hcTnI gene and protein expression, immunostaining against hcTnI protein was performed in all cell-treated animals. RFP, GFP, and hcTnI proteins co-localized in implanted subATDPCs (Figure 4.5-28D), validating the BLI analysis and providing evidence of differentiation into the cardiac lineage. However, no implanted subATDPCs were observed in the myocardium of infarcted or sham-treated animals, indicating the absence of migration from the bioactive implant to the underlying heart[75]. This results correlate with the *in vitro* results obtained for the bioactive implant of PCLMA (Figure 4.5-25).

In terms of adaptability and vascularization of the bioimplant, macroscopic and histological observations of excised hearts and cross-sections demonstrated that the bioactive implants were perfectly adapted to the mouse myocardium covering the infarcted scar (Figure 4.5-29A and B).

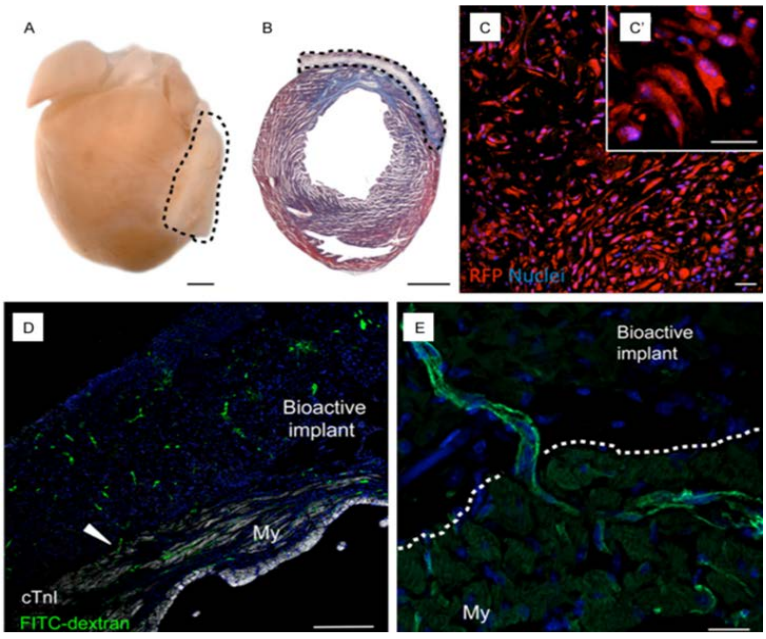

Figure 4.5-29: Adaptability and vascularization of PCLMA bioactive implant in the mouse model of MI. A) Representative image of a heart excised from a bioactive implant-treated animal. Dotted lines indicate localization of the implant. Scale bars, 1 mm. B) Masson's trichrome staining in a heart cross-section reveals the presence of a myocardial scar (blue) and the good adaptability of the bioactive implant. Scale bars, 1 mm. C) Cells inside the bioactive implant three days post-implantation were detected via the constitutively active reporter CMVp-RLuc-mRFP1 (red). C') Detail of the spindle-shape morphology of subATDPCs. Scale bars, 25 μm. D and E) Functional vessel detection with FITC-dextran (green) in mice treated with subATDPCs. Arrowheads indicate a vessel connection between the mouse myocardium and the bioactive implant in a cell-treated animal. Nuclei were counterstained with Hoechst 33342. Scale bars, 20 μm and 250 μm. Image obtained from Soler-Botija *et.al*[75].

Moreover, RFP-expressing subATDPCs were seen inside the bioactive implant and displayed the same spindle-shaped morphology observed in culture (Figure 4.5-29C and 2C'). All these

results suggested that the PCLMA elastomeric membrane confers a suitable environment for subATDPCs survival.

In parallel, it was determined whether functional vessel connections were established between the bioactive implant and the myocardium. Animals received Fluorescein isothiocyanate–dextran (FITC-dextran) through the tail vein prior to sacrifice, and it was observed that the bioactive implant was fully vascularized in all cases. Even animal controls that did not receive cell transplants showed vessel connection to the circulatory system (Figure 4.5-29D, arrowhead) and were functional (Figure 4.5-29D and 2E).

Large animal models (sheep)[92]

In parallel, experiments using large animal models were carried out by Cardio-Monde group. Specifically, sheep models, which are physiologically and biomechanically more similar to humans, were used to obtain more predictive analysis for future human use. In this model, both PEA and PCLMA elastomeric membranes were tested.

In this part of the work autologous cells were used to prepare the bioactive implants. Samples were collected from mediastinal adipose tissue undergoing myocardial infarct surgery. The samples collected were sent to IGTP group, who was responsible of cells isolation and expansion under standard conditions. The cells were labeled with fluorescent reporters as explained in the section 4.4.13, and expanded. UPV and IQS group were responsible of bioactive implants preparation before surgery. The elastomeric membranes used in this case measured 45x45 mm. After loading with the self-assembling peptide and cells, the bioactive implant was maintained under standard conditions (37 °C in 5 % CO_2 humidified atmosphere) for 24 hours. The obtained bioactive implant was placed onto the left ventricular surfaces, and the infarct regions were mostly covered. Afterwards, the pericardial sac was closed using interrupted biodegradable sutures. The animals were divided into three groups: (1) 5 animals non-treated, (2) 5 animals with a bioactive implant consisted in PEA composite, and (3) 5 animals with a bioactive implant consisted in PCLMA composite.

LV function and dimensions were measured the day that myocardial infarction was induced and 2 and 6 months post-infarction, respectively. At baseline and after infarction, the mean LV Diastolic Volume (DV) and Ejection Fraction (EF) were similar in all three groups. Over the course of 6 months, each group increased their LV end diastolic dimension compared with their baseline value. A statistically significant attenuation of LV dilation was demonstrated with the implantation of the bioactive implant (both PEA and PCLMA) compared with the non-treated control group. Functional results at 6 months showed greater benefits in the hearts treated with PCLMA bioactive implant compared with those receiving PEA bioactive implant or without

treatment. Diastolic function was improved in the PCLMA group but not in the other groups. Additionally, histopathology shows that the necrotic areas were much less prominent, mainly in the group treated with PCLMA bioimplants. Fluorescent marked cells were founded into the bioactive implant and infarct scars as well as focuses of angiogenesis (capillary network). These preliminary findings seemed to indicate that ADPSCs growing in bioactive implants and migrating to the nearby cardiac tissue could be involved in the regenerative process, promoting angiogenesis and possibly cardiomyogenesis. Furthermore, at the level of the epicardium we found minimal fibrosis interface without inflammation between both bioactive implants and the heart surface. The PCLMA bioactive implant was completely anchored and integrated to the nearest infarct area and the myocardium. In contrast, the PEA bioactive implants showed poor adhesions to the heart and the infarct scar.

In conclusion, these results demonstrated that these bioactive implants improved systolic and diastolic functions, reducing adverse cardiac dilatation in large animal models that better mimic human systems. Better results were obtained using semidegradable materials and, interestingly, no inflammatory reaction was observed after long-term implantation for any of the bioactive implants.

4.6 CONCLUDING REMARKS

The first steps or MI treatments are directed to recover blood flow. Once this goal is achieved, it is possible to focus all the efforts on mitigating the collateral problems arising from lack of blood supply. Necrotic tissue formed after MI is not static as it continues progressing through the healthy tissue and contributing to progressive ventricular dilatation. Therefore, due to continuous CM death, ECM degradation, and myocardial fibrosis it is increasingly difficult to repair the myocardial scar to obtain again a functional tissue. A spectrum of surgical procedures, cardiac resynchronization therapy (biventricular pacing), or pharmacologic therapy (e.g. angiotensin-converting enzyme inhibitors and beta-blockers) have been applied in the clinical setting in an effort to limit adverse LV remodeling. Surgical approaches include ventricular restoration with left ventricular reconstitutive surgery (Dor procedure) or ventricular wrapping with an epicardial patch[6]. However, a definitive solution that faces LV remodeling and CM death has not yet been found. The association of stem cells (1) with tissue-engineered scaffolds (2) constitutes an attractive approach. The first component is hoped to help to improve tissue functionality, while the second one could avoid ventricular chamber dilatation, which changes from a natural elliptical to spherical shape in heart failure patients.

The challenge to find an efficient regenerative therapy for heart function recovery after MI resides in the vast complexity of the heart muscle, where different factors at macroscopic and microscopic level such as heart contraction and cell connectivity must be taken into account to repair the damaged tissue. Although cell therapy appeared as an interesting approach, the environmental conditions that remain after MI are not suitable for cell survival and proliferation. For this reason, the design and fabrication of biomaterials to be used as vehicles or even to give specific signaling to the cells are of great interest. These materials must be (1) easy handling and cell-friendly, (2) reproduce heart ECM, (3) have sufficient mechanical stability and high porosity to lodge a high cell density, and (4) do not produce an inflammatory response *in vivo*. Numerous polymers (natural and synthetic) have been widely investigated for CTE, shaped in a variety of architectures[57,93,94]. These structures act as physical support for the seeded cells, allowing the exchange of oxygen and nutrients and removal of cellular secretions, to facilitate cell adhesion, survival, proliferation and differentiation[9]. On the other end, nanofibers in the form of self-assembling peptides emerged as a good system to better recreate a 3D environment[95]. 3D structures are essential for an appropriate spatial organization of cell surface receptors involved in cell–cell and cell-ECM interactions[96]. Here, a combination of elastomeric membranes with RAD16-I self-assembling peptide is proposed and analyzed. Elastomeric membranes fulfill many of the essential characteristics prescribed for necrotic myocardium repair, but fail to emulate the cardiac tissue at the nano-scale. The peptide gel network provided by RAD16-I resembles ECM environment and has been shown to increase growth and cellular

proliferation of different cell types. However, the RAD16-I poor mechanical properties are an important drawback for its implantation in the continuous beating heart[97]. Therefore, the combination of RAD16-I soft material with synthetic polymeric materials with improved elasticity and tensile strength (both PEA and PCLMA elastomeric membranes) arise as an interesting approach. Both materials would contribute to the implant success at different levels: the elastomeric membrane would be responsible for providing an adequate physical support, whereas the synthetic gel would confer an *in vivo-like* environment to the cells.

First of all, as the cells are the active component of the bioimplant it is critical to culture as many cells as possible in the composite. It has been reported that at least one billion cells are needed to be replaced in patients with heart failure[3]. Therefore, the seeding efficiency of the bioimplant was intended to be improved for further *in vivo* implantation.

After setting the two-step protocol, subATDPCs viability, growth, mobilization and progenitor phenotype maintenance in elastomeric membranes filled with peptide gel (composites) was assessed *in vitro*. The bioactive bioactive implants (both PEA and PCLMA) developed presents a good advantage as a cell vehicle for cell therapies. PEA bioactive implant has been demonstrated to allow cell proliferation to a five-fold increase after 10 days of *in vitro* culture ($p < 0.001$). However, PCLMA bioactive implant did not presented a significant increase in cell number. Additionally, it was observed a migration of subATDPCs outwards PEA elastomeric membrane (both bare and composite) but not outwards PCLMA elastomeric membrane (both bare and composite). We attribute this result to the self-assembling peptide distribution inside the microporous structure. Inside PEA scaffold the gel works as cell diffusion medium, facilitating the invasibility of the scaffold's pores upon seeding and after 10 days both the polymeric surface and the inner trabeculae were covered with cells[98]. However, inside PCLMA scaffold the nanofibers cover the trabecular structure attaching the cells on the surface. The main advantaged of the composite resides in the capacity of promoting cell mobilization outwards, which could facilitate cell grafting at the affected site. Specific to cell proliferation and migration, PEA-composite may present better properties to be used as a cell vehicle as compared to PCLMA-composite.

In other terms within the composites (for both PEA and PCLMA elastomeric membranes), subATDPCs completely covered the surface of the scaffolds and adopted an elongated shape, contacting one to each other. However, in bare scaffolds, cells remained adhered on the trabeculae and arranged forming circumferences, rather than occupying the 'empty' pores.

SubATDPCs (MSC-like) were used in this work due to their cardiogenic potential lineage. It was the primary aim to ensure that these cells in the proposed biomaterials (bare elastomeric

membrane or the composite) did not alter their gene expression. As it has been described in Materials and Methods section, the cells used for these experiments were prepared as pools of cells from 5 different patients. Therefore, it was expected slight difference in the genes analyzed depending on the pool used. For this reason, each experiment was compared with the same pool of cells growing in flat surfaces. It has been shown that subATDPCs preserved their cardiogenic potential lineage by the expression of early cardiac markers such as *TBX5* and *MEF2C* or definitive markers such as *ACTN1* and *cTnT* in PEA elastomeric membranes or *ACTN1* and *GJA1* in PCLMA elastomeric membranes. No significant differences in gene or protein expression between the cells cultured in composites, bare scaffolds and controls were observed. TBX5 early cardiac marker is critical in heart development, and it has been reported to regulate the activity of other genes by attaching to specific regions of DNA[88]. It has also been shown to interact with NKX2.5, GATA4 and MEF2C to synergistically activate target genes expression in CMs[88]. MEF2C expression, which plays a key role in myogenesis, has been related with the expression of genes such as *ACTN1* and *MHC.* In terms of definitive cardiac markers, ACTN1 is a marker of mature CM that helps to anchor the myofibrillar actin filaments. It is the major component of the contractile apparatus[99]. Interestingly, cTnT, a constituent of the troponin complex, which connects the troponin complex to tropomyosin regulating muscle contraction in response to alteration in intercellular calcium concentration, was detected in PEA elastomeric membranes. This complex controls the calcium mediated interaction between actin and myosin. In contrast with other multigene families, the skeletal and cardiac proteins of this complex are not derived from alternative splicing of exons from a single gene[100]. Therefore, they have, theoretically, the potential of being unique to the myocardium. This gene was not expressed in the pool of cells cultured in PCLMA elastomeric membranes, but GJA1 was detected at gene and protein level. This protein is the major gap junction in the heart and has a crucial role in synchronic contraction. Although these results are not conclusive to resolve a differentiation toward a cardiac phenotype, we observed that subATDPCs maintain their phenotype after 10 days of culture in both PEA and PCLMA with and without RAD16-I. Therefore, we think that neither of these biomaterials are cardio-conductive, but are able to preserve cell potentiality, which could facilitate their lineage commitment once implanted. Further analysis at longer time points and using different kind of induction (chemical or physical) would be interesting to elucidate possible cardiac differentiation at more definitive stages.

In conclusion, the proposed elastomeric scaffolds, with or without RAD16-I gel in the pores, are a non-inductive milieu where subATDPCs can survive, grow and mobilize after implantation at the ischemic tissue.

4.7 FURTHER STEPS

This chapter analyzes the behavior of subATDPCs cultured in elastomeric membranes pre-filled with RAD16-I self-assembling peptide, which aims to provide a more realistic 3D environment within the microporous of PEA or PCLMA elastomeric membranes. We consider that it is only the beginning of the *in vitro* studies for this kind of bioactive implants. A part of the more basic studies for the *in vivo* implantation, the subsequent *in vitro* assays could be interesting to better characterize the proposed concept:

- Propose a set up to electrically stimulate the bioactive implant.
- Propose a set up to mechanically stimulate the bioactive implant.
- Analyze cell behavior with chemical, electrical and mechanical stimulation alone or in combination.
- Test the effect in *in vivo* models of the developed platform using RAD16-I with the modifications proposed in Chapter 2.

All these studies could help to understand the response that the implanted cells would have *in vivo* after their implantation in an ischemic tissue. The obtained results could help to improve the bioactive implants performance.

4.8 BIBLIOGRAPHY

1. Chachques, J. C. Development of bioartificial myocardium using stem cells and nanobiotechnology templates. *Cardiol. Res. Pract.* **2011,** 806795 (2010).

2. Chachques, J. C., Pradas, M. M., Bayes-Genis, A. & Semino, C. Creating the bioartificial myocardium for cardiac repair: challenges and clinical targets. *Expert Rev. Cardiovasc. Ther.* **11,** 1701–11 (2013).

3. Ravichandran, R., Venugopal, J. R., Sundarrajan, S., Mukherjee, S. & Ramakrishna, S. Cardiogenic differentiation of mesenchymal stem cells on elastomeric poly (glycerol sebacate)/collagen core/shell fibers. *World J. Cardiol.* **5,** 28–41 (2013).

4. Giraud, M.-N., Guex, A. G. & Tevaearai, H. T. Cell therapies for heart function recovery: focus on myocardial tissue engineering and nanotechnologies. *Cardiol. Res. Pract.* **2012,** 971614 (2012).

5. Karikkineth, B. C. & Zimmermann, W.-H. Myocardial tissue engineering and heart muscle repair. *Curr. Pharm. Biotechnol.* **14,** 4–11 (2013).

6. Hashizume, R. *et al.* Biodegradable elastic patch plasty ameliorates left ventricular adverse remodeling after ischemia-reperfusion injury: a preclinical study of a porous polyurethane material in a porcine model. *J. Thorac. Cardiovasc. Surg.* **146,** 391–9.e1 (2013).

7. Christman, K. L. & Lee, R. J. Biomaterials for the treatment of myocardial infarction. *J. Am. Coll. Cardiol.* **48,** 907–13 (2006).

8. Soler-Botija, C., Bagó, J. R. & Bayes-Genis, A. A bird's-eye view of cell therapy and tissue engineering for cardiac regeneration. *Ann. N. Y. Acad. Sci.* **1254,** 57–65 (2012).

9. Castells-Sala, C. & Semino, C. E. Biomaterials for stem cell culture and seeding for the generation and delivery of cardiac myocytes. *Curr. Opin. Organ Transplant.* **17,** 681–7 (2012).

10. Albanna, M. Z., Bou-Akl, T. H., Walters, H. L. & Matthew, H. W. T. Improving the mechanical properties of chitosan-based heart valve scaffolds using chitosan fibers. *J. Mech. Behav. Biomed. Mater.* **5,** 171–80 (2012).

11. Liu, J. *et al.* Generation, Characterization and Potential Therapeutic Applications of Cardiomyocytes from Various Stem Cells. *Stem Cells Dev.* **21,** 2095–110 (2012).

12. Zammaretti, P. & Jaconi, M. Cardiac tissue engineering: regeneration of the wounded heart. *Curr. Opin. Biotechnol.* **15,** 430–4 (2004).

13. Chen, Q.-Z., Harding, S. S., Ali, N. N., Lyon, A. R. & Boccaccini, A. R. Biomaterials in cardiac tissue engineering: ten years of research survey. *Mater. Sci. Eng.* **59,** 1–37 (2008).

14. Liu, Z. *et al.* The influence of chitosan hydrogel on stem cell engraftment, survival and homing in the ischemic myocardial microenvironment. *Biomaterials* **33,** 3093–106 (2012).

15. Reis, L. a *et al.* A peptide-modified chitosan-collagen hydrogel for cardiac cell culture and delivery. *Acta Biomater.* **8,** 1022–36 (2012).

16. Bishop, J. E. & Laurent, G. J. Collagen turnover and its regulation in the normal and hypertrophying heart. *Eur. Heart J.* **16 Suppl C,** 38–44 (1995).

17. Hadjipanayi, E., Mudera, V. & Brown, R. A. Close dependence of fibroblast proliferation on collagen scaffold matrix stiffness. *Tissue Eng.* 77–84 (2009).

18. Miyagi, Y. *et al.* Biodegradable collagen patch with covalently immobilized VEGF for myocardial repair. *Biomaterials* **32,** 1280–90 (2011).

19. Cortes-Morichetti, M. *et al.* Association between a cell-seeded collagen matrix and cellular cardiomyoplasty for myocardial support and regeneration. *Tissue Eng.* **13,** 2681–7 (2007).

20. Chimenti, I. *et al.* Relative roles of direct regeneration versus paracrine effects of human cardiosphere-derived cells transplanted into infarcted mice. *Circ. Res.* **106,** 971–80 (2010).

21. Cheng, K. *et al.* Functional performance of human cardiosphere-derived cells delivered in an in situ polymerizable hyaluronan-gelatin hydrogel. *Biomaterials* **33,** 5317–5324 (2012).

22. Minato, A., Ise, H., Goto, M. & Akaike, T. Cardiac differentiation of embryonic stem cells by substrate immobilization of insulin-like growth factor binding protein 4 with elastin-like polypeptides. *Biomaterials* **33,** 515–23 (2012).

23. Heydarkhan-Hagvall, S. *et al.* The effect of vitronectin on the differentiation of embryonic stem cells in a 3D culture system. *Biomaterials* **33,** 2032–40 (2012).

24. Liau, B., Christoforou, N., Leong, K. W. & Bursac, N. Pluripotent stem cell-derived cardiac tissue patch with advanced structure and function. *Biomaterials* **32,** 9180–7 (2011).

25. Patra, C. *et al.* Silk protein fibroin from Antheraea mylitta for cardiac tissue engineering. *Biomaterials* **33,** 2673–80 (2012).

26. Haneef, K. *et al.* Development of bioartificial myocardium by electrostimulation of 3D collagen scaffolds seeded with stem cells. *Heart Int.* **7,** e14 (2012).

27. Fernandes, S., Kuklok, S., McGonigle, J., Reinecke, H. & Murry, C. E. Synthetic matrices to serve as niches for muscle cell transplantation. *Cells. Tissues. Organs* **195,** 48–59 (2012).

28. Prabhakaran, M. P., Nair, a S., Kai, D. & Ramakrishna, S. Electrospun composite scaffolds containing poly(octanediol-co-citrate) for cardiac tissue engineering. *Biopolymers* **97,** 529–38 (2012).

29. El Fray, M. & Czugala, M. Polish artificial heart program. *Wiley Interdiscip. Rev. Nanomed. Nanobiotechnol.* **4,** 322–8 (2012).

30. Huang, C.-C. *et al.* Injectable PLGA porous beads cellularized by hAFSCs for cellular cardiomyoplasty. *Biomaterials* **33,** 4069–77 (2012).

31. Dvir, T. *et al.* Nanowired three dimensional cardiac patches. *Nat. Nanotechnol.* **6,** 720–725 (2012).

32. Venugopal, J. R. *et al.* Biomaterial strategies for alleviation of myocardial infarction. *J. R. Soc. Interface* **9,** 1–19 (2012).

33. Ikonen, L. *et al.* 2D and 3D Self-Assembling Nanofiber Hydrogels for Cardiomyocyte Culture. *Biomed Res. Int.* 12 (2013).

34. Castells-Sala, C. *et al.* Current Applications of Tissue Engineering in Biomedicine. *Biochips and Tissue Chips* 0–14 (2013).

35. Gnanaprakasam Thankam, F., Muthu, J., Sankar, V. & Kozhiparambil Gopal, R. Growth and survival of cells in biosynthetic poly vinyl alcohol-alginate IPN hydrogels for cardiac applications. *Colloids Surf. B. Biointerfaces* **107,** 137–45 (2013).

36. Jung, J. P., Squirrell, J. M., Lyons, G. E., Eliceiri, K. W. & Ogle, B. M. Imaging cardiac extracellular matrices: a blueprint for regeneration. *Trends Biotechnol.* **30,** 233–240 (2011).

37. Smith, A. W. *et al.* Long-term culture of HL-1 cardiomyocytes in modular poly(ethylene glycol) microsphere-based scaffolds crosslinked in the phase-separated state. *Acta Biomater.* **8,** 31–40 (2012).

38. RECATABI PROJECT (Regeneration of Cardiac Tissue Assisted by Bioactive Implants), financially supported by the 7th Framework Programme (FP7) of the European Commission. *www.expert-reviews.com* www.recatabi.com/ (2010).

39. Carlos Semino *et al.* Bioactive implants and method for myocardial regeneration, ventricular support and elliptical shape restoration. (2013).

40. Arnal-Pastor, M., Chachques, J. C., Monleón Pradas, M. & Vallés-Lluch, A. in *Regen. Med. Tissue Eng.* (Andrades, A.) 275–303 (2013).

41. Zhang, S., Ellis-behnke, R. & Zhao, X. *Scaffolding in Tissue Engineering. CHAPTER 15: PuraMatrix : Self-assembling Peptide Nanofiber Scaffolds*. 217–248 (2006).

42. Vallés-Lluch, A. *et al.* Combining self-assembling peptide gels with three-dimensional elastomer scaffolds. *Acta Biomater.* **9,** 9451–9460 (2013).

43. Demirbag, B., Huri, P. Y., Kose, G. T., Buyuksungur, A. & Hasirci, V. Advanced cell therapies with and without scaffolds. *Biotechnol. J.* **6,** 1437–53 (2011).

44. European Commision, C. D. Advanced Therapies, European Commission. (2014). at <http://ec.europa.eu/health/human-use/advanced-therapies/index_en.htm>

45. Science Medicine Health, E. M. A. European Medicines Agency - Advanced therapies - EU. (2014). at <http://www.ema.europa.eu/ema/index.jsp?curl=pages/home/Home_Page.jsp&mid=>

46. Cuende, N. & Izeta, A. Clinical Translation of Stem Cell Therapies: a bridgeable gap. *Cell Stem Cell* **6,** 508–12 (2010).

47. Doppler, S. a, Deutsch, M.-A., Lange, R. & Krane, M. Cardiac regeneration: current therapies-future concepts. *J. Thorac. Dis.* **5,** 683–97 (2013).

48. Abdelli, L. S., Merino, H., Rocher, C. M. & Singla, D. K. Cell therapy in the heart. *Can. J. Physiol. Pharmacol.* **315,** 307–315 (2012).

49. Hoover-Plow, J. & Gong, Y. Challenges for heart disease stem cell therapy. *Vasc. Health Risk Manag.* **8,** 99–113 (2012).

50. Oldroyd, K. G., Berry, C. & Bartunek, J. Myocardial repair and regeneration: bone marrow or cardiac stem cells? *Mol. Ther.* **20,** 1102–5 (2012).

51. Chachques, J. C. *et al.* Myocardial Assistance by Grafting a New Bioartificial Upgraded Myocardium (MAGNUM trial): clinical feasibility study. *Ann. Thorac. Surg.* **85,** 901–8 (2008).

52. Jawad, H., Lyon, A. R., Harding, S. E., Ali, N. N. & Boccaccini, A. R. Myocardial tissue engineering. *Br. Med. Bull.* **87,** 31–47 (2008).

53. Stamm, C., Nasseri, B., Choi, Y.-H. & Hetzer, R. Cell therapy for heart disease: great expectations, as yet unmet. *Heart. Lung Circ.* **18,** 245–56 (2009).

54. Chachques, J. C. *et al.* Cellular cardiomyoplasty: clinical application. *Ann. Thorac. Surg.* **77,** 1121–30 (2004).

55. Genovese, J. A. *et al.* Cell Based Approaches for Myocardial Regeneration and Artificial Myocardium. *Curr. Stem Cell Res. Ther.* **7,** 121–127 (2007).

56. Patel, A. N. & Genovese, J. A. Stem cell therapy for the treatment of heart failure. *Curr. Opin. Cardiol.* **22,** 464–70 (2007).

57. Prabhakaran, M., Venugopal, J., Kai, D. & Ramakrishna, S. Biomimetic material strategies for cardiac tissue engineering. *Mat Sci Eng C* **31,** 503e13 (2011).

58. Krishnan, G. R., Hill, M. J. & Sarkar, D. *Tissue and Organ Regeneration: Advances in Micro- and Nanotechnology CHAPTER 7: Degradable Elastomers for Tissue Regeneration*. 231–264 (CRC Press, 2014). at <http://books.google.com/books?hl=en&lr=&id=fs6SAwAAQBAJ&pgis=1>

59. Pérez Olmedilla, M. *et al.* Response of human chondrocytes to a non-uniform distribution of hydrophilic domains on poly (ethyl acrylate-co-hydroxyethyl methacrylate) copolymers. *Biomaterials* **27,** 1003–12 (2006).

60. Campillo-Fernandez, A. J. *et al.* Future design of a new keratoprosthesis. Physical and biological analysis of polymeric substrates for epithelial cell growth. *Biomacromolecules* **8,** 2429–36 (2007).

61. Campillo-Fernández, A. J. *et al.* Analysis of the biological response of endothelial and fibroblast cells cultured on synthetic scaffolds with various hydrophilic/hydrophobic ratios: influence of fibronectin adsorption and conformation. *Tissue Eng. Part A* **15,** 1331–41 (2009).

62. Soria, M. *et al.* Survival and differentiation of embryonic neural explants on different biomaterials. *J Biomed Mater Res Part A* **79,** 495–502 (2006).

63. Martínez Ramos, C. *et al.* Channeled scaffolds implanted in adult rat brain. *J. Biomed. Mater. Res. A* **100,** 3276–86 (2012).

64. Rico, P., Rodríguez Hernández, J. C., Moratal, D., Monleón Pradas, M. & Salmerón-Sánchez, M. Substrate-induced assembly of fibronectin into networks. Influence of surface chemistry and effect on osteoblast adhesion. *Tissue Eng Part A* **15,** 3271–3281 (2009).

65. Soria, J. M. *et al.* Biomaterials coated by dental pulp cells as substrate for neural stem cell differentiation. *J Biomed Mater Res* **97,** 85–92 (2011).

66. Ivirico, J. L. E. *et al.* Structure and Properties of Methacrylate-Endcapped Caprolactone Networks With Modulated Water Uptake for Biomedical Applications. *J Biomed Mater Res PartB Appl Biomater.* **83,** 266–275 (2007).

67. Ivirico, J. L. E. *et al.* Proliferation and differentiation of goat bone marrow stromal cells in 3D scaffolds with tunable hydrophilicity. *J. Biomed. Mater. Res. B. Appl. Biomater.* **91,** 277–86 (2009).

68. Escobar Ivirico, J. *et al.* In vivo response of methacrylate endcapped caprolactone scaffolds. *Regen. Med.* **2,** 616 (2007).

69. Chang, H. & Wang, Y. in *"Regenerative Medicine and Tissue Engineering. - Cells and Biomateials"*. 569–588 (2011).

70. Keselowsky, B. G., Collard, D. M. & García, A. J. Surface chemistry modulates focal adhesion composition and signaling through changes in integrin binding. *Biomaterials* **25,** 5947–54 (2004).

71. Keselowsky, B. G., Collard, D. M. & Garcı, J. Surface chemistry modulates fibronectin conformation and directs integrin binding and specificity to control cell adhesion. *J. Biomed. Mater. Res.* **66A,** 247–259 (2002).

72. Leal-Egaña, A. & Scheibel, T. Interactions of cells with silk surfaces. *J. Mater. Chem.* **22,** 14330 (2012).

73. Bayes-Genis, A. *et al.* Human progenitor cells derived from cardiac adipose tissue ameliorate myocardial infarction in rodents. *J Mol Cell Cardiol.* **49,** 771–80 (2010).

74. Martinez-Estrada, O., Munoz-Santos, Y., Julve, J., Reina, M. & Vilaro, S. Human adipose tissue as a source of Flk-1+ cells: new method of differentiation and expansion. *Cardiovasc. Res.* **65,** 328–33 (2005).

75. Soler-botija, C. *et al.* Engineered 3D bioimplants using elastomeric scaffold , self-assembling peptide hydrogel , and adipose tissue-derived progenitor cells for cardiac regeneration. *Am. J. Transl. Res.* **6,** 291–301 (2014).

76. Brígido Diego, R. *et al.* Acrylic scaffolds with interconnected spherical pores and controlled hydrophilicity for tissue engineering. *J. Mater. Sci. Mater. Med.* **16,** 693–8 (2005).

77. Vilalta, M. *et al.* Dual luciferase labelling for non-invasive bioluminiscence imaging of mesenchymal stromal cell chondrogenic differentiation in demineralized bone matrix scaffolds. *Biomaterials* **30,** 4986–95 (2009).

78. Rigol, M. *et al.* Effects of adipose tissue-derived stem cell therapy after myocardial infarction: impact of the route of administration. *J. Card. Fail.* **16,** 357–66 (2010).

79. Briz, N. *et al.* Fibronectin fixation on poly(ethyl acrylate)-based copolymers. *J. Biomed. Mater. Res. B. Appl. Biomater.* **101,** 991–7 (2013).

80. Hiesinger, W. *et al.* Myocardial tissue elastic properties determined by atomic force microscopy after stromal cell-derived factor 1α angiogenic therapy for acute myocardial infarction in a murine model. *J. Thorac. Cardiovasc. Surg.* **143,** 962–6 (2012).

81. Cinca, J. *et al.* Passive transmission of ischemic ST segment changes in low electrical resistance myocardial infarct scar in the pig. *Cardiovasc. Res.* **40,** 103–12 (1998).

82. Salazar, Y., Bragos, R., Casas, O., Cinca, J. & Rosell, J. Transmural versus nontransmural in situ electrical impedance spectrum for healthy, ischemic, and healed myocardium. *IEEE Trans. Biomed. Eng.* **51,** 1421–7 (2004).

83. Geddes, L. A. & Baker, L. E. The specific resistance of biological material—A compendium of data for the biomedical engineer and physiologist. *Med. Biol. Eng.* **5,** 271–293 (1967).

84. Fallert, M. A. *et al.* Myocardial electrical impedance mapping of ischemic sheep hearts and healing aneurysms. *Circulation* **87,** 199–207 (1993).

85. Ninomiya, H. *et al.* Cadherin-dependent differential cell adhesion in Xenopus causes cell sorting in vitro but not in the embryo. *J. Cell Sci.* **125,** 1877–83 (2012).

86. Gnecchi, M. *et al.* Evidence supporting paracrine hypothesis for Akt-modified mesenchymal stem cell-mediated cardiac protection and functional improvement. *FASEB J.* **20,** 661–9 (2006).

87. Kumar, A. H. S. & Caplice, N. M. Clinical potential of adult vascular progenitor cells. *Arterioscler. Thromb. Vasc. Biol.* **30,** 1080–7 (2010).

88. Wang, C., Cao, D., Wang, Q. & Wang, D.-Z. Synergistic activation of cardiac genes by myocardin and Tbx5. *PLoS One* **6,** e24242 (2011).

89. Wilson-Rawls, J., Molkentin, J. D., Black, B. L. & Olson, E. N. Activated Notch Inhibits Myogenic Activity of the MADS-Box Transcription Factor Myocyte Enhancer Factor 2C. *Mol. Cell. Biol* **19,** 2853 (1999).

90. Lockhart, M. M. *et al.* Mef2c regulates transcription of the extracellular matrix protein cartilage link protein 1 in the developing murine heart. *PLoS One* **8,** e57073 (2013).

91. Jiang, W. *et al.* Homing and differentiation of mesenchymal stem cells delivered intravenously to ischemic myocardium in vivo: a time-series study. *Pflugers Arch.* **453,** 43–52 (2006).

92. Commision, E. CORDIS - community research and development information service. (2013). at <http://cordis.europa.eu/result/rcn/56832_en.html>

93. Xu, B. *et al.* Mechanically tissue-like elastomeric polymers and their potential as a vehicle to deliver functional cardiomyocytes. *J. Mech. Behav. Biomed. Mater.* **28,** 354–65 (2013).

94. Zhou, J. *et al.* The spatiotemporal development of intercalated disk in three-dimensional engineered heart tissues based on collagen/matrigel matrix. *PLoS One* **8,** e81420 (2013).

95. Zhang, S., Gelain, F. & Zhao, X. Designer self-assembling peptide nanofiber scaffolds for 3D tissue cell cultures. *Semin. Cancer Biol.* **15,** 413–20 (2005).

96. Santos, E., Hernández, R. M., Pedraz, J. L. & Orive, G. Novel advances in the design of three-dimensional bio-scaffolds to control cell fate: translation from 2D to 3D. *Trends Biotechnol.* **30,** 331–41 (2012).

97. Dégano, I. R. *et al.* The effect of self-assembling peptide nanofiber scaffolds on mouse embryonic fibroblast implantation and proliferation. *Biomaterials* **30,** 1156–65 (2009).

98. Martínez-Ramos, C. *et al.* Design and Assembly Procedures for Large-Sized Biohybrid Scaffolds as Patches for Myocardial Infarct. *Tissue Eng. Part C. Methods* **20,** 817–827 (2014).

99. Center, C. H. G., Genetics of Molecular, D. & the Weizmann Science, I. of. Gene Cards. *1996*

100. Messner, B., Baum, H., Fischer, P., Quasthoff, S. & Neumeier, D. Expression of messenger RNA of the cardiac isoforms of troponin T and I in myopathic skeletal muscle. *Am. J. Clin. Pathol.* **114,** 544–9 (2000).

CHAPTER 5- CONCLUSIONS

CONCLUSIONS (English)

- Three-dimensional *in vitro* models based in RAD16-I self-assembling peptide with and without RGD motifs and heparin polysaccharide modifications, where subcutaneous adipose tissue derived progenitor cells (subATDPCs) were able to form an interconnected cellular network, were developed.

- RAD16-I/RADRGD scaffold presented higher interconnections as compared to RAD16-I peptide, suggesting that RGD motif is indeed enhancing cell connections and migration. The presence of heparin presented cluster formation and looser networks but its capacity to localize growth factors is of high interest.

- 3D environment provided by RAD16-I self-assembling peptide is able to maintain the cardiac commitment of subATDPCs and in combination with chemical induction can induce overexpression of cardiac markers at gene and protein level. Neither the presence of RGD motifs or heparin polysaccharide change cardiac marker expression.

- The increase of storage modulus lead to an up-regulation of some cardiac genes, but the signaling provided by the cardiac induction media is also of high importance.

- An electro-stimulation protocol using the setup custom made by Universitat Politècnica de Catalunya (UPC) has been developed for 3D cultures based in RAD16-I self-assembling peptide.

- No differences in terms of viability, cellular network formation and condensation were observed after the application of electro-stimulation protocol in 3D cultures of subATDPCs. Therefore, it can be stated that the stipulated protocol do not cause a harmful effect to the cells.

- It was observed that at long periods of culture inside RAD16-I self-assembling peptide, subATDPCs started to migrate outwards the 3D construct. This fact is of high interest for further *in vivo* implantation of the proposed model.

- A two-steps methodology to assemble the bioactive implant was achieved.

- Both PEA and PCLMA microporous elastomeric membranes are elastomeric, hydrophobic, highly porous, and present similar electrical resistivity below the resistivity of transmural and non-transmural infarcted myocardium. Therefore, they can provide mechanical strength and geometrical definiteness to the heart and a low-resistance pathway that should contribute to facilitate the electrical signal propagation from the native heart tissue into the scaffold.

- Both proposed bioactive patches (PEA and PCLMA) intimately attach to the myocardium and remain in the position at the infarction area where they were placed suggesting resilience to the heart mechanical forces.

- SubATDPCs growing in composites were uniformly distributed whereas, on bare scaffolds, a heterogeneous layout was observed. Moreover, subATDPCs cultured on composites' surfaces were organized in a well-ordered pattern, which would facilitate cell-cell contact. Therefore, RAD16-I self-assembling peptide inside the porous provides a proper milieu for the cells.

- PEA-composites were able to proliferate and migrate outwards, but subATDPCs cultured in PCLMA-composites did not proliferate and remained inside the composite. We hypothesize that this can be caused by the lack of a 3D nanofiber network filling the microporous of the PCLMA elastomeric membrane.

- The combination of RAD16-I with this elastomeric membranes leads to the obtaining of a non-cardio-conductive biomaterial which is able to maintain the gene expression of the seeded cells.

CONCLUSIONES (Castellano)

- Se ha desarrollado un modelo tridimensional *in vitro* basado en el péptido auto-ensamblable RAD16-I con y sin motivos RGD y heparina, dónde las células progenitoras derivadas de tejido adiposo subcutáneo (subATDPCs) pueden comunicarse unas con las otras formando una red interconectada.

- Las células cultivadas en la matriz modificada con motivos RGD presentaron una mayor interconexión al ser comparadas con cultivos control de RAD16-I. Esto sugiere que el motivo RGD puede incrementar las conexiones intercelulares y la migración de las mismas. La presencia de heparina presentó la formación de agrupaciones celulares y la formación de redes más laxas, pero su capacidad de localizar factores de crecimiento es de gran interés.

- El ambiente tridimensional proporcionado por el péptido autoensamblable RAD16-I mantiene el compromiso cardíaco de las subATDPCs y en combinación con la inducción química lleva a la sobreexpresión de marcadores cardíacos a nivel de gen y proteína. La presencia de motivos RGD o el polisacárido de heparina no varía la expresión de marcadores cardiacos en comparación con RAD16-I.

- El aumento del módulo de almacenamiento provoca una sobreexpresión de algunos genes cardíacos, pero la señalización del medio sigue siendo de gran importancia.

- Se ha desarrollado un protocolo de estimulación eléctrica utilizando el sistema propuesto por la Universitat Politècnica de Catalunya (UPC) para cultivos 3D basados en el péptido auto-ensamblable RAD16-I.

- No se observaron diferencias en términos de viabilidad, formación de red celular y condensación macroscópica después de la aplicación de la estimulación eléctrica en cultivos 3D de subATDPCs. Así pues se puede concluir que el sistema no causa ningún efecto dañino a las células.

- Se ha observado que a largos periodos de cultivo en la matriz 3D de RAD16-I, las subATDPCs inician una migración hacia fuera del cultivo 3D. Esta observación resulta ser de gran interés para la posible implantación *in vivo* del modelo propuesto.

- Se ha diseñado una metodología de dos pasos para ensamblar el implante bioactivo.

- Ambas membranas elastoméricas (PEA y PCLMA) son matrices elásticas porosas muy hidrofóbicas con una resistividad eléctrica parecida y por debajo de la resistividad del miocardio infartado (transmural y no transmural). Así pues, aportan tanto fuerza mecánica y definición geométrica al corazón como un camino de baja resistencia que puede contribuir a facilitar la propagación eléctrica desde el tejido nativo al bioimplante.

- Ambos implantes bioactivos propuestos (PEA y PCLMA) se adhieren íntimamente al miocardio y se mantienen en la posición de implantación. Esto surgiere que el implante propuesto puede adaptarse a las fuerzas mecánicas del corazón.

- Las subATDPCs creciendo en los materiales compuestos se distribuyeron uniformemente, pero en las membranas sin RAD16-I se observó una distribución heterogénea. Además, las células cultivadas en los materiales compuestos se organizaron ordenadamente facilitando los contactos intercelulares. Así pues, el péptido autoensamblable RAD16-I dentro de los poros proporciona un ambiente adecuado para las células.

- Las células cultivadas en los materiales compuestos de PEA fueron capaces de proliferar y migrar hacia fuera de la plataforma, pero las cultivadas en los materiales compuestos de PCLMA no proliferaron y permanecieron dentro de la plataforma. Este resultado se puede explicar por la falta del ambiente 3D dentro de los microporos de la membrana elastomérica de PCLMA.

- La combinación de RAD16-I con membranas elastoméricas permite la obtención de una plataforma no cardio-conductiva que permite el mantenimiento de la expresión génica de las células cultivadas.

CONCLUSIONS (Català)

- S'ha desenvolupat un model tridimensional (3D) *in vitro* basat en el pèptid autoensamblable RAD16-I amb i sense modificacions de motius RGD i/o heparina, on les cèl·lules progenitores derivades de teixit adipós subcutani (subATDPCs) poden comunicar-se unes amb les altres formant una xarxa interconnectada.

- Les cèl·lules cultivades en la matriu modificada amb motius RGD van presentar una major interconnexió al ser comparades amb cultius control de RAD16-I. Això suggereix que el motiu RGD pot incrementar les connexions intercel·lulars i la migració de les mateixes. La combinació d'aquest motiu amb heparina va presentar la formació d'agrupacions cel·lulars i la formació de xarxes més laxes però la seva capacitat de localitzar factors de creixement segueix sent de gran interès.

- L'ambient tridimensional proporcionat per el pèptid autoensamblable RAD16-I manté el compromís cardíac de les subATDPCs i en combinació amb la inducció química porta a la sobre-expressió de marcadors cardíacs a nivell de gen i proteïna. La presència de motius RGD o el polisacàrid heparina no varia l'expressió d'aquests marcadors en comparació amb RAD16-I.

- L'augment del mòdul d'emmagatzematge provoca una sobre-expressió d'alguns gens cardíacs, però la senyalització del medi també és de gran importància.

- S'ha desenvolupat un protocol d'estimulació elèctrica emprant el sistema proposat per la Universitat Politècnica de Catalunya (UPC) per a cultius 3D basats en el pèptid autoensamblable RAD16-I.

- No es van observar diferencies en termes de viabilitat, formació de xarxa cel·lular i condensació macroscòpica després de l'aplicació de l'estimulació elèctrica en cultius 3D de subATDPCs. Així doncs es pot concloure que el sistema no causa cap efecte nociu per a les cèl·lules.

- S'ha observat que a llargs períodes de cultiu en RAD16-I, les subATDPCs inicien una migració cap a fora del cultiu 3D. Aquesta observació resulta ser de gran interès per a la possible implantació *in vivo* del model proposat.

- S’ha dissenyat una metodologia de dos passos per a preparar l’implant bioactiu.

- Ambdues membranes elastomèriques (PEA y PCLMA) són matrius elàstiques poroses molt hidrofòbiques amb una resistivitat elèctrica semblant i per sota de la resistivitat del miocardi infartat (transmural y no transmural). Així doncs, aporten tant força mecànica i definició geomètrica com un camí de baixa resistència que pot contribuir a facilitar la propagació elèctrica des dels teixit natiu al bioimplant.

- Ambdós implants bioactius proposats (PEA y PCLMA) s’adhereixen íntimament al miocardi i es mantenen en la posició d’implantació. Això suggereix que l’implant pot adaptar-se a les forces mecàniques del cor.

- Les subATDPCs creixent els materials compostos es van distribuir uniformement, però en les membranes sense RAD16-1 es va observar una distribució heterogènia. Les cèl·lules cultivades en els materials compostos es van organitzar ordenadament facilitant els contactes intercel·lulars. Així doncs, el pèptid autoensamblable RAD16-I dins dels porus proporciona un ambient adequat per a les cèl·lules.

- Les cèl·lules cultivades en els materials compostos de PEA van poder proliferar i migrar cap a fora de la plataforma, però en els materials compostos de PCLMA no van poder-ho fer i es van mantenir dins de la plataforma. Aquest resultat es pot explicar per la falta d’ambient 3D dins dels microporus de la membrana elastomérica de PCLMA.

- La combinació de RAD16-I amb membranes elastomèriques, permet l’obtenció d’una plataforma no cardio-conductiva que permet el manteniment del fenotip de les cèl·lules cultivades.

ANNEX

LIST OF PUBLICATIONS

[1] Castells-Sala C and Semino C E (2012) Biomaterials for stem cell culture and seeding for the generation and delivery of cardiac myocytes. *Curr. Opin. Organ Transplant.* **17** 681–7

[2] Castells-Sala C, Sanchez B, Recha-Sancho L, Puig V, Bragos R and Semino C E (2012) Influence of electrical stimulation during cardiac differentiation in 3D-cultures of SUBcutaneous Adipose Tissue Derived Progenitor Cells (subATDPCs) *Conf Proc IEEE Eng Med Biol Soc* 3–6

[3] Bussmann B M, Reiche S, Marí-Buyé N, Castells-Sala C, Meisel H J and Semino C E (2013) Chondrogenic potential of human dermal fibroblasts in a contractile, soft, self-assembling, peptide hydrogel. *J. Tissue Eng. Regen. Med.*

[4] Vallés-Lluch A, Arnal-Pastor M, Martínez-Ramos C, Vilariño-Feltrer G, Vikingsson L, Castells-Sala C, Semino C E and Monleón Pradas M (2013) Combining self-assembling peptide gels with three-dimensional elastomer scaffolds *Acta Biomater*. **9** 9451–60

[5] Castells-Sala C*, Alemany-Ribes M*, Fernández-Muiños T, Recha-Sancho L, López-Chicón P, Aloy-Reverté C, Caballero-Camino J, Márquez-Gil A and Semino C E (2013) Current Applications of Tissue Engineering in Biomedicine *Biochips and Tissue Chips* 0–14

[6] Soler-botija C, Bagó J R, Llucià-valldeperas A, Vallés-lluch A, Castells-sala C, Martínez-ramos C, Fernández-muiños T, Chachques J C, Pradas M M, Semino C E and Bayes-Genis A (2014) Engineered 3D bioimplants using elastomeric scaffold , self-assembling peptide hydrogel , and adipose tissue-derived progenitor cells for cardiac regeneration *Am. J. Transl. Res.* **6** 291–301

[7] Castells-Sala C*, Vallés-Lluch A*, Soler-Botija C*, Arnal-Pastor M, Martínez-Ramos C, Fernandez-Muiños T, Marí-Buyé N, Llucià-Valldeperas A, Sanchez, Chachques JC, Bayes-Genis A, Monleón-Pradas M, Semino CE. (under submission) Development of bioactive patch for maintenance of implanted cells at the myocardial infarcted site. *Equal contribution.

[8] Castells-Sala C*, Martínez-Ramos C*, Vallés-Lluch A, Monleón-Pradas M, Semino CE. (under submission) Bioimplant development to assist myocardial infarct using elastomeric scaffolds filled with peptide gel and adipose tissue-derived progenitor cells. *Equal contribution.

[7] Castells-Sala C, Recha-Sancho L, Sanchez B, Bragos R and Semino C E (under preparation) Three-dimensional cultures of subcutaneous adipose tissue derived progenitor cells based in RAD16-I.

[8] Martínez-Ramos C, Castells-Sala C, Vallés-Lluch A, Semino CE, Monleón-Pradas M (under preparation) SubATDPCs behavior in a bioimplant consisting of PCLMA elastomeric membrane and RAD16-I self-assembling peptide

[9] Alemany-Ribes, M.*, Castells-Sala C.*, Caballero-Camino,J., Aloy-Reverté, C., and Semino C E (under preparation) Contribution of the microenvironment on E-cadherin regulation in pancreatic cancer. *Equal contribution.

LIST OF CONTRIBUTIONS IN CONGRESS

- June 2012. Advanced Summer School. Parc Científic Barcelona "*Influence of electrical stimulation in 3D cultures of adipose tissue derived progenitor cells (ATDPCs) for cardiac regeneration purposes."* (POSTER).

- July 2012. Internacional Congress on Stem Cells and Tissue Formation. Dresden. *"Cardiac differentiation of Adipose Tissue Derived Progenitor Cells (ATDPCs) in a 3D system."* (POSTER).

- September 2012. 3rd TERMIS World Congress. Wien, Austria. *"Development of new bioactive implant to assist cardiac tissue regeneration (EU RECATABI PROJECT)"* (POSTER)

- June 2013. EMBO|EMBL Symposium Cardiac Biology, from development to regenerative medicine. Heidelberg, Germany. "Cardiac differentiation of Adipose Tissue Derived Progenitor Cells (ATDPCs) in a 3D system." (POSTER)

- November 2013. Padua Muscle Days. Padova, Italia. A bioengineering approach to restore ventricular function after myocardial infarction." (ORAL PRESENTATION)